2018

STUDY OF THE MECHANISM OF ACTION FOR Ru(II) POLYPYRIDYL COMPLEXES AS POTENTIAL ANTICANCER AGENTS

Yang Sun
University of Kentucky, yang.sun@uky.edu
Digital Object Identifier: https://doi.org/10.13023/ETD.2018.184

STUDENT AGREEMENT:

I represent that my thesis or dissertation and abstract are my original work. Proper attribution has been given to all outside sources. I understand that I am solely responsible for obtaining any needed copyright permissions. I have obtained needed written permission statement(s) from the owner(s) of each third-party copyrighted matter to be included in my work, allowing electronic distribution (if such use is not permitted by the fair use doctrine) which will be submitted to UKnowledge as Additional File.

I hereby grant to The University of Kentucky and its agents the irrevocable, non-exclusive, and royalty-free license to archive and make accessible my work in whole or in part in all forms of media, now or hereafter known. I agree that the document mentioned above may be made available immediately for worldwide access unless an embargo applies.

I retain all other ownership rights to the copyright of my work. I also retain the right to use in future works (such as articles or books) all or part of my work. I understand that I am free to register the copyright to my work.

REVIEW, APPROVAL AND ACCEPTANCE

The document mentioned above has been reviewed and accepted by the student's advisor, on behalf of the advisory committee, and by the Director of Graduate Studies (DGS), on behalf of the program; we verify that this is the final, approved version of the student's thesis including all changes required by the advisory committee. The undersigned agree to abide by the statements above.

Yang Sun, Student

Dr. Edith Glazer, Major Professor

Dr. Mark Lovell, Director of Graduate Studies

STUDY OF THE MECHANISM OF ACTION FOR Ru(II) POLYPYRIDYL COMPLEXES AS POTENTIAL ANTICANCER AGENTS

DISSERTATION

A dissertation submitted in partial fulfillment of the requirements for the degree of Doctor of Philosophy in the College of Arts and Sciences at the University of Kentucky

By

Yang Sun

Lexington, Kentucky

Director: Dr. Edith Glazer, Associate Professor of Chemistry

Lexington, Kentucky

2018

ABSTRACT OF DISSERTATION

STUDY OF THE MECHANISM OF ACTION FOR Ru(II) POLYPYRIDYL COMPLEXES AS POTENTIAL ANTICANCER AGENTS

Application of chemotherapeutic agents in current cancer treatment has been limited by adverse effects as poor selectivity results in systemic toxicity; most chemotherapy approaches also experience inherited or acquired drug resistance which lead to reduced treatment outcome. Research efforts have focused on the discovery of novel chemotherapies that overcome the limitations mentioned above. Ru(II) polypyridyl complexes with anti-cancer properties have been extensively studied as traditional cytotoxic agents and photodynamic therapy agents due to their photophysical and photochemical characteristics.

Most research has focused on the design of Ru(II) polypyridyl complexes that have affinities to nucleic acids as inspired by the classic small molecule metal complex cisplatin. Though modifying the structures of ligands on the ruthenium metal center, the hydrophilicity, charge state and photochemical properties can be tuned, resulting to Ru(II) polypyridyl complexes that act through cellular targets other than DNA.

Understanding the mechanism of action and identifying functional targets remain the challenging and complex research topic in the design and study of novel medication or candidates. With the development of semi-high throughput cytological profiling in a bacterial system, rapid investigation of the mechanism of action can be achieved to distinguish anti-cancer agents which possess different mechanisms of actions. Ru(II) polypyridyl complexes with different scaffolds have been studied and suggested to have anti-cancer properties through DNA damage response, and/or translational inhibition.

KEYWORDSs: Ru(II) polypyridyl complex, cancer, chemotherapy, mechanism of action, cytological profiling

Yang Sun

03/12/2018

STUDY OF THE MECHANISM OF ACTION FOR Ru(II) POLYPYRIDYL COMPLEXES AS POTENTIAL ANTICANCER AGENTS

By

Yang Sun

Dr. Edith Glazer
Director of Dissertation

Dr. Mark Lovell
Director of Graduate Studies

03/12/2018

TO MY FAMILY

ACKNOWLEDGEMENTS

I have had the luxury to get support from many people during the years that I pursue the Ph. D. degree in graduate school. I would first like to express my deepest gratitude to Dr. Glazer, my mentor, for her selfless help and guidance. Ever since the first day we met, she has been my inspiration in both science and life, her persistent aspiration in science has been the source of courage for me to achieve what I have done and to continue overcoming any difficulties in the future.

My committee members, Dr. Mark Lovell, Dr. Mark Watson, and Dr. Kathleen O'Connor, have been the continuous support to me for the years. I would like to thank all of them for the insightful advices during each of our meetings, and for the meaningful roles that they all have played in my life during this very important period of time. I am extremely grateful to Dr. David Heidary for the tremendous support that he has offer to me from designing my research to viewing the world as a real scientist. I would like then to thank all members of the Glazer group, including those who have move on to a new stage of their life. They have been the ground for me to start and complete the Ph. D. work. I want to thank Erin and Catherine especially for all the conversations not just about science but also on enjoying life as a graduate student. Next, I would express my appreciation to Dr. Chris Richards, he has been the major reason that I can accomplish all the microscopic researches. I want to also thank all members in the Richards group for their generous help on microscopic instrument. I would give my special thanks to Zhihui, for being an excellent collaborator but also a friend who shared many conversations. I would like to thank Dr. Thomas Wilkop in the Light Microscopy Core for giving advice on microscopic imaging. I would also thank Tricia Coakley and Megan Combs for their support as experts in metal analysis.

I want to then thank my family and friends who have been unbelievably caring and supportive. None of my work and life would be as it is without the understanding of my parents, they have always been there to listen, they have always been willing to understand my research and in general any science to know their daughter as a scientist. Thank you for being my parents.

Table of Contents

LIST OF TABLES

LIST OF FIGURES

LIST OF APPENDIX TABLES

LIST OF APPENDIX FIGURES

RESEARCH CONTRIBUTIONS

The research presented in this dissertation is completed with help and support of many scientists. Compounds synthesis, characterization, chemical and physical property studies in chapter 2 were completed by Dr. Matt Dickerson and Mr. Brock Howerton. DNA gel electrophoresis and microscopy studies were completed by Dr. Matt Dickerson. Compound studied in chapter 3 was synthesized and characterized by Mr. Brock Howerton and Dr. Erin Wachter. Compounds studied in chapter 5 were synthesized and characterized by Dr. Dmytro Havrylyuk. Cytotoxicity study of BODIPY conjugated compounds and generation of HEK cell lines stably expressing different organelle markers were completed by Dr. David Heidary. pCWori plasmid DNA and Dendra2 gene sequence was kindly provided by Dr. David Heidary.

Chapter 1 Introduction

1.1 Cancer and current treatments.

Cancer, by definition, is a group of diseases in which the abnormal cells grow and divide without control, and invade other tissues through the lymphatic and circulatory system. Failure of regulation of normal cell division and differentiation results in uncontrolled cell growth and proliferation. In recent years, cancer has remained the second leading cause of death in the United States and worldwide.[1, 2] In 2017, it is estimated that over 4,600 people will be diagnosed with cancer every day, leading to a total number of 1,688,780 new cases in the United States.[1] Cancer deaths in the US are projected to be 600,920 for 2017, which means more than 1,600 people die of cancer every day.[1] According to the statistics from National Cancer Institute's (NCI's) Surveillance, Epidemiology, and End Results (SEER) Program, the top three caner types in female are: breast cancer, which is responsible for 30% of incidences, and 14% of deaths; lung cancer, which is responsible for 12% of incidences, and 25% of deaths; and colon cancer, which leads to 8% of both incidences and deaths. In males, the top three cancer types are: prostate cancer, resulting in 19% of incidences and 8% of deaths; lung cancer, which is responsible for 14% of incidences and 27% deaths; and colon cancer, which leads to both 9% of both incidences and deaths.[1]

Current cancer treatments consist of surgery to physically remove the tumor for localized tumors, radiation therapy, and chemotherapy that typically damages a portion of cancerous cells.[3] Clinical treatments typically utilize a combination of the three methods, with multiple components in the chemotherapy prescribed, known as chemotherapy regimens. A chemotherapy regimen typically includes the type and dosage of medications used, the duration of treatment, and the frequency. In current clinical application, multiple types of drugs of different mechanisms of actions are used in combination to produce synergistic effects.[4, 5] The first successful chemotherapy regimen was MOPP, which was introduced in 1963 to treat Hodgkin's disease. This particular regimen includes mustargen, oncovin, procarbazine, and prednisone; they are administrated in a four-week cycle for several cycles by intravenous (IV) injection and oral dose.[6, 7] One component that is commonly included in many chemotherapy regimen is platinum agents, including cisplatin, oxaliplatin, and carboplatin, which have been applied in over 30 chemotherapy regimens.[7] Among the three platinum agents, cisplatin is the most commonly prescribed species in treatments of testicular cancer (BEP: bleomycin, etoposide, and cisplatin), bladder cancer (MVAC: methotrexate, vinblastine, doxorubicin, and cisplatin), lymphoma (DHAP: dexamethasone, cytarabine, and cisplatin), and lung cancer (MVP: mitomycin, vindesine, and cisplatin; PEI: cisplatin, etoposide, and ifosfamide).[8, 9, 7]

Recent advances in drug discovery have provided novel treatment approaches, including immunotherapy, that have seen promising results, and there are chemotherapeutic agents that are able to target certain biomarkers of cancer cells. A majority of the targeted therapies approved by the FDA are small molecule kinase inhibitors, such as imatinib mesylate, commonly used under brand name Gleevec. This is a small molecule tyrosine kinase inhibitor that effectively inhibits the fusion protein kinase Bcr-Abl in Philadelphia chromosome-positive chronic myelogenous leukemia (CML) and acute lymphoblastic leukemia (ALL).[10, 11, 12, 13] Positive results associated with such selective drugs include increasing survival rates with fewer side effects, but there are also challenges in targeted therapy. Cancer cell resistance occurs with targeted therapy by mutation of the targets, and the development of precision medication for certain targets can be difficult and time consuming.[14, 11, 15] For these reasons, the systemic chemotherapy that generally damages common cell targets remain the main stream for current chemotherapy.

1.2 Cisplatin is a commonly used chemotherapeutic agent.

Cis-diamminedichloroplatinum (II), also known as cisplatin (brand name Platinol), is one of the most widely used metal-based chemotherapeutic agents for cancer (Figure 1A). Barnett Rosenberg's study showing *E. coli* cell division inhibition led to the discovery of cisplatin in 1965, and he also demonstrated the anti-tumor activity of this platinum based small molecule in later research.[16,17,18] Following the approval by FDA in 1978 for the treatment of testicular and ovarian cancer, cisplatin has been used to treat various types of cancer since then, including bladder, lung, and head and neck cancer, and provides an overall cure rate of testicular cancer higher than 90%.[19,20] The discovery of cisplatin also led to the extensive study of platinum and other metal based compounds for their biological properties and potential medical applications.[21, 22]

The generally accepted mechanism of action of cisplatin is DNA damage induced by covalent platinum - DNA adducts; therefore, DNA has been considered the primary functional target of cisplatin. Cisplatin mainly enters cells by passive diffusion,[23,24] the chloride ligands on platinum are then displaced by water molecules in the cell, generating an active aquated species, which is positively charged, and has higher affinity to DNA molecules. The active species binds to DNA with loss of the water ligands and forms stable covalent bonds primarily with purine bases at the N7 position, causing intrastrand (on a single strand) and interstrand (on two strands) crosslinks, as shown in Fig. 1B.[25] The DNA - cisplatin adducts lead to distortions of DNA structure, which are recognized by damage recognition proteins including HMGB proteins, DNA damage repair proteins, and transcription factors. This triggers DNA repair pathways, whose failure leads to apoptosis, a form of programmed cell death.[26]

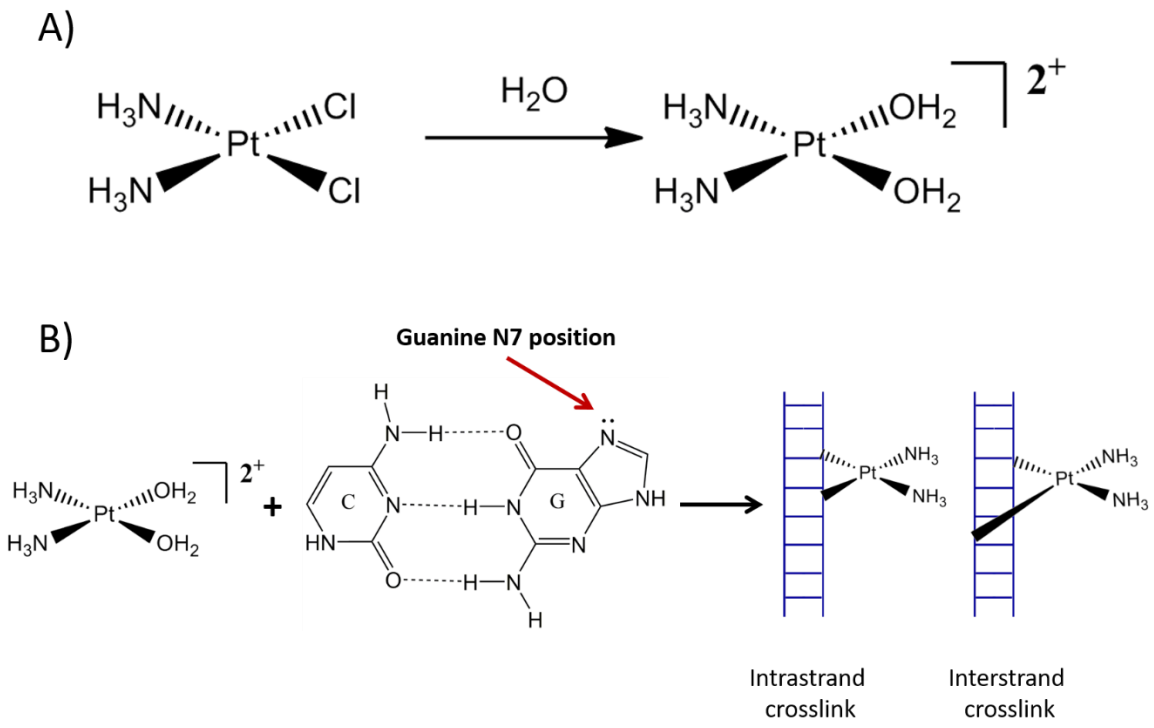

Figure 1.1 DNA damaging mechanism of cisplatin. A) Formation of cisplatin diaqua active species via hydrolysis. B) The diaqua form of cisplatin forms covalent cisplatin-DNA adducts at N7 position of guanine and results in both interstrand and intrastrand crosslinks of DNA.

Similar to many chemotherapeutic agents, cisplatin has a limited spectrum of anticancer activity, and the utilization of cisplatin in cancer treatment is also largely limited by adverse-effects due to its non-selectivity. Since cisplatin affects normal cells as well as cancer cells, it causes several systemic toxicities.[26] Cisplatin affects the kidneys of patients, resulting in nephrotoxicity; it also causes neurotoxicity and ototoxicity, severe nausea and vomiting, and myelosuppression. These side-effects have limited the clinical application of cisplatin.[26] Another major limitation of cisplatin treatment is the intrinsic or acquired drug resistance of cancer cells. The mechanism of cisplatin resistance is complex and is currently not fully understood. Several different mechanisms have been shown to be associated with resistance behavior, including but not limited to decreased cellular accumulation, inactivation of cisplatin by sulfur containing molecules, enhanced nucleotide excision DNA repair mechanism, and defects in signaling pathways leading to apoptosis. In most cisplatin resistant cells, there is more than one mechanism involved.[27] Reduced cellular accumulation of cisplatin is mainly caused by decreased uptake. Recent research shows copper transport protein (CTR1) assists in the uptake of cisplatin, and increased CTR1 expression level results in increased cisplatin accumulation and cytotoxicity.[28] Cisplatin resistance due to reaction with sulfur compounds has been shown with glutathione. Glutathione is a short peptide consisting

of three amino acid residues: cysteine, glutamic acid, and glycine. Cisplatin is able to covalently bond to the thiolate anion of glutathione, and as a result, loses the ability to crosslink DNA, which leads to tolerance of cisplatin. In cisplatin resistant bladder tumor cells, elevated levels of glutathione are observed while the glutathione levels are lower in testicular cells, which are intrinsically sensitive to cisplatin treatment.[29] Other cysteine-rich proteins such as metallothioneins also contribute to the inactivation of cisplatin through a similar mechanism.[27]

In cisplatin resistant cells, the ability to repair cisplatin - DNA adducts and to tolerant the DNA lesions is enhanced; in other words, sensitivity to cisplatin is decreased. Nucleotide excision repair (NER) is responsible for removal of most DNA lesions caused by cisplatin.[4, 30] In mammalian cells, NER requires about 20 proteins to excise the damaged nucleotides, reconstruct the DNA by replacing new nucleotides, and sealing the repaired strand.[31] Deficient NER is usually associated with cisplatin sensitivity, while cisplatin resistant cells exhibit increased NER proficiency to repair cisplatin - DNA lesions. The increased repair efficiency in cisplatin resistant cells is also positively correlated with specific enzymes, including XP complementation group A (XPA) and excision repair cross-complementation group 1 (ERCC1). These two enzymes are key players in nucleotide excision repair. It has been reported that cisplatin resistance is correlated with overexpression of ERCC1 and XPA.[32, 33] In addition to NER, another repair mechanism, mismatch repair (MMR) detects the cisplatin induced DNA damage. MMR fails to repair the damage which leads to apoptotic signaling, so this repair mechanism serves more as a signaling pathway, and it has been reported that cisplatin resistant cells usually have a defect in MMR. In cisplatin resistant cells, there are more changes in signaling pathways other than the mismatch repair that inhibit apoptosis caused by cisplatin treatment. Some studies suggest that cisplatin resistant cells fail to activate several mitogen activated protein kinase (MAPK) family members, for example, P38 MAPK and c-JNK, and therefore result in deficient apoptotic signaling.[34,35] Many cisplatin resistant cells express high level of apoptosis inhibitors or low levels of proapoptotic proteins.[36] It has been reported that cisplatin resistant ovarian cancer cells express reduced levels of the proapoptotic protein Bax.[37] In addition, the cisplatin sensitive testicular cancer cells express high levels of Bax to promote apoptosis and low level of apoptotic inhibitor Bcl-2.[38]

1.3 Alternative platinum complexes as anticancer agents.

After the discovery and clinical application of cisplatin, platinum based small molecules have been the focus of intense research to design novel molecules that retain anticancer activity with reduced systemic toxicity and drug resistance.[39] Investigation of molecules with a platinum center generally have similar features: (i) neutral complexes; (ii) square planar structures; (iii) two *cis* amine groups and two *cis*-coordinated leaving groups.[21, 40, 41] Several analogous drugs acting

through similar DNA binding mechanisms have been developed and approved by drug administration agencies around the world for cancer treatments (Figure 1.2).

Carboplatin is a second-generation platinum drug that was approved by the FDA in 1989 for treatment of multiple types of cancer including ovarian cancer, lung cancer, and breast cancer. The alteration in the chelating ligand, dicarboxylate replacing the two chloride ligands in cisplatin, makes the leaving group bigger and more stable than chloride. This slows drug metabolism, and reduces the side effects compared to cisplatin. The major side effects of carboplatin include nausea, vomiting, and myelosuppression.[21, 42, 43] Another platinum based drug that has been globally approved for clinical application is oxaliplatin (Figure 1.2). Here, the platinum center in oxaliplatin coordinates with a 1,2-diaminocyclohexane (DACH) ligand and a bidentate oxalate ligand. Developed as an improvement of cisplatin, oxaliplatin has a shifted anticancer spectrum compared with the first and second generations of platinum drugs. It has been mainly used to treat colorectal cancer and gastrointestinal cancers that are resistant to cisplatin and carboplatin.[44, 5] The altered anticancer spectrum of oxaliplatin has been thought to be associated with the alteration in DNA binding and DNA damage responses.[22, 45] Recent researches, however, have indicated the differences could be a result of novel mechanisms relating to ribosome biogenesis that are not associated with cisplatin and carboplatin mechanisms of action.[46, 44] The side effects of oxaliplatin includes peripheral neurotoxicity, nausea, vomiting, and fatigue.[47, 48]

Nedaplatin, heptaplatin, and lobaplatin are cisplatin analogous drugs that are approved for clinical treatments in certain countries. Nedaplatin is currently approved for treatments of lung cancer, head and neck cancer in Japan.[49, 50] This molecule has greater water solubility due to the glycolate chelating group that replaces the two chloride ligands in cisplatin (Figure 1.2). [49, 21] Heptaplatin is now approved by Korean drug administration agency for treatment of gastric cancer, the platinum center is chelated to a malonate group and a 2-(1-methylethyl)-1,3-dioxolane-4,5-dimethanamine group which contains a seven-numbered ring.[21, 51] The efficacy of heptaplatin in cisplatin resistant gastric cancer cells has been reported to be associated with less involvement of metallothionein.[51] Lobaplatin is currently approved in China to treat breast cancer, lung cancer, and chronic myelogenous leukemia (CML).[52, 21] Lobaplatin contains a 1,2-bis(aminomethyl)cyclobutane ligand and a lactic acid serves as the leaving group, it is formulated as a diastereometric mixture.[53, 21]

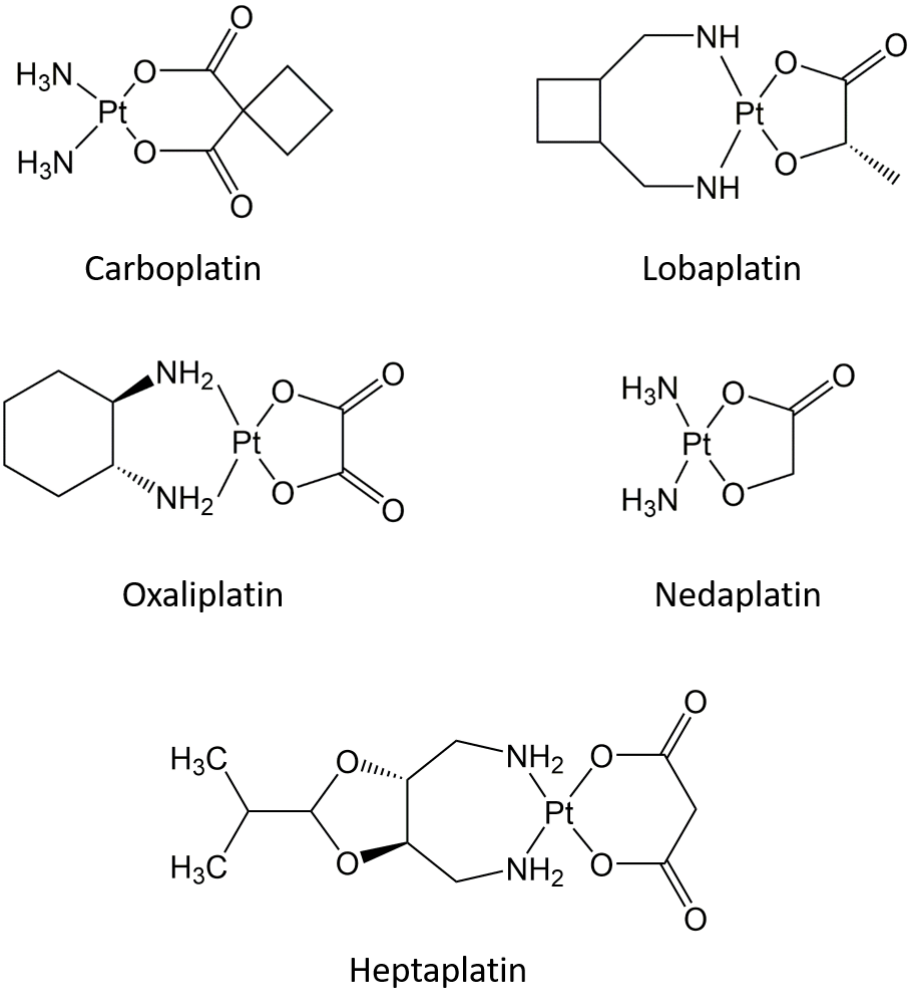

Figure 1.2 Platinum based drugs that have approved for clinical treatments of cancers.

Platinum based drugs such as carboplatin and oxaliplatin which are analogous to cisplatin, however, do not completely eliminate side-effects and drug resistance.[54, 55, 56, 57] More platinum containing molecules with modified structures have been studied for possible medical applications.[21] Besides the cisplatin analogous drugs that have approved for clinical applications, a number of platinum compounds have been developed and studied for their anticancer properties. The possibility of using platinum (IV) compounds as prodrugs to release platinum (II) compounds that are analogous to cisplatin has been explored, and several candidates have entered clinical trials for their therapeutic applications. Tetraplatin (tetrachloro(*trans*-1,2-diaminocyclohexane) platinum (IV)), also known as ormaplatin, is reduced to an active platinum (II) species dichloro(*trans*-1,2-diaminocyclohexane) platinum (II) that is similar to oxaliplatin.[21, 58] In Phase I clinical trials, it showed activity against cisplatin-resistant cancers, but severe neurotoxicity was observed as well.[59, 60, 61] Iproplatin (*cis*,*trans*,*cis*-dichlorodihydroxobis(isopropylamine)platinum (IV)) also produces

active platinum (II) species that covalently bind to DNA and induces cytoxicity against cancer cells. Iproplatin has been studied in Phase I to III clinical trials for ovarian cancer, head and neck cancer, with the major side effects of iproplatin being myelosuppression, nausea, and vomiting.[21, 62, 63] Satraplatin (*trans,cis,cis*-bis(acetato)amminecyclohexylaminedichloroplatinum (IV)) is featured as an oral bioavailable agent. It is reduced in the bloodstream, producing six different platinum (II) species that are DNA crosslinking agents.[21, 64] Phase II clinical trial in lung cancer and head and neck cancer patients showed reduced neurotoxicity and nephrotoxicity side effects.[65, 66, 21]

1.4 Non-platinum metal compounds as potential anticancer agents.

Besides all the efforts invested on platinum based anticancer agents, non-platinum based drugs with alternate metal centers also have been the subject of increasing research interest as they offer the possibility of novel targets and mechanisms of action with reduced drug resistance and general toxicity.[67, 68] The availability for expanded coordination chemistry, and the photophysical and photochemical properties of transition metals make them favored research candidates for the medicinal chemistry field.[69, 70] Molecules with anticancer properties have been prepared and studied with transition metals including iron (Fe), cobalt (Co), copper (Cu), nickel (Ni), ruthenium (Ru), rhodium (Rh), palladium (Pd), gold (Au), osmium (Os), and iridium (Ir).[71, 70, 41] While none of these transition metal compounds have been approved by FDA for clinical treatment, they have been studied in clinical trials and preclinical studies with not just DNA associated mechanism, but also novel mechanisms of action.[72]

Dinuclear cobalt compounds with alkyne ligands have been reported to exhibit cytotoxicity in multiple cancer cell lines;[73, 72] furthermore, it was revealed that the cytotoxicity didn't correlate with the DNA binding property. The lead compound, [2-acetoxy-(2-propynyl)benzoate]hexacarbonyldicobalt (Co-ASS, Figure 1.3A), a cobalt alkyne compound with an aspirin derivative, has shown ability to inhibit cyclooxygenase enzymes (COX-1 and COX-2); and the COX inhibition has correlated well with the cytotoxicity in cancer cells.[74, 75] Further studies have proved additive and synergistic effects of Co-ASS in combination with the tyrosine kinase inhibitor, imatinib.[76, 72] Efforts have been invested in cobalt (III) compounds that are activated by the hypoxia environment and the slightly acidic pH in cancer cells to cause cytotoxicity.[77, 72] Cobalt (III) compounds containing nitrogen mustards (Figure 1.3B) are reduced to cobalt (II) compounds in hypoxic cells, releasing the nitrogen mustard ligand to damage DNA of cancer cells.[78, 79]

Copper plays essential roles in a number of cellular events and regulatory pathways, besides its role as an enzyme co-factor. Copper (II) compounds have received considerable research interests as they exhibit activities in cancer cells through mechanisms that differ from cisplatin.[71, 70] It has been generally considered that the cytotoxicity of copper compounds are the result of the

reactive oxygen species (ROS) generation and oxidative DNA cleavage.[71, 70] It is also notable that copper compounds containing dithiocarbamates (Figure 1.3C) selectively target the proteasome in cancer cells.[80, 71, 81]

Research on ruthenium compounds has drawn increasing research interest as the octahedral coordination geometry and three dimensional architecture of ruthenium offers the potential for higher degrees of site selectivity towards biological molecules such as DNA and protein compared to the square planer geometry of most platinum based compounds. This may lead to lower toxicity and possible reduced adverse effects.[82, 83, 84, 85] Current ruthenium compounds studied for anticancer properties act through both DNA dependent and independent mechanisms. Two ruthenium (III) compounds, NAMI-A (imidazolium trans-imidazoledimethyl sulfoxide-tetrachlororuthenate, Figure 1.3E) and KP1019 (trans-[tetrachlorobis(1H-indazole, Figure 1.3F) ruthenate]) have been studied in clinical trials. Both NAMI-A and KP-1019 form various ruthenium species in the biological environment and the active species generated readily react with biological molecules including DNA.[72, 86, 87] It has been reported that both compounds induce DNA damage responses and apoptosis in cancer cells, though the mechanism is not fully understood. NAMI-A is primarily effective in inhibiting tumor metastasis *in vivo*, while KP1019 is active against both primary and metastatic tumors.[88, 89, 90]

Ruthenium (II) arene compounds containing 1,3,5-triaza-7-phosphoadamantane ligands, also known as RAPTA compounds (Figure 1.3D), are another type of ruthenium compounds with favorable anticancer properties.[82, 91] RAPTA compounds have exhibited similar anti-metastasis properties as NAMI-A both in animal studies and in cell migration and invasion assays, and they have also shown strong interactions with protein but relatively low affinity with DNA, suggesting the possible mechanism is not through DNA, as with classical platinum compounds. It has been reported that RAPTA compounds binds to the histone proteins of chromosomes.[91, 71, 40, 82]

Ruthenium (II) polypyridyl compounds have been investigated for their photophysical and photochemical properties as photodynamic therapy agents, and their nucleic acid affinity is responsible for their use as DNA damaging agents.[92, 71] Recently, a novel type of ruthenium (II) photosensitizer TLD1433 (Figure 1.3H) has been studied in Phase I clinical trial for bladder cancer and has received positive results. TLD 1433 has shown the capability to generate singlet oxygen as a type II photosensitizer. Inspired by work from the Glazer group[93, 94, 95], McFarland and co-workers have also made multifunctional ruthenium (II) polypyridyl compounds (Figure 1.3G) capable of both photo induced DNA covalent binding and singlet oxygen generation by introducing steric bulk.[96, 97]

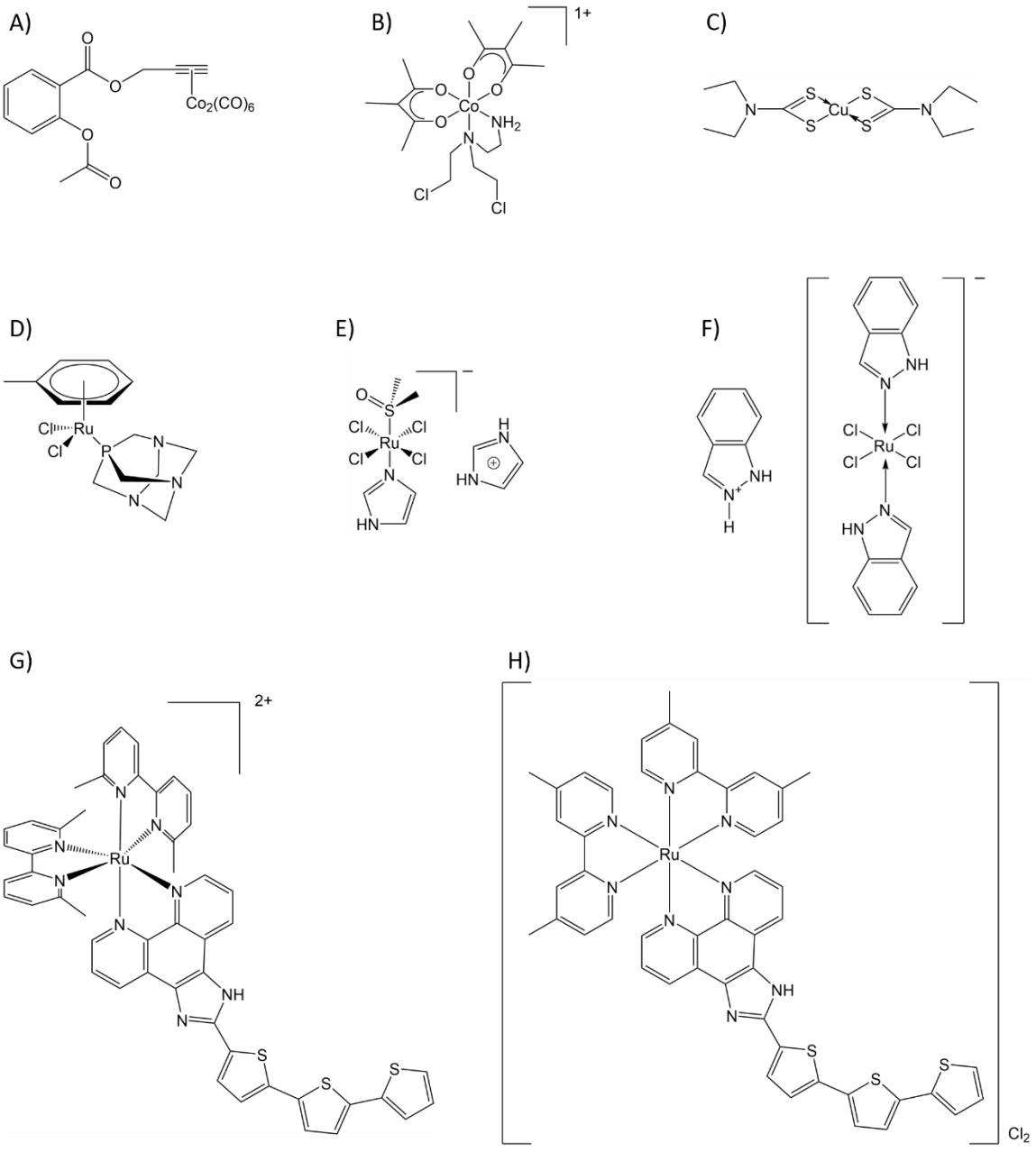

Figure 1.3 Representative metal compounds currently in researches as potential anti-cancer agents.

1.5 Current drug discovery and mechanistic studies.

With the advancement of techniques in synthetic chemistry and analytical chemistry, the numbers of new molecules have been hugely increased, which calls for the development of biochemical approaches for mechanistic studies with increased efficiency and comprehensive understanding. Of all the chemotherapy related research areas, mechanism elucidation remains one of the most challenging ones, as it requires complex approaches including analytical chemistry, biochemistry, and molecular and cell biology to study an enormous number of biomolecules in

complex cell environments.[98, 99] As a fully understanding of mechanism of action is not required by FDA, there are a considerable number of medications that have been approved and prescribed without much knowledge of their mechanism, and this could be a major concern for clinical prescriptions since understanding mechanism helps to better determine the appropriate dosing and predict potential side effects.[100] Knowledge of the mechanism is a vital component in drug discovery as it offers insights on clinical application. Lack of this knowledge could ultimately lead to failure of clinical trials for novel drug candidates and undesired adverse effects for medications currently in use.[98, 100] Most commonly, mechanistic studies are achieved by direct biochemical methods including affinity based binding and activity studies; cell biology approaches to understand the cellular events in responses to treatments, and more comprehensive genomic and proteomic approaches to gain a system level understanding.[101] With all these methods, the efficiency in both time and cost remains a major challenge to overcome.

Another approach is high-content screening (HCS), employing automated imaging and data processing. This phenotypic analysis has aided drug discovery for separating agents with potential novel mechanism by classifying molecules with known mechanisms of action and identifying active molecules that fall into potential new catagories.[26, 102] First described by Giuliano *et al.* in 1997[103], the technique didn't gain significant application until the late 2000s when automated high resolution imaging techniques were more commonly applied. High-content screening utilizes multiple fluorescent reporters in living cells and automated microscopy to probe biological phenotypic changes such as cell viability, metabolism, and morphology.[104, 105] Compared with current approaches, HCS is superior in probing the effects of drugs in living whole cells, not evaluating interactions with an isolated single target, which offers the possibility to discover unexpected targets and mechanisms as well as confirming engagement of a drug candidate with desired biological entities.[106, 105] The technique is also favored over other cell-based assay because of the fact that it is highly multiplexed, allowing for combination of multiple fluorescent labels and image analysis systems. HCS is able to provide up to one hundred parameters from a single experimental set up, which radically expands the quantity of temporal and spatial data obtained compared with single pathway analysis.[107, 105, 108] The highly automated imaging and analysis system also enables the ability of HCS to reduce human bias,[109, 110] though the potential still persists depending on specifics of experimental design factors prior to imaging analysis.

High-content screening, however, does have certain limitations when it is applied in drug discovery and target validation. One major challenge of utilizing HCS is the huge amount of data generated, as the multi-channel fluorescence microscope typically takes thousands of images that are 512 x 512 to 2048 x 2048 pixels. As a result, these image sets can be over 50 TB in file size.[111,

[112] Proper storage and management of these data therefore requires continuous caution. Another factor that limits application is that the data formats obtained using instruments from different manufactures don't translate well, which adds to the difficulty of analyzing the large data sets.[113, 114] Many parameters in HCS are calculated using multiple quantifiable features directly extracted from the imaging including compartment/organelle morphologies (nucleus, mitochondria, golgi apparatus, endoplasmic reticulum), these morphological features are usually described by a set of properties produced by statistics and software algorithms and are sometimes subtle compared with classical cell morphological descriptors. Commonly used data analysis methods also include normalizing different fluorescent intensities to cell nuclei staining in cells while the cell itself is also defined by computational algorithms estimating the plasma membrane. These highly manipulated data therefore lead to false-positive and false-negative results, making it a challenge to interpret the data sets.[108, 112]

A related analytical approach is cytological profiling, a type of phenotypic analysis in bacterial cells, which has been used to evaluate mechanisms of action for antibiotics and discover novel anti-bacterial agents[115, 116]. It has been demonstrated that antibiotics with mechanisms of action involving different biological processes induce distinct phenotypic changes[117, 118]. Accordingly, antibiotics inhibiting replication, transcription, or translation can be distinguished by analysis of specific phenotypic features. Historically, the discovery of cisplatin by Rosenberg was first motivated by the observation of the antibacterial activity of cisplatin on *E. coli*. More studies have also confirmed the biological activities of natural product antitumor antibiotics in bacteria, especially in *E.* coli.[119, 120, 121] Notably, in the bacterial cytological profiling by Pogliano and coworkers, molecules were tested that are commonly used anti-cancer agents targeting DNA replication and transcription; however, although phenotypic changes consistent with molecules with a similar mechanism of action were observed in their studies, there was a failure to make the connection between the anti-cancer agents and their biological activities in bacteria.[116] These studies support the possibility to use bacteria as a cytological profiling system for mechanistic studies of anti-cancer agents targeting the biological processes common in both prokaryotic and eukaryotic cells. Given the genetic simplicity of the bacterial system, it can be quickly determined if an anti-cancer agent works through a target that has a prokaryotic analogue. Furthermore, it can be proposed that by classifying phenotypic feature changes induced by compounds with known biological effects, bacterial cytological profiling would be capable of distinguishing *anti-cancer agents* whose mechanisms involve conserved biological processes utilized by both eukaryotic and prokaryotic cell type. This would offer a rapid and convenient approach to predict mechanisms of action for newly synthesized or discovered molecules.

Both high-content screening and the cytological profiling are based on the phenotypic changes in responses to the drug/chemical treatments, which is recognized as reverse chemical biology, in contrast to the commonly applied target based approach in drug discovery (forward chemical biology).[122, 123, 124] While target-driven approaches have been considered as streamlined and efficient in drug discovery, Swinney and Anthony discovered in their investigation of therapeutic agents the FDA approved during 1999 to 2008 that the majority of new molecular entities (NMEs) were discovered through the phenotypic based approaches.[125, 122] In both HCS and cytological profiling, the observations are reflections of complex biological effects of treatments and the global responses from the whole cell/organism. It is important to realize the phenotypic changes are indications of possible targets and mechanisms, and conclusions may be drawn only from comparison to agents with known mechanisms of action, as the phenotype does not directly identify cellular targets and mechanisms.

In this report, mechanistic studies of light activated ruthenium compounds synthesized in the Glazer lab as potential anticancer agents will be discussed. Some of these ruthenium-based compounds can be selectively activated by light of certain wavelengths only in the desired treatment region, offering increased selectivity and decreased adverse effects, and may also provide potentially novel mechanisms of actions. Others behave as traditional cytotoxic agents that do not require light activation. Three types of ruthenium polypyridyl complexes, representing different classes of compounds with different scaffolds, charge states, and biological activities, were studied *in vitro* and *in vivo* (with cell assays) to elucidate their biological targets and mechanism of action. Eukaryotic cell studies and bacterial cytological profiling were carried out to understand the mechanism of action for different ruthenium polypyridyl complexes. Two classes of ruthenium compounds were found to act through mechanisms and biological targets that have been reported for metal based anticancer agents. In contrast, ruthenium complex with hydroxyquinoline ligands exhibited a novel translation inhibition related mechanism, as demonstrated through bacterial cytological profiling and confirmed in cancer cells.

Chapter 2. Mechanistic studies of Ru(II) polypyridyl compounds with disparate charge state and hydrophilicity

COPYRIGHT INFORMATION

RESEARCH CONTRIBUTIONS

The research presented in this chapter is completed with help and support of other scientists. Compounds synthesis, characterization, chemical and physical property studies were completed by Dr. Matthew Dickerson and Mr. Brock Howerton. DNA gel electrophoresis and microscopy studies were completed by Dr. Matthew Dickerson.

2.1 Introduction.

Metal complexes have been studied for decades as potential cytotoxic agents, because of the unprecedented and continued success of cisplatin as a chemotherapeutic.[126, 127] Investigations into Ru(II) polypyridyl complexes have been particularly extensive, because of their ease of synthesis, appealing chemical, physical, and photophysical characteristics, and their high affinities for nucleic acids. Most early studies focused on characterizing the *in vitro* interactions of these complexes with DNA,[128, 129, 130, 131] and quantifying the potencies of the compounds both as traditional cytotoxic agents and as light-activated agents for photodynamic therapy (PDT) or phototherapy. In recent years, attention has shifted to understanding the cellular localization[132, 133, 134, 135] properties of Ru(II) complexes, along with their mechanisms of cellular uptake[135, 136] and cytotoxicity, providing a deeper understanding of how these compounds elicit their biological activities.

An attractive feature of Ru(II) polypyridyl complexes that makes them particularly useful for applications as biological probes and effectors is the diversity of the chemical structures that are readily available through modifications of the coordinated ligands.[137] However, most biological studies have focused on complexes that carry an overall charge of +2 or greater. This significantly limits the chemical structures and physical properties of the molecules under investigation. A question that occurred to us was this: To what degree could the biological properties of a chemically inert Ru(II) complex be tuned by chemical modification of the ligands surrounding the metal center?

To address this question, we have investigated the biological activities, cellular uptake, localization, and mechanism of cell killing of two simple Ru(II) complexes that are commonly used dyes for solar cell research or biological staining, but have not been previously explored as PDT agents. Ru(bathophenanthroline)$_3$ (**1**; Figure 2.1) is a hydrophobic molecule with a high DNA binding affinity,[138, 139] while Ru(bathophenanthroline disulfonate)$_3$ (**2**; Figure 2.1) is hydrophilic and possesses a high affinity for proteins.[140, 141, 142] Both complexes are efficient singlet oxygen ($^1O_2$) generators with the same quantum yields for $^1O_2$ production (Φ_Δ) and similar molar extinction coefficients (ε).[143] Both are luminescent, allowing for analysis by fluorescence microscopy. However, although the photophysical properties of the compounds are almost identical, the physical properties of the two Ru(II) compounds are quite dissimilar (see Table 2. 1). Compound **1** carries an overall charge of +2, while **2** has an overall charge of −4. They also have very different hydrophilicities, as indicated by their partition coefficient or log *P* values. Given the radically different physical properties of the complexes, we anticipated differences in their biological effects that could provide information for future rational design of lightactivated cytotoxic agents.

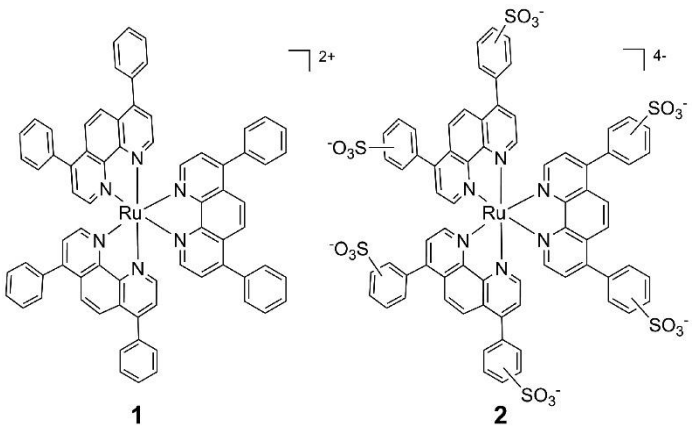

Figure 2.1 Structures of Ru(II) compound **1** Ru(bathophenanthroline)$_3$ and compound **2** Ru(bathophenanthroline disulfonate)$_3$

Considering the established dogma of the field, it would be expected that the negatively charged compound **2** would not enter cells[144] and would suffer low efficacy, while the positively charged, DNA-binding compound **1** would prove the more effective PDT agent. Instead, our findings run counter to this prediction. Here, we show large differences in potency, cellular uptake, localization, and mechanism of cytotoxicity of these agents, illustrating that radical modulation of biological properties is possible with ligand modifications of simple homoleptic Ru(II) polypyridyl complexes that are substitutionally inert. Most importantly, our results also prove that a significantly greater range of charge states and physical properties of Ru(II) complexes are compatible with potential application as PDT agents.

Table 2.1 Physical and photophysical properties of **1** and **2**

Property	Compound **1**	Compound **2**
Charge	+2	-4
Log *P*	1.8 ± 0.02	-2.2 ± 0.12
λ_{max} (nm)	460[a]	462[a]
ε ($M^{-1}cm^{-1}$)	29,500[a]	29,300[a]
λ_{em} (nm)	632[a]	632[a]
Φ_{PL}	0.101[b]	0.176[c]
Φ_{Δ}	0.42[a,d]	0.43[a,d]

[a]From ref. [145]; [b]From ref. [146]; [c]From ref. [147]; [d]Determined in D_2O.

2.2 Investigation of DNA damage and cytotoxicity induced by both Ru(II) compounds.

As both **1** and **2** are efficient catalysts for the light-activated generation of $^1O_2$ (Φ_{Δ} = 0.42, 0.43),[145] it was expected that the two compounds would act as sensitizers for PDT. Accordingly, their DNA damaging properties were assessed with pUC19 plasmid DNA and analyzed by gel

electrophoresis (Figure 2.2). Each compound was incubated with plasmid and irradiated with 40 J/cm^2 of visible light (>400 nm) or kept in the dark. Compound **1** is known to bind strongly with DNA, and precipitation of DNA with the complex was observed at concentrations above 31.3 μM both in the light and in the dark (Figure 2.2A). In contrast, **2** is a much more hydrophilic molecule, and the negatively charged sulfonate functional groups were anticipated to cause electrostatic repulsions between the complex and the negatively charged backbone of the DNA. Consistent with low DNA affinity,[148] no DNA precipitation or smearing was observed with up to 500 μM of **2** (Figure 2.2B). When exposed to light, both **1** and **2** induced single strand DNA breaks, creating relaxed circular plasmid. This is likely due to the photogeneration of $^1O_2$ that mediates the DNA damage. However, for **2**, the amount of relaxed circle plasmid did not exhibit any concentration dependence above 125 μM, suggesting either a reduction in Φ_Δ as the concentration of the complex is increased, or alternative quenching mechanisms that impede DNA damage.

As both compounds are capable of light-induced DNA damage, the cytotoxicity of **1** and **2** were evaluated in the A549 human non-small cell lung cancer, the HL60 human promyelocytic leukemia, and the Jurkat human T lymphoblastoid cell lines in the presence and absence of 7 J/cm^2 of >400 nm light. The IC_{50} values across the cell lines for **1** ranged from 0.62 to 3.75 μM in the dark. Upon irradiation, potency was increased to a range of 0.075 to 0.35 μM, resulting in an average phototoxicity index (PI = IC_{50} (dark)/IC_{50} (light)) of 10- to 20-fold (Figure 2.2, Table 2.2).

In marked contrast to the high toxicity of **1** in the absence of light, no toxicity was observed in the dark with **2** across all cell lines at concentrations up to 300 μM. However, compound **2** was effective in killing cells when irradiated, with IC50 values ranging from 3.3 μM to 17.3 μM, consistent with the concentrations required for *in vitro* DNA damage. This provides for a large therapeutic window, as no cell death is observed for samples in the absence of irradiation.

Surprisingly, not only was compound **1** toxic to cells upon irradiation, it also induced cell death far more rapidly in HL60 cells than traditional DNA damaging agents such as cisplatin. Complete cell death was observed within 2 h of irradiation with **1** (see Figure S1.1 in Appendix). The compound also induced cell death in the dark, but more slowly, with ~30% viable cells remaining at 24 h. In marked contrast to **1**, compound **2** induced cell death after irradiation only after a long delay, with 70% viable cells remaining at 24 h and 55% remaining at 48 h.

The significant disparity in the potency, phototoxicity index (PI), and rates of cell killing for the two compounds despite their equivalent abilities to sensitize $^1O_2$ strongly suggested that they were acting through different cellular mechanisms, possibly by interacting with different biological targets. As the compounds are substitutionally inert, they are unlikely to covalently

modify biomolecules. This complicates target identification by isolation of protein or nucleic acid components of the cells, so the subcellular localization was investigated instead.

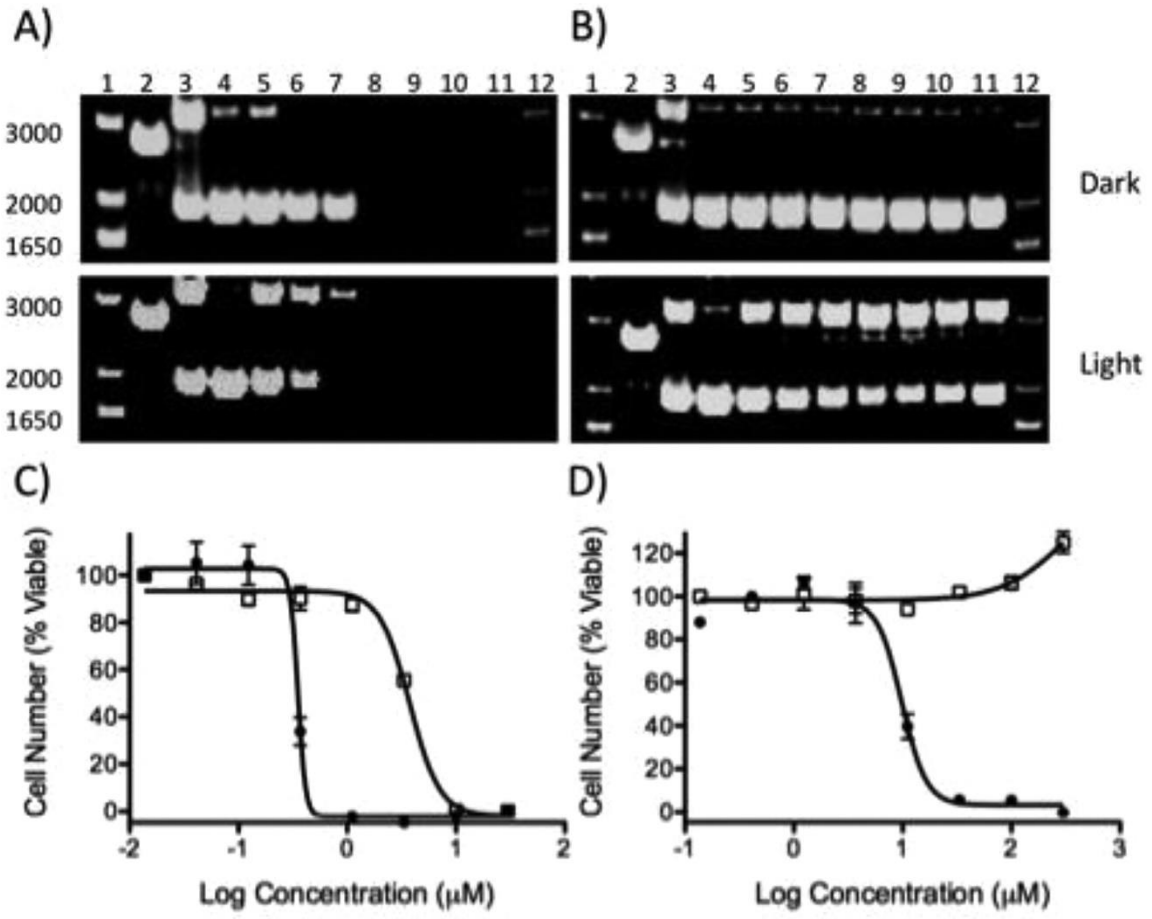

Figure 2.2 Agarose gel electrophoresis of pUC19 with increasing concentrations of (A) **1** and (B) **2** in the dark or irradiated (λ > 400 nm). Lanes 1 and 12: DNA molecular weight standard; lane 2: linear (reaction with EcoRI); lane 3: relaxed circle (reaction with Cu(phen)2); lanes 4−11: 0, 8.25, 16.5, 31.3, 62.5, 125, 250, and 500 μM compound. Cytotoxicity dose response of (C) **1** and (D) **2** in the dark (open squares) or irradiated (closed circles). HL60 cells were incubated for 72 h with compound prior to quantification of viability.

Table 2.2 Cytotoxicity IC_{50} values (μM) in various cell lines[a]

Compound	HL60 Light	HL60 Dark	A549 Light	A549 Dark
1	0.35 ± 0.18	3.75 ± 0.18	0.11 ± 0.02	0.62 ± 0.08
2	9.81 ± 1.09	>300	17.25 ± 9.82	>300
Cisplatin	3.1 ± 0.2	3.1 ± 0.2	3.4 ± 0.6	3.5 ± 0.2

[a]IC_{50} values are averages from three measurements.

Table 2.2 Cytotoxicity IC_{50} values (μM) in various cell lines[a] (*continued*)

Compound	Jurkat Light	Jurkat Dark	PI[b] Jurkat
1	0.075 ± 0.004	1.63 ± 0.11	21.7
2	3.31 ± 0.36	>300	>90
Cisplatin	0.5 ± 0.07	0.5 ± 0.07	1

[a]IC_{50} values are averages from three measurements. [b]The phototoxicity index (PI) is the ratio of the dark and light IC_{50} values.

2.3 Altered cellular uptake and subcellular localization of Ru(II) compounds.

Both **1** and **2** are emissive, allowing for direct visualization in cells. Flow cytometry and fluorescence microscopy were used to provide relative uptake values, the time dependence of compound uptake, and information on the subcellular localization of the compounds. To optimize signal intensity, **1** was assayed at 5 μM while 20 μM was required for **2**. Flow cytometry with A549 cells revealed greater uptake of **1** compared with **2** at time points of 2 and 24 h, with an 11.6-fold and 8.2-fold difference in signal, respectively (see Figure S1.2 in Appendix). Between the time points of 2 and 24 h, the average emission of cells incubated with **1** increased by 2.8-fold while the amount of **2** increased by 4-fold. This data was supported by direct quantification of the number of ruthenium atoms per cell using inductively coupled plasma−optical emission spectroscopy (ICP-OES; see Tables S1.1 and S1.2 in Appendix). The relative amount of compound **1** in cells versus the cell media increased ∼4-fold from 2 h to 24 h, from 5.4% to 22%.[149] Much less of compound **2** entered the cells, with a maximal uptake of 0.7% at 24 h. While low, this degree of uptake of the −4-charged **2** is comparable to cisplatin, a neutral compound, dosed at the same concentration (20 μM, 0.8% at 24 h).

The emission of **1** and **2** was also measured in A549 cells using an ApoTome microscope (the adherent cell line was chosen to facilitate the required wash steps to allow for the use of fluorescent reporters). The relative rates of uptake of each of the complexes were analyzed as a function of time, and both **1** and **2** were visible inside cells as early as 2 h after compound addition (see Figure S1.3 in Appendix), consistent with the flow cytometry and ICP-OES results. Images were taken at 2, 8, 18, and 24 h, and intracellular levels of both complexes appeared to plateau at 8 h. The uptake data showed good agreement between the three techniques and two cell lines, suggesting similar behavior in adherent and suspension cell lines.

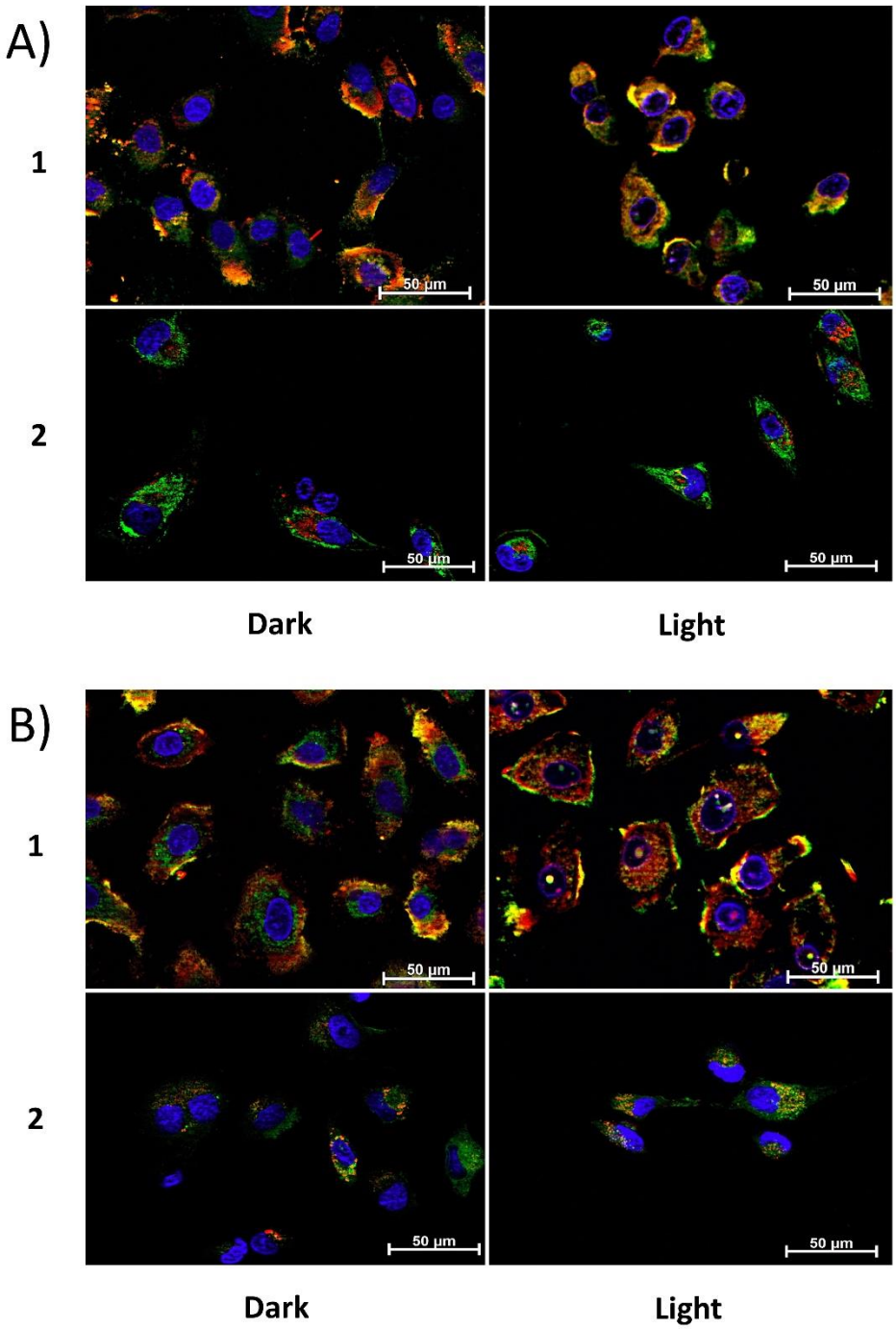

Figure 2.3 ApoTome microscopy showing subcellular localization of **1** and **2** at 8 h. Co-localization of **1** and **2** in mitochondria or lysosomes is indicated by the apparent yellow emission. (A) Mitotracker Green FM was used to image mitochondria. (B) Lysotracker Green DND-26 was used to image lysosomes. Red color denotes intrinsic emission of **1** and **2**, whereas blue color denotes Hoechst staining of the nucleus. The yellow color occurs due to overlap of the red emission from the ruthenium complexes and green emission of the organelle-specific dyes, indicating colocalization. Compound **1** localizes in both the mitochondria and the lysosomes while **2** was not predominantly found in either organelle.

Differences in the intracellular localization of **1** and **2** were evaluated by determining colocalization of luminescence of the compounds and fluorescent markers of organelles in A549 cells. Overlap in signals between the compounds, nucleus, mitochondria, and lysosome was measured over a 24 h period. Compounds **1** and **2** have very different localization profiles, as exemplified by the imaging 8 h after dosing (see Figure 2.3). Compound **1** substantially localized to lysosomes and the mitochondria in the absence of light, while **2** remained primarily in the cytosol. Exposure to light did have an impact on compound localization, where **1** induced nuclear localization of both the mitochondrial and lysosome markers (see Figures 2.3A and 2.3B, top), indicating that photoinduced damage mediated by **1** reduced the integrity of the nuclear membrane. In contrast, **2** was primarily observed in lysosomes after irradiation, and did not co-localize with mitochondria (Figures 2.3A and 2.3B, bottom). In addition, irradiation in the presence of **2** did not result in the appearance of organelle markers in the nucleus, suggesting the nuclear membrane remained intact. Neither **1** nor **2** was found to associate with the plasma or nuclear membranes.

2.4 Mitochondrial function and time dependence for cell death.

As compound **1** appeared to localize within mitochondria, it was hypothesized that this may account for its high toxicity in the absence of irradiation. To determine if either **1** or **2** caused a reduction in mitochondrial function, mitochondrial membrane potential was measured using tetramethylrhodamine ethyl ester (TMRE) (see Figure 2.4). TMRE is a cationic dye that accumulates in active mitochondria as a result of the negative membrane potential ($\Delta_{\psi m}$). Inactive or depolarized mitochondria exhibit a decreased membrane potential, and TMRE does not localize in these organelles. Compound **1** induced rapid and complete depolarization of mitochondria both in the dark and upon irradiation (Figure 2.4B, C). However, surprisingly, cell viability did not parallel mitochondrial potential. While mitochondrial function was completely impaired at 2 h post treatment with **1** in the dark, viability decreased slowly, with 44% ± 6% viable cells remaining after 24 h. In contrast, both mitochondrial function and cell viability fell to 0% within 2 h of irradiation. Thus, while **1** completely impedes mitochondrial function within 2 h even in the absence of light, irradiation induced additional damage that results in rapid cell death, along with the loss of mitochondrial function.

In contrast to compound **1**, **2** did not significantly reduce the mitochondrial potential over a 24 h period either when irradiated or kept in the dark. Irradiation did reduce cell viability to 70% ± 12% at 2 h and 59% ± 4% after 24 h, but this occurred without a significant decrease in the relative mitochondrial potential (Figure 2.4E), indicating that **2** does not act through inhibition of mitochondrial function. These results strongly suggest that mitochondrial failure plays a role in the

dark toxicity of **1**, and the lack of mitochondrial localization and inhibition may explain the comparatively low dark toxicity of **2**.

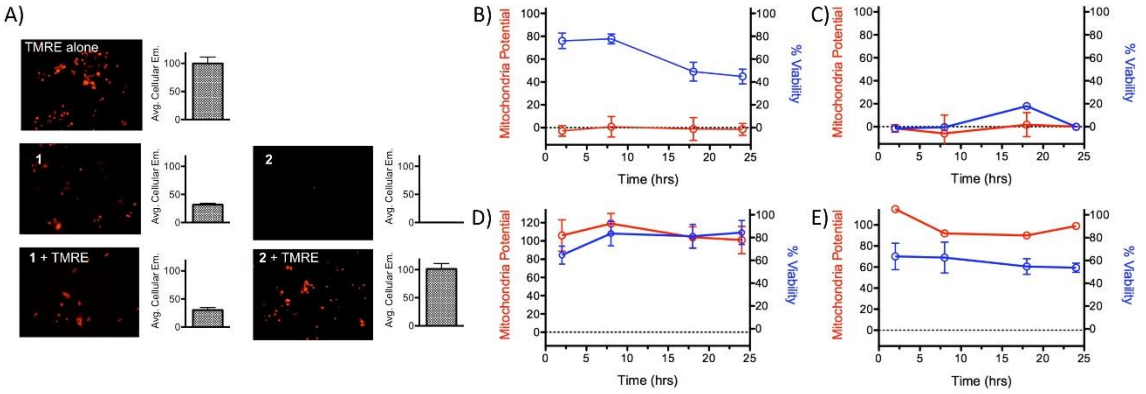

Figure 2.4 (A) Example images and quantification of the emission of tetramethylrhodamine ethyl ester (TMRE) in the presence and absence of **1** and **2**. Compound **1** does not show increased TMRE emission over background emission of **1**, while compound **2** does not add to the TMRE emission. Mitochondrial potential and cell viability of A549 cells as a function of time for (B) **1**, in the dark; (C) **1**, irradiated; (D) **2**, in the dark; and (E) **2**, irradiated. TMRE was used to quantify membrane potential; values are relative to a no-compound control value of 100.

2.5 Ru(II) compounds induce cell death through disparate mechanisms.

Most compounds used for PDT that generate singlet oxygen induce apoptosis. Given the different cellular localization properties and time profiles for cell death induced by **1** and **2**, the mechanism of cell death was investigated. Indicators of apoptotic cell death (activation of PARP and caspase 3 through proteolysis) were determined in HL60 cells treated with either **1** or **2** (Figure 2.5A). The known apoptotic-inducing compounds, cisplatin and doxorubicin, were run in parallel. Compound **1** induced the proteolytic activation of both PARP and caspase 3 within 2 h of irradiation (Figure 2.5A). In the absence of light, cleaved PARP and caspase 3 were observed with **1**, but only after 18 and 24 h, and to a lesser degree. In the absence of irradiation, the amount of inactive procaspase 3 did not change.

Exposure of **2** to light also induced PARP cleavage as early as 2 h, but unlike **1**, increasing amounts of cleaved PARP were observed over the course of 24 h (Figure 2.5A). The increase in the level of activated caspase 3 also occurred on a slower time scale than PARP cleavage, with the protein initially observed at 18 and 24 h. This suggests that the irradiated samples undergo apoptosis that is not primarily signaled through caspase 3. Conversely, cells treated with **2** and protected from light did not display PARP or caspase 3 cleavage, which is consistent with viability measurements indicating no cytotoxicity in the absence of light. The level of procaspase 3 also did not change over 24 h, further confirming a lack of cytotoxicity under these conditions.

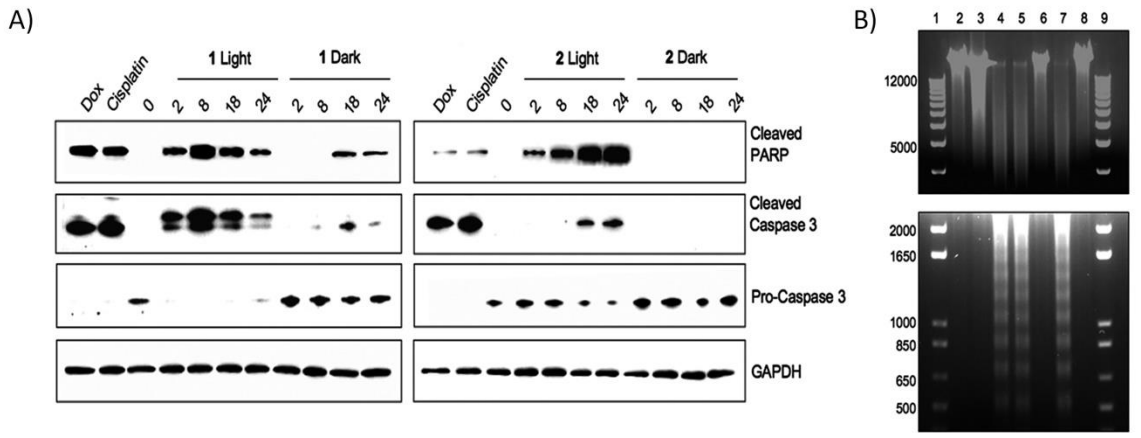

Figure 2.5 (A) Western blot of cleaved PARP, caspase 3, and pro-caspase 3. GAPDH is used as a loading control. (B) Agarose gel electrophoresis of genomic DNA harvested from HL60 cells after treatment with various agents. Lanes 1 and 9: ladder; lane 2: no compound control; lane 3: 10% EtOH, 24 h (necrosis control); lane 4: cisplatin, 24 h (apoptosis control); lane 5: **1**, irradiated, 8 h; lane 6: **1**, in the dark, 8 h; lane 7: **2**, irradiated, 24 h; and lane 8: **2**, in the dark, 24 h.

Since **2** showed strong PARP induction without significant caspase 3 activation, as compared to **1** and cisplatin or doxorubicin, a mechanism of cell death through necrosis was explored. The level of an alternate 55 kDa PARP fragment was determined by immunoblot as a marker for necrosis (see Figure S1.6 in Appendix), with 10% (v/v) ethanol used as a positive control.[150] Exposure of HL60 cells to **1** produced this fragment at significant levels both when protected from light and when irradiated, which is consistent with necrosis. Cisplatin and doxorubicin also produced this cleavage product, indicating that some cells had progressed into necrosis (Figure S1.6 in Appendix). In contrast, cells exposed to **2**, both in the presence and absence of irradiation, produced a lower level of the 55 kDa PARP fragment, similar to the untreated cells, suggesting necrosis is not a significant cell death pathway for this compound.

To support the assessment of the disparate mechanisms of cell death induced by **1** and **2**, the degradation pattern of genomic DNA was investigated. DNA laddering is observed as a result of DNA fragmentation stemming from the executionary phase of apoptosis. In contrast, necrotic cell death lacks this characteristic laddering effect, allowing differentiation between these two mechanisms. HL60 cells were exposed to both Ru(II) complexes, cisplatin, and 10% ethanol, followed by genomic DNA isolation and resolution by gel electrophoresis. As expected, the apoptosis inducer, cisplatin, initiated DNA fragmentation, resulting in a laddering pattern on the gel (Figure 2.5B). This laddering was absent in the cells treated with ethanol and compounds **1** and **2** in the dark. However, both compounds **1** and **2** displayed similar laddering patterns as cisplatin when irradiated, suggesting apoptosis is a contributing cell death pathway for both compounds

when irradiated. In contrast, given the cytotoxicity of **1** in the dark and the presence of the 55 kDa PARP fragment, it appears that necrotic cell death is a significant pathway for **1**. For compound **2**, the absence of DNA laddering is a result of the lack of cytotoxicity of the negatively charged compound.

Flow cytometry was also employed to further corroborate the assessment of the mechanism of cell death using Annexin V/propidium iodide (PI) or Annexin V/Hoechst staining to differentiate apoptotic versus necrotic cell death. Fluorescent Annexin V conjugates recognize the translocation of phosphatidylserine to the outer leaflet of the cell membrane during apoptosis. PI and Hoechst were used as nuclear stains to distinguish between live and dead cells; while PI is most commonly used, Hoechst was also applied, because of spectral interference of **1** and **2** with PI. The presence of significant populations of PI positive cells in the absence of Annexin V staining for **1** both in light and in the dark demonstrate that necrosis is a significant cell death pathway for this compound (see Figures S1.7 and S1.8 in Appendix; 5% and 14%, respectively, at 2 h). In contrast, compound **2** produced large populations of Annexin V positive cells (55% at 24 h), showing an apoptotic pathway (see Figures S1.9 and S1.10 in Appendix). Similarly, Hoechst staining was consistent with necrosis as a contributing pathway for **1** in the dark and in light, while **2** induced apoptosis.

2.6 Conclusion.

The goal of phototherapy is to achieve cell death in cancerous or abnormal tissues that are irradiated, while protecting healthy tissues that are not exposed to light. As a result, the compounds developed for this application should possess large "therapeutic windows" where the toxicity in the dark is minimized. This has proven to be challenging for many inorganic agents developed for PDT applications. The rational design of new and more efficacious compounds would be facilitated by (1) a better understanding of the mechanisms of action that induce dark
toxicity for promising PDT agents, and (2) the identification of chemical features that eliminate dark toxicity. The investigations of the biological activities of these two simple Ru(II) complexes provide guidance for both approaches toward improved PDT agents.

While compound **1** demonstrated notable potency when irradiated (0.075−0.35 μM, depending on cell line), the toxicity of the compound in the dark (0.62 to 3.75 μM) reduces its potential as a PDT agent. Imaging studies showed both mitochondrial and lysosomal localization, and assessment of mitochondrial potential indicated that **1** immediately inhibits mitochondrial function. However, the disconnect between the time dependence of the inhibition of mitochondrial function and the reduction in cell viability in the dark shows that disruption of mitochondrial membrane potential does not lead to rapid cell death. It is possible that the cells treated with **1** and kept in the dark survive for several hours, despite the complete abrogation of

mitochondrial function, due to the Warburg effect, where cancer cells exhibit a reduced reliance on oxidative phosphorylation and increased dependence on glycolysis for energy production.

After 72 h, cell death is complete for **1** in the dark. The obliteration of mitochondrial function would explain the observation of necrotic cell death in this case.[151] In contrast, when **1** is irradiated, it appears that a combination of necrotic and apoptotic pathways are activated. Cell death is so rapid (with most cells undergoing death at 2 h, as indicated by Trypan Blue staining) that necrosis is likely to be a primary pathway for a majority of cells. The breakdown of membrane integrity is apparent not only for the plasma membrane, but also for the membranes of organelles, as cells treated with **1** and irradiated showed nonspecific nuclear localization of both Mitotracker and Lysotracker. The high dark toxicity, mitochondrial localization, and induction of necrotic death pathways may reduce the potential of compounds structurally similar to **1** for PDT.

In marked contrast, compound **2** was found to possess several features that encourage further exploration of derivatives or similar compounds. While uptake was low, it was comparable to that of cisplatin, despite the overall charge of −4. Most importantly, **2** exhibited IC_{50} values on the order of 3.3−17.3 μM when exposed to light, with no observed toxicity in the dark. A slight increase in intracellular accumulation was observed upon irradiation, possibly due to induction of plasma membrane damage that facilitated compound uptake. Once inside the cell, the compound remained in the cytosol, with no observable localization to the mitochondria or inhibition of mitochondrial function. Furthermore, the light-induced cell death mediated by **2** occurred by apoptosis, in contrast to the mitochondrial targeting of **1**, which resulted in necrosis. One possibility to explore is that PDT compounds that avoid mitochondrial localization will exhibit lower toxicity in the absence of light than those that associate with the mitochondria. It is anticipated that structural modifications that result in a modest increase in cellular uptake could sufficiently drive down potency to make improved derivatives of **2** that maintain large therapeutic windows.

Given the high binding affinities of most Ru(II) complexes for DNA (Kb > 106), it was previously believed that the compounds would preferentially localize in the nucleus, and indeed several do.[132, 133, 152, 153, 154] However, recent fluorescence and electron microscopy studies have shown localization of several Ru(II) compounds in the mitochondria, suggesting it is a common target.[155, 156] Other reports indicate membrane accumulation and disruption,[135, 157] along with apoptosis pathways that are mediated by the mitochondria.[158, 159] Gasser and co-workers have shown in a recent report that this mitochondrial localization was, in fact, required for cytotoxicity for a lead compound in a structure− activity relationship study of a family of Ru(II) polypyridyl complexes.[160]

While mitochondrial accumulation results in cytotoxicity, this mechanism is not likely to be compatible with a PDT-type approach where such redox-active compounds are required to be essentially nontoxic in the absence of photons. Alternatively, targeting moieties such as nuclear localization signals can be conjugated to the coordinated ligands to affect the affinity of the complex for biological molecules and regulate cellular uptake and subcellulation localization.[136d, 160, 161] This approach requires significant chemical modifications, and the targeting often fails to increase cytotoxicity.

While microscopy is a powerful tool to assess compound localization, imaging experiments can cause relocalization of compounds that induce production of $^1O_2$ or perform other photochemical reactions when exposed to light.[162] Previous studies on porphyrins used for PDT applications also have demonstrated this phenomenon,[163] including uptake and relocalization of an anionic tetrasulfonated porphyrin.[164] For this reason, it is important to perform imaging using a minimum of light exposure, and to probe for compound relocalization by comparing to conditions where the treated cells have been exposed to significant light doses.

This current study shows that simple ligand modifications produce complexes with divergent physical properties and, correspondingly, different biological activities. Compound **1**, despite its high DNA affinity, localizes to the mitochondria and induces rapid membrane depolarization and necrotic cell death. It is possible that this will be a common problem for compounds containing the bathophenanthroline ligand. Compound **2**, despite its overall charge of −4, is taken up into cancer cells to a sufficient degree to mediate light-induced cell death through an apoptotic pathway. The absence of mitochondrial localization may be the factor that eliminates the dark toxicity of this Ru(II) complex. The incorporation of the sulfonic acids into the ligands is likely responsible for the alteration in subcellular localization, suggesting a possible general approach to reducing dark toxicity for other Ru(II) complexes developed for applications in phototherapy.

2.7 Materials and methods.

Materials. Ru(bathophenanthroline)$_3$ (**1**) and Ru-(bathophenanthroline disulfonate)$_3$ (**2**) were synthesized using previously established procedures.[141, 145] All cell lines were purchased from ATCC. Cell culture media, heat-inactivated fetal bovine serum (FBS), 4−20% tris-glycine precast gels, Dulbecco's phosphate buffered saline (DPBS), penicillinstreptomycin solution (pen-strep), and 0.4% Trypan Blue solution were from Invitrogen. 35 mm wide, 4-compartment CELLview cell culture dishes were obtained from USA Scientific. Serum supreme was from Lonza. Hoechst 33342, Lysotracker Green DND-26 and Mitotracker Green FM were purchased from Invitrogen. Propidium iodide (PI) and FITC-Annexin V were obtained from BD Science. Trimethylrhodamine

ethyl ester (TMRE) was purchased from Sigma−Aldrich. Antibodies for PARP-1, procaspase 3, and GAPDH were from Santa Cruz Biotechnology, Inc., while cleaved PARP and cleaved caspase 3 was from Cell Signaling Technology. RIPA buffer was purchased from Santa Cruz Biotechnology, Inc. Clarity Western ECL Substrate was from Bio-Rad. An apoptotic DNA-ladder kit was purchased from Roche Applied Science.

DNA gel electrophoresis. Compounds were mixed with 40 μg/mL pUC19 plasmid DNA in 10 mM potassium phosphate buffer, pH 7.4. To determine the effect of light, samples were irradiated with light (>400 nm) from a 200 W light source for total light doses of 40 J/cm^2. Samples were then incubated for 12 h at room temperature in the dark. Single- and double-strand DNA break controls were prepared, and the DNA samples were resolved on agarose gels, as described previously.[165] In brief, samples were resolved on a 1% agarose gels prepared in tris-acetate buffer with 0.3 μg of plasmid/lane. The gels were stained with 0.5 μg/mL ethidium bromide in tris-acetate buffer at room temperature for 40 min, destained with tris-acetate buffer, and imaged on a ChemiDoc MP System (Bio-Rad).

Cell cytotoxicity determination. Human alveolar adenocarcinoma cell line A549, Human promyelocytic leukemia cell line HL60, and Human T lymphocyte cell line Jurkat cells were maintained in media supplemented with 10% FBS and 50 U/mL pen-strep at 37 °C with 5% CO_2, with DMEM used for A549 cells, and IMDM and RPMI 1640 used for HL60 and Jurkat cells respectively. Cells were assayed in Opti-MEM supplemented with 1% serum supreme and 50 U/mL pen-strep and seeded into 96 well plates at a density of 1.5×10^3 cells/well for A549 cells, 2×10^4 cells/well for HL60 cells, and 1×10^4 cells/well for Jurkat cells followed by a 6 h incubation at 37 °C, 5% CO_2. Cells were dosed with serial dilutions of compound and incubated for 18 h. They were then irradiated with 7 J/cm^2 light (>400 nm) in 30 sed pulses or kept in the dark. Cell viability was determined 72 h later by measuring the conversion of resazurin to resorufin,[165] using a SpectraFluor Plus Plate Reader (Tecan).

Intracellular measurement of Ru complexes by flow cytometry. A549 cells were seeded in Opti-MEM with 1% serum supreme at a density of 2×10^5 cells/ml in 25 cm^2 cell culture flasks and incubated overnight. A concentration of 5 μM of **1** and 20 μM of **2** were added to the cells and incubated for 2 or 24 h protected from light; the concentration of 20 μM was selected for **2** to correspond with the IC_{50} of the complex when irradiated with light. A concentration of 5 μM was used for **1** for compatibility with fluorescent imaging. After 2 and 24 h the media was removed, cells were washed twice with DPBS, trypsinized, and collected by centrifugation at 125 × g for 4 min. The cells were resuspended in Opti-MEM, filtered through 40 μm cell strainers, and analyzed

on a FACSCalibur (Becton−Dickenson) with an excitation wavelength of 488 nm and emission measured at 650 nm. A minimum of 30,000 events were measured for each sample.

ApoTome structured illumination imaging of Ru complex uptake. The ApoTome microscope was used to resolve fine features of cellular structure. This instrument averages the fluorescence of three separate images to greatly reduce out-of-plane fluorescence. A549 cells were seeded in 35 mm, four-compartment CELLview culture dishes at a density of 5×10^4 cells per compartment in a 500 μL volume and incubated for 24 h in Opti-MEM containing 1% FBS, followed by the addition of 5 μM **1** or 20 μM **2** and time points measured at 2, 8, 18, or 24 h. Media was removed at each time point, cells rinsed with DPBS, and incubated in Opti-MEM with 16 μM Hoechst 33342 and 0.15 μM Lysotracker Green DND-26, or 16 μM Hoechst 33342 and 0.2 μM Mitotracker Green FM. Cells were incubated for 30 min, then washed three times with DPBS and imaged at 50× magnification using an ApoTome structured illumination fluorescent microscope (Carl Zeiss AG).

Mitochondrial membrane potential measurement. A549 cells were seeded at 2×10^4 cells/well in 24 well plates and incubated for 18 h, followed by the addition of 5 μM **1** or 20 μM **2**. They were incubated for an additional 8 h, and then irradiated with light as described for cell cytotoxicity measurements or kept in the dark. The cells were incubated for an additional 2, 8, 18, or 24 h, washed with DPBS, followed by the addition of 0.5 μM TMRE in Opti-MEM, and incubated for 30 min. The cells were then washed twice with DPBS and imaged. The change in TMRE signal was determined by the difference in fluorescence between compound treated cells in the presence and absence of TMRE. Fluorescence was measured at 10× magnification using an ApoTome microscope in normal fluorescence mode. Images were processed and the average cell fluorescence was calculated using ImageJ software. Samples dosed with **1** and **2** were compared to untreated A549 cells (n =3) to give the relative mitochondrial potential.

Cell viability as a function of time. HL60 cells were seeded in Opti-MEM at a density of 1×10^6 cells/mL and incubated for 2 h. The cells were then dosed with **1** or **2**, incubated for 8 h, irritated as above or protected from light, and incubated for 2, 8, 18, 24, or 48 h. As HL60 cells grow in suspension, Trypan Blue staining was employed in place of resazurin to simplify and accelerate cell viability analysis. At each time point, a 10 μL cell suspension was mixed with an equal amount of Trypan Blue solution and cell viability determined by manual counting with a hemocytometer.

Apoptosis marker immunoblotting. HL60 cells were cultured, dosed with **1** and **2**, then irradiated as above or protected from light. Cells were harvested 0, 2, 8, 18, or 24 h after treatment, pelleted by centrifugation at 124 × g for 5 min, washed twice with DPBS, and lysed in RIPA buffer

supplemented with 5 mM sodium pyrophosphate for 15 min on ice. The insoluble fraction was removed by centrifugation at 20,800 × g for 10 min at 4 °C. The supernatant was collected and the protein concentration determined by BCA assay. 10 μg of protein was loaded onto 4−20% tris-glycine gels, followed by transfer to nitrocellulose membranes. After blocking with 5% nonfat milk in DPBS with 0.1% Tween20 (PBST) for 1 h at room temperature, the membrane was immunoblotted with PARP-1 at a 1: 500 dilution, procaspase 3, cleaved caspase 3, and cleaved PARP at 1: 1,000 dilutions, or GAPDH at a 1: 2,000 dilution in 5% nonfat milk overnight at 4 °C. Immunoblots were washed with PBST for 10 min four times and incubated for 1 h with secondary antibodies at a 1: 10,000 dilution for GAPDH and at a 1: 5,000 dilution for all other antibodies. Detection was performed using Clarity Western ECL substrate and imaged with the ChemiDoc MP System.

DNA laddering gel electrophoresis. HL60 cells were cultured, dosed with **1** and **2**, then photoactivated or protected from light as detailed above. Cells were harvested 2 h after photoactivation for **1** or after 24 h for **2**, pelleted by centrifugation at 124 × g for 5 min, washed twice with DPBS, and prepared with an apoptotic DNA-ladder kit as per manufacturer instructions. Gel electrophoresis was carried out using a 1% agarose gel containing 0.5 μg/mL ethidium bromide with 1 μg DNA loaded per lane and run for 90 min at 75 V. Gel imaging was performed with the ChemiDoc MP System.

Quantification of metal complex uptake by ICP-OES. HL60 cells were seeded in Opti-MEM at a density of 1×10^6 cells/mL in 25 cm^2 cell culture flasks, cultured overnight, then dosed with 5 μM **1**, 20 μM **2**, or 20 μM cisplatin. Cells treated with Ru complexes were incubated for 8 h, protected from light before irradiating or kept in the dark. Cells were collected after 2 and 24 h by centrifugation at 124 × g for 5 min. The cell media was transferred to separate 15 mL centrifuge tubes, and cells were washed twice with DPBS. 2 mL of concentrated HNO_3 was added to media samples while cell pellets were resuspended in 5 mL of 20% (v/v) HNO_3. All samples were heated at 110 °C for 3 h. After digestion, the volume of all cell samples was adjusted to 5 mL and media samples were adjusted to 10 mL with deionized (DI) water. The metal content was analyzed using a VISTA-PRO CCD simultaneous inductively coupled plasma optical emission spectrometer (Varian, Inc.) with detection at 240.272, 245.657, and 267.876 nm for ruthenium and 214.424, 217.468, and 265.945 nm for platinum, with a replicate reading time of 60 sec. Yttrium (1 ppm) in 1% nitric acid was employed as an internal standard. The percentage intracellular metal ratio in 107 cells was calculated by normalizing the metal amount to 10^7 cells, and then divided by the total metal amount in both media and cells.

Cell death by flow cytometry. HL60 cells were cultured, dosed with **1** and **2**, then irradiated or protected from light. Cells were harvested 2 and 24 h after treatment, pelleted by centrifugation at 124 × g for 5 min, washed twice with DPBS, stained for 15 min with FITC-Annexin V and PI or FITCAnnexin V and Hoechst 33342, because of the interference between the emission of **1** and PI. Cells were analyzed with a FACSCalibur (Becton−Dickenson). A minimum of 20,000 events were measured for each sample.

Chapter 3. Mechanistic studies of Ru (II) polypyridyl compounds that form DNA adducts as potential photodynamic therapy agents

RESEARCH CONTRIBUTIONS

The research presented in this chapter is completed with help and support of many scientists. Compound studied in chapter 3 was synthesized and characterized by Mr. Brock Howerton and Dr. Erin Wachter.

3.1 Introduction.

The fortuitous observation of filamentous growth of *E. coli* by Barnett Rosenberg led to the discovery of cisplatin, one of the most important and widely used chemotherapeutic agents.[16-18] Cisplatin, and its later generation analogues, are essential components in the clinical treatment of ovarian, testicular, small cell lung, and head and neck cancers.[24, 25, 166] The administration of platinum drugs, however, is limited by adverse side-effects, including nephrotoxicity, neurotoxicity, ototoxicity and other complications.[39, 167] Drug resistance (either intrinsic or acquired) compromises the efficacy of platinum drugs as well.[36, 168, 27] These deficiencies have necessitated the development of new chemotherapeutic agents to overcome such obstacles.

A great deal of effort has been applied in the field of medicinal inorganic chemistry to identify cytotoxic agents that replicate the efficacy of cisplatin, with the hope of adding to our current arsenal of chemotherapeutic drugs.[169, 170, 41] While many of the new chemical entities show promise, the understanding of their biological activities is often incomplete. The very nature of inorganic agents (with variable charge states, geometries, and coordination numbers, all of which can be altered by speciation) adds to the challenge, and can result in polypharmacology.[170, 171] As a result, elucidation of the biological effects of potential medicinal inorganic agents has lagged far behind chemical innovation. Organic or inorganic agents developed through target-based drug discovery avoid some of these pitfalls, but undesired off-target effects are prevalent for these systems as well. Thus, mechanistic studies are necessary even for compounds designed to inhibit single, well-validated targets.[172, 122, 173]

Despite multiple technological advances, the identification of the mechanism of action for cytotoxic compounds remains a time consuming and challenging process. While simple *in vitro* systems can provide key insights, there are undeniable advantages to work in living cells. Bacteria are intrinsically simpler systems than eukaryotic cells, with *E. coli* containing only 4,288 genes,[174, 175] as opposed to the approximately 30,000 genes found in the human genome.[176, 177] Essential processes are homologues between bacteria and eukaryote, including DNA replication, transcription and translation. It is well known that many agents that are toxic to eukaryotic systems also have antibacterial activities, though many orthogonal variations do exist between the two.[178, 179]

Rosenberg's classical experiment illustrated that a simple prokaryotic system could be employed to discover anticancer agents. Recently, other groups, including those of Lippard and Brabec, have utilized *E. coli* phenotypic assays as a qualitative means to characterize potential anticancer agents, and as with cisplatin, showed a good correlation between activity in the prokaryotic system and cancer cells.[180, 181, 182] We also have an interest in simple biological systems,

to utilize them as a tool to investigate mechanistic details of anticancer agents. Our premise is that compounds which are found to be active in mammalian cells but not *E. coli* can be expected to affect processes or targets absent in the simpler biological system. Alternatively, *compounds* which show similar activities in the two cell types can be logically deduced to inhibit processes common to both. Thus, it should be possible to use *E. coli* as a first pass screen to radically reduce the number of likely biological entities or processes targeted by cytotoxic agents. Furthermore, *E. coli* is readily amenable to genetically encoded reporter systems, allowing for additional phenotypic analysis to be used to rapidly parse mechanistic features of active compounds.[122, 183] This approach could greatly expedite mechanism of action studies.

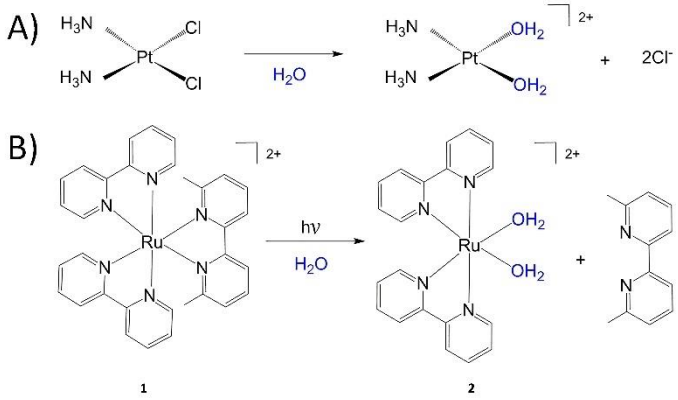

Figure 3.1 Thermal hydrolysis of A) cisplatin and B) the photochemical hydrolysis of compound **1**

Here we describe studies that demonstrate that *E. coli* is an excellent model for mammalian systems to investigating the effects of metal complex inhibition of cell growth, and phenotypic changes consistent with DNA damage. A promising light-activated Ru(II) complex developed in our laboratory[165] (Compound **1**, Figure 3.1) was compared to cisplatin, along with three organic antibiotics. Noteworthy differences were observed between the inorganic compounds and organic compounds in the bacterial system; these differences directly correlate with their different mechanisms of action. Moreover, differences between compound **1** and cisplatin in mammalian cells suggest more subtle disparities in their mechanistic features, which offers the possibility to maintain anticancer efficacy without experiencing the same resistance profile by altering the metal center from platinum to ruthenium.

3.2 Comparison of compound efficacies in *E. coli* and mammalian cancer cells.

The capacity of *E. coli* to serve as a model system for cancer cells was first evaluated by comparing the relative cytotoxicities of the metal complexes in the two cell types. The ruthenium complex prodrug (compound **1**), and cisplatin were tested in dose response, along with the

antibiotics rifampicin, tetracycline and nalidixic acid. Optical density was used to quantify the response in *E. coli*. The activity of **1** was evaluated both in the absence of light and after light activation (described as "dark" and "light"; irradiation results in the formation of compound **2**; Figure 3.1). The half maximal inhibitory concentration (IC_{50}) value was compared with the minimum inhibitory concentration (MIC),[184] an important clinical standard [parameter184, 185, 186, 187] that effectively defines the lowest concentration to achieve a complete inhibition effect. As shown in Table 3.1, IC_{50} values of 2.6 and 2.0 μM for light-activated **1** and cisplatin were obtained in *E. coli*, with MIC values that were 2 – 3-fold higher.

Table 3.1 Cytotoxicity values and inhibition of protein production in *E. coli* and HL60 cells.

	E. coli			**HL60**
	MIC (μM)	Growth Inhibition IC_{50} (μM)	Dendra2 Production Inhibition IC_{50} (μM)	Cytotoxicity IC_{50} (μM)
1 light	6.1 ± 0.8	2.6 ± 0.4	77 ± 3	3.4 ± 0.3
1 dark	> 300	> 300	> 300	> 300
Cisplatin	4.4 ± 0.5	2.0 ± 0.1	85 ± 11	2.6 ± 0.4
Rifampicin	0.6 ± 0.3	0.3 ± 0.1	2.8 ± 0.3	n.d.[a]
Tetracycline	10 ± 1.1	4.8 ± 0.7	1.3 ± 0.2	n.d.[a]
Nalidixic Acid	5.2 ± 2.0	2.6 ± 0.4	4.6 ± 0.1	n.d.[a]

[a]Cytotoxicity values of antibacterial antibiotics were not determined in mammalian cells.

The biological activity of cisplatin and compound **1** was also studied in human promyelocytic leukemia HL60 cells. Upon light irradiation, **1** exhibited an IC_{50} of 3.4 μM, similar to the IC_{50} of 2.6 μM for cisplatin. No cytotoxic effect was seen for compound **1** at 300 μM in the dark, resulting in a phototoxicity index (PI) of > 88. As expected, the cytotoxicity of cisplatin was not affected by treatment with light. These experiments demonstrated that light irradiated **1**, like cisplatin, is cytotoxic in both prokaryotic and eukaryotic cells, and with very similar potencies, suggesting the mechanism of action is through general cellular targets or biological processes present in both cell types.

3.3 Comparison of cellular uptake and nucleic acid metallation between compound I and cisplatin.

Cellular uptake of the metals in *E. coli* was measured by atomic absorption spectroscopy (AAS; see Table 3.2). Light irradiation of compound **1** resulted in a 5-fold increase in cellular uptake, with a total of 10% of the dosed compound localized in *E. coli* cells. Only 6% of the dosed cisplatin was found in the cells. Genomic DNA and total RNA isolation was performed after 24 h of treatment, followed by AAS analysis for ruthenium or platinum. While no ruthenium was found with either of the nucleic acids for compound **1** in the dark, 1.3% of the ruthenium was found with

the DNA when the compound had been exposed to light. This corresponds to a ratio of 2000 nucleotide bases per metal center (nt / mc). Only 0.5% of ruthenium was found with the RNA, providing a ratio of 3800 nt / mc. As a result, compound **1** appears to be slightly more reactive with DNA than RNA, with about a 1.5–2-fold difference between the metal levels in the two nucleic acids. A similar trend of increased reactivity with DNA over RNA was observed for cisplatin, with a ratio of 3000 nc / mc in DNA and 4700 nt / mc in RNA.

Table 3.2 Cellular metal uptake and metal content with different nucleic acids measured by AAS.

	E. coli			**HL60**		
	Cellular uptake[a]	DNA nt / mc [b]	RNA nt / mc[c]	Cellular uptake[a]	DNA nt / mc[b]	RNA nt / mc[c]
1 light	10%	2000 ± 200	3800 ± 600	0.6%	4800 ± 400	5000 ± 700
1 dark	2%	-[d]	-[d]	0.1%	-[d]	-[d]
Cisplatin	6%	3000 ± 200	4700 ± 900	0.7%	7000 ± 200	7800 ± 700

[a]Cellular uptake was calculated as metal content measured in cells divided by total metal content in both cell samples and cell culture media samples. Cellular uptake in *E. coli* cells were normalized to 10^9 cells and HL60 cellular uptake was normalized in 10^7 cells. [b]DNA nt /mc was calculated as DNA nucleotide bases (μmol) divided by metal content measured in DNA sample (μmol). [c]RNA nt /mc was calculated as RNA nucleotide bases (μmol) divided by metal content measured in DNA sample (μmol). [d]Ruthenium level in DNA and RNA samples were under detection limit (< 2 ppb).

Compound accumulation in mammalian cells was also assessed. After 24 h treatment with 20 μM compound **1**, 0.6% of dosed ruthenium was found in HL60 cells with light irradiation, in contrast to only 0.1% present when the cells were kept in the dark. These results indicate that the prodrug form is taken up much less effectively than the active species. The metal content of the active compound in cells is comparable to the 0.7% of cisplatin that accumulated under the same conditions. Isolation of DNA and RNA and metal content analysis revealed that no nucleic acid-bound ruthenium was observed for **1** in the dark, but treatment of **1** with light resulted in 4800 nt / mc in DNA, and 5000 nt / mc in RNA. This corresponds to 1.3% of the cellular ruthenium found with the DNA and 2% in the RNA. Quantification of the metal binding of cisplatin gave 7000 nt / mc in DNA and 7800 nt / mc in RNA (1.1% and 1.5%). The nucleotide base to metal center ratios were close, but consistently a slightly higher reactivity was observed with DNA for both irradiated compound **1** and cisplatin.

It has been reported by DeRose *et al*. that platinum accumulates more in the cellular RNA than DNA.[188] This is partly due to the higher abundance of RNA in the cell (10–50-fold). Despite this difference in abundance for the different nucleic acids, DeRose demonstrated that there is a 3.8-fold preference for cisplatin to react with DNA vs. RNA in *S. cerevisiea*, with 1661 nt / mc in DNA and 6369 nt /mc in RNA after 12 h of treatment at 100 μM.[188] While our study used 20 μM

of cisplatin treatment for 24 h with cells, we observed the same preferential metal binding with DNA over RNA in both *E. coli* and mammalian cancer cells, though we observed a closer nt / mc ratio between DNA and RNA. This similar binding trend across different cell types reveals once more that cisplatin exhibits a general DNA damaging ability in both eukaryotic and prokaryotic systems. The similar biological accumulation characteristics of compound **1** and cisplatin in bacterial, yeast, and mammalian cells suggest a mechanism of action through common biological targets or processes present in both prokaryotic and eukaryotic cell types, though multiple subsequent events may be involved that induce the cytotoxic effects.

3.4 Phenotypic analysis of *E. coli* distinguishes DNA damaging agents from transcription and translation inhibitors.

1) Filament Size. For imaging studies, the MIC was used in order to more closely mimic physiological conditions; data was also taken at 10x MIC. As anticipated, elongated *E. coli* cells were observed after treatment with cisplatin and compound **1** in the presence of light. Treatment with **1** in the absence of light didn't induce *E. coli* filamentous growth, and the cells were characterized by the same short rod shaped morphology as the untreated control.

To gain a more quantitative understanding of filament formation in populations, cells in multiple views (~200 per condition) were chosen for size analysis. Treatment with compound **1** at 10x MIC and light exposure caused a shift in population distribution, where 73% and 68% of cells were filamentous for **1** and cisplatin, respectively. At 100 μM compound **1**, cells over 40 μm in length were the major population group (29%), and only 5% of the cells were in the ≤5 μm size range. The same trend was seen after cisplatin treatment. In contrast, at the MIC, both the filament length and % filamentous population were lower, with 30% and 41% of cells forming filaments for cisplatin and **1** (Figure 3.3E and S2.4 in Appendix). As shown in the histograms in Figure 3.2E and H, both the no treatment control and dark control for compound **1** exhibited a dominant population (over 97%) of cells in the ≤5 μm size range, which represents the normal *E. coli* cell size.

It has been observed that many compounds induce filamentous growth of *E. coli*. In order to determine how this morphological feature corresponds to the compounds' mechanisms of action, we compared the metal-based compounds to two commonly used antibiotics that inhibit transcription or translation, and one gyrase inhibitor. Rifampicin prevents transcription by binding and inhibiting the bacterial DNA-dependent RNA polymerase (RNAP)[189, 190, 191] and tetracycline inhibits translation via binding to the 30S subunit of the ribosome, preventing entrance of aminoacyl-tRNAs to the A-site. These compounds were selected as agents that do not induce DNA damage.[192, 193, 194] Nalidixic acid, which inhibits gyrase and induces DNA double strand breaks, was also investigated as a DNA damaging agent control.[195]

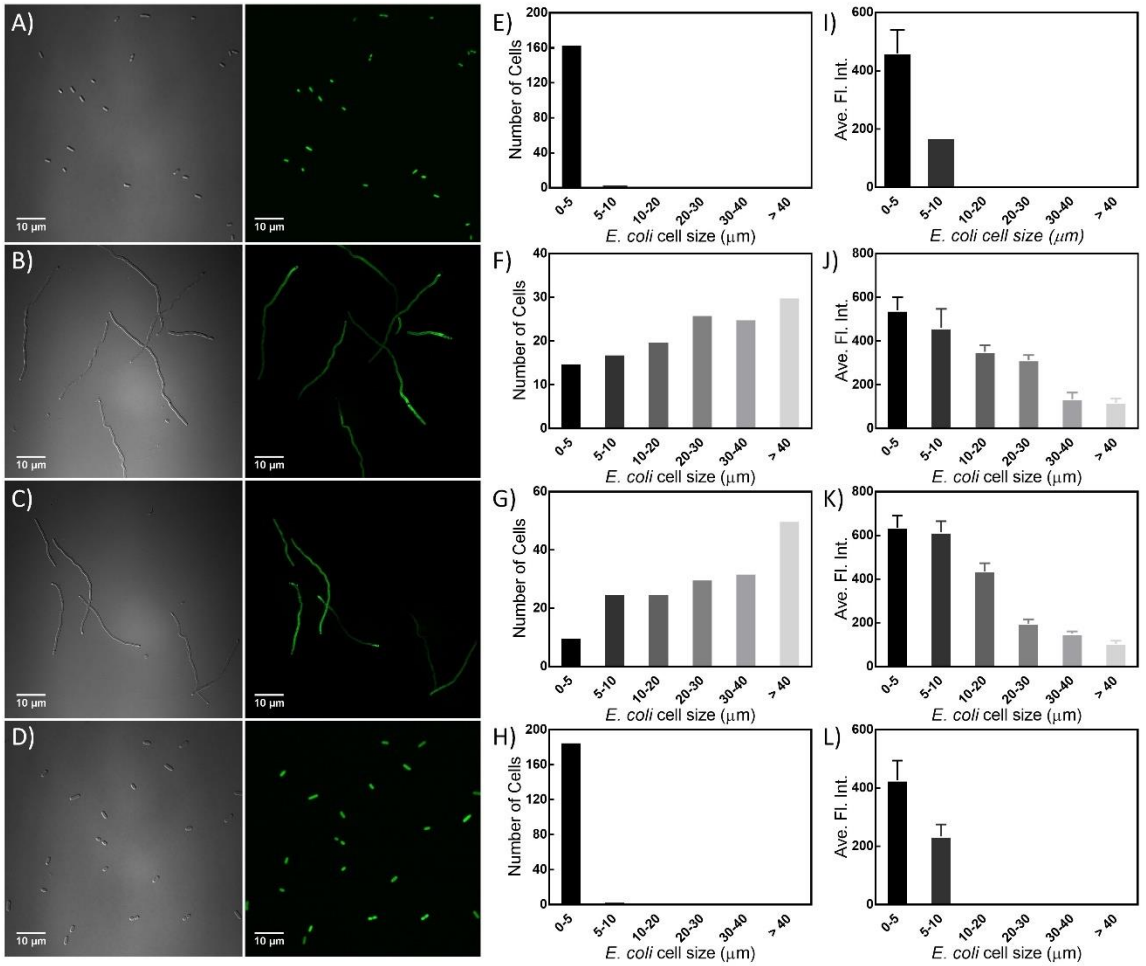

Figure 3.2 Complex **1** induces filamentous growth and decreased protein production in *E. coli*. Bright field and fluorescent imaging of *E. coli* cells. A) N. C. control, B) cisplatin, C) compound **1** with light, D) compound **1** in the dark. Size distribution histograms of *E. coli* cells associated with the conditions for A) - D): E) N. C. control, F) cisplatin, G) compound **1** with light, H) compound **1** in the dark. Histograms of average fluorescence intensity correlated to cell size with the different treatments: I) N. C. control, J) cisplatin, K) compound **1** with light, L) compound **1** in the dark. Cells were treated with 100 µM of each compound for 6 h before imaging.

All antibiotics were able to induce *E. coli* filaments, but the populational size analysis revealed the major populations of *E. coli* varied significantly in length. Tetracycline treatment at the MIC resulted in a large fraction (88%) of the cell population of normal length, with 22% forming short (5–10 µm) filaments. In marked contrast, nalidixic acid induced significant filamentation, and the filaments were the dominant populations (100%; average length of 51 µm). For rifampicin, a concentration of 10x MIC was required to induce filaments. Treatment resulted in 70% with a length ≤5 µm, and the remaining 30% were short filaments of 5–10 µm (Figure S2.2 in Appendix). This initial analysis made clear that compound **1**, cisplatin, and nalidixic acid induced

longer filaments that were a more dominant portion of the population under all treatment conditions than the antibiotics that inhibited transcription or translation.

2) Membrane Integrity. The membrane stain FM4-64 was used to confirm that the observed filaments were single cells and to visualize membrane integrity. As shown in Figure 3.3A and B, filaments were formed by single living cells upon compound treatment. No disruption of the cell membrane was observed, indicating that the phenotypic changes were not associated with cell lysis. This is consistent with results that were obtained utilizing trypan blue staining of HL60 cells, which indicated that neither of the two metal compounds act as membrane damaging agents. Thus, the abnormal features observed occur in living cells and are not an artifact resulting from physical disruptions of cellular integrity. In addition, the mechanism of action does not entail membrane damage.

3) Nucleoid Morphology and Number. DNA staining and analysis of over 30 cells per treatment condition revealed trends for the impact of the compounds on *E. coli* nucleoids. Multiple nucleoids were observed in some cells for all treatments that induced filamentous growth. However, the different compound classes resulted in significant differences in DNA content and distribution.

Both rifampicin and tetracycline treatment produced filaments with a regular distribution of DNA, while nalidixic acid, cisplatin, and light irradiated **1** caused expansion, fragmentation, and irregular distribution of nucleoids (Figure 3.3A and B). Rifampicin treatment (at 10x MIC) produced the fewest nucleoids, with the majority of filaments containing a single nucleoid that spread along the length of the cell. Tetracycline, in contrast, produced a number of nucleoids in each of the filaments, and the nucleoids were compact and regularly distributed throughout the cell.

In cells treated with nalidixic acid and the metal compounds, the size and distribution of the nucleoids were quite varied. In order to quantify this observation, the %STD (the ratio of the standard deviation to the average nucleoid size, used as a measurement of variability) was calculated, where the %STD was 38% for the no treatment control. The %STD was 50–55% for the transcription and translation inhibitors. In the metal complex and nalidixic acid treated systems, however, the %STD was greater than 100%, indicating the standard deviation of nucleoid size largely exceeded the average size of the nucleoids. This wide range of nucleoid size implicates issues of DNA fragmentation and failure of DNA segregation after DNA replication.[196] The morphological changes in the bacterial nucleoids treated with the metal compounds and nalidixic acid demonstrate a multifaceted process as a consequence of DNA damage, in contrast with compounds that act to inhibit transcription or translation.

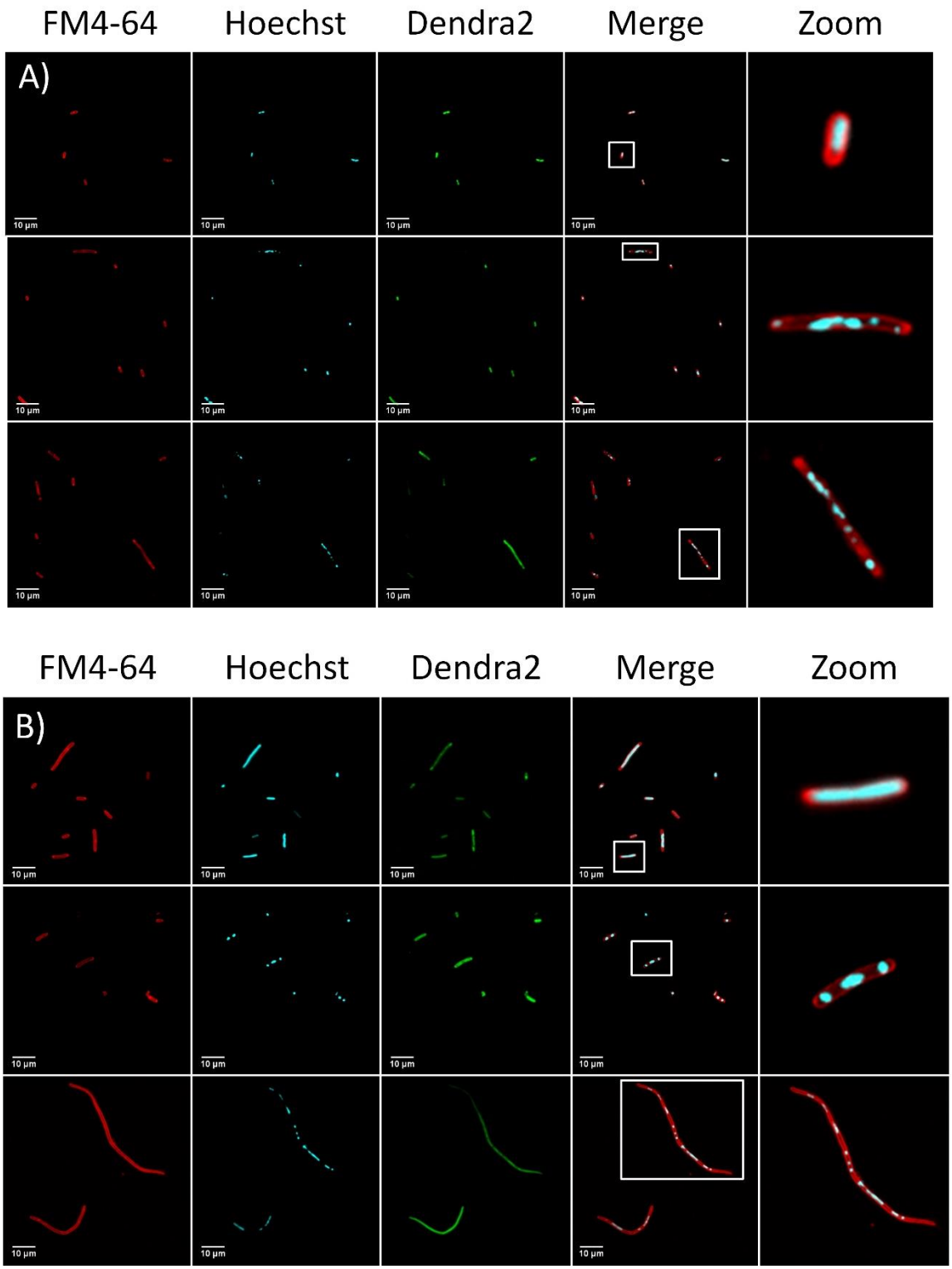

Figure 3.3 Phenotypic profiles of compounds with different mechanisms of action in *E. coli* cells. Fluorescent imaging: A) Top: N. C. control; Middle: cisplatin; Bottom: compound **1** with light; B) Top: rifampicin; Middle: tetracycline; Bottom: nalidixic acid. The merge is the combination of the Hoechst and FM4-64 membrane stain. Scale bars: 10 µm.

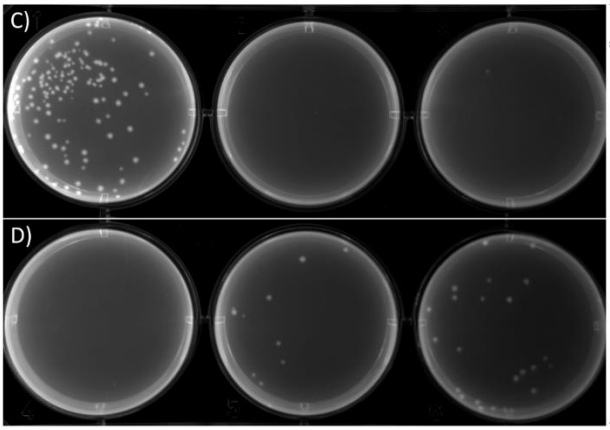

E)	Treatment Concentration	Ave. Filament Size (μm)	Filamentous Population	Nucleoid Morphology
Cisplatin	MIC	9 ± 4	30%	Segregation; Random distribution
	10x MIC	25 ± 22	73%	
Compound 1	MIC	10 ± 4	41%	Segregation; Random distribution
	10x MIC	24 ± 21	68%	
Rifampicin	MIC	N/A	0%	Normal sized and localization
	10x MIC	8 ± 3	30%	Expansion
Tetracycline	MIC	10 ± 2	22%	Compaction; Even distribution
	10x MIC	16 ± 4	52%	
Nalidixic acid	MIC	51 ± 7	100%	Segregation; Random distribution

Figure 3.3 (*continued*) Phenotypic profiles of compounds with different mechanisms of action in *E. coli* cells (*continued*). Colony forming experiment with various compounds: C) Left: N. C. control; Middle: cisplatin; Right: compound **1** with light; D) Left: nalidixic acid; Middle: rifampicin; Right: tetracycline. Cells were treated with each compound at MIC for 6 h before imaging or colony forming. E) Quantitative and qualitative analysis of *E. coli* filamentous growth and nucleoid morphology phenotypes in response to compounds treatment.

It is well established that the processes of transcription and translation are closely coordinated in *E. coli*, and the "transition model" posits, in part, that coupled transcription-translation and membrane association of the growing protein impacts nucleoid morphology. Thus, any process that interferes with mRNA production and protein synthesis could be reflected in the nucleoids. A recent report has demonstrated that transcription and translation inhibitors affected *E. coli* nucleoid shape and spatial distribution, with expansion observed with treatment of rifampicin and compaction with tetracycline.[196] This is qualitatively similar to our results. In addition, treatment with nalidixic acid resulted in the observation of fragmented nucleoids,[196] similar to our imaging results with this compound and the metal complexes. This supports our hypothesis that nucleoid morphology can be used as a phenotypic indicator of DNA damage.

A colony forming assay was performed to provide further support for the assignment of a DNA damaging mechanism of action (Figure 3.3C and D). Cells were treated at the MIC for each compound, the media removed, and the cells spread on an agarose plate. Only cells treated with the transcription and translation inhibitors were able to form colonies; the metal complexes and nalidixic acid were clearly cytotoxic at their MIC. This suggests that these three compounds induce irreversible damage to the *E. coli*.

4) Protein Production. Cisplatin and other platinum-based agents are known to interfere with protein production. Some question remains, however, if this is an important feature that induces cell death. Several experiments have quantified the impact on protein production after transfection of already metalated plasmids into living systems.[197, 198] To study the process and impact of DNA metalation, we treated *E. coli* with the metal complexes and subsequently

monitored protein production. This couples the quantitation of protein levels in the detection of the fluorescent protein to the preceding natural sequence of events that impact transcription/translation, and allows for observation of important features that may play a role, such as compound uptake, localization within the cell, or sequence-dependent interactions with the nucleic acid.

Cells undergoing death will slow or cease protein production, which produces a similar phenotype to cells that are under the influence of a transcription or translation inhibitor. To discriminate between inhibition of protein production and induction of cell death, we used a photoconvertible protein, Dendra2, as a reporter, since it is able to provide information on both aspects of cell viability and new protein production simultaneously.[199] Dendra2 undergoes a photochemical conversion, transforming from a green fluorescent protein to a red fluorescent protein when exposed to 405 nm light. The photoconverted "Red" Dendra2 emission provided a stable internal reference for cell health and cell number for all samples, while new protein production (after light exposure) is reflected in the "Green" Dendra2 emission. Both forms are stable and persist in living cells with half-lives ($t_{1/2}$) on the order of 50 to 70 h.[200, 201, 202] The two forms of the protein thus provide spatial and temporal tracking of Dendra2 formed before and after light exposure.

A clear negative correlation was seen between protein production and cell size, where filamentous cells with longer filament lengths exhibited a lower fluorescence intensity, reflecting a reduction in the amount of new Dendra2 protein being produced. As shown in Figure 3.2, after 24 h of treatment with compound **1**, the average fluorescence intensity of the cell population with the largest length (> 40 μm) dropped by over 70% compared to the control population. Other populations with increased cell lengths exhibited a 30 – 70% decrease in fluorescence intensity. The same trend was seen in cisplatin treated cells, where the fluorescence intensity decreased by 15 – 80%, depending on the length of the filament. Both compound dose and the time of treatment was found to have an effect on filament formation and protein production (see Figure S2.3 – S2.5 in Appendix).

The production of Dendra2 was quantified by dose response, providing IC_{50} values for inhibition of protein production. For this experiment, Dendra2 production was induced in *E. coli* with IPTG and allowed to proceed for 3 h prior to photoconversion, followed by compound treatment. Protein production was quantified using the ratio of the average fluorescent intensity of the two forms of Dendra2, as shown in Figure 3.4, the transcription inhibitor rifampicin and translation inhibitor tetracycline exhibited IC_{50} values for inhibition of Dendra2 production that matched well with growth inhibition (within 3-10 fold; see Table 3.1 and Figure 3.4). In contrast, both compound **1** and cisplatin displayed a greater disparity between inhibition of protein

production and cell growth inhibition. The 30-40 fold decrease in potency reflects that the mechanism of action of cisplatin and compound **1** is not solely (or primarily) through transcription or translation inhibition. In contrast, nalidixic acid, which induces DNA double strand breaks, was far more effective at inhibiting protein production, suggesting that this may contribute to its mechanism of action. These results implicate other biological effects as likely being responsible for the enhanced toxicity of the metal compounds.

Interestingly, while cisplatin has been described as a transcription inhibitor, it was the least effective of the four compounds tested for inhibition of protein production. The impact of the DNA damage induced by platinum compounds on protein production has been comprehensively and conclusively proven, along with the restoration of protein production when the appropriate DNA repair mechanisms are activated to remove the lesions. However, our studies suggest that the implication of inhibition of protein production by cisplatin is of secondary importance in *E. coli*, as the concentrations required to observe significant impacts on this process in far exceed the toxic dose for the compound.

In an analogous study, Lippard and coworkers tested cisplatin in mammalian cells containing a genetically encoded fluorescent reporter system.[203] Very good agreement was observed between the concentrations required to inhibit protein synthesis and to induce cytotoxicity evaluated via a colony counting assay in that report. The reason for the disparity in the ability of cisplatin to inhibit protein production in *E. coli* compared to the HeLa cells used by Lippard is unclear. It is particularly surprising, given the very similar values we found for DNA and RNA metallation in *E. coli* and HL60 cells, as described above.

5) Protein distribution. The use of a photoconvertible protein allows for a spatiotemporal analysis of protein content. This provides the opportunity to address intriguing questions such as the impact of interruption of cell division and filamentous growth on the activity of ribosomes for new protein production, and the redistribution of existing protein within a filamentous cell. Fluorescent imaging was performed to probe the effects of the different compounds on protein distribution in single cells. Compounds were dosed after photoconversion, and imaging was performed 6 h later. As shown in Figure 3.4A and B, both the "Red" Dendra2 (the internal control of pre-treatment protein level) and the "Green" Dendra2 (reflecting protein synthesis after treatment) was distributed throughout the cell as the healthy cells underwent multiple cell divisions. Both Red and Green forms of Dendra2 were also found within the filamentous cells where cell division was blocked by either DNA damaging agents or transcription/translation inhibitors. It has been reported that disruption of DNA replication and double strand breaks resulting from nalidixic acid treatment could lead to uneven distribution of ribosomes in filamentous cells.[196] However, we did not observe

any particular spatial sequestration of active ribosomes, or alternatively, protein diffusion is sufficiently rapid to prevent observation of any localization.

3.5 Comparison of *in vitro* and in cell protein production.

Previously, we reported an *in vitro* transcription and translation assay (IVTT) with compound **1** and cisplatin using green fluorescent protein (GFP) as a fluorescent reporter.[199] In this assay, either a plasmid containing the GFP gene or the mRNA transcript for GFP were allowed to react with varying concentration of compound **1** or cisplatin before addition of the nucleic acids to a cancer cell lysate containing transcription and translation machinery. Both metal compounds inhibited GFP production with a clear dose response. Interestingly, the IC_{50} value for inhibition of protein production was ~3 μM for both compounds. The ratio of DNA nucleotides or RNA nucleotides to each metal center (nt / mc) was then calculated at the IC_{50} for protein synthesis inhibition. The values for compound **1** were 1140:1 for DNA and 820:1 for RNA, while the values for cisplatin were 600:1 for DNA and 610:1 for RNA.

In the current uptake studies, *E. coli* cells were dosed at 20 μM, which is approximately 10 times higher than the IC_{50} value for growth inhibition, but well below the IC_{50} value for inhibition of protein synthesis, as determined by Dendra2 production (see Table 3.1). In order to compare the *in vitro* experiment to the cell data, extrapolation of the ratio for DNA and RNA nucleotides per metal center at the IC_{50} value for *in vivo* protein synthesis inhibition were performed as detailed in Appendix. The calculated values were remarkably close to the values from the *in vitro* transcription and translation assay, with DNA nt / mc ratios of 520:1 for compound 1 and 700:1 for cisplatin. The RNA nt / mc ratio was 1000:1 for compound 1 and 1090:1 for cisplatin.

This analysis of the ratio of DNA or RNA bases to metal centers suggests the functional inhibition of protein synthesis by covalent adducts to DNA and mRNA by compound **1** and cisplatin is similar in *E. coli* and the *in vitro* assay. It is notable that in a living cell, where the reaction conditions are much more complex than the buffered system of IVTT assay, the IC_{50} values to inhibit protein synthesis were diminished by over 60-fold relative to the IVTT assay. However, the ratio between DNA or RNA bases and the metal center for inhibition of protein production remain quite consistent. The increase in the IC_{50} values in cells suggests two conclusions: 1) inhibition of protein synthesis is not the factor that induces cell death, and 2) both compounds suffer from off-target binding to biological molecules. The latter is known to be a major issue for many currently administered drugs, especially cisplatin

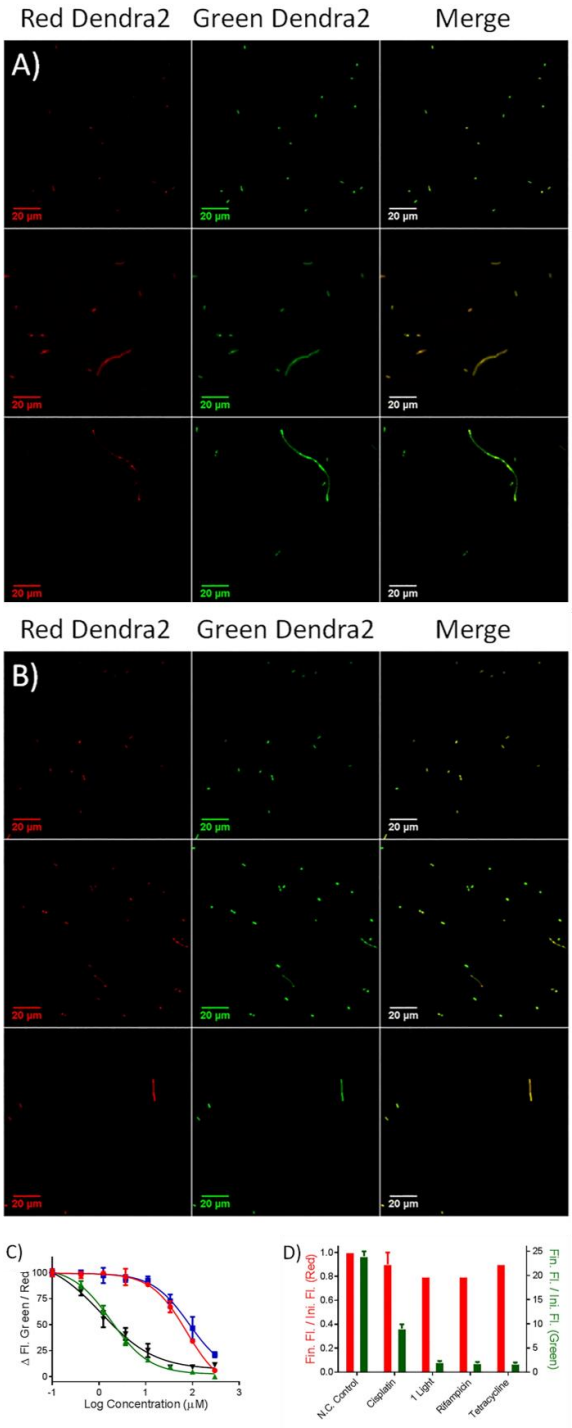

Figure 3.4 Dendra2 distribution in *E. coli* cells. A) Top: N. C. control; Middle: cisplatin (100 µM); Bottom: compound **1**, light (100 µM). B) Top: compound **1**, dark (100 µM); Middle: rifampicin (3 µM); Bottom: tetracycline (48 µM). Scale bars: 20 µm. Cells were treated for 6 h before imaging. C) Dose response of Dendra2 production inhibition measured at 0 and16 h after photoconversion of Dendra2 and treatment with cisplatin (blue), compound **1** with light (red), rifampicin (green), tetracycline (black). D) Dendra2 production inhibition after 16 h treatment.

The role of off-target binding was also supported by the AAS analysis of metal content with the different nucleic acids in *E. coli* and mammalian cells, as only a minor component of the metal compounds entered the cells, and of this, only 1.3% and 1.26% of cellular ruthenium from compound **1** and 0.98% and 1.12% of the cellular platinum from cisplatin were found with genomic DNA in the two systems. If one includes the < 2% of metal present in the RNA as on-target damage, this means over 96% of the cellular metal is reacting with potentially non-relevant targets. Extending this argument, if off-target binding could be eliminated, cytotoxicity IC_{50} values would be reduced to nanomolar concentrations if the same levels of cellular uptake could be maintained. This may lead to another method to improve the potency of currently used drugs: instead of focusing on the generation of analogues that are more potent against nucleic acids, analogues with reduced off-target binding could be more effective. It was anticipated that the ruthenium compound would fare better than cisplatin in avoiding off-target binding, due to its lower affinity for hydrophobic proteins such as human serum albumin (HSA) and thiols such as glutathione (GSH), but this has not been found to be the case in cells.[165, 204] As the preferred binding partners are not the same for the platinum and ruthenium complexes, it will be important to identify the primary off-target biomolecules responsible for sequestering the ruthenium in order to rationally design derivatives that avoid these species to increase the potency of these inorganic compounds.

3.6 Ru and Pt compounds induce distinct cellular responses in mammalian cells.

The cellular effect of compound **1** was also studied in mammalian cells, with a focus on proteins involved in cell signaling and cell death. As shown in Figure 3.5, the effect of compound on cell cycle and apoptosis were studied using flow cytometry, immunoblotting for apoptotic markers, and DNA fragmentation. No cell-cycle specific arrest point was observed with compound **1** treatment, while a sub G1 population of 20% of cells was observed after 24 h. Flow cytometry analysis of apoptosis vs. necrosis using Annexin V/propidium iodide (PI) indicated that compound **1** induced cell death through apoptosis as the dominant mechanism. While cisplatin induced necrosis in a small fraction (5%), less than 2% of cells treated with compound **1** were characterized as necrotic. Immunoblotting of caspase 3 and PARP cleavage showed a time dependent induction of apoptosis; in addition, isolation of genomic DNA showed fragmentation, which is consistent with apoptotic cell death. All apoptotic reporters were clearly observed at 24 h.

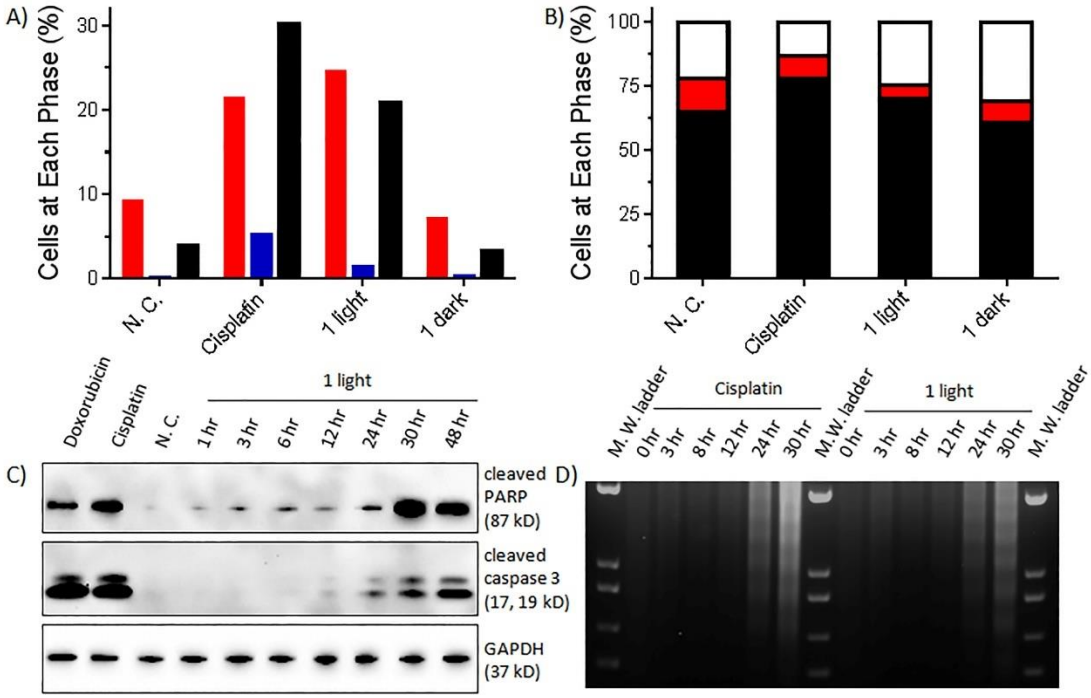

Figure 3.5 Compound **1** induces apoptosis in HL60 cells without cell cycle arrest. A) Flow cytometry by PI/Annexin V in HL60 cells; Red = apoptotic cells, Blue = necrotic cells, Black = dead cells. B) Flow cytometry by PI in HL60 cells; Black = G1; Red = G2; White = S phase. C) Immunoblotting of cleaved PARP and cleaved caspase 3 in HL60 cells. GAPDH was blotted as loading control. D) Agarose gel electrophoresis of DNA laddering. HL60 cells were treated for 24 h befor flow cytometry. Treatment condition in all panels: compound **1**, 20 μM; cisplatin, 20 μM; doxorubicin, 1 μM.

The tumor suppressor protein p53 regulates cell growth and cell cycle checkpoints to eliminate proliferation. It is one of the most commonly mutated genes in cancer, resulting in loss of its regulatory function.[205, 206] Both p53/p21 and chk1 are involved in G1/S and G2/M cell cycle checkpoints in response to DNA damage.[207, 208] In order to probe the role of p53 in response to compound **1**, immunoblotting was performed in A549 cells. This non-small cell lung cancer cell line contains functional p53, in contrast with the p53 deficient HL60 cell line. While both cisplatin and doxorubicin were able to induce apoptosis in the absence of functional p53 in HL60 cells (Figure 3.5), the A549 cell line demonstrated clear induction of p53 for these two compounds. In contrast, compound **1** did not induce elevated expression of p53, and didn't significantly alter its phosphorylation or expression of p21 (Figure 3.6A).

Another surprising difference observed between the platinum and ruthenium compounds is that p-chk1, which is involved in G2/M cell cycle arrest in response to DNA damage, was not induced by treatment of compound **1** in either cell line, while both cisplatin and doxorubicin both induced phosphorylation of chk-1. This finding is consistent with the fact that no cell cycle arrest

point was seen in HL60 cells upon treatment with compound **1** and light, in contrast to cisplatin and doxorubicin. However, phosphorylation of γ-H2AX, an early sensor of DNA damage, was observed after 6 h of treatment with **1**, indicating DNA damage even in the absence of chk1 activation.

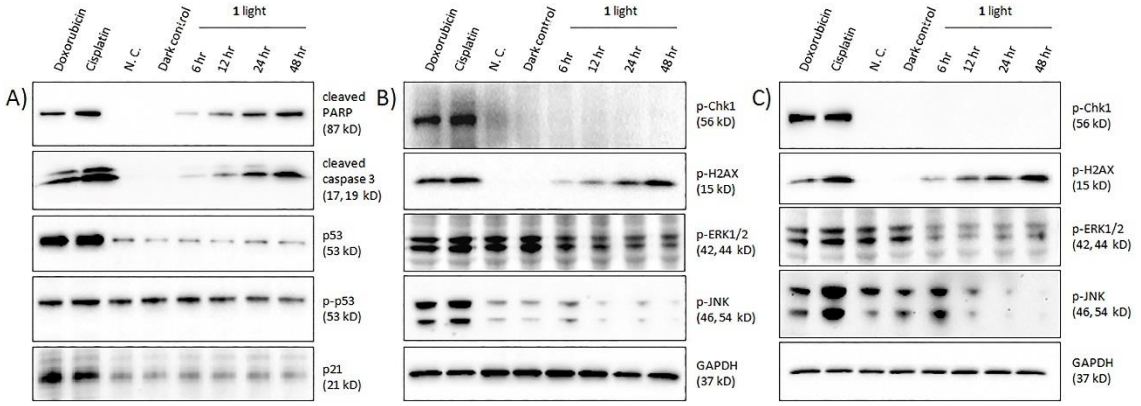

Figure 3.6 Immunoblotting of apoptotic markers and cell signaling proteins in A) and B) A549 cells; C) HL60 cells. Cells were treated with 20 μM of compound **1** for specified time periods, cisplatin (20 μM) and doxorubicin (2 μM) at 24 h of treatment were used as controls. GAPDH was used as loading control.

Pro-survival and pro-apoptotic pathways, including MAPK pathways were examined, and consistent signaling behaviors after compound **1** treatment were observed in both cell lines. The ERK pathway has been reported to facilitate cell survival and prevent apoptosis.[209, 210] As shown in Figure 3.6, this pathway was inactivated by compound **1** in both A549 and HL60 cell lines; in contrast, both cisplatin and doxorubicin didn't downregulate this pro-survival pathway. The JNK pathway has been reported to act as a pro-apoptotic pathway in response to cellular stress induced by DNA damage, and is mainly activated by mismatch repair signals.[209, 34] Both cisplatin and doxorubicin were able to induce phosphorylation of JNK in A549 and HL60 cells at 24 h, though different phosphorylation levels in HL60 cells were observed, which might indicate possible phosphorylation time course differences. Phospho-JNK was seen as early as 6 h after doxorubicin treatment in HL60 cells while cisplatin induced phospho-JNK was seen to increase to maximum level at 24 h.[211, 212] Surprisingly, compound **1** didn't activate the JNK pathway to the same extent as cisplatin or doxorubicin. The phosphorylation level was slightly increased within 6 to 12 h of treatment with compound **1** in both cell lines, but then decreased over time. This, along with the previously discussed markers, indicate a different DNA damage response for compound **1** either from altered cell signaling pathways or by a different class of DNA damage.

3.7 Addressing the cytotoxic species, the metal center or the ligand?

In recently published works, Bonnet and others raised the question of the cytotoxic species generated in the photoejection of Ru(II) comlexes,[213, 214] and the possibility of the dissociating ligand, rather than the metal center, being responsible for the cytotoxic effects of strained Ru(II) compounds. To further the understanding of the mechanisms of actions of Ru(II) compounds on the basis of our knowledge on compound **1** from works described in this chapter, the aquated species compound **2** produced in the photoejection of compound **1** (see Figure 3.1) was synthesized and studied in parallel with the free ligand, 6,6'-dimethyl-2,2'-bipyridine (dmbpy).

Table 3.3 Cytotoxicity IC_{50} values (μM) of compound **1** and **2** in *E. coli*.

	Light	Dark
Compound **1**	3.2	>300
Compound **2**	2.2	2.2
Dmbpy	>300	>300
Compound **2** + dmbpy	2.8	2.6

As shown in Table 3.3, compound **2** showed IC_{50} values of 2.2 μM in both light irradiated and dark conditions, in close agreement with the cytotoxicity of compound **1** with light irradiation in *E. coli*. The free ligand, however, failed to induce cytotoxic effects, either in light or dark conditions. When dosed with the ligand, compound **2** exhibited IC_{50} values of 2.8 and 2.6 μM, which is not only close to the cytotoxic properties of compound **1** with light treatment and can be attributed to the cytotoxicity of compound **2**.

Cellular metal accumulation and metal content with nucleic acid in the cell was examined in both *E. coli* and HL60 cells as described for compound **1** to determine the nucleic acid binding properties of compound **2**. As anticipated, similar amounts of ruthenium were found in the cells treated with **2** in both light and dark conditions. This is in agreement with ruthenium levels in cells treated with **1** and subjected to light irradiation. Further studies of genomic DNA and total RNA isolated from both types of cells revealed compound **2** exhibits very similar nucleic binding ratios and preferences compared with **1**. The DNA or RNA nucleotide to metal center ratio in prokaryotic and eukaryotic cells are consistent for both compounds, and reflect the same trend that the metal species bind to and react with DNA with a slightly higher preference. This result offers direct evidence that compound **2**, as the aquated metal species generated from photoejection of **1**, possesses similar cellular uptake and nucleic acid binding properties as the light irradiated parent compound **1**.

Table 3.4 Cellular Ru content with different nucleic acids measured by AAS

	E. coli			HL60		
	Cellular uptake[a]	DNA nt / mc [b]	RNA nt / mc[c]	Cellular uptake[a]	DNA nt / mc[b]	RNA nt / mc[c]
2 light	0.1%	2600 ± 300	4300 ± 500	0.7%	4200 ± 600	5400 ± 700
2 dark	0.1%	3000 ± 400	4000 ± 400	0.5%	5200 ± 600	6000 ± 800
1 light	0.1%	2000 ± 200	3800 ± 600	0.6%	4800 ± 400	5000 ± 700

[a]Cellular uptake was calculated as metal content measured in cells divided by total metal content in both cell samples and cell culture media samples. Cellular uptake in *E. coli* and HL60 cellular uptake was normalized in 10^7 cells. [b]DNA nt /mc was calculated as DNA nucleotide bases (μmol) divided by metal content measured in DNA sample (μmol). [c]RNA nt /mc was calculated as RNA nucleotide bases (μmol) divided by metal content measured in DNA sample (μmol).

As discussed in section 3.4, phenotypic profiling has been used to understand the mechanism of action for several cytotoxic agents targeting different biological processes. With the prediction that compound **2** is mainly responsible for the cytotoxic effects upon light irradiation of compound **1**, phenotypic features in *E. coli* cells treated with compound **2** and the free ligand dmbpy were studied and compared with that induced by molecules studied in section 3.4. At the MIC determined as in table 3.3, compound **2** was able to induce similar filamentous growth of *E. coli* cells, and 38% and 42% of the cellular populations were filamentous in light and dark conditions respectively. The average filament size was 11 μm either with light irradiation or just dark treatment; this also agreed with the filament size of cells treated with compound **1** in light condition. Further observation of the nucleoid morphology revealed a random distribution of irregular sized DNA pieces in filamentous cells, which is also consistent with the phenotypic features induced by compound **1**. The free ligand was dosed at a much higher concentration, 300 μM, as no MIC was determined from the dose response studies. At this highest dose, however, only 3% to 4% of filamentous cells were observed, which is the same level as naturally occurred under no treatments; the filament size is much smaller than that induced by compound **1** and **2** treatment.

Combine the cytotoxicity, metal content bount to cellular nucleic acids, and phenotypic analysis, it appears that the Ru(II) center is responsible for the biological effects observed. The free dmbpy ligand doesn't show significant cytotoxicity against *E. coli* cells, nor does it induce phenotypic changes. In marked contrast to the ligand molecule, compound **2** has similar IC50 values as compound **1** following light activation, and the cellular accumulation of compound 2 is comparable to that of compound 1 with consistent nucleic acid binding properties. Phenotypic features very similar to those induce by compound **1** were observed with compound **2** treatment.

The answer now to the question addressed for this section is that compound **1** generates both the aquated metal species compound **2** and the free ligand dmbpy, and among the two, it is the metal product, compound **2**, that is mainly responsible for the cytotoxic effects induced by light irradiated compound **1** through a DNA damaging mechanism of action.

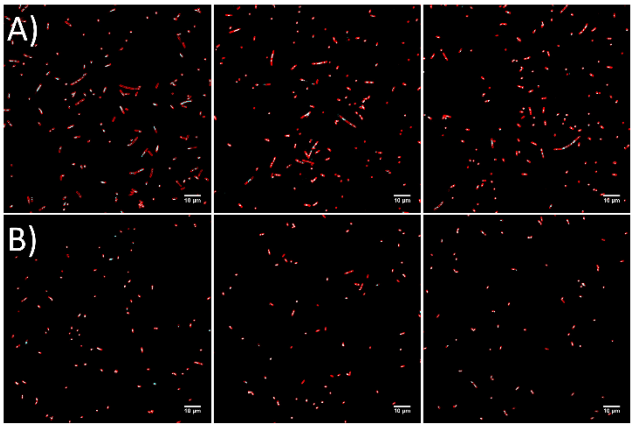

C)

	Avg. Filament Size (μm)	Filamentous Population
2 light	11 ± 2	38%
2 dark	11 ± 4	42%
Dmbpy light	6 ± 1	4%
Dmbpy dark	7 ± 1	3%

Figure 3.7 Compound **2** induced filamentous growth of *E. coli* cells. A) Left: compound **2** light; Middle: compound **2** dark; Right: compound **1** light; B) Left: dmbpy light; Middle: dmbpy dark; Right: N. C. control. The image is the merge of the Hoechst and FM4-64 membrane stain. Scale bars: 10 μm. Cells were treated with each compound at MIC for 6 h before imaging. C) Quantitative analysis of *E. coli* filamentous growth and nucleoid morphology phenotypes in response to compounds treatment.

3.8 Conclusion.

This work indicates that a combination of phenotypic screening based on *E. coli* imaging and protein production using Dendra2 as a fluorescent reporter allows for rapid investigations of mechanisms of action for cytotoxic agents which may have similar activities in mammalian cells. We found that a combination of these two experimental parameters facilitates discriminating DNA damaging agents from agents that work solely as transcription or translation inhibitors. While filaments are formed by all classes of compound, filament size and population distribution was radically different depending on the mechanism of action. Furthermore, the observation of irregular bacterial nucleoids, easily visualized using Hoechst staining, was associated with DNA damage, while regular nucleoid size, shape, and distribution was associated with compounds that do not directly affect DNA.

These studies in bacterial and mammalian cells highlight the capacity of performing rapid studies of anticancer agents in a simple biological model system. Phenotypic studies and quantitative analysis reveal similarities in biological activities between complex **1** and cisplatin. The different cellular response to the compounds in cancer cells, however, suggest diverse pathway regulation resulting from the DNA damage, which offers a possibility to maintain efficacy without experiencing the same resistance by altering the metal center.

Last but not the least, phenotypic profiling in *E. coli* provides identification of the cytotoxic species generated from the photoejection of compound **1** that is relevant to the mechanism of action of the parent compound, proving the metal center product, compound **2**, not the free ligand, is responsible for the DNA damaging mechanism and the sequential cytotoxic effects.

E. coli have been used in the past as model systems to probe binding characteristics of drugs, such as cisplatin, with proteins using NMR.[215, 216] Phenotypic analysis in bacteria by microscopy is now gaining more attention, primarily to identify the cellular pathways affected by antibiotics,[116, 217] but a recent report identified anticancer activity for a molecule characterized by cytological profiling.[218] We believe this is a burgeoning area that will accelerate the pace of drug discovery.

While these studies bring us closer to understanding the mechanism of action of a particular cytotoxic ruthenium complex, it also raised several provocative questions. These include the following: 1) Why is the cytotoxic potency of cisplatin and other inorganic putative DNA damaging agents the same in *E. coli* and mammalian cells when DNA damage recognition and repair pathways that are unique to eukaryotic systems are implicated as playing a key role in their mechanism of action? 2) While more of the metal complexes are taken up in *E. coli* than the HL60 cells, the nt / mc ratio remains quite consistent for both DNA and RNA. What biological entities are responsible for the enhanced sequestration of the metals in the *E. coli*, and is it possible that similar molecules play a role in cisplatin-resistant cancer cells? 3) Why does DNA packing not play a greater role in determining the degree of metallation? DNA is packaged in different ways and to different degrees of compaction in the two cells types, and if the more highly exposed, transcriptionally active sequences where the primary target, we would anticipate greater potency for inhibition of Dendra2 production. We believe that addressing these basic questions may be very important to the rational development of improved DNA targeting agents, and see *E. coli* as an excellent system to seek the answers.

3.9 Materials and methods.

E. coli culture maintenance. The Dendra2 gene was cloned into a pCW-ori plasmid modified to contain an N-terminal 6x histidine tag with multiple restriction enzyme cloning sites. Escherichia coli BL21(DE3) competent cells transformed with pCWori plasmid containing Dendra2 gene (pCWori-Dendra2) were cultured in Luria Broth (LB) at 37°C with 180 rpm shaking.

Mammalian cell maintenance. Human promyelocytic leukemia HL60 cells were purchased from ATCC. Dulbecco's modified eagle medium (DMEM), Iscove's modified Dulbecco's medium (IMDM), Opti-MEM I reduced serum medium, heat inactivated fetal bovine serum (FBS),

Penicillin/Streptomycin (5, 000U/mL), Trypsin-EDTA (0.5%), Dulbecco's phosphate buffered saline (DPBS), Trypan Blue Solution (0.4%) were purchased from Life Technologies.
HL60 cells were maintained in IMDM supplemented with 10% FBS and 50 U/mL of Penicillin/Streptomycin. A549 cells were maintained in DMEM with the same supplements. Cells were maintained at 37°C with 5% CO2.

Cytotoxicity determination. E. coli BL21(DE3) cells transformed with pCWori-Dendra2 plasmid were plated in M63 minimal medium at 4 x 10^6 cells per well in 96 well flat bottom transparent tissue culture treated plates (Greiner Bio One). Compounds were dosed from 0 – 300 μM, followed by 3 min of light irradiation (7 J/cm^2 blue light (> 400 nm)). The cells were then incubated for 16 hours with the compounds, and cell growth was determined by measurement of the optical density at 600 nm using a SpectraMax Multiwell Plate Reader (Molecular Devices). HL60 cells were plated in Opti-MEM supplemented with 1% FBS and 50 U/mL of Penicillin/Streptomycin at 30,000 cells per well in 96 well flat bottom transparent tissue culture treated plates (Greiner Bio One). Compounds were dosed from 0 – 300 μM, and incubated for 16 hours, followed by light irradiation with 7 J/cm^2 blue light (> 400 nm) in 30 second pulses for a total light exposure of 3 minutes. The cells were then incubated for 72 hours, and cell viability determined by conversion of resazurin to resorufin. Dark controls were run in parallel. The emission of resorufin was measured on a SpectraFluor Plus Plate Reader (Tecan). The data were normalized to the untreated control and fitted to a sigmoidal dose response model using Prism 6.02 to determine IC_{50} values. Minimal inhibitory concentration (MIC) was fitted to the model published by Lambert et al using Prism 6.02.[185]

Protein synthesis inhibition. E. coli BL21DE3 cells transformed with pCWori-Dendra2 were cultured in LB medium to an OD_{600} of 0.8. Cells were then resuspended in M63 minimal media and induced with 0.5 mM IPTG for 3 hours at 37°C with 180 rpm shaking. Photoconversion of Dendra2 was carried out with a 405 nm LED flood array (Loctite) with a total light exposure time of 2 minutes. Cells were then plated in 96 well plates at 6 x 10^7 cells per well. Green and red emission was measured directly after photoconversion using a SpectraMax Multiwell Plate Reader (Molecular Devices) for a baseline evaluation of Dendra2 protein (t = 0 hour). For green emission, an excitation wavelength of 491 nm and emission wavelength of 538 nm was used; for red emission, the excitation wavelength was 544nm and emission wavelength was 590 nm. Compounds were then dosed from 0 μM to 300 μM, and compound **1** was activated with light as described above. The cells were incubated for 16 hours before the green and red emission was measured again for an evaluation of protein synthesis with compound treatment (t = 16 hours). The average

fluorescence ratio of green/red at t = 0 hour and t = 16 hours was calculated, the values were normalized, and the data fitted to a sigmoidal dose response.

E. coli filamentous growth. E. coli were cultured as above and plated at 3 x 10^8 cells per well in 24 well flat bottom transparent tissue culture treated plates (Greiner Bio One). IPTG was added at a concentration of 0.5 mM for induction of Dendra2 production. Compound treatment was then carried out, with cells dosed at the MIC or 10 x MIC for each compound and cultured at 37°C with 180 rpm of shaking for 6 and 16 hours before imaging.

E. coli cell imaging. After compound treatment, *E. coli* cells were centrifuged at 5, 510 x g for 2 minutes, washed twice with PBS, and 3 x 10^7 cells were resuspended in 1 mL of PBS. The fluorescent dyes FM4-64 and Hoechst 33342 were added to a final concentration of 5 μg/mL and 10 μg/mL respectively. The cells were protected from light for 20 minutes, and then 2 μL of cell suspension was placed on a slide and a cover glass was applied before imaging. Imaging was carried out on an Olympus IX2-RFAEVA-2 microscope with the following filter settings: Dendra2 (green), excitation filter: 473/10 nm BrightLine® single-band bandpass filter, FF01-473/10-25 (Semrock, Rochester, NY, USA); emission filter: 525/50 nm BrightLine® single-band bandpass filter, FF03-525/50-25 (Semrock, Rochester, NY, USA). Dendra2 (red) and FM4-64, excitation filter: HQ 550/30 (Chroma, Bellows Falls, VT, USA); emission filter: 664 nm EdgeBasic long-pass edge filter, BLP01-664R-25 (Semrock, Rochester, NY, USA). Hoechst 33342, excitation filter: BP 360-390 (Chroma, Bellows Falls, VT, USA); emission filter, HQ470/30 M (Chroma, Bellows Falls, VT, USA). Imaging data was processed and analyzed with ImageJ.

Metal uptake in bacterial cells. *E. coli* were cultured in M63 minimal medium as discussed above and dosed with 20 μM compound **1** or cisplatin. Cells treated with compound **1** were irradiated with 7 J/cm^2 blue filtered light (> 400 nm) for a total of 3 minutes, or were protected from light. Cells were collected 24 hours after compound addition by centrifugation at 5, 510 x g for 5 minutes. The culture medium was separated for analysis, and cells were washed twice with PBS and pelleted. Both cell content and medium were heated at 110 °C for 3 hours with 20% (v/v) HNO_3. Total RNA and genomic DNA were isolated using Qiagen kits. RNA and DNA samples were digested in HNO_3 as described above. Following sample digestion, the metal content was analyzed using a Varian AAS with a replicate reading and a spiked reading. Cellular uptake was calculated as following:

$$\text{Cellular uptake} = \frac{\text{Metal measured in cell sample (μmol)}}{\text{Metal in cell sample + media (μmol)}} \times 100\%$$

Genomic DNA and total RNA were quantified by measuring their absorbance at 260 nm. Mass to DNA nucleotide pair conversion was calculated using the average molecular weight of DNA nucleotide pairs. The number of DNA nucleotide bases per metal center was calculated as following:

$$\text{DNA nt./mc.} = \frac{\text{2 x DNA nucleotide base pairs (µmol)}}{\text{Metal measured with DNA samples (µmol)}}$$

Mass to RNA nucleotide base conversion was calculated using the average molecular weight of RNA nucleotide bases. Number of RNA nucleotide bases per metal center was calculated as following:

$$\text{RNA nt./mc.} = \frac{\text{RNA nucleotide bases (µmol)}}{\text{Metal measured with RNA samples (µmol)}}$$

Metal uptake in HL60 cells. HL60 cells were plated in Opti-MEM supplemented with 1% FBS and 50 U/mL Penicillin/Streptomycin at a density of 1x 10^6 cells/mL in 25 cm^2 cell culture flasks, and dosed with 20 µM compound **1** or cisplatin. Cells treated with compound **1** were incubated 12 hours protected from light before irradiating with 7 J/cm**2** blue filtered light (> 400 nm) in 30 second pulses for a total of 3 minutes, or protected from light. Cells were collected 24 hours after compound addition by centrifugation at 124 x g for 5 minutes. The culture media was separated for analysis, and cells were washed twice with PBS. Total RNA and genomic DNA were also isolated, and the nucleic acids, cell content, and media were prepared for analysis as described above.

Immunoblotting. HL60 cells were harvested 0, 1, 3, 6, 12, 24, 30 and 48 hours after treatment, pelleted by centrifugation at 124 x g for 5 minutes, washed twice with DPBS. A549 cells were plated at 2 x 10^5 cells per well in 6 well flat bottom transparent tissue culture treated multiwell plates and in the same treatment condition detailed for HL60 cells. Cells were harvested at 0, 6, 12, 24 and 48 hours after treatment. All cells were lysed in RIPA buffer supplemented with 5 mM sodium pyrophosphate (2 x 10^6 cells/100 µL) for 15 minutes on ice. The insoluble fraction was removed by centrifugation at 20, 817 x g for 10 minutes at 4 °C. The supernatant was collected and the protein concentration was determined by BCA assay. 20 µg of protein was loaded onto 4-12% bis-tris gels and followed by transfer to nitrocellulose membranes. After blocking with 2.5% BSA in DPBS with 0.1% Tween20 (PBST) for 1 hour at room temperature, the membrane was immunoblotted with the following primary antibodies and correspondence dilutions. Cleaved caspase 3, cleaved PARP, p-p53, p21, p-Chk1, p-JNK and γ-H2AX at 1: 1, 000 dilutions; p53 and p-ERK at 1: 500 dilutions; and GAPDH at a 1: 2, 000 dilution in 2.5% BSA overnight at 4 °C. Immunoblots were washed with PBST for 10 minutes for four times and incubated for 1 hour with

secondary antibodies at a 1: 10, 000 dilution for GAPDH and 1: 5, 000 dilutions for all other antibodies. Detection was carried out with Clarity Western ECL Substrate and imaged with a ChemiDoc MP System (Bio-Rad).

DNA fragmentation. HL60 cells were cultured, and treated as described above. Cells were harvested at 0, 3, 8, 12, 24 and 30 hours after treatment, pelleted by centrifugation at 124 x g for 5 minutes, washed twice with DPBS, and prepared with an apoptotic DNA-ladder kit as per manufacturer instructions (Rosch). Gel electrophoresis was carried out using a 1 % agarose gel containing 0.5 μg/mL ethidium bromide for 90 minutes at 75 V. Gel imaging was performed with the ChemiDoc MP.

Flow cytometry. HL60 cells were cultured, and treated as detailed previously. Cells were harvested at 24 hours after treatment, pelleted by centrifugation at 124 x g for 5 minutes, washed twice with DPBS. For cell death mechanism analysis, cells were stained 15 minutes with FITC-Annexin V and PI; for cell cycle analysis, cells were stained 15 minutes with PI only. Cells were analyzed with a FACSCalibur (Becton-Dickenson). A minimum of 20, 000 events were measured for each sample.

Chapter 4. Bacterial cytological profiling differentiates anticancer agents with various mechanisms of actions

RESEARCH CONTRIBUTIONS

The research presented in this chapter is completed with help and support of other scientists. The pCWori plasmid DNA and Dendra2 gene sequence was kindly provided by Dr. David Heidary.

4.1 Introduction.

Small molecule compound screening as starting a point for the development of a drug is traditionally evaluated for biological effects by one of two methods. The first involves isolating the biological molecule target and identifying chemical "hits" by assaying activity of the target in the presence of compound libraries. The second focuses on screening compound libraries in complex systems, such as bacterial or mammalian cells. While the first approach allows one to have clear knowledge of the effect of compounds on the specific biological target, the second approach is necessary when the target cannot be isolated, or when efforts must be focused on its cell based activity.

When screening compounds in complex systems, elucidating the mechanism of action through target identification is an essential step. It also remains one of the most challenging problems in drug discovery.[219] Though the precise mechanism or functional target is not required for a drug to be approved by the FDA, as illustrated by the fact that many medications are prescribed without mechanistic understanding, knowledge of the biological mechanisms and targets of potential drugs could, however, reduce the chances of clinical trial failure.[220, 100] Knowing the mechanism not only improves our understanding of how the compound results in a biological activity, but can be used to improve potency while minimizing adverse effects in treatments as a single or combination medication.[221, 222] Current drug discovery progress can also benefit from mechanistic studies of therapeutic agents that are either approved by the FDA or in clinical trials.

Mechanistic studies and target identification are common methods used to solve the "black box" problem, and involve considerable time and effort, due to the enormous number of biomolecules present in the cellular environment and the complex networks involving all possible molecular and cellular processes.[223, 224, 98, 225] Affinity based techniques have played an important role in target validation and mechanism elucidation studies, either independently or in combination with computational approaches.[226, 227, 173] This approach, however, is time consuming and requires stringent validation to remove false targets identified in the isolation process. Phenotypic screening, on the other hand, offers insights into the performance of drugs in more biologically relevant environments, allowing the possibility to discover novel cellular targets and mechanisms.[228, 122, 229, 230] Recent advancements in microscopy have made it possible to carry out imaging-based phenotypic profiling with semi-automated or automated settings, combined with statistical evaluation of parameters extracted from imaging results.[116, 231, 232, 233]

Mammalian cell systems have been in dominant use in phenotypic profiling for anti-cancer agents.[230, 234] The role of microbial system, especially bacterial system, however, has been underestimated despite their role in the discovery of novel antibiotics,[235, 115, 236, 237] some of which

also possess anticancer activity. Ever since the discovery of the first commonly used platinum based anti-cancer agent cisplatin in *E. coli* by Rosenberg,[16, 18] there have been studies showing cytotoxic effects of anti-cancer agents in this simple system related to their known mechanisms.[45, 238] Lippard recently reported phenotypic changes in *E. coli* induced by a platinum molecule and the correlation between cytotoxic effects in cancer cells and bacterial cells.[239] In the bacterial cytological profiling results of Pogliano, three molecules used for anti-cancer chemotherapy were included and induced significantly distinct phenotypic changes.[116]

Here in this chapter, we describe phenotypic profiling with anti-cancer molecules in *E. coli*. A combination of cytotoxic and cytostatic analysis helped to distinguish molecules with mechanisms involving DNA damage, transcription inhibition, and translation inhibition. Cellular imaging was performed with statistical evaluation of phenotypic feature changes, and the comprehensive data evaluation led to classification and separation of molecules inducing DNA damage, transcription inhibition, and translation inhibition, proving that a fast assessment of mechanisms of actions can be done in this simple system for anti-cancer agents that target common biological targets in mammalian and bacterial cell systems.

4.2 Correlation of cytotoxicity in mammalian cells and bacterial cells.

In order to study anticancer agents in *E. coli*, it was essential to determine if they possessed cytotoxicity in bacterial cells first. As prokaryotic system lacks eukaryotic-exclusive organelles and biological processes, anticancer agents with DNA damaging mechanism were chosen for this study as DNA has been the most common target for many chemotherapeutic agents, and is a common biological target in both prokaryotic and eukaryotic cells. Determination of cytotoxicoty in human promyelocytic leukemia HL60 cells and *E. coli* cells were done by the resorufin assay and by the OD_{600} assay, as described in previous chapters. As shown in Figure 4.1, all the studied molecules exhibit cytotoxicity in E. coli, despite the fact that their cytotoxicities have previously been primarily studied in mammalian cells. For most of the studied anticancer molecules, the ratio of IC_{50} values in HL60 cells and *E. coli* cells falls into a one log unit range, which means the cytotoxicity in two cell types are within a 10-fold range. This relatively small shift in cytotoxicity suggests these anticancer molecules act through mechanisms involving common targets in cancer cells and *E. coli*.

A translational inhibitor, puromycin, was also chosen for this study for its ability to inhibit translation by inducing premature chain termination of translation in both prokaryotic and eukaryotic cells.[240] Notably, puromycin clustered with the molecules that had IC_{50} values in both HL60 and *E. coli* cells that fell in the one log unit range. The nitrogen mustard compound bis(2-chloroethyl) amine (BCEA), and the topoisomerase II inhibitor, doxorubicin, however, were both

shifted significantly from this range. As shown in Figure S3.7 in the Appendix, the linear regression of IC_{50} values in *E. coli* and in HL60 cells for all molecules was y = 0.009x + 3.936, with the R^2 value being 0.001, suggesting the linear regression poorly fitted the data. When the two data points for BCEA and doxorubicin were removed, the linear regression was y = 0.045x + 1.191 and the R^2 incresed to 0.368. This improvement in goodness of fit suggested that BCEA and doxorubicin largely affected the linear regression. Doxorubicin has been known to possess multiple mechanisms to induce cytotoxic effects including DNA intercalation and reactive oxygen species (ROS) associated mechanism.[241, 242] One possible explanation is that doxorubicin induces cytotoxic effects in HL60 cells through both eukaryotic-exclusive mechanisms and common mechanisms, while the cytotoxicy in *E. coli* cells were only induced through mechanisms that are commonly present in both cell types. The shift of BCEA cytoxicity in *E. coli* cells compared with other two nitrogen mustard compounds could be possibly explained by the reduced reactivity of the nitrogen in the secondary amine BCEA in the SN_2 reactions that alkylate DNA bases.

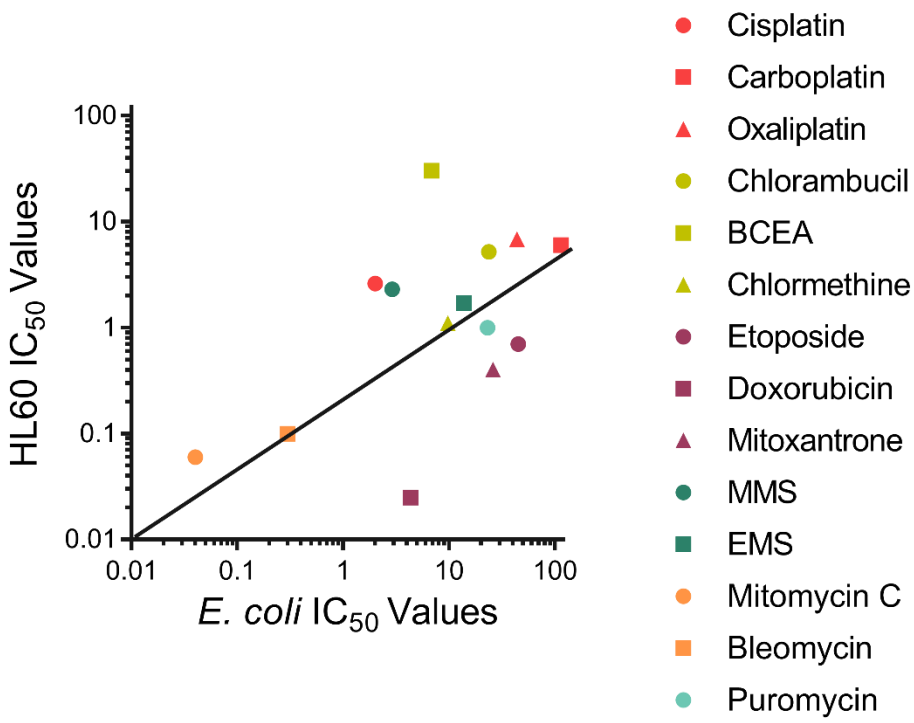

Figure 4.1 Correlation of cytotoxicity in cancer cells and *E. coli*. IC_{50} values in HL60 cells were determined 72 hours after treatement; IC_{50} values in *E. coli* cells were determined 16 hours after treatments. The fit line on the scatter plot represent a y = 0.1x linear correlation.

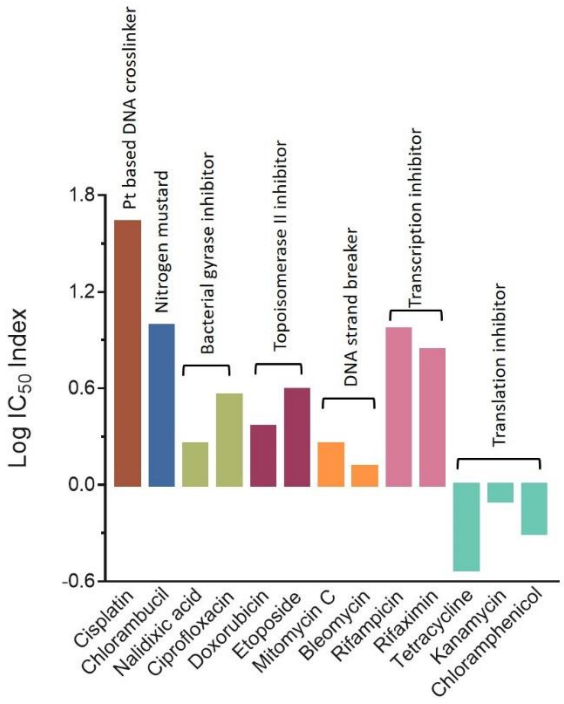

Figure 4.2 The ratio of IC_{50} values for growth inhibition vs. translation inhibition depend on the class of drug. IC_{50} values for growth inhibition in *E. coli* were measured 16 hours after drug treatment, while inhibition of translation was measured by following the production of Dendra2 in a 16-hour time course after drug treatment. The IC_{50} index is defined as the IC_{50} value for translation inhibition/IC_{50} value for growth inhibition.

4.3. Relationship between cytotxicicty and translation inhibition.

The concentration of drug required to induce growth inhibition and the concentration to prevent protein synthesis were independently measured in *E. coli*. For each compound, the ratio of the IC_{50} values from translation inhibition and growth inhibition was established to determine the "IC_{50} index". Compounds known to inhibit translation displayed a negative IC_{50} index value, indicating that the IC_{50} value for translation was more potent than for growth inhibition (Figure 4.2). Compounds with other mechanisms of action had much higher IC_{50} values for translation inhibition. Among the molecules with DNA damaging mechanisms, cisplatin and chlorambucil, two DNA alkylating and crosslinking agents which require nucleotide excision repair (NER) as the major DNA damage repair mechanism, had translation inhibition IC_{50} values that were 43-fold and 9.7-fold above their IC_{50} value for growth inhibition respectively. Bacterial gyrase inhibitors (nalidixic acid, ciprofloxacin), topoisomerase II inhibitors (doxorubicin, etoposide) and the commonly used chemotherapeutic agents mitomycin C and bleomycin are all DNA damaging molecules resulting in strand breaks and therefore requiring homologous recombination repair (HR) in *E. coli*. In contrast to the DNA alkylating agents, these molecules had a smaller IC_{50} index value,

which was less than 5. The IC_{50} index analysis was not able to clearly distinguish the difference between inhibitors of transcription from the single strand break DNA damaging molecules, as the IC_{50} index values of transcription inhibitors (rifampicin, rifaximin) and nitrogen mustard compounds (chlorambucil, BCEA, and BCEMA) fell in a close range.

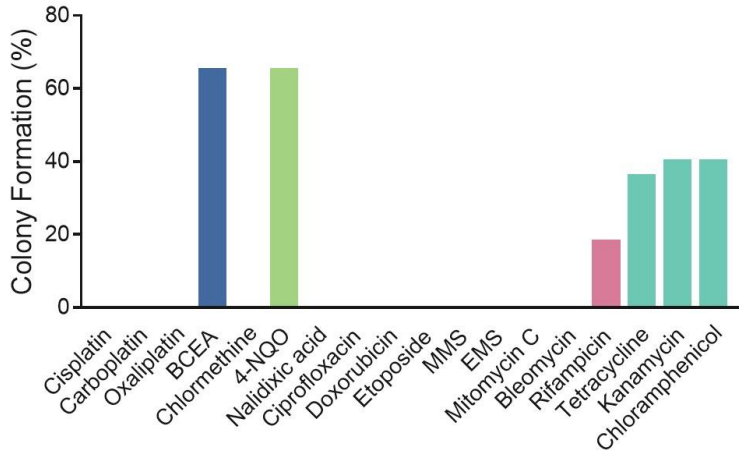

Figure 4.3 Drugs with a DNA damaging mechanism of action are cytotoxic, while drugs that inhibit transcription and translation are cytostatic in a colony forming assay. *E. coli* were treated with drugs at their minimal inhibitory concentration (MIC) for 6 hours, and then the cells were washed to remove the drugs. The cells (~500) were plated on LB agar and colonies allowed to form for 16 hours. Colonies were counted and normalized to the untreated control.

4.4 Establishing a relationship between cytostatic and cytotoxic drugs.

In order to discriminate between transcription inhibitors and the single strand DNA damaging agents, compounds were evaluated for their ability to inhibit colony formation. *E. coli* were treated with compound for 6 hrs at their MIC before the cells were transferred to fresh media without drug. Most DNA damaging molecules induced total inhibition of colony formation, regardless of their mechanism of action (Figure 4.3). Interestingly, bis(2-chloroethyl) amine and 4-nitroquinoline-1-oxide treatment were only able to reduce colony formation by 40%, similar to that seen for the translation inhibitors, where a 60% reduction was observed. This result suggests that altered kinetics in DNA damage repair and responses result in intermediate colony formation inhibition. The colony formation assay could distinguish between transcription inhibition and DNA damage, as the number of detected colonies decreased by 80% after rifampicin treatment, while no colonies were detected for any of the DNA damaging agents. This result is consistent with cytostatic effects associated with inhibition of transcription and/or translation, in contrast to cytotoxic effects caused by DNA damaging molecules.

4.5 *E. coli* phenotypic changes as a function of drug class.

The IC_{50} index and colony formation could be used to narrow down the mechanism of action for several drug classes, but it was found that the combination of the two experiments could not conclusively define the mechanism. It was hypothesized that imaging of *E. coli* could be used to quickly measure several phenotypic parameters which could correlate more effectively with drug class. Accordingly, high resolution imaging was performed using stains to visualize DNA and the cell wall, providing additional cytological features for analysis. Hoechst 33342 (cyan) was used for DNA and FM4-64 (red) was used to stain the cell wall.

Normal *E. coli* cells have length of 2 μm and diameter of 1 μm, giving two-dimensional cellular size of 2 μm^2. Most cells were observed to contain one nucleoid, though cells about to undergo division were observed with two equal sized nucleoids. Upon treatment of molecules targeting different stages of protein production, dramatic changes in single *E. coli* cell and DNA morphology were observed (Figure 4.4). Regardless of drug treatment, the diameter remained constant, but significant changes in length were observed. Cells treated with nalidixic acid exhibited an increase in length that was on average 35 times longer than untreated *E. coli*. They also displayed many fragments of DNA that were irregular in both size and distribution within the cell (Figure 4.4B). Staining of the cell walls confirmed that the changes in length are the result of filamentous growth of a single *E. coli* cell, and not due to the alignment of multiple *E. coli* cells that were adjacent to one another after cell division. Both rifampicin and tetracycline treated cells formed shorter filaments than nalidixic acid, and the DNA morphology was distinct between the two drugs. Cells treated with rifampicin exhibited an expanded, diffuse nuclear staining, distributed throughout the cell with equal intensity. Tetracycline resulted in punctate staining of the DNA, with multiple pieces of similar size occurring with a relatively regular distribution within the cell.

Given the distinctive phenotypic changes observed for these drugs, the study was expanded to include several representatives from each drug class to determine if the correlation between the phenotypic parameters of cell length and DNA morphology and each drug's mechanism of action was robust. All molecules tested were quantified as to the percentage of cells that formed filaments, the average length of the filaments, the number of distinct DNA pieces identified per cell, and the variation in the size of DNA pieces per cell (Figure 4.5). Among the studied molecules, all were able to induce filaments, though both the percent of the cellular population and filament sizes varied significantly. Molecules that induce DNA strand breaks, including bacterial gyrase inhibitors (ciprofloxacin, nalidixic acid), topoisomerase II inhibitors (etoposide, doxorubicin, mitoxantrone), molecules that mimic ionizing radiation (MMS, EMS), bleomycin, and mitomycin C, all induced filamentous populations of over 50% of cells. Other DNA damaging molecules that induce DNA

crosslinking (Pt containing molecules and nitrogen mustards) were only able to induce filaments in less than 50% of cells (17% - 40%; average = 28% ± 11%). Transcription inhibitors (rifampicin, rifaximin) and translation inhibitors (tetracycline, kanamycin, chloramphenicol, and puromycin) induced filamentous populations of 25% - 30% and 23% - 29%, respectively. Notably, translation inhibitors had to be dosed as 10x MIC to observe filaments; all other drugs were dosed at 1x MIC. Under those conditions, the values for the filamentous populations for transcription (1x MIC) and translation (10x MIC) inhibitors were very close (standard deviation = 2.7%).

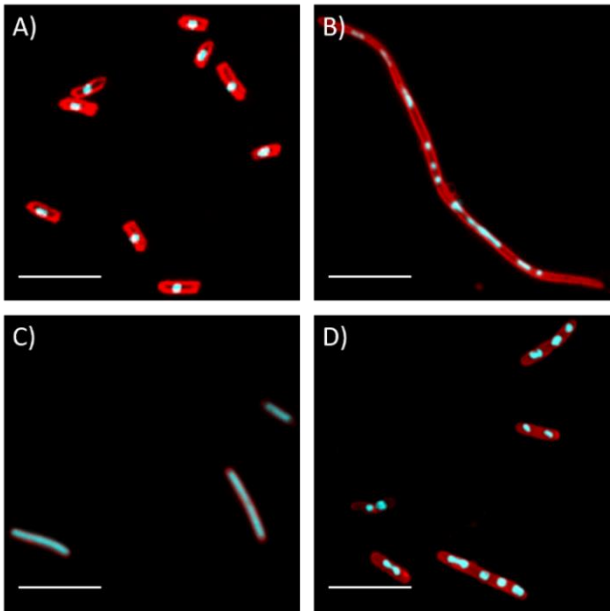

Figure 4.4 Distinctive DNA morphology is observed with treatments targeting different stages of protein production. A) Untreated; B) Nalidixic Acid; C) Rifampicin; D) Tetracycline. *E. coli* cells were treated at their MIC for 6 hours and then stained and imaged. FM4-64 (red) was used to stain the cell wall while Hoechst 33342 (cyan) was used for DNA. The stains were incubated with the cells for 15 minutes prior to imaging with wide-field epifluorescence microscopy. Scale bar represent 5 μm in all images.

The average filament size, as shown in Figure 4.5B, varies upon treatments with different molecules at biologically relevant concentrations. Both transcription inhibitors and translation inhibitors induced filaments with average length within 5-fold of normal cells. Molecules inducing DNA strand breaks resulted in filaments with average lengths that were over 10-fold that of normal cells, and the filaments induced by these molecules also have considerably wider distribution of filament size, resulting in correspondingly long whiskers in the box and whisker plot (Figure 4.5B; representative histograms shown in 4.5C). Treatments with DNA crosslinking molecules resulted in average filament sizes that were generally within 5-fold of normal *E. coli*, with oxaliplatin and chlormethine identified as outliers, inducing more filaments with increased length, and resultantly large error whiskers.

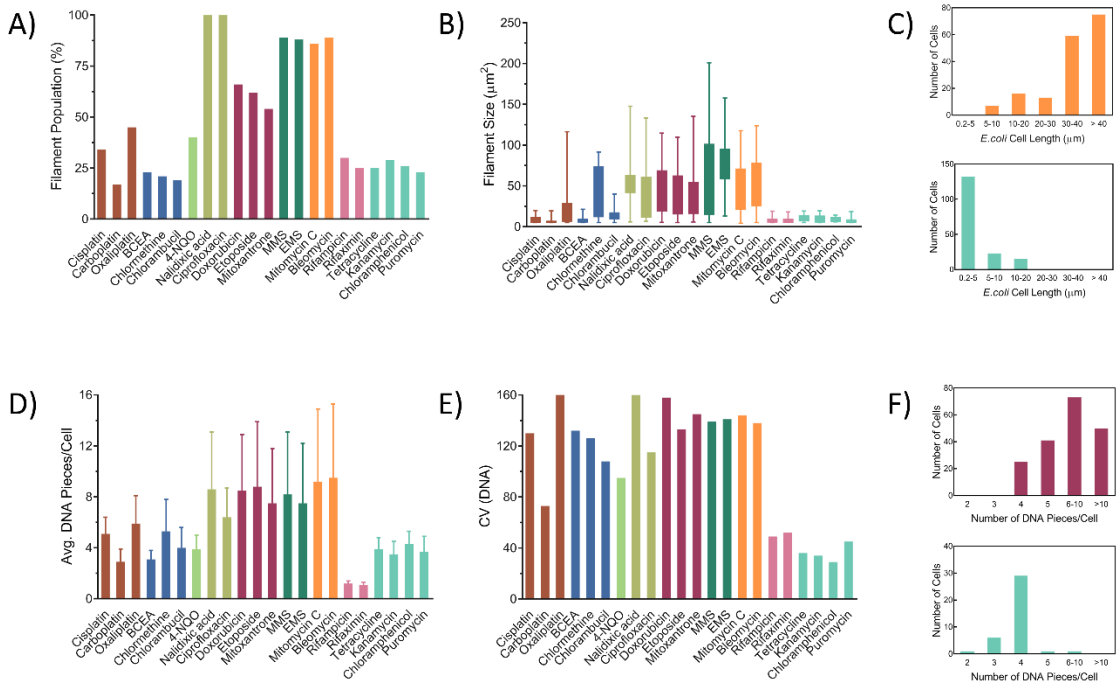

Figure 4.5 Phenotypic change observed in *E. coli* correlates with drugs' mechanism of action. Cells were treated with drugs at their MIC for 6 hours prior to imaging, translation inhibitors were dosed at 10 x MIC for phenotypic changes. To quantify the population distribution, multiple fields of view were analyzed for a total of 300-500 cells. **A)** Graph of filament population induced by different drug molecules; a cutoff of 5 μm was used for identification as a filament. **B)** The overall (in whisker)and major 50% (25% to 75%, in box) range of the E. coli filaments size. Error bars depict the maximum and minimum size of E. coli filaments. **C)** Histograms of *E. coli* cell length for DNA strand breakers (orange, top) and translation inhibitors (cyan, bottom). The histograms reflect the standard deviations associated with the data in **B)**. **D)** The average number of DNA pieces in each filament. Error bars depict the standard deviation, which is a reflection of the population distribution. **E)** The coefficient of variation (CV) for the size of the DNA piece in each filament. **F)** Histograms of the number of DNA pieces per *E. coli* for topoisomerase II inhibitors (maroon, top) and translation inhibitors (cyan, bottom). The histograms reflect the standard deviations associated with the data in **D)**. Molecules of diverse mechanisms are color coded as follows: ● Pt based DNA crosslinker; ● nitrogen mustard; ● oxidizing agent; ● bacterial gyrase inhibitor; ● topoisomerase II inhibitor; ● ionizing radiation mimicking agent; ● DNA strand breaker; ● transcription inhibitor; ● translation inhibitor.

The DNA material in the filaments was characterized by two phenotypic features: the average number of DNA pieces per filament (Figure 4.5D) and the degree of variation of the sizes of DNA pieces in the filaments, described as the "coefficient of variation" (CV) of the size of the DNA pieces (Figure 4.5E). Nearly all molecules resulted in the observation of multiple pieces of DNA in the filaments; the exception was transcription inhibitors, which resulted in single nucleoids per cell. DNA damaging molecules that induce strand breaks, in particular, produced the greatest number of DNA pieces in the filaments; there was also significant variation in the size of each

piece, resulting in high CV values. Fewer pieces of DNA were observed with other classes of DNA damaging molecules and translation inhibitors, as shown in Figure 4.5D and F.

All four translation inhibitors in the study produced DNA pieces that were condensed into similar size, resulting in very small CV values, as shown in Figure 4.5E; the DNA pieces were distributed at regular distances within the filaments. A histogram depicting the number of DNA pieces per cell is shown in 4.5F, which revealed that the vast majority of cells treated with translation inhibitors contain 4 nucleoids. DNA damaging molecules that work by various mechanisms, in contrast, all induced DNA pieces of irregular sizes, so the CV values for DNA piece sizes were above 50 or more (5.4E). There was also greater variation in the number of pieces of DNA from cell to cell, leading to larger standard deviations (5.4D) and histograms that show large populations of cells containing each 4, 5, 6–10, and >10 DNA pieces.

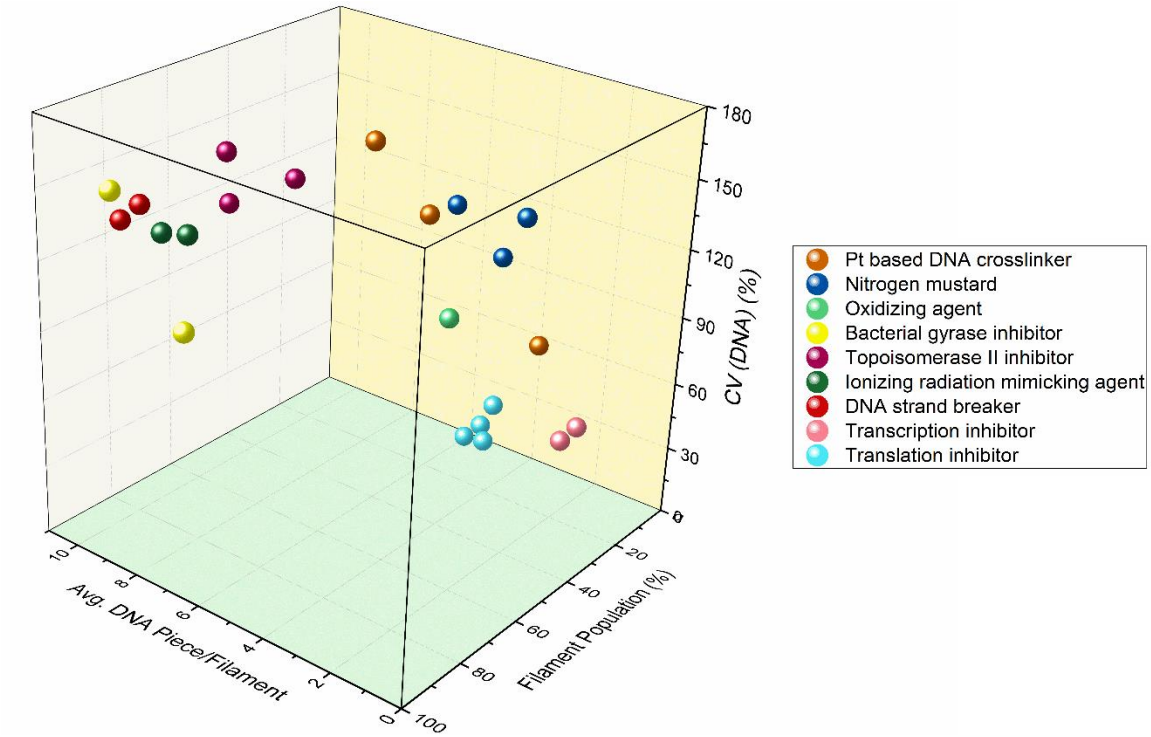

Figure 4.6. Distinguishing anticancer agents with different mechanisms based on phenotypic characteristics in *E. coli*. Cells were treated with molecules at their MIC for 6 hours prior to imaging. Translation inhibitors were dosed at 10 x MIC for analysis of phenotypic changes. The same phenotypic features are shown as used for Figure 4.5.

As each individual phenotypic feature does not fully provide the information needed to distinguish molecules with different mechanisms of action, a comprehensive analysis with multiple phenotypic features was used to generate a multidimensional scatter plot in Figure 4.6. The similarity in the phenotypic features observed upon treatments with compounds with the same

mechanism of action resulted in clustering in this 3D plot, as exemplified by all translation inhibitors; the transcription inhibitors formed a similarly tight cluster. Based on variation in phenotypic features, molecule that directly damage DNA formed two loosely clustered groups. The bacterial gyrase inhibitors, topoisomerase II inhibitors, DNA alkylating molecules that mimic ionizing radiation, and DNA strand breaking molecule bleomycin, formed one cluster group to the upper left of the cluster plot. Notably, mitomycin C, with a known mechanism of action involving DNA intrastrand and inter strand crosslinks, was also found in this cluster. This observation could be associated with the reported DNA double strand breaks and the involvement of DNA double strand break repair following mitomycin C treatment.[243, 244, 245] Another loose cluster formed containing the Pt based DNA crosslinking molecules, nitrogen mustard molecules, and oxidizing molecule 4-NQO.

4.6 Dose effects on the phenotypic profiling of DNA damaging molecules.

While it was possible to distinguish some mechanisms of action through the preceding analysis, only loose clusters formed for certain classes of molecules, indicating that additional parameters would be needed to obtain diagnostic information that correlated to specific mechanisms of DNA damage. Initial studies indicated that there were compound dose- and time-dependent effects on *E. coli* phenotypic features that might prove helpful to distinguish between different compound classes. Accordingly, a phenotypic profiling study was performed with three Pt-containing molecules (cisplatin, carboplatin, and oxaliplatin) at 0.1 x MIC, 1 x MIC, and 5 x MIC, and with three topoisomerase II inhibitors (etoposide, doxorubicin, and mitoxantrone) at 0.1 x MIC and 1 x MIC.

As shown in Figure 4.7, when dosed at different concentrations, distinct phenotypic features were observed for the studied molecules. Fewer *E. coli* cells formed filaments in response to treatments at the lower compounds dose, 0.1 x MIC, and the filaments were of much smaller size. As the drug concentration increased, the profiles were similar among the three Pt containing molecules, with a relatively steady increase in the filamentous population. However, the profile for the average filament size varied for oxaliplatin in comparison to carboplatin and cisplatin, with oxaliplatin forming filaments of the same size at both 1 and 5 x MIC. In contrast, both cisplatin and carboplatin exhibited a greater increase in filament length for the last two concentrations, from 1 to 5 x MIC, resulting in a greater relative increase in size vs. the 10-fold increase in concentration at lower doses (0.1 to 1 x MIC). This analysis suggests that there is a notable difference in the mechanism of action of oxaliplatin compared to the two other platin agents.

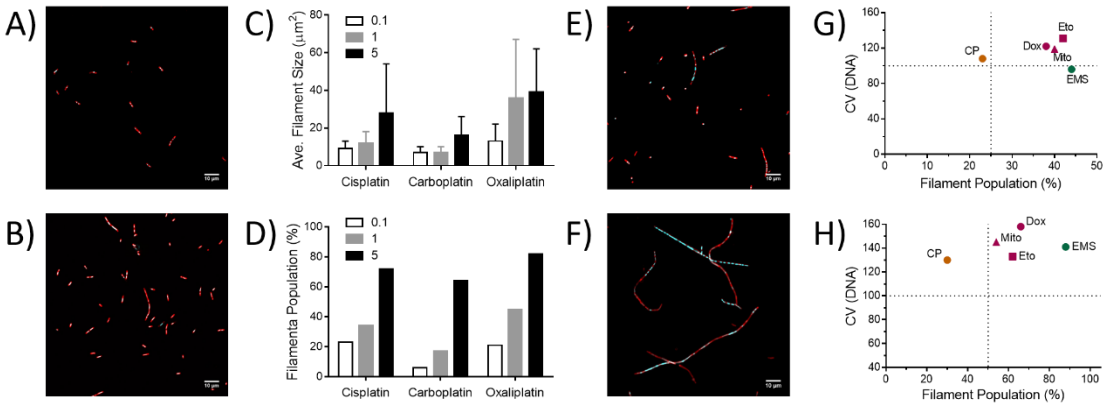

Figure 4.7 Drugs that damage DNA via different mechanisms of action can be distinguished using bacterial cytological profiling as a function of drug concentration. *E. coli* cells were treated with drugs for 6 hours before imaging and cytological profiling. **A)** Representative image of *E. Coli* treated with cisplatin at a dose corresponding to 0.1 x MIC and **B)** 1 x MIC. **C)** Plot of the average filament size and distribution for platinum drugs at 0.1, 1, and 5 x the MIC value. **D)** Plot of the population of filaments over 5 µm for the platinum drugs as function of MIC value. **E)** Image of *E. coli* treated with doxorubicin at 0.1 x MIC and **F)** 1 x MIC. Scatter plots of the filament population versus the CV for the DNA size in cells treated at **G)** 0.1 x MIC and **H)** 1 x MIC of different DNA damaging agents. The scale bar in all microscope images corresponds to 10 µm.

A dose effect study was also performed for three topoisomerase II inhibitors at 0.1 x MIC and 1 x MIC; higher doses were not possible due to the high cytotoxicity of these compounds in *E. coli*. Similar dose effects were observed on phenotypic features such as filament population, average filament size, and the number of DNA pieces per filament. The lower concentration led to smaller filamentous populations (ca. 70% vs. ca. 80%) and smaller filament size. The CV for DNA piece size, however, remained similar at the two treatment conditions.

The three molecules were compared to two other DNA damaging agents with different mechanisms: cisplatin, a DNA crosslinker, and EMS, an alkylating agent that can result in multiple strand breaks and is used as a ionizing radiation mimic.[246, 247] All five DNA damaging compounds have similar CV values (as is the case for all the DNA damaging agents; see Figure 4.5E). When examined in 2D scatter plots of filament population and CV (DNA), the three topoisomerase II inhibitors formed a tight cluster that could be easily separated from cisplatin at both dose concentrations. The effects of EMS could be distinguished from the topo II inhibitors when the filament population was compared at both 0.1 x MIC and 1 x MIC; EMS produced a larger shift (from ca. 45% to 90%) over this concentration range than the topo II inhibitors (from ca. 40% to 60%). This analysis suggests that the phenotypic profiling of DNA damaging molecules can be used to identify compounds with the same mechanism of action and distinguish them from others that appear similar but have different mechanisms by comparison of suitable features over a dose range.

4.7 Discussion.

E. coli have been extensively used as model systems in the discovery and mechanistic studies of antibiotics[236, 235, 115], but are not usually considered in studies for the mechanisms of action for anti-cancer agents. The results from our phenotypic profiling, however, prove it is feasible to use this simple bacterial system to rapidly elucidate mechanisms of anticancer agents. The combination of phenotypic profiling features distinguishes DNA damaging agents, transcription inhibitors, and translation inhibitors; furthermore, anticancer agents inducing different types of DNA damage can be distinguished.

Previously, cytotoxic effects in *E. coli* have been reported for FDA approved Pt-based agents and some other anti-cancer agents[238a, 238b, 248]. For our approach it was essential to understand the cytotoxicity correlation in mammalian cells and *E. coli* cells. To our satisfaction, all the studied agents showed cytotoxic effects, and the cytotoxicity in *E. coli* is usually within one log range of that in mammalian cells (Figure 4.1). This correlation validates the proposal to study anti-cancer agents with specific mechanisms in *E. coli, and* is consistent with Rosenberg's original experiments and Lippard's findings for some more recent Pt compounds[239].

The colony formation assay and study of protein synthesis inhibition study were used to further understand the correlation between the mechanism of action and cytotoxic vs. cytostatic effects. In the colony formation study, most DNA damaging molecules showed cytotoxic effects, with inhibition of the formation of any colony after treatment at a biologically relevant concentration (the MIC). Transcription and translation inhibitors, however, showed mainly cytostatic effects, resulting in 20 – 40% of colony formation with treatment at the same condition. Among the categories of molecules being studied, DNA damaging agents and transcription inhibitors require higher concentration to achieve inhibition of protein production, while translation inhibitors exhibited lower IC_{50} values for translation inhibition than that needed for growth inhibition (resulting in negative values for the log IC_{50} ratio shown in Figure 4.2). This allows for identification of translation inhibitors. Combining these simple studies, the studied molecules were categorized into groups by mechanisms for DNA damage, transcription inhibition, and translation inhibition, which agrees with the known individual mechanisms of the molecules.

Further studies of single cell and DNA morphological changes, using statistical evaluation, offered clearer separation of molecules with various mechanisms. Observations of DNA spreading along the length of the cells in response to transcription inhibition and the compact DNA pieces of similar size regularly distributing in the cell for translation inhibition were consistent with previous reports[249, 117]. DNA damaging agents, in sharp contrast, induced generally larger population of *E. coli* cells that were filamentous, and the filament lengths exceed those of cells treated with

transcription inhibitors and translation inhibitors (Figure 4.4). The filaments induced by DNA damaging agents also had highly variable number of DNA pieces per cell, and with much more irregular sizes, which, in combination with the filament population and average filament size, created different phenotypic profiles of *E. coli* in response to treatments of molecules with different mechanisms of DNA damage. A key feature of our analysis is to use biologically relevant concentrations (generally at MIC) and to recognize the effect of drug concentration on phenotype. We found that both transcription inhibitors and translation inhibitors can be distinguished from DNA damaging molecules as shown in both a 2D bar graph (Figure 4.5) and the 3D scatter plot (Figure 4.6) utilizing the key phenotypic features. Transcription inhibitors, rifampicin and rifaximin, are closely cluster in the 3D scatter plot, and feature smaller filament population, small average filament size, and generally a single piece of DNA spreading throughout the entire filament. All four translation inhibitors, including three antibiotics and one mammalian and bacterial translation inhibitor, puromycin, were distinguished from other molecules as they exhibited more regularly sized and evenly spaced DNA pieces in each filament, which is reflected by the smaller CV values. The clustering of puromycin with other antibiotics (tetracycline, kanamycin, and chloramphenicol) supports the capacity of *E. coli* phenotypic profiling to study mammalian translation inhibitors. DNA damaging molecules, depending on their individual mechanisms of actions, were separated into different groups as they induce 1) different types of DNA damage and 2) DNA repair mechanisms. DNA double strand breaks can be induced by direct interactions with molecules such as bleomycin, or molecules that alkylate DNA and lead to subsequent DNA damage repair processes generating double strand breaks. Ionizing radiation mimicking molecules methyl methanesulfonate (MMS) and ethyl methanesulfonate (EMS), and DNA strand breaking molecules mitomycin C directly alkylate DNA and induces base excision repair (BER) and nucleotide excision repair (NER); these repair processes can lead to secondary DNA damage which is usually double strand break. Another major source of DNA double strand break is the failure of re-ligation process of type II DNA topoisomerase as a result of interference with the enzyme by type II DNA topoisomerase inhibitors. Bacterial gyrase inhibitors ciprofloxacin and nalidixic acid, and topoisomerase II inhibitors doxorubicin, etoposide, and mitoxantrone all induce DNA double strand breaks through this mechanism. DNA double strand breaks induced by the antitumor antibiotics bleomycin is mainly through reactive oxygen species associated DNA cleavage. DNA damage induced by these molecules requires double strand break repair which is homology directed repair (HDR) due the lack of non-homologous end joining (NHEJ) in *E. coli*[250]. Topoisomerase II inhibitors (doxorubicin, etoposide, and mitoxantrone), bleomycin, and mitomycin C have been commonly used in cancer chemotherapy, and the relatively similar phenotypic features observed

after treatments with these molecules and bacterial gyrase inhibitors (ciprofloxacin and nalidixic acid) offer insights that molecules inducing DNA strand breaks in mammalian cells can also induce DNA damage and repair responses in *E. coli* of the same type. Other molecules that mainly induce covalent adducts with DNA bases include nitrogen mustard compounds (chlorambucil, chlormethine, and BCEA), and Pt-containing DNA crosslinkers (cisplatin, carboplatin, and oxaliplatin). The DNA damage induced by these molecules is usually repaired by base excision repair (BER) and nucleotide excision repair (NER)[238d, 251]. A comprehensive analysis of phenotypic features including filament population, average filament size, and DNA morphology show that DNA damaging molecules inducing double strand breaks and HDR are separated from DNA damaging molecules that mainly induces DNA adduct formation and BER and NER repair. Slightly different is a molecule that induces direct oxidative damage, 4-NQO, which also showed a similar phenotypic profile to those requiring BER and NER as major repair mechanism[252].

Thus far, there have been three Pt-containing agents approved by the FDA for cancer chemotherapy, and their therapeutic effects are considered to be associated with DNA damage induced from DNA crosslinking. In a dose-dependent phenotype analysis of the three Pt-containing molecules, however, we are surprised to discover that oxaliplatin showed phenotypic features that are different from cisplatin and carboplatin. While it has long been assumed that all Pt agents share the same mechanism of action, a previous report showed that oxaliplatin induces altered DNA damage responses in *E. coli* compared with cisplatin and carboplatin[45]. In a recent report by Lippard and Hemann, an RNAi signature study showed mechanism of oxaliplatin may involve ribosome toxicity over DNA damage[44]. The shifted oxaliplatin phenotypic profile we observed in *E. coli* provided insights into a novel mechanism of oxaliplatin before it was demonstrated in mammalian cells. This study highlights that compounds with potentially multiple mechanisms of action can be distinguished from similar compounds that have fewer biological effects.

Similar dose dependent studies were performed with topoisomerase inhibitors that induce DNA double strand breaks. As expected, some phenotypic features such as the filament population were dose dependent at 0.1 x MIC and 1 x MIC. However, other phenotypic features like the CV for DNA piece size showed consistency over the dose range. We propose that this consistency in DNA morphology indicates this is a key phenotypic feature associated with the compounds' mechanisms of action. The phenotypic feature profiles for the topoisomerase inhibitors were differentiable when compared with the DNA crosslinking agent cisplatin and the ionizing mimicking molecule EMS at 0.1 x MIC and 1 x MIC, suggesting the phenotypic profiling results are consistent across dose points for molecules with the same mechanism of action, but differ when the mechanisms of action are different. This provides separation of these molecules over a wide

dose range and provides another simple method to differentiate molecules with similar phenotypic features at a single dose point.

Research on morphological features of bacteria involving microscopy techniques have been performed in antibiotic research, but it is only recently that compilation and systematic analysis of various phenotypic features of cell and DNA morphology have been performed[116]. Reports from Pogliano prove that phenotypic features in *E. coli* are associated with the mechanisms of action for antibiotics, and the profiling can be used to classify anti-bacterial agents by their mechanisms. Our research includes commonly used chemotherapeutic agents that are usually studied only in mammalian cells and proves that when the mechanisms of actions involve general steps of the central dogma, it is feasible to study and identify the mechanism in *E. coli*. This would offer much faster insights into the possible mechanism of action and help to direct subsequent studies. As prokaryotic cell system lack organelles and biological processes exclusively found in mammalian cells, it is impossible to study those targets in *E. coil.* This disadvantage, however, could also be used as a fast method to discover if the mechanism involves common targets in both cell types, or rather only mammalian cell-exclusive targets, leading to rapid elimination of several potential mechanisms of action.

4.8 Materials and Methods

Cloning and expression of Dendra2 in E. coli. The gene encoding the photoconvertable protein, Dendra2, was cloned into a pCWori plasmid modified to contain an N-terminal 6x histidine tag with multiple restriction enzyme cloning sites.[253] The pCWori-dendra2 plasmid was transformed into BL21(DE3) competent cells and selected on carbenicillin containing LB-Agar plates. A single colony was selected and cultured in Luria Broth (LB) at 37°C with 180 rpm shaking. The density of the *E. Coli* was calculated using the equation OD_{600} of 1.0 = 8 x 10^8 cells/ml. (http://www.genomics.agilent.com/biocalculators/calcODBacterial.jsp)

Cytotoxicity determination. BL21(DE3) cells transformed with pCWori-Dendra2 plasmid were plated in M63 minimal medium at 4 x 10^6 cells per well in a 96 well flat bottom transparent tissue culture treated plate (Greiner Bio One). Compounds were added to the *E. Coli* such that the final concentration ranged from 0 - 300 µM. The cells were incubated for an additional 16 hours in an incubated shaker at 180 rpm and 37 ˚C. After 16 hours, the cell density was measured as described above. The OD_{600} values were normalized to the untreated *E. coli* cell control and fitted to a sigmoidal dose response equation using GraphPad Prism 6.02 to determine the IC_{50} values. To obtain the minimal inhibitory concentration (MIC), the OD_{600} values were fitted to the model published by Lambert et al. using GraphPad Prism 6.02.[185]

Protein synthesis and degradation measurements in E. coli with Dendra2. BL21(DE3) cells transformed with pCWori-Dendra2 were cultured in LB medium to an OD_{600} of 0.8. Cells were pelleted, the LB removed, the cells resuspended in M63 minimal medium, and induced with 0.5 mM Isopropyl β-D-1-thiogalactopyranoside (IPTG) for 3 hours at 37 °C with 180 rpm shaking. Photoconversion of Dendra2 was carried out with a 405 nm LED flood array (Loctite, 0.6mW) with a total light exposure time of 2 minutes. Cells were then plated in 96 well plates at 6×10^7 cells per well. Green and red emission was measured immediately after photoconversion using a SpectraMax Multiwell Plate Reader (Molecular Devices) for a baseline evaluation of Dendra2 protein (t = 0 hours). For the green emission, an excitation wavelength of 491 nm and an emission wavelength of 538 nm were used; for the red emission, the excitation wavelength was 544 nm and the emission wavelength was 590 nm. Compounds were then added to the cells at concentrations ranging from 0 to 300 μM. The cells were incubated for an additional 16 hours before the green and red emission was measured again to quantify the change in protein synthesis due to compound treatment (t = 16 hours). The average fluorescence ratio of green/red at t = 0 hour and t = 16 hours was calculated, the values were normalized, and the data were fitted to a sigmoidal dose response using GraphPad Prism 6.02.

E. coli colony formation assay. BL21(DE3) cells transformed with pCWori-Dendra2 were cultured in LB medium to an OD_{600} of 0.08. Cells were resuspended in M63 minimal medium and plated at 3×10^8 cells per well in 24 well flat bottom transparent tissue culture treated plates (Greiner Bio One). Cells were dosed at MIC for each compound and cultured for 6 hours in an incubator shaker set to 37 °C and 180 rpm. The OD_{600} was measured for each treatment condition followed by the removal of culture that contained ca. 500 cells. Cells were pelleted by centrifuging at 8,600 xg for 2 minutes and the media was removed. Cells were then washed twice in 1 mL of sterile filtered PBS by centrifuging at 8,600 x g for 2 minutes, and the PBS was removed. Cells were resuspended in 50 μL of M63 medium and spread on agar coated wells prepared in 6 well plates. The agar plates were incubated at 37 °C for 16 hours. Images of the colonies were obtained using a ChemiDoc imager (Bio-Rad). Data analysis was done with object analysis function in ImageJ to quantify the number of colonies for each treatment condition, and normalized to the untreated control.

E. coli filamentous growth. E. coli BL21(DE3) cells transformed with pCWori-Dendra2 were cultured in LB medium to an OD_{600} of 0.08. Cells were then resuspended in M63 minimal medium and plated at 3×10^8 cells per well in 24 well flat bottom transparent tissue culture treated plates (Greiner Bio One). IPTG was added at a final concentration of 0.5 mM, followed by the

addition of compounds at desired concentrations. The cells were cultured for 6 hours in an incubator shaker set to 37 °C and 180 rpm.

E. coli cell imaging. After compound treatment, the OD_{600} was measured for each treatment condition followed by the removal of culture that contained 4 x 10^5 cells. The cells were centrifuged at 8,600 xg for 1 minute, aspirated, and washed twice with 1 mL of sterile filtered PBS with centrifugation at 8,600 xg for 1 minute, and PBS was removed. Cells were then resuspended in 150 µL of sterile filtered MilliQ water, and plated on a poly-D-Lysine (100 µg/mL) coated 1.5# cover glass bottom 35 mm culture dish. Cells were allowed to settle on the culture dish for 1 hour before gently rinsing with 150 µL of PBS. FM4-64 and Hoechst 33342 were added to the cells at concentrations of 5 and 10 µg/mL respectively. The cells were incubated at room temperature and protected from light for 20 minutes. The solution was removed from the cells followed by rinsing with 150 µL of PBS. Imaging was carried out on an Olympus IX2-RFAEVA-2 microscope or a Nikon A1R+ confocal microscope. For the Olympus microscope, a 60 x oil or a 100 x oil objective was used. Hoechst 33342 was visualized using the excitation filter BP 360-390 (Chroma, Bellows Falls, VT, USA), and emission filter HQ470/30 M (Chroma, Bellows Falls, VT, USA). To view Dendra2 (green), a 473/10 nm BrightLine® single-band bandpass filter FF01-473/10-25 (Semrock, Rochester, NY, USA) was used as the excitation filter, and a 525/50 nm BrightLine® single-band bandpass filter, FF03-525/50-25 (Semrock, Rochester, NY, USA) was used as the emission filter. FM4-64 was visualized with a HQ 550/30 (Chroma, Bellows Falls, VT, USA) as the excitation filter, and a 664 nm EdgeBasic long-pass edge filter, BLP01-664R-25 (Semrock, Rochester, NY, USA) as the emission filter. The imaging channel sequential was set as FM4-64, Dendra2 (green), and Hoechst 33342. For each single field of view, a 1024 x 1024 pixel image was taken. Imaging on the Nikon A1R+ confocal microscope was performed with a 100 x oil objective and the zoom in factor was 1 x. Hoechst 33342 was visualized on the 405 nm channel with 5% laser excitation and 100% gain, offset was -25% to -50%. Dendra2 (green) was viewed on the 488 nm channel with 1% laser excitation and 25% gain, offset was -25% to -50%. FM4-64 was visualized on the 561 nm channel with 5% laser excitation and 50% gain, offset was -25% to -50%. Imaging channel sequential was set as FM4-64, Dendra2 (green), and Hoechst 33342. For each single field of view, a 1024 x 1024 pixel image was taken, and a 3 x 3 image stitch was taken using the same setting.

Analysis of E. Coli images for filaments and DNA morphology quantification. Images were processed and analyzed using the ImageJ software. For each single image, to analyze cell filaments, the threshold of FM4-64 channel was adjusted to match the original image, and any particles smaller than 0.2 μm^2 were excluded from measurements; size exclusion was only applied in FM4-64 channel for cell size and number analysis. All measurement results from "Analyze Particles"

were saved in a Microsoft Excel file. The filament population (%) was calculated as the percentage of all particles larger than 5μm^2, and the average filament size and standard deviation of filament size was also calculated using the statistical function of Microsoft Excel. To analyze DNA morphology, the threshold for Hoechst 33342 channel was adjusted to match original image. The ROI manager was used to match the DNA with the cell, and a certain filament was selected and set as region of interest (ROI). Then the number of DNA pieces of each filament was obtained by "Analyze Particles". In each treatment condition, 30-50 filaments were selected and analyzed. All measurement data were saved in Microsoft Excel files. The average DNA pieces in filaments were calculated by dividing the number of all DNA pieces by number of filaments. The average size of DNA pieces, and standard deviation of DNA pieces, were also calculated with the statistical function of Microsoft Excel. To obtain the magnitude of variation in sizes of DNA pieces, the coefficient of variation (CV) was calculated by dividing the standard deviation of DNA pieces by the average size of DNA pieces.

Chapter 5. Elucidation of the mechanism of action of Ru(II) polypyridyl compounds containing hydroxyquinoline (HQ) ligand

RESEARCH CONTRIBUTIONS

The research presented in this chapter is completed with help and support of other scientists. Compounds synthesis, characterization, chemical and physical property studies were completed by Dr. Dmytro Havrylyuk and Mr. Brock Howerton. The cytotoxicity study of BODIPY conjugated compounds and generation of HEK cell lines stably expressing different organelle markers were completed by Dr. David Heidary. The pCWori plasmid DNA and Dendra2 gene sequence was kindly provided by Dr. David Heidary.

5.1 Introduction.

The small molecule 8-hydroxyquinoline (HQ) and its derivatives have a broad variety of medicinal applications including anticancer, antibacterial, and antifungal effects.[254, 255] In the past few decades, research interest in HQ and its derivatives has been focused on both developing novel chemically modified molecules and understanding the mechanism of actions of HQs.[256] The presence of nitrogen and oxygen atoms in the HQ makes it a suitable bidentate chelating agent for metals.[256] Free HQ ligands can thus bind endogenous metals and aid in their transport, or alternatively, can form metal complexes with new properties.

The metal chelating property of HQ and derivatives have raised research interest in synthesizing metal complexes containing HQs as ligands. Many transition metal compounds bearing HQ ligands have been synthesized and studied for their biological activities including antimicrobial and anticancer properties. Liu and co-workers have reported ruthenium polypyridyl compounds containing HQ ligand showing antitumor activities.[257] A series of antitumor metal compounds containing HQ ligands with platinum (II), copper (II), and iron (III) as metal centers have been reported by Hong Liang and co-workers.[258, 259, 260] A gallium (III) compound, KP46, containing the HQ ligand (tris(8-quinolinolato)gallium) has been successfully tested in renal cancer in a Phase I clinical trial.[261]

Efforts have also been made to understand the mechanisms of actions for the metal compounds containing HQ and derivative ligands. Given the fact that classical metal compounds approved by the FDA for chemotherapy are mostly DNA damaging agents, much of the previous and current research focused on the nucleic acid interacting ability of metal compounds with HQ ligands. Liang and Alemán have both reported DNA binding properties and associated cytotoxicities of zinc and gold compounds with HQ ligands.[262, 263] Studies on ruthenium compounds with HQ ligand by Liu, however, indicate alternative mechanisms that are not DNA related, but rather through interactions with basic fibroblast growth factors (bFGF) and inhibition of ERK and Akt pathways.[257]

It has been previously reported by our group that by chelating HQ ligands with ruthenium metal centers, the cytotoxicity of the HQ compounds is significantly increased in cancer cells.[264] The mechanism of action of Ru(II) HQ compounds, however, remains unclear. In addition to understanding of the structure activity relationship (SAR), it is also important to elucidate the functional targets and mechanisms of actions to improve the chemical design of HQ compounds, and to increase the possibility of the HQ compounds serving as potential candidates for cancer chemotherapy.

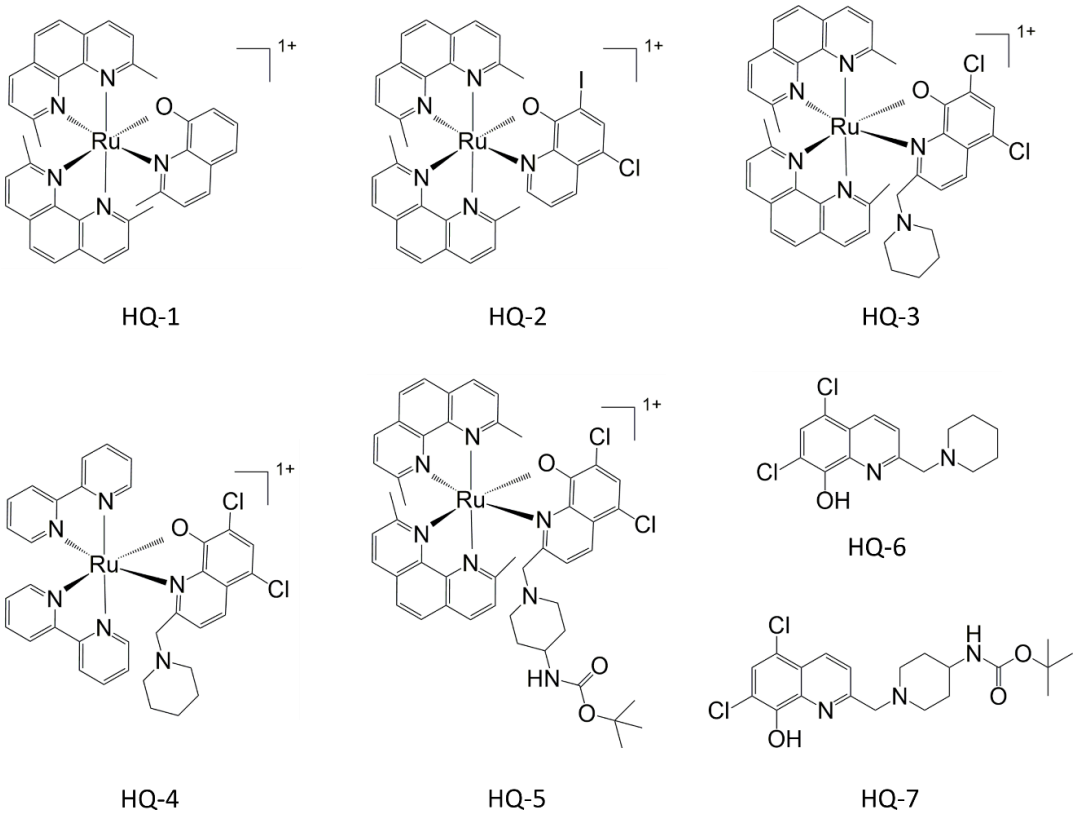

Chart 5.1 Structures of compounds HQ-1 to HQ-7.

5.2 Cell death kinetics and uptake of HQ compounds in mammalian cells.

Cell death kinetics and cellular accumulation were studied in human promyelocytic leukemia HL60 cells. As shown in Figure 5.1, both Ru(dmphen)$_2$-8-hydroxy-2-methylquinoline (**HQ-1**) and Ru(dmphen)$_2$-clioquinol (**HQ-2**) were able to induce > 50% and > 90% cell death in 24 hours for **HQ-1** and **HQ-2** respectively. In a washout study, HL60 cells were treated with a certain concentration (20 μM) of both compounds for specified periods of time (3, 6, 12, 24 hours), followed by removal of compound and incubation with compound free media for 72 hours before cell death was quantified. In all treatment conditions, over 95% of cell death was observed, even with only 3 hours of treatments with **HQ-1** and **HQ-2**. A detailed washout study performed with **HQ-1** examining the effects of decreased treatment time showed that 30 minutes of **HQ-1** treatment lead to 90% of cell death. This suggests that treatment of 30 minutes or less with HQ compound is able to induce the maximum cytotoxic effects.

As the cytotoxicity could be affected by the cellular accumulation of compounds, ruthenium content was determined using inductively coupled plasma optical emission spectrometry (ICP-OES) in HL60 cells (Figure 5.1C). After 6 hours of treatment with **HQ-1**, the cellular

ruthenium content level was 1.18 x 10^9 ruthenium atoms per HL60 cell, which was 10-fold more than the ruthenium content in cells treated with $Ru(bpy)_2dmbpy$ (compound **1**), a light-activated Ru(II) polypyridyl compound described in Chapter 3. The ruthenium content level increased to 1.68 x 10^9 ruthenium atoms per HL60 cell after 20 hours; treatment of **HQ-1**, comparing to 1.30 x 10^8 ruthenium atoms per HL60 cell in compound **1** treated cells. The cellular metal content study revealed the fact that **HQ-1** accumulates in HL60 cells much faster than compound **1**, and this fast accumulation primarily occurs during the first 6 hours after treatment.

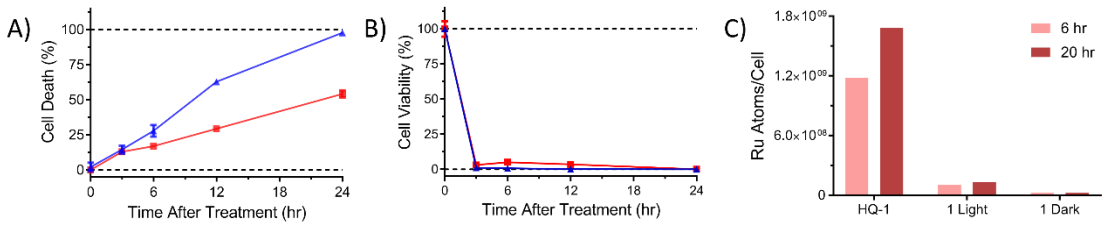

Figure 5.1 HQ compounds induce quick cell death and fast cellular accumulation in HL60 cells. In both A) and B), **HQ-1** is represented in red, and **HQ-2** is represented in blue. A) Time dependence for cell death. HL60 cells were treated with 2 μM of compounds, and cell death was determined by Trypan Blue staining of membrane corruption at various time points. B) Wash out experiment. HL60 cells were treated with 2 μM of compounds, and after certain periods of time (3, 6, 12, 24 hours) the cells were washed and incubated in compound free media. Cell death was determined 72 hours later by resorufin conversation. C) Relative metal uptake. HL60 cells were treated with 20 μM of compounds, after 6 hour and 20 hour, cells were isolated and Ru(II) metal content was determined with ICP-OES.

The rapid cellular accumulation of **HQ-1** could possibly contribute to the fast cell death and the very short treatment time needed to exhibit maximum cytotoxicity. Given the lack of direct correlation of cytotoxicity values to measured ruthenium level in the cell (IC_{50} values in Table 3.3, and Table S4.1 in Appendix), the shift in cell death kinetics can't be solely attributed to elevated cellular uptake or different uptake kinetics. Thus, the cytotoxicity of **HQ-1** and **HQ-2** likely involves a mechanism of action where the two compounds have different potencies. Though it can be predicted that other HQ compounds likely accumulate in cells at similar level, further studies on cellular uptake of other HQ compounds listed in Table S4.1 is to be done in future work.

5.3 HQ compounds induce apoptosis in mammalian cells through a p53 independent pathway.

Apoptosis induced by **HQ-1** and **HQ-2** was confirmed by immunoblotting in the human alveolar adenocarcinoma A549 cell line and flow cytometry in HL60 cell line (see Figure 5.2). A549 cells were used for the immunoblot analysis rather than HL60 cells because HL60 cells are naturally p53 deficient and therefore A549 cells were used to study p53 related mechanism.Cells at early apoptotic and late apoptotic phases were determined in HL60 cells by propidium iodide

(PI) and fluorescein isothiocyanate (FITC)-Annexin V staining. The cells positively stained with FITC-Annexin V but not PI are characterized as early apoptotic, while cells positively stained with both PI and FITC-Annexin V are identified as late apoptotic cells, and therefore can be distinguished from the viable cells that are not stained by either of the fluorophore. As shown in Figure 5.2B and C, treatment with **HQ-1** didn't induce significant apoptosis at 3 hour; by 8 hour, there were 10% of cells at early apoptotic phase and 5% of cells at late apoptotic phase, similar to the untreated control. These number increased to 25% and 40% at 16 hour. In **HQ-2** treated cells, a similar trend was observed; after 8 hours of treatment, there were 6% of early apoptotic cells and 7% of late apoptotic cells, while at 16 hour, 20% of early apoptotic cells and 43% of late apoptotic cells were observed. This flow cytometry determination of apoptotic cells over 16 hours after treatment confirmed that the cytotoxic effects happen quickly after HQ compound treatments.

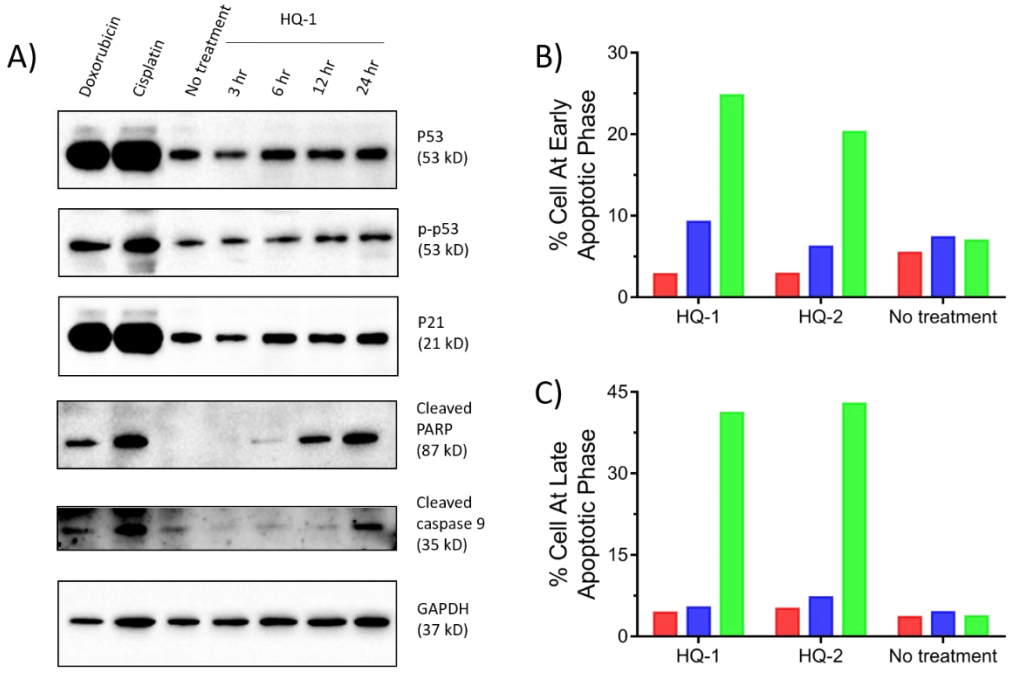

Figure 5.2 HQ compound induces apoptosis in cancer cells through p53 independent pathways. A) A549 cells were treated with 2 μM of HQ-1 for specific periods (3, 6, 12, and 24 hours respectively); cisplatin (20 μM) and doxorubicin (2 μM) at 24 hours of treatment were used as controls. GAPDH was used as loading control. HL60 cells were treated with 2 μM of HQ compounds for specific periods (3, 8, and 16 hours) before analysis by flow cytometry. Cells with positive FITC-Annexin V staining and negative PI staining were identified as early apoptotic cells as in B); cells with both positive FITC-Annexin V and PI staining were identified as late apoptotic cells as in C). Red, 3 hour; blue, 8 hour; green, 16 hour.

Hallmarks of apoptosis such as PARP and caspase 9 cleavage were observed by immunoblotting in A549 cells as early as 12 hours. The cleavage of PARP and caspase 9 indicate the executionary phase of intrinsic apoptosis downstream of mitochondria permeabilization and release of cytochrome c into cytoplasm. Interestingly, no significant changes in p53 expression and phosphorylation were seen in A549 cells, and p21 expression was not changed as well. This result suggests the cytotoxicity and apoptosis induced by **HQ-1** is not through p53 dependent pathways, which play central roles in cellular stress responses. In contrast, the commonly used chemotherapeutic agents doxorubicin and cisplatin both induced dramatic increases in p53 and p21 expression and p53 phosphorylation. This result indicates the HQ compounds likely have different mechanism of action compared with doxorubicin and cisplatin as they induce alternations in signaling pathways that are key components of cellular activities.

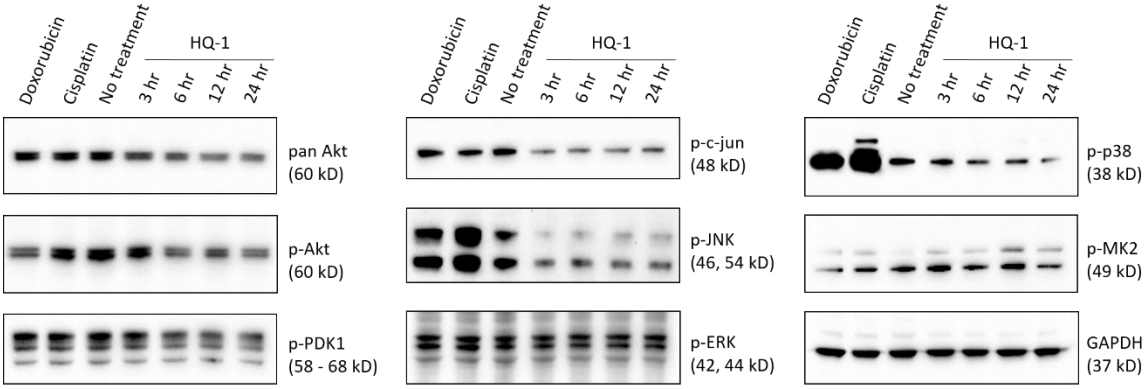

Figure 5.3 HQ compound induces downregulation of Akt pathways in A549 cells. A549 cells were treated with 2 μM of HQ-1 for specific periods (3, 6, 12, and 24 hours respectively). Cell lysates were made for immunoblotting, with cisplatin (20 μM) and doxorubicin (2 μM) at 24 hours of treatment used as controls. GAPDH was used as loading control.

Detailed studies on cell signaling pathways involved in cellular stress response, cell growth, and proliferation by immunoblotting in A549 cells revealed that HQ compounds induce altered signaling pathways (Figure 5.3). Compared with doxorubicin and cisplatin, **HQ-1** induced down regulation of both JNK and c-jun phosphorylation, suggesting the JNK mitogen-activated protein kinases (MAPKs) pathway was inhibited upon treatment of **HQ-1**; the treatment also didn't activate p38 phosphorylation, suggesting the p38 MAPK pathway was not activated in response to **HQ-1** treatment; ERK phosphorylation remained at basal level for all treatment conditions. These three MAPKs pathways are mainly responsible for cell proliferation, survival and apoptosis regulation in response to cellular stress.[265, 266, 267] Another significant change in signal transduction was down

regulation of the Akt pathway upon treatment of **HQ-1**. Both Akt expression (pan Akt) and the phosphorylation (p-Akt) were inhibited as early as 6 hours after treatment of **HQ-1**, the same inhibition was also observed for PDK-1 phosphorylation, the upstream activator of Akt pathway, proving that down regulation of the Akt pathway occurs in response to **HQ-1** treatment. The Akt pathway is a key signal transduction pathway in cell survival and growth by regulating a wide range of downstream signals.[268, 269, 270] The down regulation of the Akt pathway by **HQ-1** reveals that the mechanism of action is associated with the inhibition of cell growth and proliferation activities. Notably, similar inhibition of the Akt pathway was also reported by Jie Liu *et al*., with inhibition of ERK pathway.[257] These results also suggest that the mechanisms of HQ compounds possibly involve Akt inhibition to promote cell death.

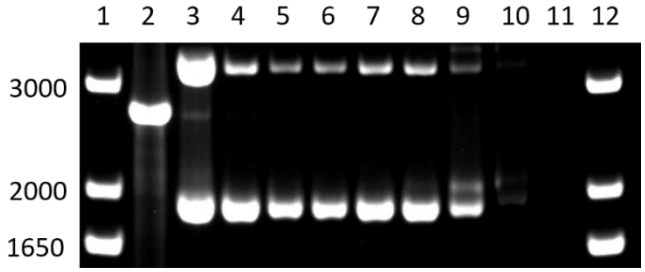

Figure 5.4 DNA gel electrophoresis of compound HQ-1. Agarose gel electrophoresis of pUC19 plasmid treated with compound HQ-1. Lane 1, and 12: molecular weight marker; Lane 2: double strand breaks caused by EcoR1 (linear DNA); Lane 3: single strand breaks caused by $Cu(phen)_2$ reaction (relax circle); Lane 4 – 11, DNA treated with compounds dosed at increasing concentration (2-fold dilution per lane) from 0 to 500 μM.

5.4 Cytotoxicity of HQ compounds is not associated with cell membrane disruption or DNA damage.

The rapid cell death kinetics and cellular ruthenium accumulation raised the question if the HQ compounds exhibit cytotoxic effects through corruption of the cell membrane. Both mammalian cells and *E. coli* cells were studied to understand if the cell membrane was compromised with HQ compound treatment. In the cell death kinetics studies, HL60 cells were stained with Trypan Blue which is commonly used in the dye exclusion test as it enters the cells that are permeable during apoptosis or necrosis and is excluded from viable cells. Upon treatment with compound **HQ-1** and **HQ-2**, the dead cells that were stained as dark color by Trypan Blue had intact membranes. In a microscopy study of human embryonic kidney (HEK) cells to be discussed in detail in later sections (Figure 5.9 – 5.13), the lack of fluorophore-conjugated HQ compounds highlighting the cell membrane also suggested that the cell membrane is not the primary target of HQ compounds in mammalian cells. In the bacterial cytological profiling studies in *E. coli* used to further understand the mechanism of action of the HQ compounds, it was also observed the *E. coli*

cells were intact after HQ compounds treatment (Figure 5.6). Studies in both eukaryotic cells and prokaryotic cells have demonstrated the HQ compounds don't act through disrupting the cell membrane as a detergent.

It has been reported that metal complexes bearing HQ ligand may interact with DNA as intercalators[271, 272] or alkylating agents[273]; a previous study by Glazer lab members Mr. Brock Howerton and Dr. David Heidary, however, proved the ruthenium compound, **HQ-2**, didn't affect the function of DNA in the process of central dogma.[264] DNA gel electrophoresis also confirmed there was no visible DNA mobility shift at the cytotoxic concentrations (the IC_{50} in HL60 and *E. coli*) observed with **HQ-1** treated pUC19 plasmid DNA. In fact, the concentrations needed for **HQ-1** to induce a DNA mobility shift was significantly higher than the concentrations to induce cytotoxic effects in both eukaryotic and bacterial cells, suggesting DNA was not the target involved in HQ compounds' activity.

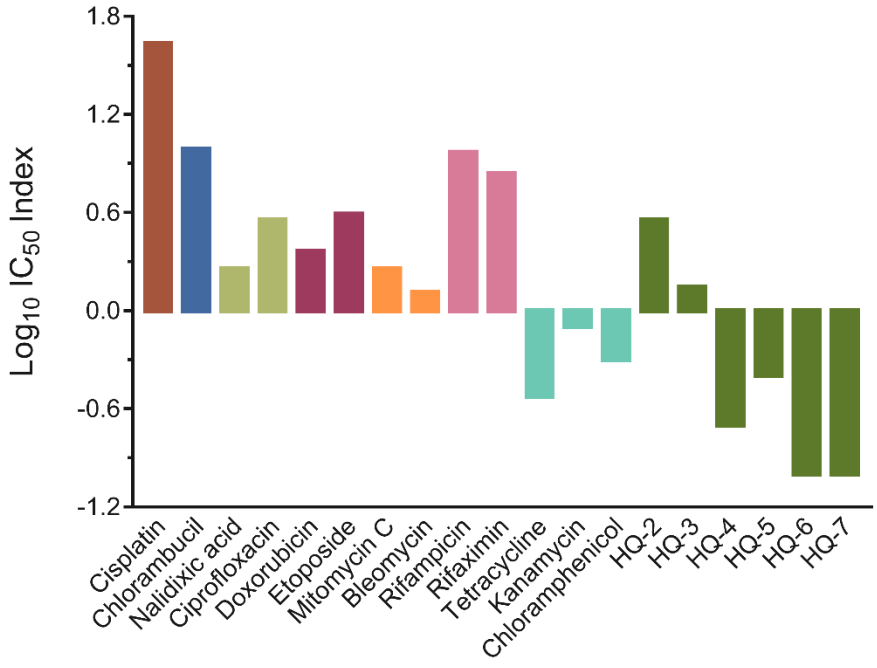

Figure 5.5 HQ compounds induce translation inhibition in *E. coli*. IC50 values for growth inhibition in *E. coli* were measured 16 hours after drug treatment, while inhibition of translation was measured by following the production of Dendra2 in a 16-hour time course study after drug treatment. The IC50 index is defined as the IC50 value for translation inhibition/IC50 value for growth inhibition.

5.5 HQ compounds exhibit cytotoxicity in association with translation inhibition in *E. coli*.

Given the complexity of the eukaryotic cells, *E. coli* was employed as a simple model system to study the mechanism of action of the HQ compounds. By comparing the IC_{50} values for growth inhibition and translation inhibition in *E. coli*, the IC_{50} index was determined. This index is described in Chapter 4; in brief, the IC_{50} index is the IC_{50} for translation inhibition/IC_{50} of growth

inhibition. The Log value of the IC_{50} index was used to get a quick comparison of the two IC_{50} values, as shown in Figure 5.5. DNA damaging molecules and transcription inhibitors all have positive Log IC_{50} index values, which means the concentration needed for translation inhibition is larger than that needed to achieve growth inhibition, suggesting the mechanism of cytotoxicity of these molecules are unlikely to be through translation inhibition. The translation inhibitors, however, all have negative Log IC_{50} index values, suggesting a smaller IC_{50} value of translation inhibition compared with growth inhibition, and indicating that the mechanism of cytotoxicity is likely through translation inhibition. Interestingly, most of the HQ compounds studied also have a negative Log IC_{50} index value, indicating that the mechanism of action of HQ compounds could be associated with translation inhibition effects.

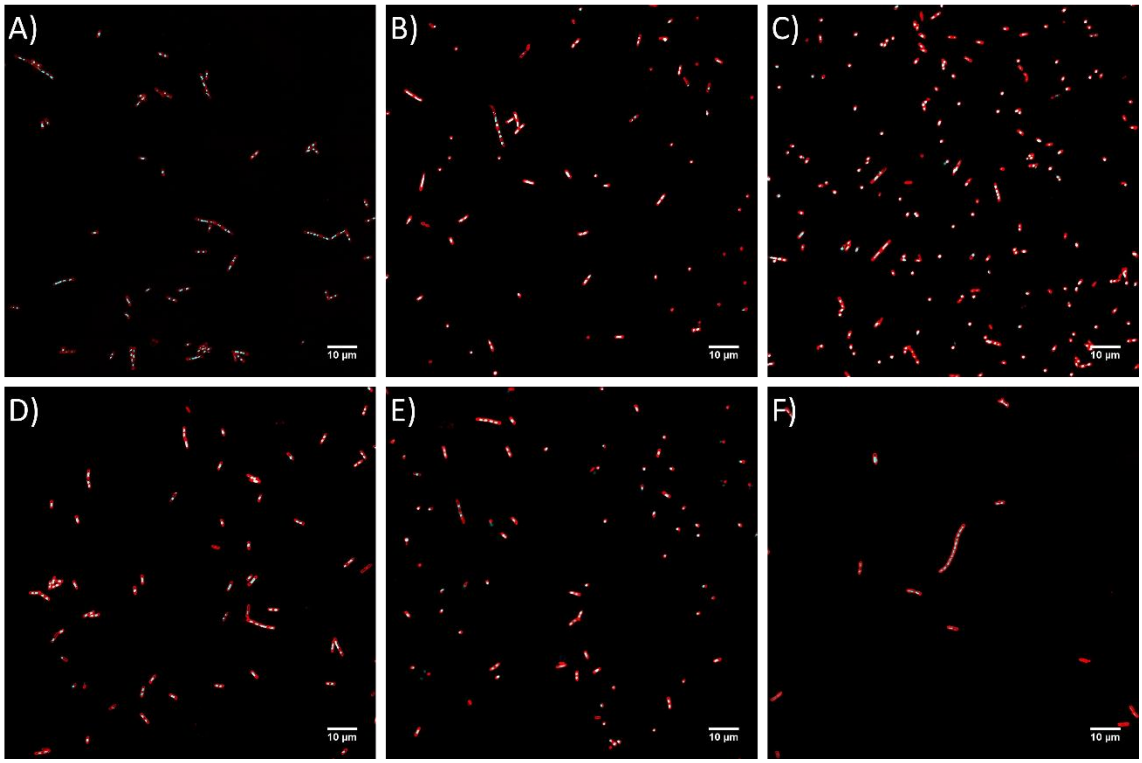

Figure 5.6 HQ compounds induce phenotypic feature changes in *E. coli* that are typical of translation inhibitors. A) HQ-2; B) HQ-3; C) HQ-4; D) HQ-5; E) HQ-6; F) HQ-7. *E. coli* cells were treated at 5 x MIC of each compound for 6 hours and then stained and imaged. FM4-64 (red) was used to stain the cell wall while Hoechst 33342 (cyan) was used for DNA. The stains were incubated with the cells for 15 minutes prior to imaging with Nikon A1R confocal epifluorescence microscopy. Scale bar represent 10 µm in all images.

In a previous research, Glazer group members, Dr. Heidary and Mr. Brock Howerton studied the ability of **HQ-2** to inhibit transcription and/or translation activity using a coupled *in vitro* transcription and translation (IVTT) assay, and reported that **HQ-2** didn't affect the transcription or translation process.[264] While it seems the observation of translation inhibitory

effects in *E. coli* is not consistent with the reported IVTT results, it is noteworthy that the IVTT assay uses the T7 promoter and an EMCV IRES (encephalomyocarditis virus internal ribosomal entry site) to facilitate *in vitro* protein synthesis using Hela cell lysate(1-Step Human Coupled IVT Kit, Thermo Fisher Scientific). The incorporation of the two viral RNA elements could possibly explain the results that **HQ-2** didn't show inhibitory effects in the IVTT assay. The IRES is a RNA element that allows the ribosome to initiate translation bypassing the 5'-cap of eukaryotic mRNA which is essential for the majority of eukaryotic translation activities.[274, 275] The 5'-cap independent translation through IRES, therefore, don't require certain eukaryotic initiation factors (eIFs) to initiate translation process in eukaryotic cells while those specific eIFs and the bacterial analogous initial factors (IFs) could be the target of HQ compounds to achieve translation inhibitions as the translation initiation factors are relatively conserved.[276, 277, 278] Moreover, the 5'-cap independent translation has been reported to contribute to cell survival in response to cell stress and translation inhibition. [279] It could then be explained that **HQ-2** didn't show effects in the IVTT assay was because of the introduction of a possible salvage mechanism.

5.6 *E. coli* phenotypic profiling identifies HQ compounds as potential translation inhibitors.

To further understand the mechanism of action of HQ compounds, microscopy based cytological profiling was performed as described in Chapter 4. Similar to the translation inhibitors tetracycline, kanamycin, and chloramphenicol, HQ compounds didn't induce significant phenotypic changes in *E. coli* when dosed at the minimal inhibitory concentration (MIC). Instead, a concentration of 5 x MIC was required for each HQ compound to induce the phenotypic changes without significant cell killing. Surprisingly, all HQ compounds were able to induce similar phenotypic changes as those induced by classical antibiotics with direct translation inhibition mechanisms. In response to HQ compounds treatments, a subpopulation of *E. coli* cells formed filaments with multiple DNA pieces of uniform size distributing evenly in the cells (Figure 5.6, Figure 4.4D). This is different from transcription inhibitors, for which there was a single piece of DNA spreading the length of the filament observed though the population of cells forming filaments; the average filament sizes were similar for the two treatments. Compared with molecules with DNA damaging mechanisms, HQ compounds didn't induce irregularly sized DNA pieces, and the population percent forming filaments and the average filament size were generally smaller than most DNA damaging molecules.

Detailed statistical evaluation of the data was performed for the same phenotypic features as described in Chapter 4. The key features that serve to distinguish molecules with different mechanism of action include the % filament population, average filament size, average DNA pieces per filament, and the coefficient of variation (CV) of DNA piece size. These features were analyzed

and compared between molecules with known mechanisms of actions and the HQ compounds with unknown mechanisms. As shown in Figure 5.7, in response to HQ compound treatments, about 30% to 40% of cells formed filaments that were over 5 µm in length and the average size of the observed filaments was below 10 µm. These data were consistent with imaging observations, and distinguished HQ compounds from most DNA damaging molecules. An analysis of the average DNA pieces in each filament revealed differences between HQ compounds, transcription inhibitors, and DNA damaging molecules. Unlike transcription inhibitors, most HQ compounds induced multiple pieces of DNA in filaments, but the number of DNA pieces were generally smaller than those induced by DNA damaging molecules. The HQ compounds also induced DNA pieces of regular sizes, similar to the translation inhibitors, generating smaller CV values of DNA piece sizes compared with all DNA damaging molecules. These phenotypic profiling results helped to separate HQ compounds from molecules with DNA damaging or transcription inhibition mechanisms.

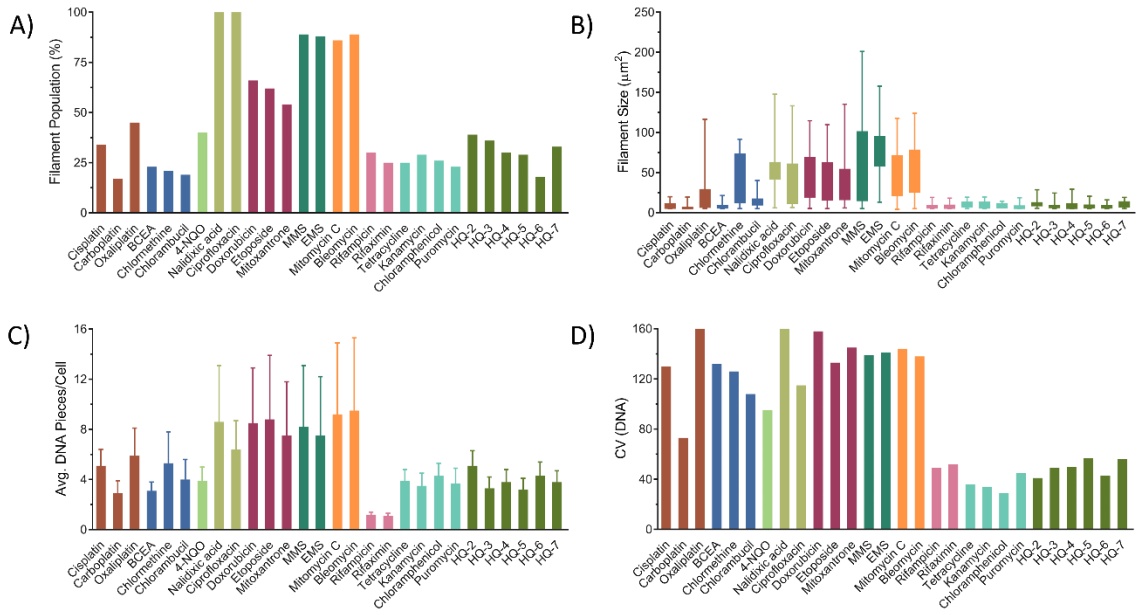

Figure 5.7 HQ compounds induce similar phenotypic profiles to translation inhibitors. Cells were treated with drugs at the MIC for 6 hours prior to imaging, while translation inhibitors were dosed at 10 x MIC and HQ compounds were dosed at 5 x MIC. Multiple fields of view were analyzed for 300-500 cells. A) Graph of filament population (%) as a function of drug where *E. coli* of over 5 µm were identified as filaments. B) Box and whisker plot shows the dispersity of the overall (whisker) and major 50% (25% to 75%, in box) range of the *E. coli* filaments. C) The average number of DNA pieces in each filament as a function of drug. The error bar is not an error in measurement; rather it is a reflection of dispersity in the number of DNA pieces per cell, similar to the variation in the DNA piece size. D) The coefficient of variation (CV) for the size of the DNA piece in each filament. Molecules of diverse mechanisms are color coded as follows: ● Pt based DNA crosslinker; ● nitrogen mustard; ● oxidizing agent; ● bacterial gyrase inhibitor; ● topoisomerase II inhibitor; ● ionizing radiation mimicking agent; ● DNA strand breaker; ● transcription inhibitor; ● translation inhibitor; ● HQ compounds.

Data from phenotypic profiling were also used in a multi-dimensional data analysis. The filament population (%), average number of DNA pieces in filament, and CV of DNA piece sizes were used for all molecules with a known mechanism of action and the HQ compounds. In the 3D scatter plot, all HQ compounds (shown in purple, Figure 5.8) clustered with translation inhibitors (shown in cyan), and this cluster is well separated from transcription inhibitors and molecules with DNA damaging mechanisms. This multi-parameter phenotypic profiling in *E. coli* strongly suggested HQ compounds possess a mechanism of action involving translation inhibition. Though this result is obtained in a bacterial system, given that the translation process is a common step in the central dogma of molecular biology and is present in both prokaryotic and eukaryotic cell system, the cytotoxic effects of HQ compounds in cancer cells could possibly involve translation inhibition as well. Indeed, these results were consistent with concurrent studies on inhibition of protein translation in mammalian cells (performed by Dr. David Heidary; unpublished results).

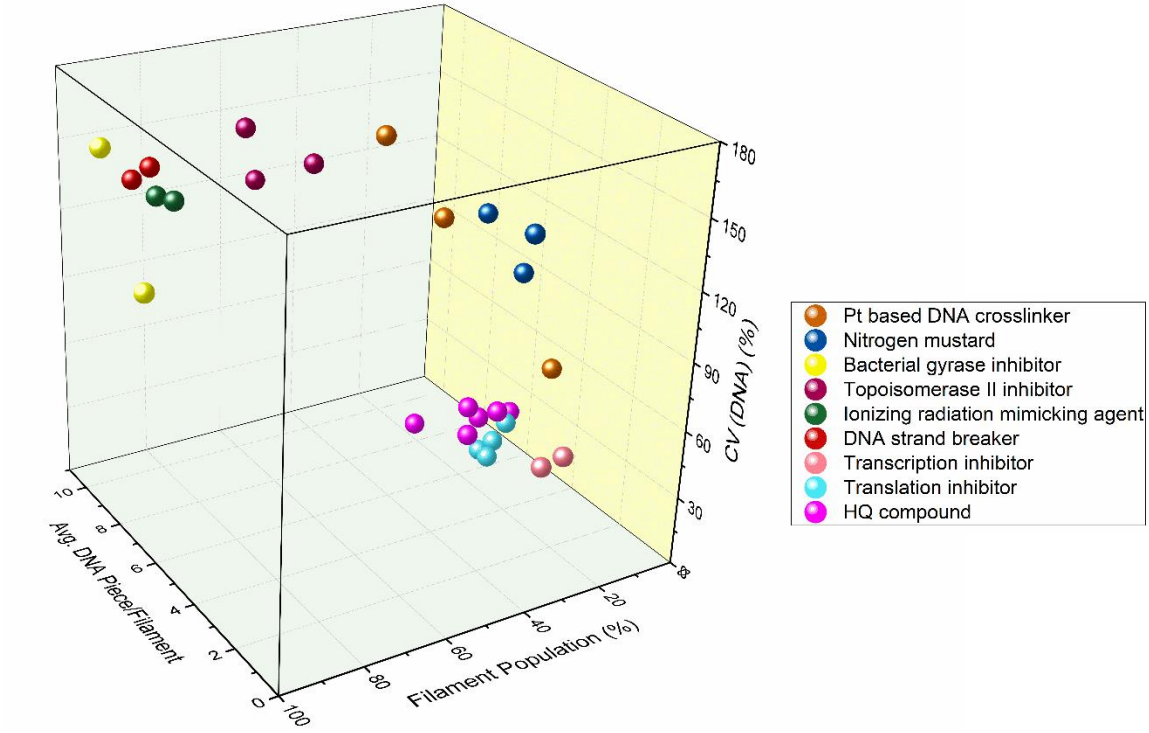

Figure 5.8 Distinguishing HQ compounds from molecules with DNA damaging or transcription mechanisms based on the phenotypic change observed in *E. coli*. Cells were treated with molecules at their MIC for 6 hours prior to imaging, translation inhibitors were dosed at 10 x MIC, HQ compounds were dosed at 5 x MIC for phenotypic changes. Same phenotypic features as used for Figure 5.6 were analyzed with OriginPro 2017.

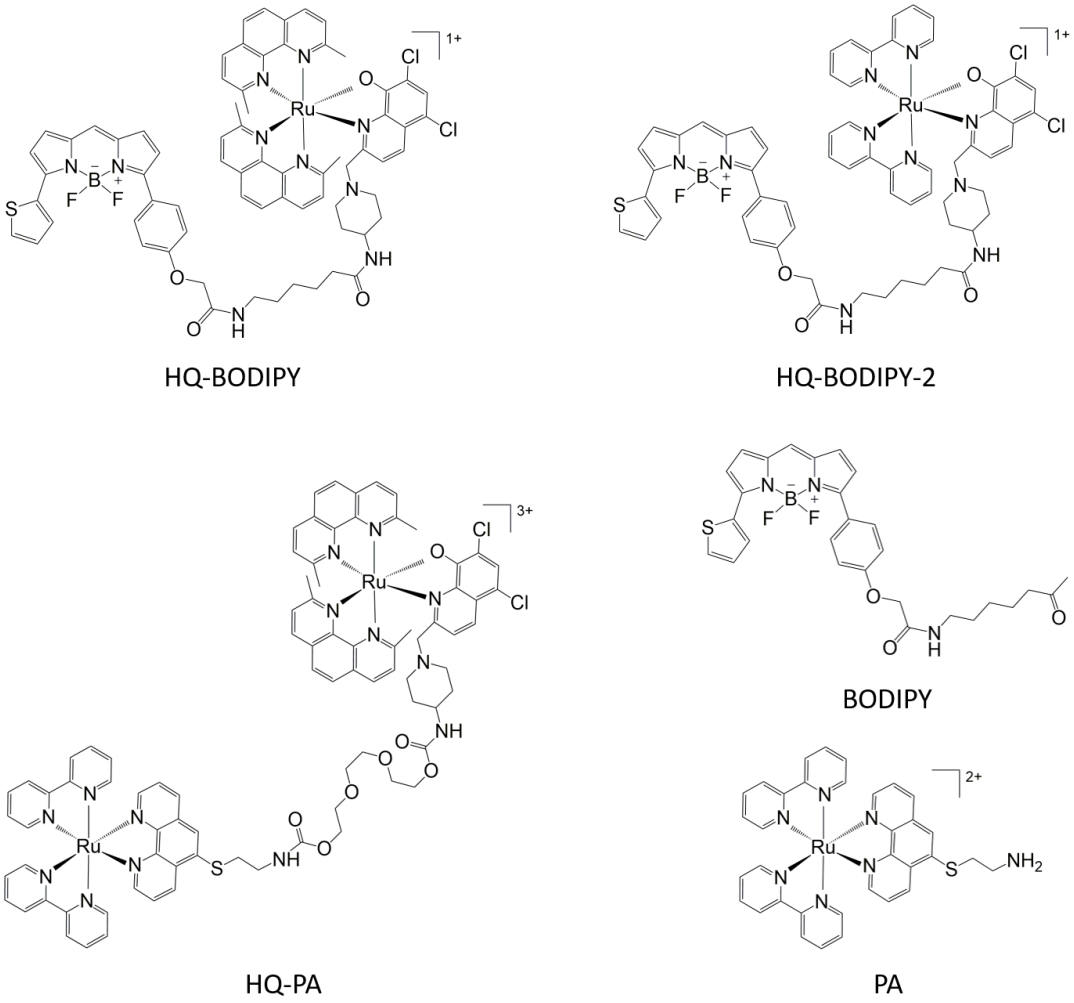

Chart 5.2 Structures of probes and conjugated HQ compounds used in live cell imaging for subcellular localization study.

5.7 Investigation of subcellular localization of HQ compounds in living cells through BODIPY conjugation.

Bacterial cytological profiling suggested the mechanism of action of HQ compounds likely involves translation inhibition. Given the complexity of eukaryotic cell structure and the significantly increased number of possible targets, any conclusions obtained from bacterial cells required confirmation in mammalian cells. Additional imaging studies offered an approach to rapidly determine if the HQ might be interacting with the translational machinery in mammalian cells. For this purpose, a red fluorophore boron-dipyrromethene TR-X (BODIPY) was conjugated to the ruthenium polypyridyl compound containing the hydroxyquinoline ligand ($Ru(dmphen)_2$-5,7-dichloro-8-hydroxyquinoline) to form the conjugated compound (**HQ-BODIPY**) by a group member Dr. Dmytro Havrylyuk. The biological activity of **HQ-BODIPY** was confirmed in

mammalian cells by another group member, Dr. David Heidary. With the efforts and support of scientists in the group, it was possible to directly study the localization of HQ compounds in mammalian cells, and detect the colocalization with eukaryotic organelles. Multicolor fluorescence confocal microscopy was employed using Human Embryonic Kidney cell lines (HEK) stably expressing GFP conjugated organelle marker proteins to determine the localization of the BODIPY conjugated HQ compound (**HQ-BODIPY**); Hoechst 33342 dye was used to stain the nucleus.

Protein synthesis associated organelles were of primary interest; as bacterial cytological profiling revealed translation inhibition effects, the endoplasmic reticulum (ER) and ribosome were therefore studied first. ER targeted transmembrane domain (CytERM) with enhanced green fluorescent protein (EGFP)[280, 281] and large ribosomal subunit protein 10A (RPL10A) with GFP[282] have been used to visualize the two organelles. HEK cells expressing either ER targeted transmembrane domain with GFP (CytERM-GFP) or large ribosomal subunit protein 10A with GFP (RPL10A-GFP) were treated with **HQ-BODIPY** for 6 hours and stained with Hoechst 33342. As shown in Figure 5.9, the overlay of red fluorescent channel from **HQ-BODIPY** and the green channel from CytERM-GFP generated the bright yellow region in the cells, suggesting that there was colocalization of **HQ-BODIPY** at the ER. Further analysis of GFP (green) and BODIPY (red) showed a strong correlation with the Pearson's correlation coefficient (PCC) of 0.80, as listed in Table S4.3 in the Appendix, which revealed the correlation of HQ compound and the protein synthesis organelle. Notably, the cytoplasmic accumulation of free BODIPY dye also resulted in partial colocalization in the ER with a PCC value of 0.60, suggesting BODIPY could contribute to the localization of **HQ-BODIPY** (Figure 5.18). The ribosome, however, was not identified as a direct target of HQ-BODIPY, as the compound didn't accumulate in this structure (Figure 5.10). This ribosomal protein has both nuclear and cytoplasmic distribution as ribosomal proteins are normally transported into nucleus for ribosome biogenesis.[283] Both **HQ-BODIPY** and free BODIPY localized in cytosol, so there was no overlap with nuclear ribosomal protein. In both HQ-BODIPY and free BIDOPY treated cells, there was no detectable colocalization of the BODIPY fluorescence and GFP fluorescence as indicated by the lack of a yellow region in the merged images, and the poor PCCs listed in Table S4.3 in Appendix (-0.03 for **HQ-BODIPY** and 0.03 for free BODIPY, respectively).

The Golgi apparatus is the organelle responsible for packing protein into vesicles that are involved in protein transportation and secretion, and therefore could be one of the possible target of the HQ compounds. Direct visualization of **HQ-BODIPY** in HEK cells expressing the Golgi apparatus marker, human galactosyltransferase (GalT) with GFP (GalT-GFP)[284], showed that **HQ-BODIPY** didn't localize in this organelle (Figure 5.11), nor did the free BODIPY control. The well

separated BODIPY fluorescence (red) and the GalT-GFP fluorescence (green) in the merged images clearly showed the lack of colocalization of **HQ-BODIPY** and the Golgi apparatus. Low correlation between the Golgi marker and the BODIPY including both free BODIPY and **HQ-BODIPY** is also reflected by the low PCC values listed in Table S4.3. As the organelle with a dominant role to produce energy needed for all cellular activities, mitochondria has drawn significant research interest and there have been several ruthenium compounds targeting mitochondria,[285, 158, 286] including a ruthenium polypyridyl complex targeting mitochondria reported in Chapter 2. For this reason, a mitochondria marker mitochondrial matrix-targeted photoactivable GFP (mito-paGFP)[287] was used to visualize this organelle. As shown in Figure 5.12 and Figure 5.18, there was medium overlap of red fluorescence from **HQ-BODIPY** and the green fluorescence from mito-paGFP, the correlation level as indicated by PCC (0.33 to 0.3 for **HQ-BODIPY**, and 0.55 to 0.34 for free BODIPY) also suggested that the observed HQ compound accumulated in the mitochondria is most likely the artificial effects of BODIPY localization.

Human purine nucleoside phosphorylase with GFP (PNP-GFP) was used as the marker protein of peroxisomes. As shown in Figure 5.13 and Figure 5.18, the BODIPY conjugated HQ compound **HQ-BODIPY** and the fluorophore BODIPY both had partial colocalization with peroxisome as indicated by the yellow region observed in the merged images. Pearson's correlation coefficients also suggest a medium to strong correlation with the green fluorescence detected from PNP-GFP and the red fluorescence detected from **HQ-BODIPY** and free BODIPY. The PCC values ranged from 0.6 to 0.7 in both **HQ-BODIPY** and BODIPY treated cells (Table S4.3 in Appendix). It is again indication of the localization of HQ compounds could be affected by the localization of the conjugated fluorophore.

The same organelle imaging was done with BODIPY conjugated to another HQ compound $Ru(bpy)_2$-5,7-dichloro-8-hydroxyquinoline (**HQ-BODIPY-2**). This compound was also synthesized by Dr. Dmytro Havrylyuk by using a different polypyridyl scaffold which produces less active compounds. Dr. David Heidary evaluated the biological activity in mammalian cells. Since **HQ-BODIPY-2** didn't show cytotoxic effects in HL60 cells, it was used as a negative control to understand the localization of HQ compounds and the connections between the localization and cytotoxic effects. Similar results were observed in HEK cells showing partial colocalization of **HQ-BODIPY-2** with the ER (PCC was 0.80). The similar colocalization of **HQ-BODIPY**, **HQ-BODIPY-2**, and BODIPY at the ER suggested the connection between translation inhibitory effects and the subcellular localization of HQ compounds is to be further validated by isolating organelles for direct metal amount analysis or conjugating a different fluorophore to HQ compounds (Figure S4.1, S4.2, and Table S4.3 in Appendix).

5.8 HQ compounds partially colocalize with endoplasmic reticulum (ER).

The highly consistent imaging results for **HQ-BODIPY**, **HQ-BODIPY-2**, and the BODIPY control indicated that the subcellular localization of both BODIPY conjugated HQ compounds is largely dominated by the subcellular localization of the commonly applied commercial organic probe BODIPY. It was therefore necessary to use an alternative probe to visualize the HQ compounds in mammalian cells. Certain luminescent ruthenium(II) polypyridyl complexes have the potential to be used as novel probes in cellular imaging because they have many appropriate properties, including low cytotoxicity and high photostability.[288, 289] Our group has extensively studied the photophysical and photochemical properties of Ru(II) polypyridyl complexes, and as described in Chapter 2, the subcellular localization of two Ru(II) polypyridyl complexes has been studied utilizing the intrinsic luminescence of those two molecules. To further understand the subcellular localization of HQ compounds, Dr. Dmytro Havrylyuk used a Ru(II) compound, $Ru(bpy)_2$phenamine (PA), as the alternative probe, and a HQ compound was conjugated to the probe. The conjugated compound (**HQ-PA**) was then used to study the subcellular localization of HQ compounds. As shown in Figure 5.14 to 5.17, no clear subcellular localization of PA in the selected organelles were detected as the red fluorescence from PA and green fluorescence from organelle markers were not observed, suggesting PA has no organelle localizing preferences. This result is consistent with the low PCC values for PA and all organelle markers. The conjugated molecule **HQ-PA** exhibited subcellular localization in the ER as shown by the yellow region from the overlap of **HQ-PA** (red) and the organelle marker CytERM-GFP (green). The result was also confirmed by the high PCC values, suggesting a strong correlation as shown in Table S4.4 in the Appendix. However, unlike **HQ-BODIPY** and **HQ-BODIPY-2**, the molecule **HQ-PA** didn't show subcellular localization in other organelles, including the mitochondria and peroxisome (Figure 5.18).

BODIPY-based fluorophores have been frequently and widely conjugated to various targets as imaging probes.[290, 291] The research utilizing BODIPY includes examining subcellular localization of targets of interests in living cells.[292, 293] BODIPY has also gain commercial applications as manufactured imaging reagents because of the low cytotoxicity and broad fluorescent properties that can be easily tuned by simple chemical modifications.[290, 294] However, the live cell imaging results of **HQ-BODIPY**, **HQ-BODIPY-2**, and BODIPY showed that BODIPY may preferably localize in certain organelles (ER and peroxisome in this study) and alter the subcellular localization of the molecules of interest conjugated to BODIPY. Recently, Zhang *et al.* reported silver mediated modification of BODIPY produced a derivative with enhanced ER localization.[295] This research has also confirmed the BODIPY derivatives have certain subcellular

localization preferences. Ru (II) chromophores have been used as staining reagents such as SYPRO Ruby in proteomics researches.[296] Increased research interests have been drawn to utilize Ru (II) complexes as novel imaging probes as they have low cytotoxicity and rich photophysical and photochemical properties that allow easy chemical designs.[297, 298, 299] The imaging results of luminescent Ru (II) molecule PA and the conjugated HQ molecule **HQ-PA** described in this chapter has also shown that Ru (II) polypyridyl complexes are superior in live cell imaging studies of subcellular localization as they have minimized subcellular localization preferences.

5.9 Conclusion.

Ruthenium polypyridyl compounds bearing HQ ligands have received much research interest, with most previous and current research still focused on nucleic acid associated biological activity.[300,] Our research, however, developed HQ-containing Ru(II) complexes that are highly potent, and the potency depended on not only the HQ structure, but also the structure of the Ru(II) complex co-ligands. Moreover, the HQ compounds induce cytotoxicity through a non-DNA target, and the mechanism of action of HQ compounds is associated with translation inhibition in both bacterial and mammalian cells.

The mammalian cell death kinetics and cellular uptake studies showed the HQ compounds were more efficient in accumulating in cells and inducing cell death compared with cisplatin or ruthenium compounds described in previous chapters that have a DNA related mechanism. The cell signaling pathway studied in cancer cells revealed downregulation of the Akt pathway which plays a central role in cell proliferation, growth, and survival regulation.[270, 269] Liu *et al.* has reported consistent Akt pathway inhibition in cancer cells by ruthenium polypyridyl compounds containing HQ ligand by immunoblottings[257], suggesting a common cell signaling pathway in response to HQ compound treatment. To further elucidate the possible target and mechanism of action, bacterial cytological profiling obtained using high-resolution imaging as described in previous chapters was employed. Quite to our surprise, all studied HQ compounds induced phenotypic feature changes that were typical of translation inhibitors, and the statistical evaluation of multiparameter plots revealed the tight cluster of translation inhibitors and HQ compounds, indicating HQ compounds have translation inhibition effects in bacterial cells. Organelle labeling in live mammalian cells also showed HQ compounds were partially localized in the ER, a primary protein synthesis machinery, supporting the premise that HQ compound act through translation associated mechanisms. No HQ compound was observed in either the nucleus or mitochondria, the two targets that have been extensively studied. With this data, in combination with bacterial cytological profiling and mammalian cell signaling studies, it could be concluded that ruthenium polypyridyl compounds with a HQ ligands act through direct or indirect translation inhibition effects other than DNA

damaging mechanisms that have been previously assumed. In this study, the possibility of utilizing luminescent Ru (II) polypyridyl compounds as novel imaging probes were also investigated through the conjugation of PA to HQ compound, in comparison to the commonly applied commercial fluorophore BODIPY, the Ru (II) molecule PA showed no preference of localizing in organelles and therefore was more suitable for the study of subcellular localization in living cells.

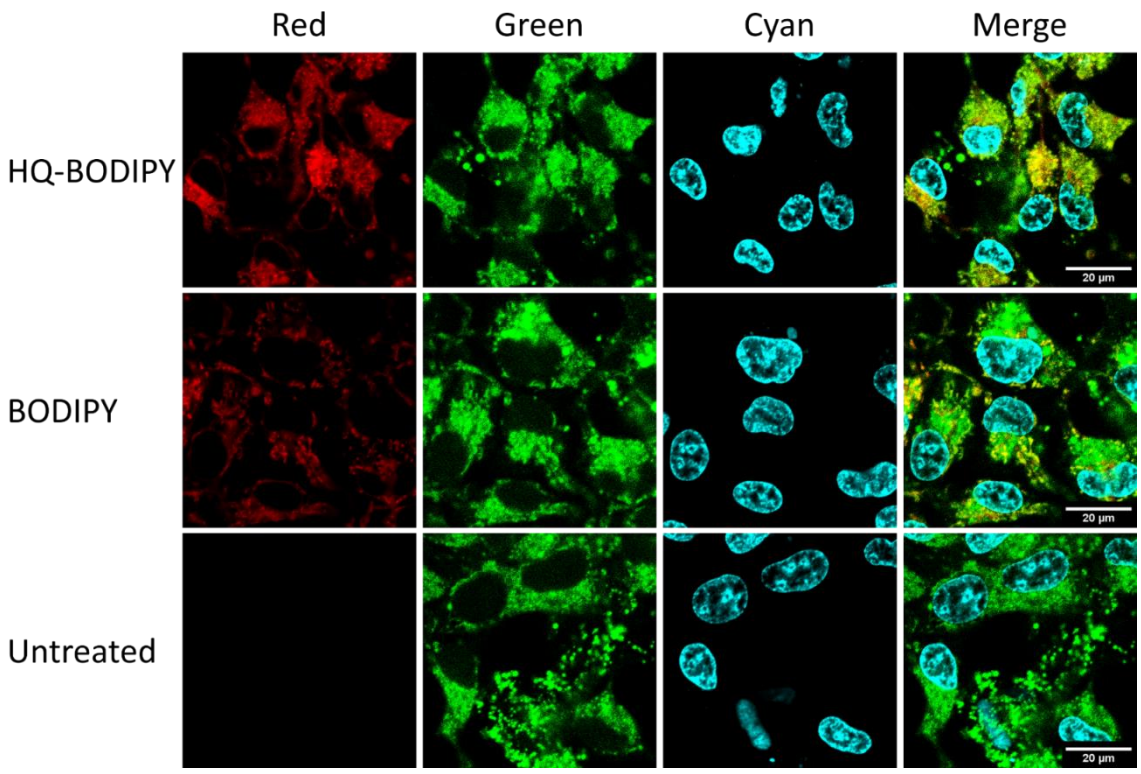

Figure 5.9 HQ compound shows partial colocalization with the endoplasmic reticulum (ER). HEK cells stably expressing ER targeted transmembrane domain with GFP (CytERM-GFP) were treated with 2 µM of HQ-BODIPY or free BODIPY for 6 hours prior to imaging; untreated cells were used as controls. Cells were incubated with Hoechst 33342 for 15 minutes before being imaged with a Nikon A1R confocal microscope. Red, BODIPY; Green, CytERM-GFP; Cyan, Hoechst 33342. All scale bars represent 20 µm.

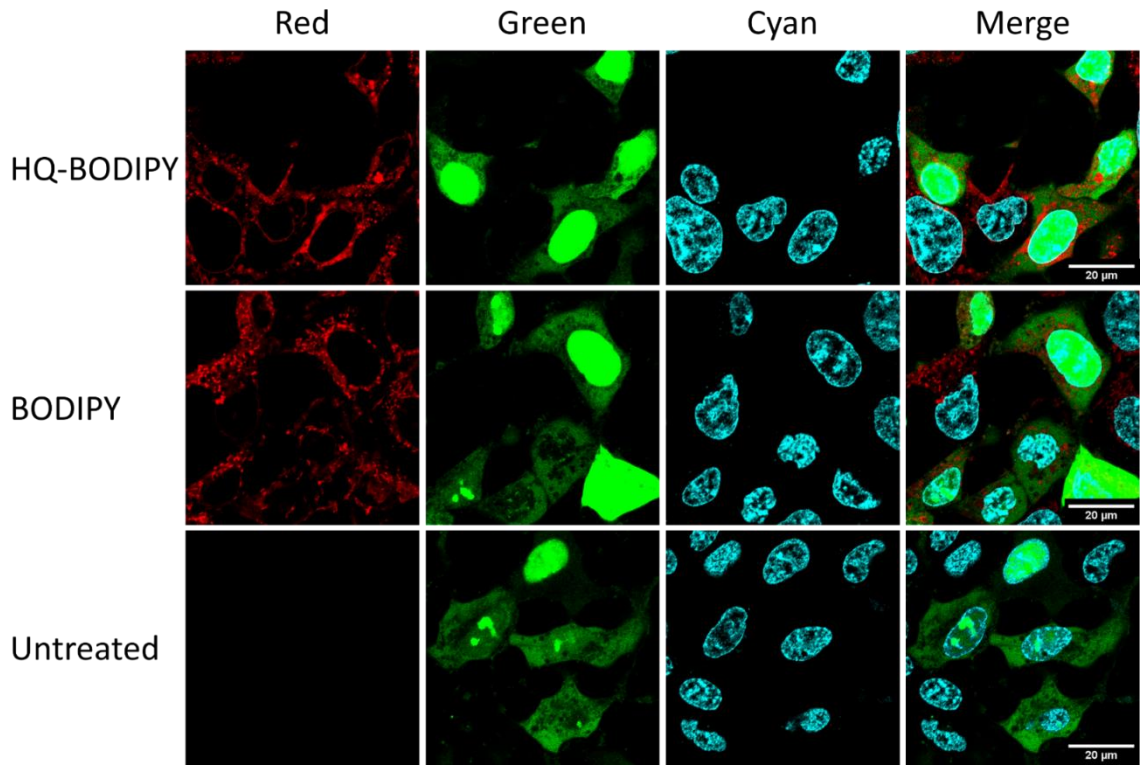

Figure 5.10 HQ compound shows no colocalization with the ribosome. HEK cells transfected with large ribosomal subunit protein 10A with GFP (RPL10A-GFP) were treated with 2 µM of HQ-BODIPY or free BODIPY for 6 hours prior to imaging; untreated cells were used as controls. Cells were incubated with Hoechst 33342 for 15 minutes before being imaged with a Nikon A1R confocal microscope. Red, BODIPY; Green, RPL10A-GFP; Cyan, Hoechst 33342. All scale bars represent 20 µm.

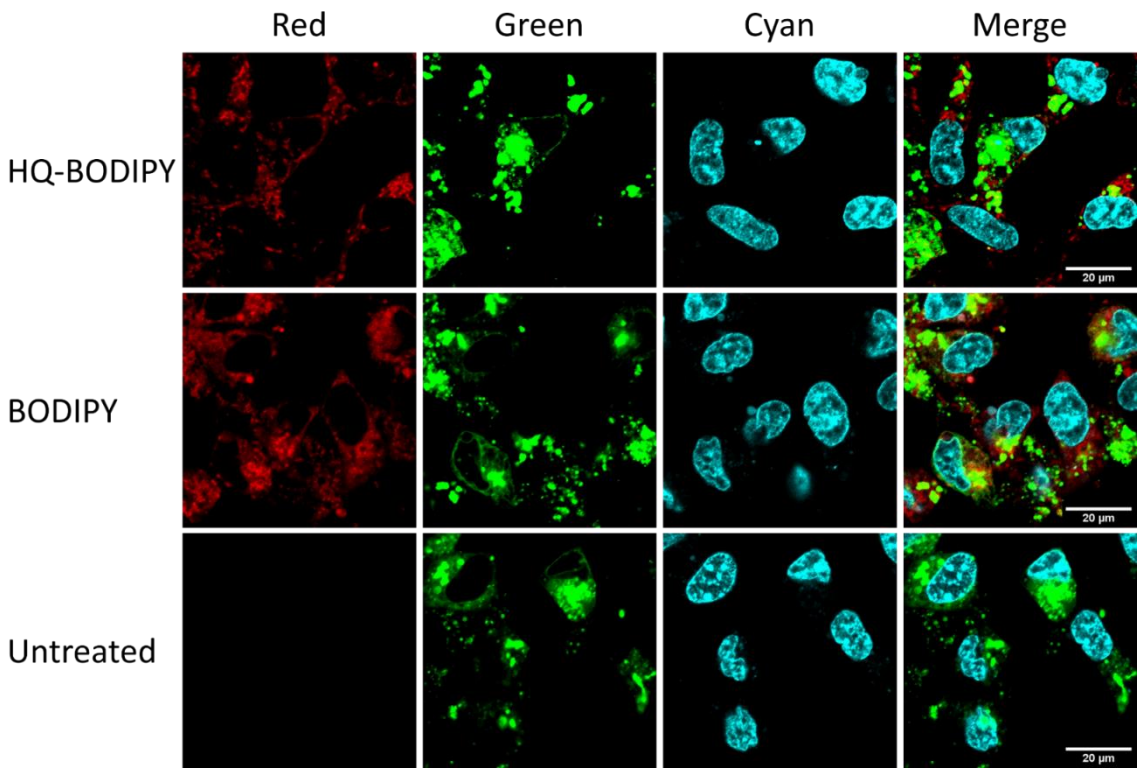

Figure 5.11 HQ compound shows no colocalization with the Golgi apparatus. HEK cells stably expressing human galactosyltransferase (GalT) with GFP (GalT-GFP) were treated with 2 µM of HQ-BODIPY or free BODIPY for 6 hours prior to imaging; untreated cells were used as controls. Cells were incubated with Hoechst 33342 for 15 minutes before being imaged with Nikon A1R confocal microscope. Red, BODIPY; Green, GalT-GFP; Cyan, Hoechst 33342. All scale bars represent 20 µm.

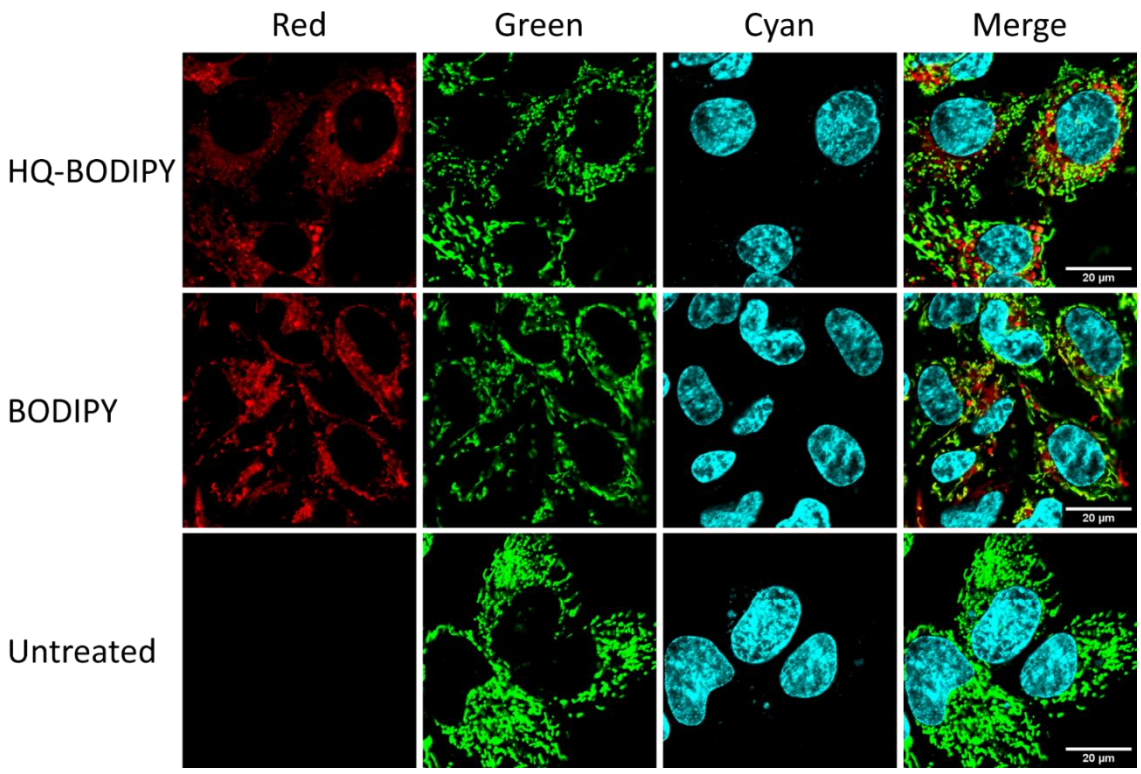

Figure 5.12 HQ compound shows no colocalization with mitochondria. HEK cells stably expressing mitochondrial matrix-targeted photoactivable GFP (mito-paGFP) were treated with 2 µM of HQ-BODIPY or free BODIPY for 6 hours prior to imaging; untreated cells were used as controls. Cells were incubated with Hoechst 33342 for 15 minutes before being imaged with a Nikon A1R confocal microscope. Red, BODIPY; Green, mito-paGFP; Cyan, Hoechst 33342. All scale bars represent 20 µm.

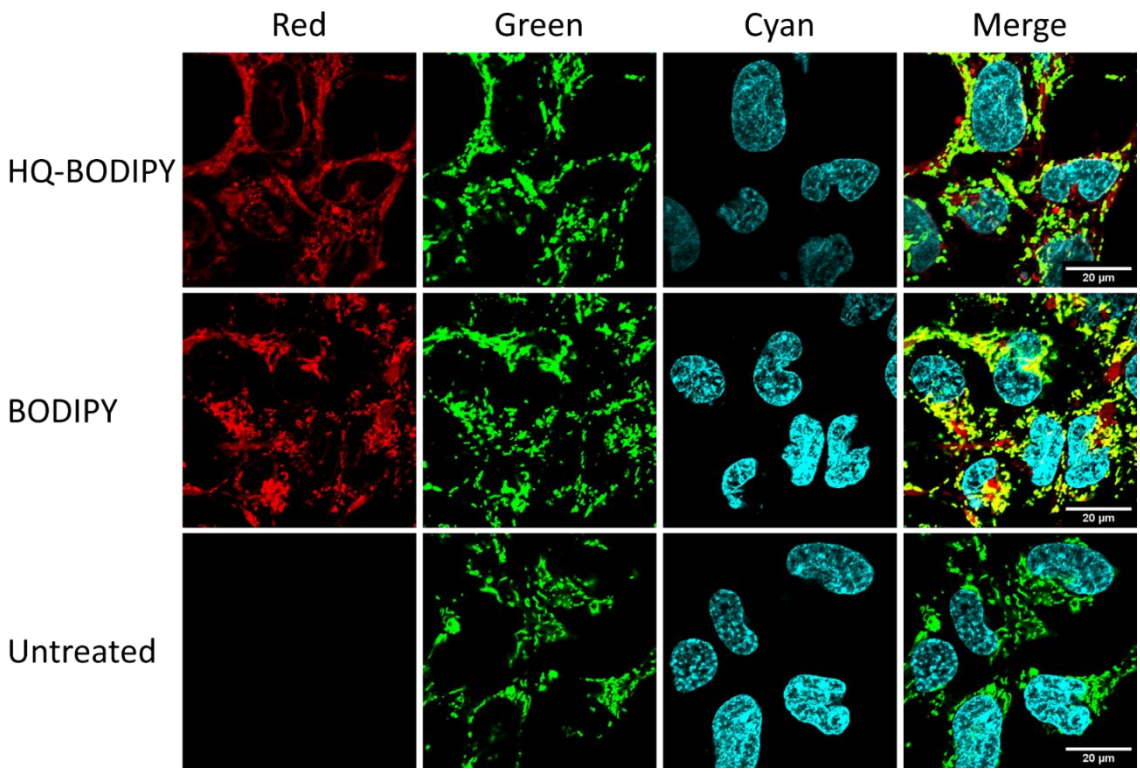

Figure 5.13 HQ compound shows partial colocalization with peroxisomes. HEK cells stably expressing human purine nucleoside phosphorylase with GFP (PNP-GFP) were treated with 2 µM of HQ-BODIPY or free BODIPY for 6 hours prior to imaging; untreated cells were used as controls. Cells were incubated with Hoechst 33342 for 15 minutes before being imaged with a Nikon A1R confocal microscope. Red, BODIPY; Green, PNP-GFP; Cyan, Hoechst 33342. All scale bars represent 20 µm.

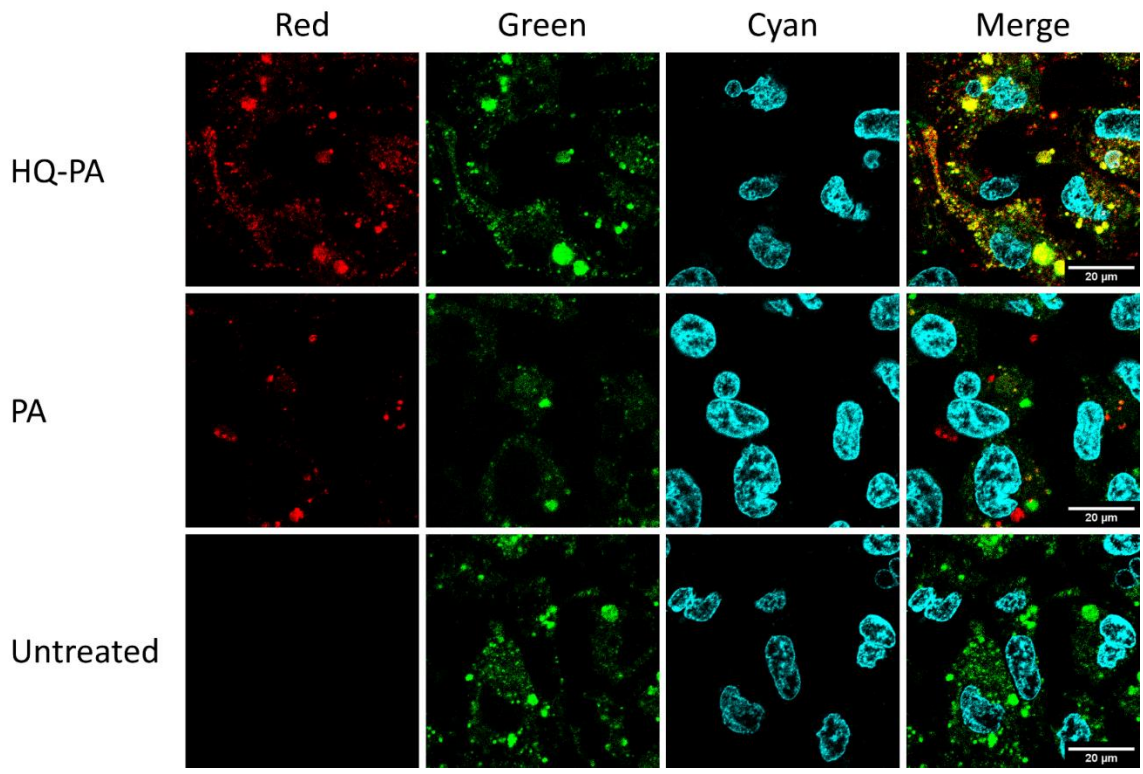

Figure 5.14 HQ compound shows partial colocalization with the endoplasmic reticulum (ER). HEK cells stably expressing ER targeted transmembrane domain with GFP (CytERM-GFP) were treated with 2 µM of HQ-PA or free PA for 6 hours prior to imaging; untreated cells were used as controls. Cells were incubated with Hoechst 33342 for 15 minutes before being imaged with a Nikon A1R confocal microscope. Red, PA; Green, CytERM-GFP; Cyan, Hoechst 33342. All scale bars represent 20 µm.

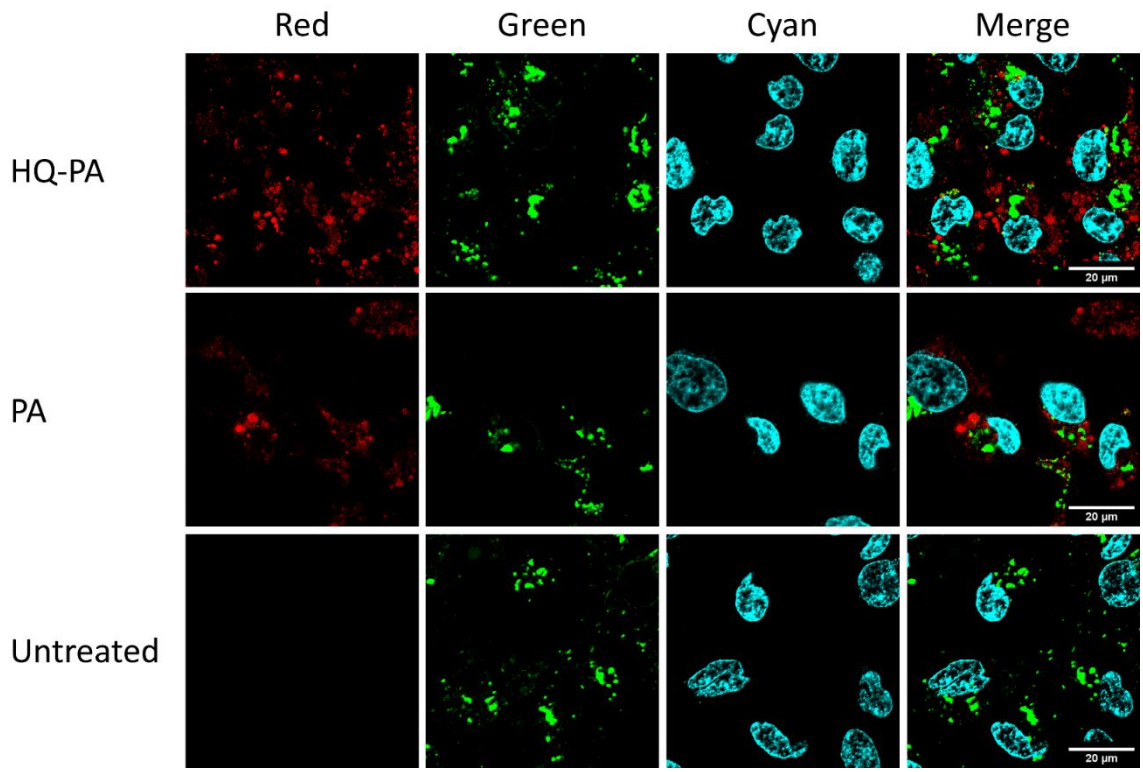

Figure 5.15 HQ compound shows no colocalization with the golgi apparatus. HEK cells stably expressing human galactosyltransferase with GFP (GalT-GFP) were treated with 2 µM of HQ-PA or free PA for 6 hours prior to imaging; untreated cells were used as controls. Cells were incubated with Hoechst 33342 for 15 minutes before being imaged with a Nikon A1R confocal microscope. Red, PA; Green, GalT-GFP; Cyan, Hoechst 33342. All scale bars represent 20 µm.

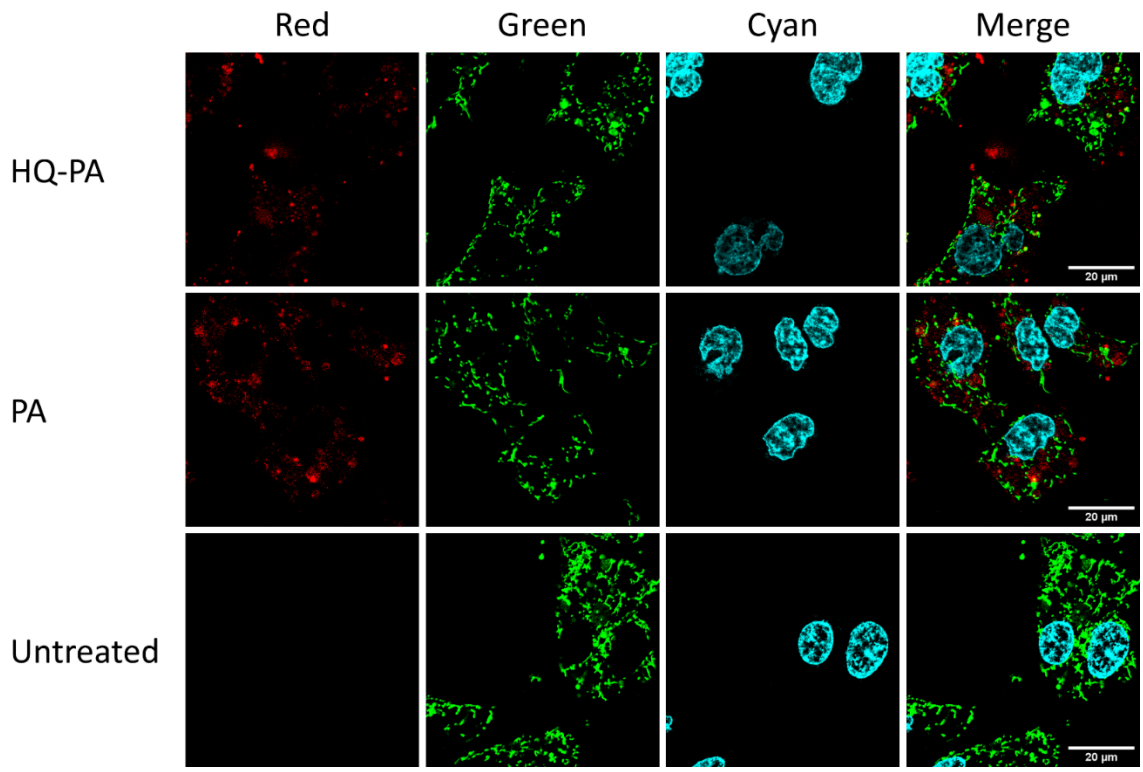

Figure 5.16 HQ compound shows no colocalization with mitochondria. HEK cells stably expressing mitochondrial matrix-targeted photoactivable GFP (mito-paGFP) were treated with 2 µM of HQ-PA or free PA for 6 hours prior to imaging; untreated cells were used as controls. Cells were incubated with Hoechst 33342 for 15 minutes before being imaged with a Nikon A1R confocal microscope. Red, PA; Green, mito-paGFP; Cyan, Hoechst 33342. All scale bars represent 20 µm.

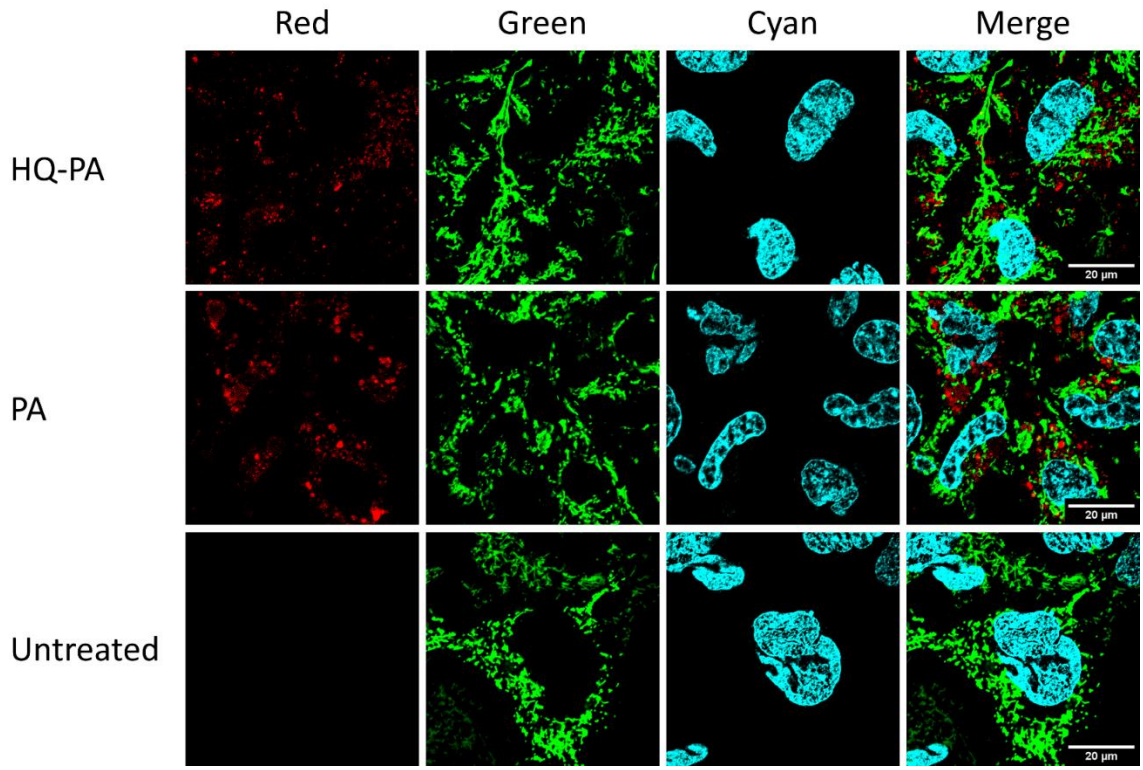

Figure 5.17 HQ compound shows no colocalization with peroxisome. HEK cells stably expressing human purine nucleoside phosphorylase with GFP (PNP-GFP) were treated with 2 µM of HQ-PA or free PA for 6 hours prior to imaging; untreated cells were used as controls. Cells were incubated with Hoechst 33342 for 15 minutes before being imaged with a Nikon A1R confocal microscope. Red, PA; Green, PNP-GFP; Cyan, Hoechst 33342. All scale bars represent 20 µm.

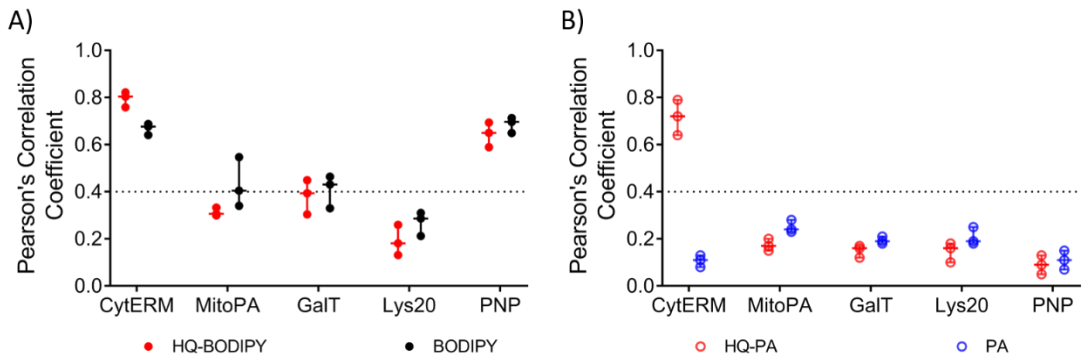

Figure 5.18 BODIPY alters subcellular localization of HQ compound while PA doesn't. Pearson's Correlation Coefficients (PCCs) between red channel (BODIPY, PA, HQ-BODIPY, and HQ-PA) and green channel (organelle markers) were determined for A) BODIPY conjugation; B) PA conjugation in HEK cell lines stably expressing different organelle markers using NIS Elements AR software. Red circle(solid), HQ-BODIPY; black circle (solid) BODIPY; red circle (open), HQ-PA; blue circle (open), PA. Organelle markers: CytERM, endoplasmic reticulum marker; MitoPA, mitochondria marker; GalT, Golgi apparatus marker; Lys20, lysosome marker; PNP, peroxisome marker. Medium correlation is indicated at the dot line at 0.4.

5.10 Materials and methods.

Note: all studied compounds were synthesized by Dr. Dmytro Havrylyuk or Mr. Brock Howerton. All HEK cell lines containing clonal, stably expressed organeller markers were generated by Dr. David Heidary.

E. coli culture maintenance. The Dendra2 gene was cloned into a pCW-ori plasmid modified to contain an N-terminal 6x histidine tag with multiple restriction enzyme cloning sites. Escherichia coli BL21(DE3) competent cells transformed with pCWori plasmid containing Dendra2 gene (pCWori-Dendra2) were cultured in Luria Broth (LB) at 37°C with 180 rpm shaking. *Mammalian cell maintenance.* Human promyelocytic leukemia HL60 cells were purchased from ATCC. Dulbecco's modified eagle medium (DMEM), Iscove's modified Dulbecco's medium (IMDM), Opti-MEM I reduced serum medium, heat inactivated fetal bovine serum (FBS), Penicillin/Streptomycin (5, 000U/mL), Trypsin-EDTA (0.5%), Dulbecco's phosphate buffered saline (DPBS), Trypan Blue Solution (0.4%) were purchased from Life Technologies. HL60 cells were maintained in IMDM supplemented with 10% FBS and 50 U/mL of Penicillin/Streptomycin. A549 cells and HEK cells were maintained in DMEM with the same supplements. Cells were maintained at 37°C with 5% CO2.

Cytotoxicity determination. E. coli BL21(DE3) cells transformed with pCWori-Dendra2 plasmid were plated in M63 minimal medium at 4 x 10^6 cells per well in 96 well flat bottom

transparent tissue culture treated plates (Greiner Bio One). Compounds were dosed from 0 – 300 μM, followed by 3 min of light irradiation (7 J/cm^2 blue light (> 400 nm)). The cells were then incubated for 16 hours with the compounds, and cell growth was determined by measurement of the optical density at 600 nm using a SpectraMax Multiwell Plate Reader (Molecular Devices). HL60 cells were plated in Opti-MEM supplemented with 1% FBS and 50 U/mL of Penicillin/Streptomycin at 30,000 cells per well in 96 well flat bottom transparent tissue culture treated plates (Greiner Bio One). Compounds were dosed from 0 – 300 μM, and incubated for 16 hours. The cells were then incubated for 72 hours, and cell viability determined by conversion of resazurin to resorufin. The emission of resorufin was measured on a SpectraFluor Plus Plate Reader (Tecan). The data were normalized to the untreated control and fitted to a sigmoidal dose response model using Prism 6.02 to determine IC_{50} values. Minimal inhibitory concentration (MIC) was fitted to the model published by Lambert et al using Prism 6.02.[185]

Protein synthesis and degradation measurements in E. coli with Dendra2. E. coli BL21DE3 cells transformed with pCWori-Dendra2 were cultured in LB medium to an OD_{600} of 0.8. Cells were then resuspended in M63 minimal media and induced with 0.5 mM IPTG for 3 hours at 37°C with 180 rpm shaking. Photoconversion of Dendra2 was carried out with a 405 nm LED flood array (Loctite) with a total light exposure time of 2 minutes. Cells were then plated in 96 well plates at 6 x 10^7 cells per well. Green and red emission was measured directly after photoconversion using a SpectraMax Multiwell Plate Reader (Molecular Devices) for a baseline evaluation of Dendra2 protein (t = 0 hour). For green emission, an excitation wavelength of 491 nm and emission wavelength of 538 nm was used; for red emission, the excitation wavelength was 544nm and emission wavelength was 590 nm. Compounds were then dosed from 0 μM to 300 μM, the cells were incubated for 16 hours before the green and red emission was measured again for an evaluation of protein synthesis with compound treatment (t = 16 hours). The average fluorescence ratio of green/red at t = 0 hour and t = 16 hours was calculated, the values were normalized, and the data fitted to a sigmoidal dose response.

E. coli filamentous growth. E. coli were cultured as above and plated at 3 x 10^8 cells per well in 24 well flat bottom transparent tissue culture treated plates (Greiner Bio One). IPTG was added at a concentration of 0.5 mM for induction of Dendra2 production. Compound treatment was then carried out, with cells dosed at the desired concentration for each compound and cultured at 37°C with 180 rpm of shaking for 6 hours before imaging.

E. coli cell imaging. After compound treatment, the OD_{600} was measured for each treatment condition followed by the removal of culture that contained 4 x 10^5 cells. The cells were centrifuged at 8,600 xg for 1 minute, aspirated, and washed twice with 1 mL of sterile filtered PBS with

centrifuging at 8,600 xg for 1 minute and PBS was removed. Cells were then resuspended in 150 µL of sterile filtered MilliQ water, and plated on a poly-D-Lysine (100 µg/mL) coated 1.5# cover glass bottom 35 mm culture dish. Cells were allowed to settle on the culture dish for 1 hour before gently rinsing with 150 µL of PBS. FM4-64 and Hoechst 33342 were added to the cells at concentrations of 5 and 10 µg/mL respectively. The cells were incubated at room temperature and protected from light for 20 minutes. The solution was removed from the cells followed by rinsing with 150 µL of PBS. Imaging was carried out on an Olympus IX2-RFAEVA-2 microscope or a Nikon A1R+ confocal microscope. For the Olympus microscope, a 60 x oil or a 100 x oil objective was used. Hoechst 33342 was visualized using the excitation filter BP 360-390 (Chroma, Bellows Falls, VT, USA), and emission filter HQ470/30 M (Chroma, Bellows Falls, VT, USA). To view Dendra2 (green), a 473/10 nm BrightLine® single-band bandpass filter FF01-473/10-25 (Semrock, Rochester, NY, USA) was used as the excitation filter, and a 525/50 nm BrightLine® single-band bandpass filter, FF03-525/50-25 (Semrock, Rochester, NY, USA) was used as the emission filter. FM4-64 was visualized with a HQ 550/30 (Chroma, Bellows Falls, VT, USA) as the excitation filter, and a 664 nm EdgeBasic long-pass edge filter, BLP01-664R-25 (Semrock, Rochester, NY, USA) as the emission filter. The imaging channel sequential was set as FM4-64, Dendra2 (green), and Hoechst 33342. For each single field of view, a 1024 x 1024 pixel image was taken. Imaging on the Nikon A1R+ confocal microscope was performed with a 100 x oil objective and the zoom in factor was 1 x. Hoechst 33342 was visualized on the 405 nm channel with 5% laser excitation and 100% gain, offset was -25% to -50%. Dendra2 (green) was viewed on the 488 nm channel with 1% laser excitation and 25% gain, offset was -25% to -50%. FM4-64 was visualized on the 561 nm channel with 5% laser excitation and 50% gain, offset was -25% to -50%. Imaging channel sequential was set as FM4-64, Dendra2 (green), and Hoechst 33342. For each single field of view, a 1024 x 1024 pixel image was taken, and a 3 x 3 image stitch was taken using the same setting.

Analysis of E. coli images for filaments and DNA morphology quantification. Images were processed and analyzed using the ImageJ software. For each single image, to analyze cell filaments, the threshold of FM4-64 channel was adjusted to match the original image, and any particles smaller than 0.2 μm^2 were excluded from measurements, size exclusion was only applied in FM4-64 channel for cell size and number analysis. All measurement results from "Analyze Particles" were saved in Microsoft Excel file. The filament population (%) was calculated as the percentage of all particles larger than 5μm^2, and the average filament size and standard deviation of filament size was also calculated using the statistical function of Microsoft Excel. To analyze DNA morphology with the most accuracy, in each field of view, a duplication image of the original image was made. The original image was used as the reference to adjust the threshold of the duplicate

image to make sure only the correct pixels that were present in the original image were captured and included for image analysis. ROI manager was used to match DNA with cell, and a certain filament was selected and set as region of interest (ROI). Then the number of DNA pieces of each filament was obtained by "Analyze Particles". In each treatment condition, 30-50 filaments were selected and analyzed. All measurement data were saved in Microsoft Excel files. The average DNA pieces in filaments were calculated by dividing the number of all DNA pieces by number of filaments. The average size of DNA pieces, and standard deviation of DNA pieces, were also calculated with the statistical function of Microsoft Excel. To obtain the magnitude of variation in sizes of DNA pieces, coefficient of variation (CV) was calculated by dividing the standard deviation of DNA pieces by the average size of DNA pieces.

HQ compound uptake in HL60 cells. HL60 cells were plated in Opti-MEM supplemented with 1% FBS and 50 U/mL Penicillin/Streptomycin at a density of 1x 10^6 cells/mL in 25 cm^2 cell culture flasks, and dosed with 20 μM compound **HQ-1**. Cells were collected 6 hours and 20 hours after compound addition by centrifugation at 124 x g for 5 minutes. The culture media was separated for analysis, and cells were washed twice with PBS. Total RNA and genomic DNA were also isolated, and the nucleic acids, cell content, and media were prepared for analysis as described in Chapter 4.

Immunoblotting. HL60 cells were treated with 2 μM of **HQ-1,** harvested 3, 6, 12, and 24 hours after treatment, pelleted by centrifugation at 124 x g for 5 minutes, washed twice with DPBS. A549 cells were plated at 2 x 10^5 cells per well in 6 well flat bottom transparent tissue culture treated multiwell plates and in the same treatment condition detailed for HL60 cells. Cells were harvested at 3, 6, 12, and 24 hours after treatment. All cells were lysed in RIPA buffer supplemented with 5 mM sodium pyrophosphate (2 x 10^6 cells/100 μL) for 15 minutes on ice. The insoluble fraction was removed by centrifugation at 20, 817 x g for 10 minutes at 4 °C. The supernatant was collected and the protein concentration was determined by BCA assay. 20 μg of protein was loaded onto 4-12% bis-tris gels and followed by transfer to nitrocellulose membranes. After blocking with 2.5% BSA in DPBS with 0.1% Tween20 (PBST) for 1 hour at room temperature, the membrane was immunoblotted with the following primary antibodies and correspondence dilutions. Cleaved caspase 9, cleaved PARP, p-p53, p21, p-JNK, p-c-jun, p-PDK1, pan Akt, p-Akt, p-MK2, and p-p38 at 1: 1, 000 dilutions; p53 and p-ERK at 1: 500 dilutions; and GAPDH at a 1: 2, 000 dilution in 2.5% BSA overnight at 4 °C. Immunoblots were washed with PBST for 10 minutes for four times and incubated for 1 hour with secondary antibodies at a 1: 10, 000 dilution for GAPDH and 1: 5, 000 dilutions for all other antibodies. Detection was carried out with Clarity Western ECL Substrate and imaged with a ChemiDoc MP System (Bio-Rad).

Flow cytometry. HL60 cells were treated with 2 μM of HQ compounds for 3, 8, and 16 hours respectively, cells were pelleted by centrifugation at 124 x g for 5 minutes, washed twice with DPBS before flow cytometry. For cell death mechanism analysis, cells were stained 15 minutes with FITC-Annexin V and PI, cells with positive FITC-Annexin V staining and negative PI staining were identified as early apoptotic cells; cells with both positive FITC-Annexin V and PI staining were identified as late apoptotic cells. Cells were analyzed with a FACSCalibur (Becton-Dickenson). A minimum of 20, 000 events were measured for each sample.

Mammalian cell organelle labeling. Cell lines were prepared by Dr. David Heidary and provided for imaging studies. Plasmids containing ER targeted transmembrane domain with GFP (CytERM-GFP), large ribosomal subunit protein 10A with GFP (RPL10A-GFP), human galactosyltransferase (GalT) with GFP (GalT-GFP), mitochondrial matrix-targeted photoactivable GFP (mito-paGFP), and human purine nucleoside phosphorylase with GFP (PNP-GFP) genes were purchased from Addgene. The plasmids were transfected into human embryonic kidney (HEK) cells, and selected with corresponding selection markers respectively. HEK cells expressing CytERM-GFP, GalT-GFP, mito-paGFP, and PNP-GFP were from selection of stable cell lines and HEK cells expressing RPL10A-GFP were from selection of transient transfection.

Mammalian cell imaging of BODIPY-labeled HQ compounds. BODIPY® TR-X NHS Ester (Succinimidyl Ester) was purchased from Thermo Fisher Scientific. BODIPY-labeled compounds were synthesized and provided by Dr. Dmytro Havrylyuk. HEK cells expressing different organelle markers were treated with 2 μM of **HQ-BODIPY**, **HQ-BODIPY-2**, or BODIPY for 6 hours prior to imaging. The treatment was removed by replacing culture media with treatment free media, cells were stained with Hoechst 33342 for 15 minutes and then rinsed with PBS for three times. Imaging was done with on a Nikon A1R+ confocal microscope with a 100 x oil objective for ER and ribosome labeling and a 60 x oil objective for other organelle labeling, and the zoom in factor was 1 x. Hoechst 33342 was visualized on the 405 nm channel with 5% laser excitation and 100% gain, offset was -25% to -50%. Organelle labeling (green) was viewed on the 488 nm channel with 1% laser excitation and 25% gain, offset was -25% to -50%. BODIPY was visualized on the 561 nm channel with 5% laser excitation and 50% gain, offset was -25% to -50%. Imaging channel sequential was set as BODIPY, GFP, and Hoechst 33342. For each single field of view, three 1024 x 1024 pixel images were taken, and the images were analyzed with ImageJ. Quantification of colocalization with organelle markers was performed by determination of Pearson's correlation coefficient (PCC) with NIS-Elements AR software.[301, 302]

Mammalian cell imaging of PA-labeled HQ compound. PA-labeled compound was synthesized and provided by Dr. Dmytro Havrylyuk. HEK cells expressing different organelle

markers were treated with 2 μM of **HQ-PA** or PA for 6 hours prior to imaging. The sample preparation and imaging settings were the same as described above. Imaging channel sequential was set as PA, GFP, and Hoechst 33342. For each single field of view, three 1024 x 1024 pixel images were taken, and the images were analyzed with ImageJ. Quantification of colocalization with organelle markers was performed by determination of Pearson's correlation coefficient (PCC) with NIS-Elements AR software.[301, 302]

Chapter 6 Conclusion

The possibility of utilizing metal complexes in cancer treatment has drawn increased research interest. Though many efforts have been spent on platinum-based compounds following the discovery and application of cisplatin, compounds containing non-platinum metal centers have emerged as potential improved alternatives to cisplatin to achieve enhanced anticancer spectrum and reduced adverse effects. Among those non-platinum metal compounds, our group has taken particular research interest in Ru(II) compounds because of their unique features. The octahedral geometry and the three-dimensional architecture of ruthenium makes it possible to bond with structurally diverse ligands, including heterocycles containing nitrogen and/or oxygen, and therefore makes more complicated structures. The Ru(II) complexes have been known to possess lower cytotoxicity; as Fe and Ru shares similar outermost shell electron configuration, Ru(II) complexes can be transported by transferrin proteins which are responsible to transport Fe for cellular activities. Ru(II) complexes are also known for rich photophysical properties; luminescent Ru(II) complexes have been developed as cellular imaging probes. Moreover, the chemical and physical properties of Ru(II) complexes can be easily tuned by modifying the ligands coordinated to ruthenium center and the anions, resulting in rich chemical diversity.

The major goal of this research was to elucidate functional targets and mechanisms of action for ruthenium (II) polypyridyl complexes as potential anticancer agents. Platinum complexes approved by the FDA, such as cisplatin, carboplatin, and oxaliplatin, have been commonly used as contemporary chemotherapeutic agents. While they are considered to act through DNA damaging mechanisms, their clinical application has been limited by acquired or intrinsic drug resistance and the adverse effects due to the non-selectivity and systematic toxicity of the drugs. These platinum compounds have been inspiring to scientists and provided direction for designing, synthesizing, and studying novel compounds bearing metal centers with anticancer properties. On the other hand, the development of metal compounds with possible medicinal applications have called for mechanistic research to understand their biological targets and mechanisms of action. Mechanistic research aids the design of novel compounds, as with a better understanding of SAR, it is possible to design compounds with specific targets. It is also important to gain knowledge of the mechanism for any compounds that will possibly be tested in clinical trial or prescribed as medications.

Ruthenium compounds with different scaffolds can have different charge states and hydrophilicities, which are very likely to affect the biological targets and mechanisms of action. Elucidating the mechanisms of action for ruthenium compounds with different scaffolds is therefore important. As revealed in this research, Ru(II) polypyridyl compounds that were structurally diverse had shown the ability to interact with different functional targets involved in

diverse biological processes, and the ability to localize in different subcellular structures/organelles. In turn, understanding the mechanism of action helps logical design and synthesis of molecules with certain mechanisms or biological targets.

As many metal compounds are inspired by cisplatin, the DNA crosslinking agent, it is not surprising that the majority of metal compounds are designed as DNA binding molecules and therefore have positive charges. While many believe that negatively charged compounds may not enter the cell and thus can't act as cytotoxic agents, the study of two structurally similar compounds with positive and negative charges led to a different conclusion. Ru(bathophenanthroline)$_3$ is a hydrophobic molecule with positive charge, and Ru(bathophenanthroline disulfonate)$_3$ is a negatively charged hydrophilic molecule. Both molecules generate singlet oxygen with same quantum yields and are luminescent. Trace metal analysis by ICP-OES proved that not only Ru(bathophenanthroline)$_3$ had an elevated cellular uptake, as expected, but that Ru(bathophenanthroline disulfonate)$_3$ also accumulated in human cancer cells, and at a higher level than cisplatin, which is neutral. Both molecules were able to induce cytotoxicity, but through distinct mechanisms, and microscopy imaging helped to identify different cellular localization patterns for the two molecules. This research has a profound impact on understanding the mechanism of ruthenium polypyridyl compounds, as it shows the possibility to achieve radically different biological activities by simple ligand modification. This study demonstrated that ruthenium compounds with a significantly greater range of physical properties are compatible with potential medicinal applications.

The next research focus was the mechanism of action of a cisplatin inspired molecule, Ru(bpy)$_2$dmbpy, a prodrug which must be activated by light to induce biological effects. Gel electrophoresis confirmed DNA covalent adducts, and bioanalytical studies of nucleic acid isolated from *in vitro* treatment offered more details on the preference for reaction with DNA over RNA in both mammalian cells and bacterial cells. While similar results have been published on *in vitro* studies for cisplatin, our research demonstrated that this ruthenium prodrug had a similar nucleic acid interacting behavior as the known DNA crosslinking chemotherapeutic agent cisplatin. Cell biology studies showed the ruthenium compound induced altered cellular responses compared to cisplatin. The apoptosis induced by Ru(bpy)$_2$dmbpy was through p53-independent pathways, and no cell cycle arrest was observed, so treatment with this compound didn't trigger typical cisplatin response pathways. Instead, the down regulation of cell survival and growth pathways was observed. These facts suggest though some of the biological targets – DNA and RNA - are similar, the actual cellular responses are different, and it raises the possibility to retain cytotoxicity but minimize parallel drug resistance to cisplatin.

Mechanistic studies involve a great deal of time and effort to identify the target and determine the mechanism for potential drug molecules. These first two studies mainly utilized the well-established approaches to investigate the mechanism of action for Ru(II) polypyridyl complexes. However, given the commonly existing metal speciation resulted from the alternations of charge states, geometry, and ligands, additional tools and approaches were sought to provide new insights for medicinal inorganic chemistry. Mammalian cell system has been the primary choice for mechanistic studies, requiring consideration of the huge number of biomolecules present in eukaryotic cellular environment and the complex networks involving all possible molecular and cellular processes. Bacterial cell system, especially *E. coli*, however, have the potential to serve as simplified model systems that help to rapidly distinguish mechanisms if the targets and mechanism of action are common to both prokaryotic and eukaryotic cells. In fact, a multiparameter cytological profiling evaluation, based on the phenotypic features in *E. coli* treated with molecules with known mechanisms involving different phases of the central dogma, demonstrated the capability to separate molecules into different categories based on their individual mechanism of action. This phenotypic profiling included FDA approved anticancer agents and molecules that are commonly known antibiotics. The drugs were classified into subgroups in agreement with previous reports, based on their mechanism of action. A combination of cytotoxic studies, cellular imaging, and statistical evaluation of phenotypic features made it possible to classify molecules inducing DNA damage, transcription inhibition, and translation inhibition. Molecules that induced DNA strand breaks or DNA alkylating and crosslinking, or molecules induced repair processes through double strand break repair (DSBR) pathways or nucleotide excision repair (NER) pathway could be readily distinguished from each other. This study proved that a fast assessment of mechanisms of actions can be done in a simple biological system, *E. coli*, for anticancer agents targeting common biological targets in mammalian and bacterial cell systems.

To validate the application of bacterial cytological profiling to enrich the understanding of metal complexes with unknown mechanisms of action, $Ru(bpy)_2dmbpy$ was evaluated. This light activated system, and its proposed Ru(II) species product, $Ru(bpy)_2(H_2O)_2$, were both studied in *E. coli*. Key phenotypic features revealed similar *E. coli* cytological profiling in response to both light irradiated $Ru(bpy)_2dmbpy$ treatment and cisplatin; equally importantly, the compound $Ru(bpy)_2(H_2O)_2$ also induced similar cytological profiling in *E. coli*. This result not only provided the evidence that the ruthenium metal species generated from photo-induced ligand ejection was responsible for the biological effects of Ru(II) polypyridyl compounds, but also showed that the similar cytological profile was the reflection of similar mechanism of action to cisplatin, the control compound with a known mechanism of action.

Another class of ruthenium polypyridyl compounds studied were the HQ compounds, ruthenium compounds with hydroxyquinoline and its derivatives as a chelating ligand. The HQ compounds developed in the Glazer laboratory were reported with outstanding cytotoxic potency, but the mechanism of action was unclear. Mammalian cell studies showed fast kinetics of cellular accumulation and cell death in response to HQ compound treatment, but investigations into cell signaling pathways and cell cycle arrest failed to point to a specific mechanism of action. The *E. coli* cytological profiling analysis revealed the mechanism of action of HQ compound was associated with translation inhibition, which was consistent with studies in mammalian cells. Live cell organelle labelling and cell imaging also confirmed the colocalization of HQ compound with the endoplasmic reticulum (ER), the site of protein synthesis machinery. This was the first report on translation inhibition related mechanism of HQ Ru(II) compounds, and very few other inorganic systems are known with this mechanism of action. In this study, the commercially available fluorophore BODIPY and the Ru(II) molecule PA were both used as the imaging probes, however, the widely used imaging reagent BODIPY showed surprisingly high preference of subcellular localization in several organelles including the endoplasmic reticulum and the peroxisomes. The Pearson's correlation coefficients (PCCs) were used to evaluate the localization of imaged molecules in the organelles. The BODIPY and the BODIPY conjugated molecules all showed significantly elevated PCC values in peroxisomes (BODPY, 0.71; **HQ-BODIPY**, 0.70; **HQ-BODIPY-2**, 0.72) compared with the Ru(II) polypyridyl molecule PA (PA, 0.15; **HQ-PA**, 0.13). This result showed that the subcellular localization preference of BODIPY had artificial effects that dominated the localization of the molecules conjugated to this imaging probe. BODIPY is one of the most commonly applied imaging probes, and this calls into question its use. The live cell imaging study showed that Ru(II) polypyridyl compounds could be improved imaging reagents as they have little preference for subcellular localization.

To fulfill the research goal of elucidating the mechanism of action for ruthenium compounds, a number of established analytical, biochemical, and cell biology assays and techniques were employed. The research utilized direct studies such as DNA binding and damage assays, trace metal analysis of biological samples, and visualization of compounds in the cells; indirect research approaches like cellular signaling regulation, growth and death regulation, and phenotypic feature changes were also used to gain knowledge of cellular responses and the mechanisms of actions. The ruthenium compounds with different scaffolds exhibited different, and in some cases, novel mechanisms, involving different organelles and biomolecules. This work demonstrated that mechanistic studies support chemistry, providing key information to aid in the design and optimization of ruthenium compounds with novel mechanism or targets.

Appendix A. Supplemental tables and figures in chapter 2.

Note: Compound codes are chapter-specific.

Compound 1 = $[Ru(bathophenanthroline)_3]^{2+}$

Compound 2 = $[Ru(bathophenanthroline\ disulfonate)_3]^{4-}$

Table S1.1 The % intracellular metal measured by ICP-OES. HL60 cells were treated with 5 μM of **1**, 20 μM **2**, or 20 μM cisplatin for 2 hrs and 24 hrs. The metal levels in cell and media were measured by ICP-OES, and % intracellular levels were normalized in 107 cells. The metal levels were quantified by detection at three different wavelengths (n = 3).

Compound	2 hrs		24 hrs	
	Light	**Dark**	**Light**	**Dark**
1	11.64 ± 0.34%	5.37 ± 1.15%	23.30 ± 0.52%	15.42 ± 0.89%
2	0.35 ± 0.04%	0.20 ± 0.01%	0.71 ± 0.08%	0.42 ± 0.01%
Cisplatin	0.25 ± 0.01%		0.83 ± 0.03%	

Table S1.2 Metal atoms per cell measured by ICP-OES. HL60 cells were treated with 5 μM of **1**, 20 μM **2**, or 20 μM cisplatin for 2 hrs and 24 hrs. The metal levels in cells and media was measured by ICP-OES, and the number of metal atoms per cell was calculated using the cell number obtained using trypan blue and manual counting. The metal levels were quantified by detection at three different wavelengths (n = 3).

Compound	2 hrs		24 hrs	
	Light	**Dark**	**Light**	**Dark**
1	$4.58 \pm 0.13 \times 10^7$	$2.15 \pm 0.46 \times 10^7$	$8.64 \pm 0.18 \times 10^7$	$6.42 \pm 0.36 \times 10^7$
2	$1.69 \pm 0.18 \times 10^7$	$0.93 \pm 0.03 \times 10^7$	$3.38 \pm 0.38 \times 10^7$	$2.05 \pm 0.03 \times 10^7$
Cisplatin	$3.22 \pm 0.52 \times 10^7$		$9.34 \pm 0.28 \times 10^7$	

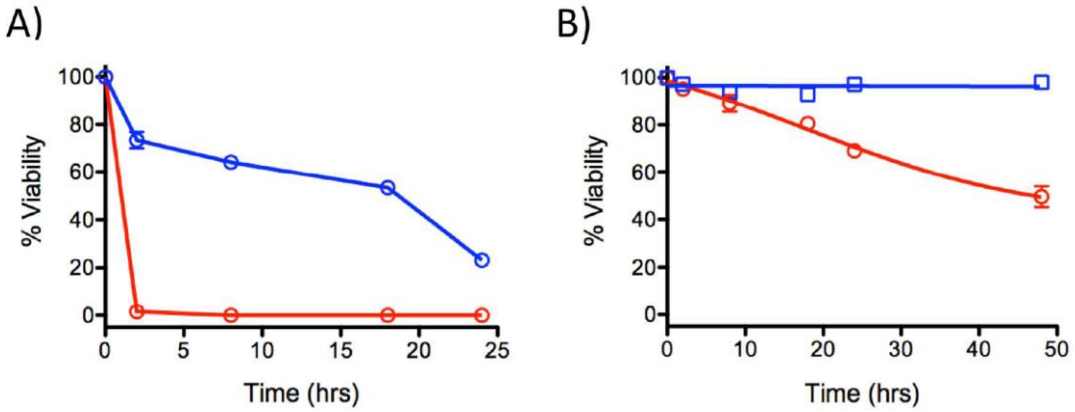

Figure S1.1 Time dependence of cell death in HL60 cells. A) Compound **1**; B) compound **2**. Blue, dark; red, irradiated. Viability was determined using Trypan Blue dye exclusion and manual counting.

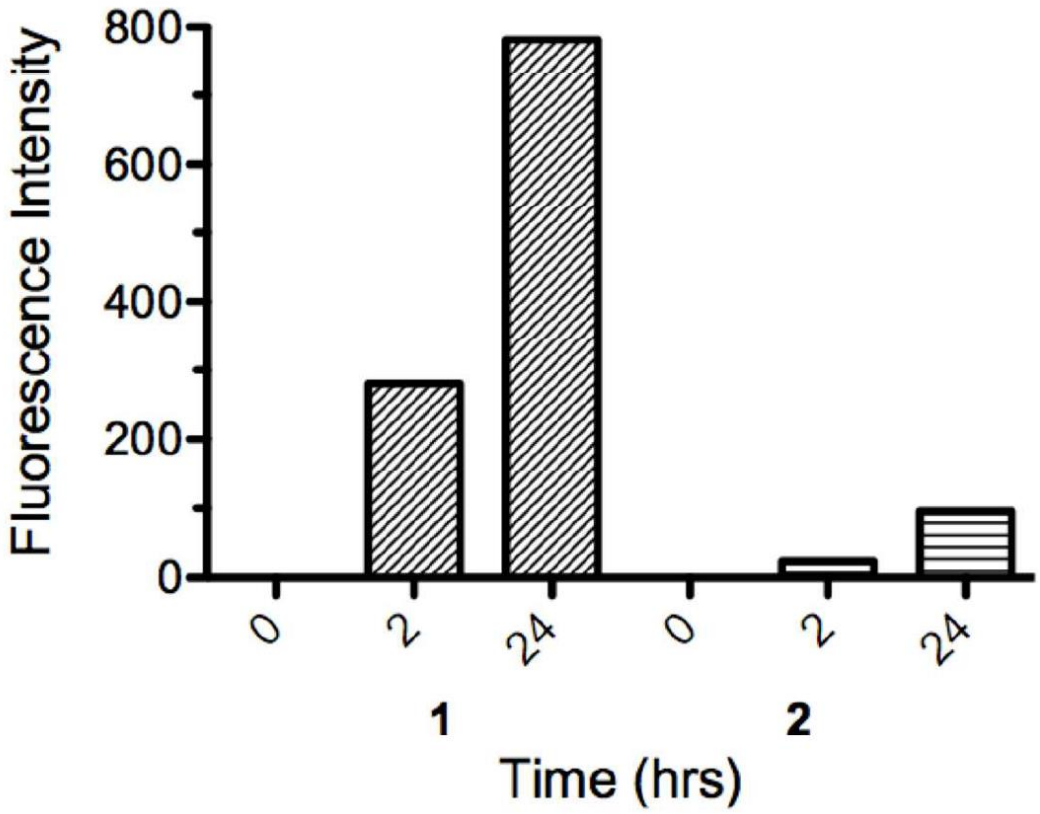

Figure S1.2 Time dependence of compound uptake and average emission intensity per cell in A549 cells determined by flow cytometry.

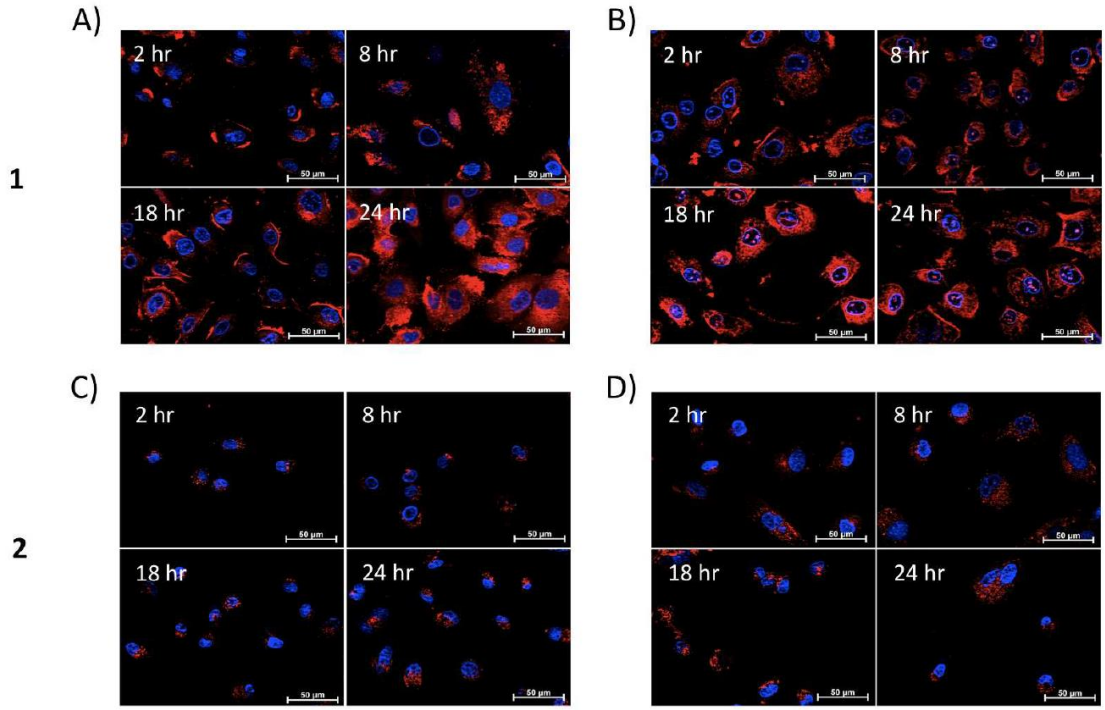

Figure 1.3 Time dependence of compound uptake in A549 cells measured by ApoTome microscope. The ruthenium compounds' emissions are shown in red and Hoechst was used to stain the nucleus (blue). A) **1**, dark; B) **1**, light; C) **2**, dark; D) **2**, light.

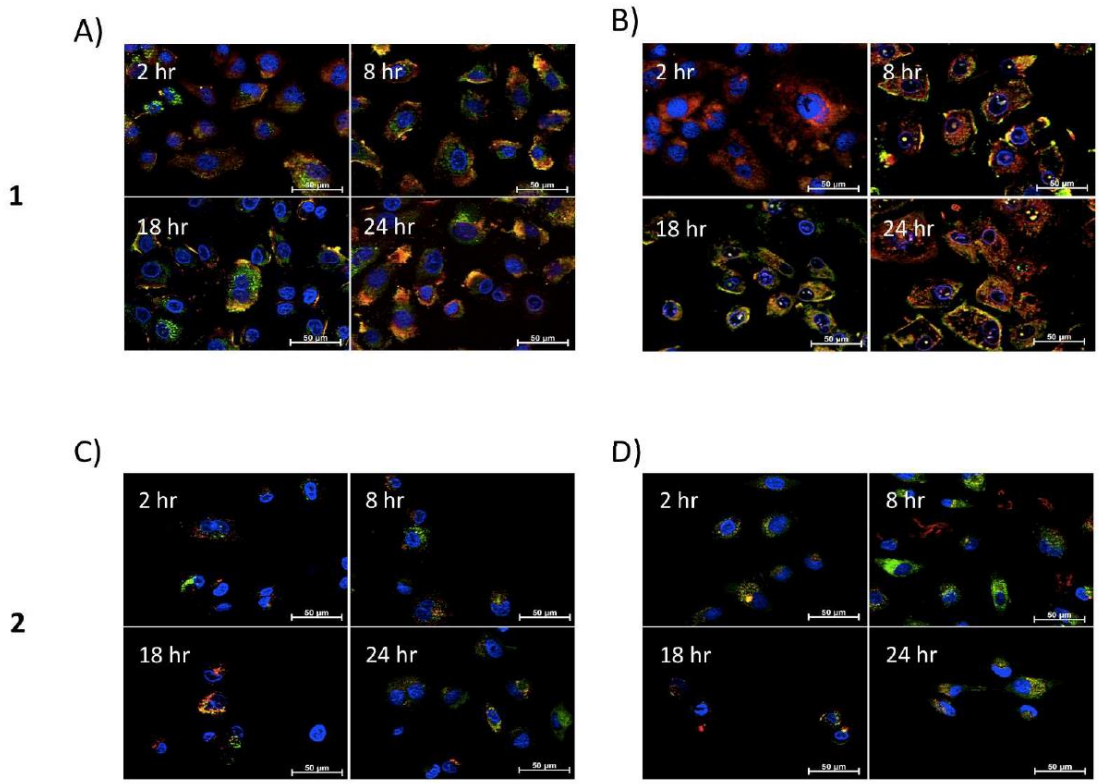

Figure S1.4 Time dependence of compound localization in lysosomes in A549 cells measured by ApoTome microscope. Lysotracker green was used to visualize lysosomes. A) **1**, dark; B) **1**, light; C) **2**, dark; D) **2**, light.

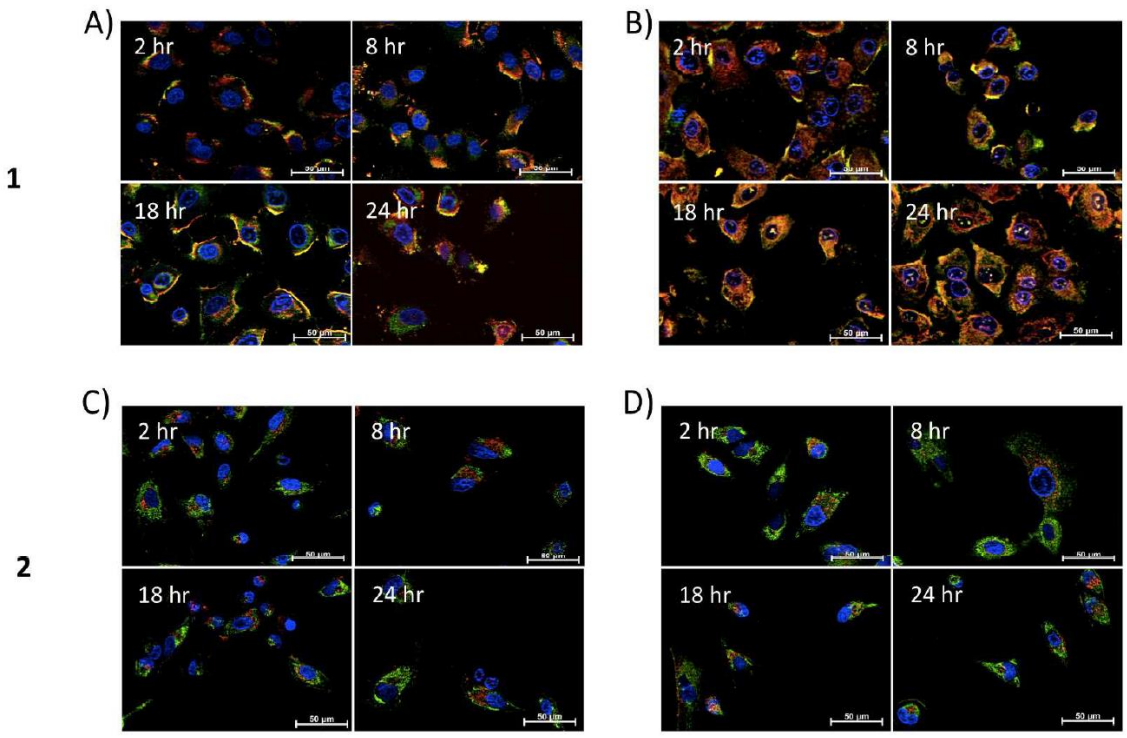

Figure S1.5 Time dependence of compound localization in mitochondria in A549 cells measured by ApoTome microscope. Mitotracker green was used to visualize mitochondria. A) **1**, dark; B) **1**, light; C) **2**, dark; D) **2**, light.

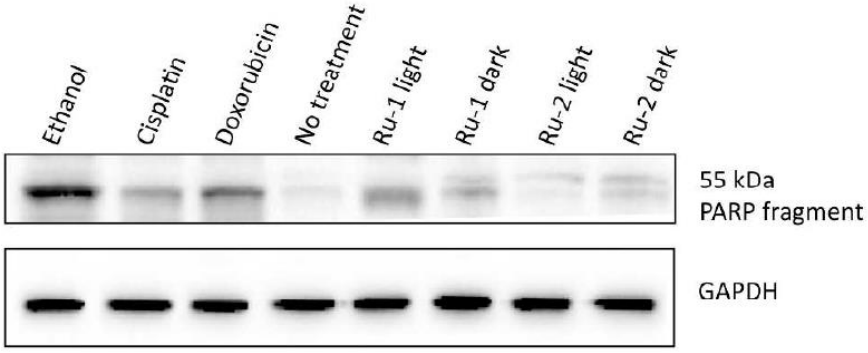

Figure S1.6 Western blotting of 55 kDa PARP fragment shows contribution from necrotic cell death for 10% ethanol, cisplatin, doxorubicin, **1**, and **2**.

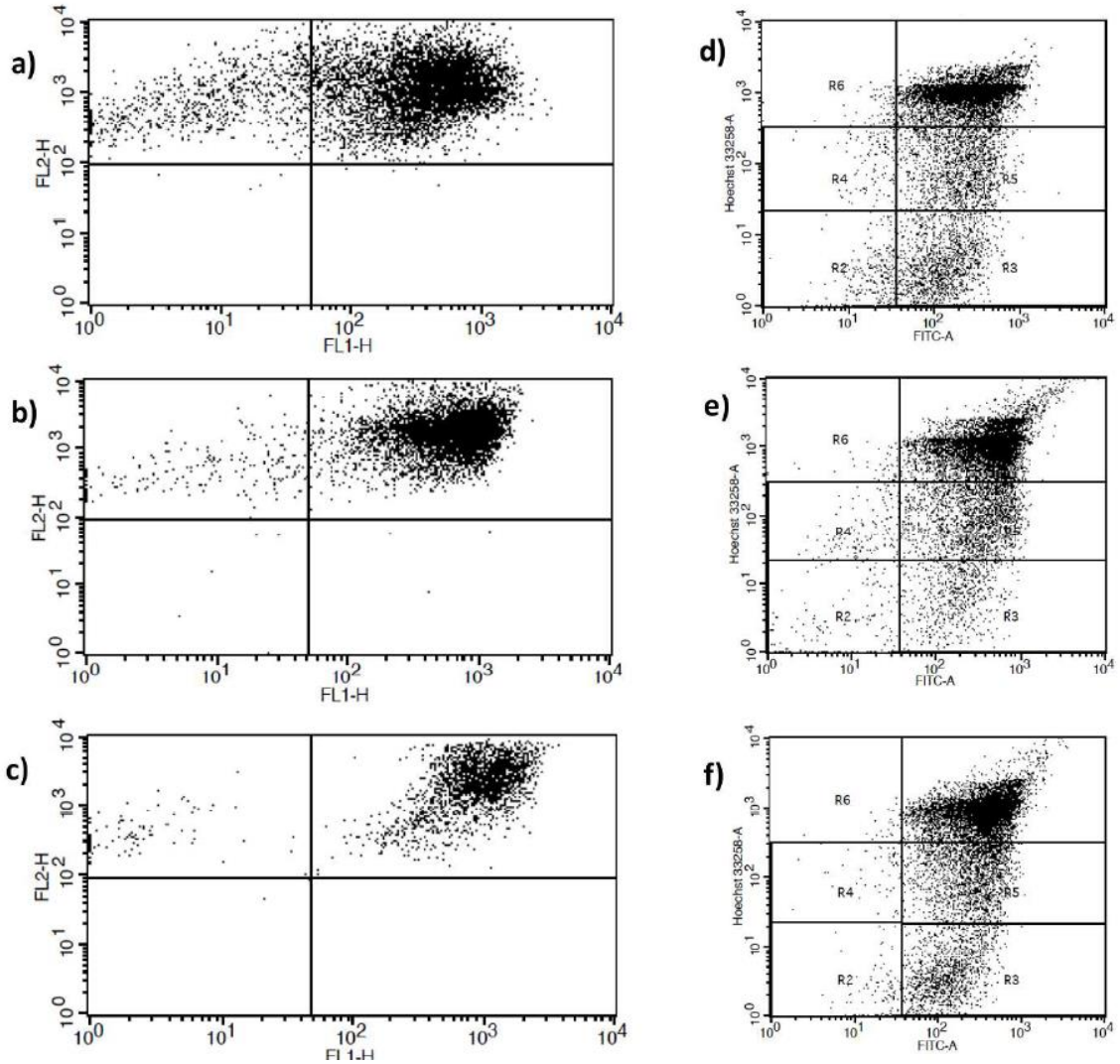

Figure S1.7 Flow cytometry analysis of apoptosis induced by **1** after light exposure. Annexin V was used in conjunction with Propidium Iodide (left) or Hoechst (right) staining. A) and D) 2 hours; B) and E) 8 hours; C) and F) 24 hours. Induction of cell death is rapid, and while there are many cells that are classified as late apoptotic (or necrotic), a very small percentage can be classified as early apoptotic (Annexin V positive cells, both PI or Hoechst negative).

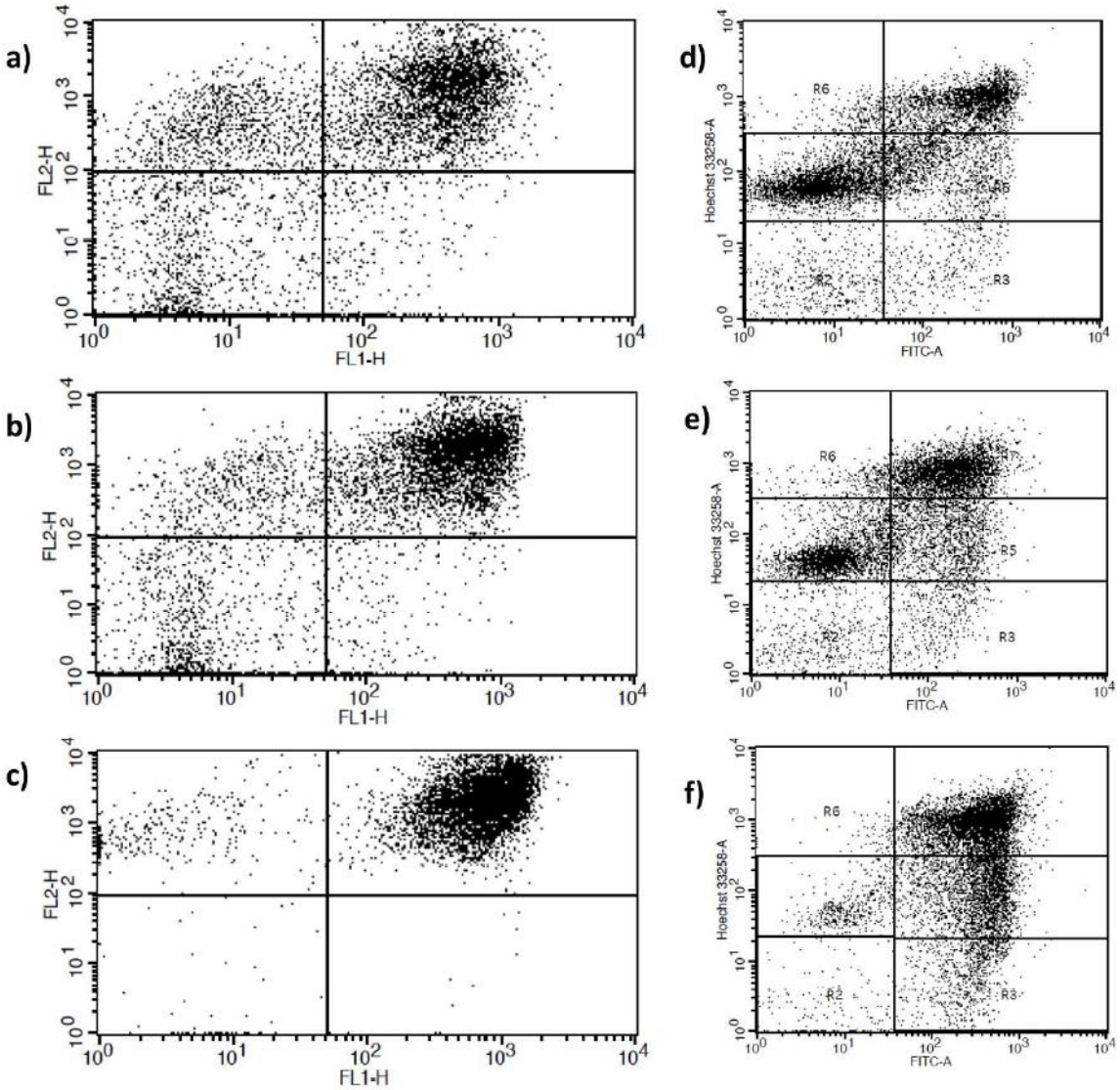

Figure S1.8 Flow cytometry analysis of apoptosis induced by **1** protected from light. Annexin V was used in conjunction with Propidium Iodide (left) or Hoechst (right) staining. A) and D) 2 hours; B) and E) 8 hours; C) and F) 24 hours. At all time points there are many cells that are classified as late apoptotic (or necrotic), but at 2 and 8 hours there are Annexin V negative cells that are both PI or Hoechst positive, indicating necrosis, along with some fraction of early apoptotic cells (Annexin V positive cells, both PI or Hoechst negative).

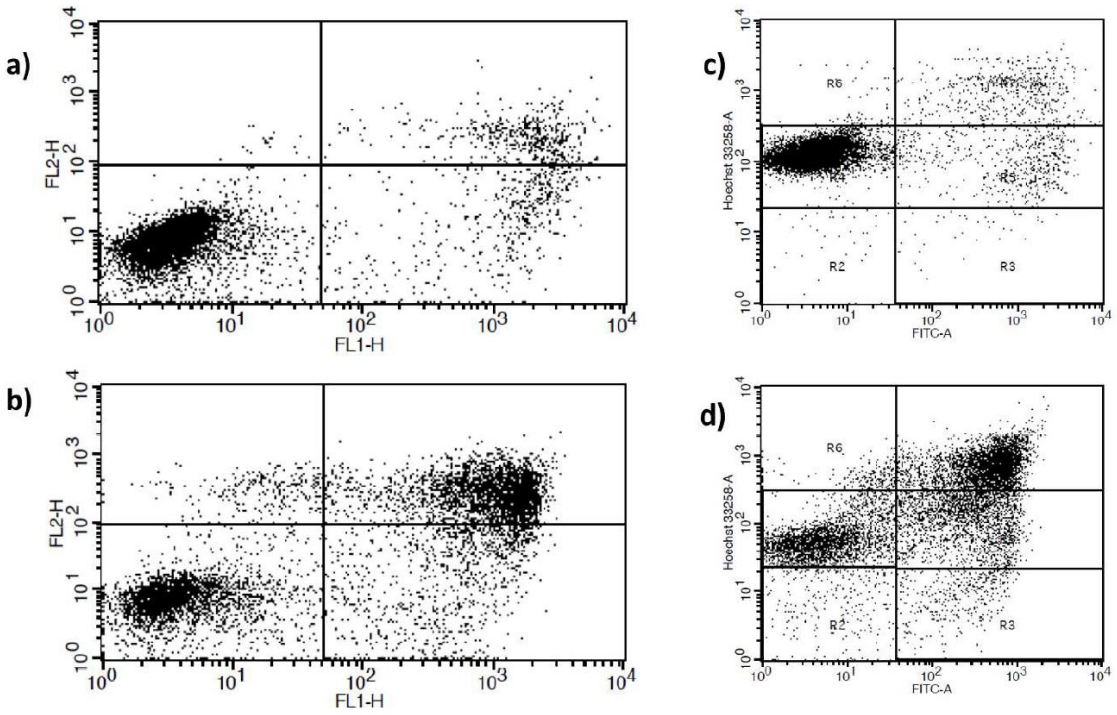

Figure S1.9 Flow cytometry analysis of apoptosis induced by **2** after light exposure. Annexin V was used in conjunction with Propidium Iodide (left) or Hoechst (right) staining. A) and C) 2 hours; B) and D) 24 hours. There are a significant fraction of early apoptotic cells (Annexin V positive cells, both PI or Hoechst negative).

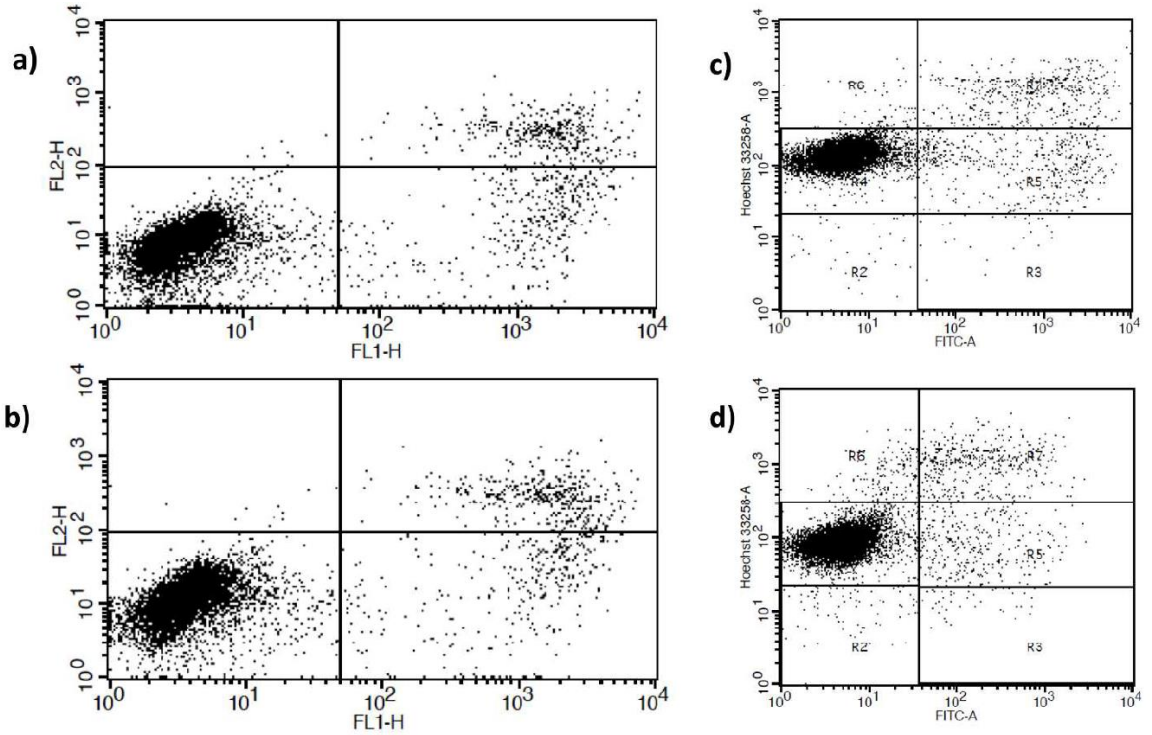

Figure S1.10 Flow cytometry analysis of apoptosis induced by **2** protected from light. Annexin V was used in conjunction with Propidium Iodide (left) or Hoechst (right) staining. A) and C) 2 hours; B) and D) 24 hours. The compound does not induce significant cell death.

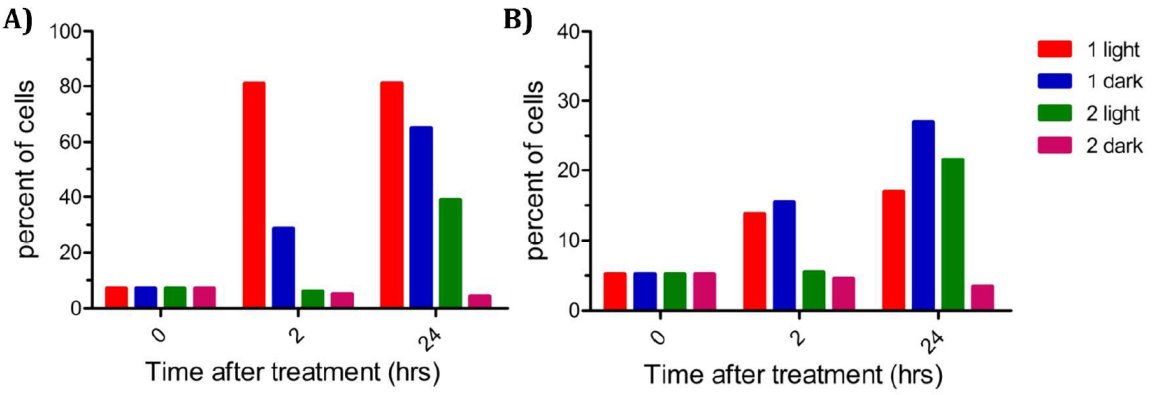

Figure S1.11 Cell death study by flow cytometry comparing ratio of early apoptotic vs. dead cells. HL60 cells were treated with 5 μM **1** or 20 μM **2** for 2 hrs and 24 hrs and stained by Hoechst 33342 and FITC conjugated Annexin V. The percent of A) dead cells and B) early apoptotic cells were measured by flow cytometry.

Appendix B. Supplemental tables and figures in chapter 3.

Note: Compound codes are chapter-specific.

Compound 1 = $[Ru(bpy)_2(6,6'\text{-dmbpy})]^{2+}$

Table S2.1 Cellular metal content with different nucleic acids measured by AAS.

	E. coli		**HL60**	
	Percentage of metal bound with genomic DNA[a]	Percentage of metal bound with total RNA[b]	Percentage of metal bound with genomic DNA[a]	Percentage of metal bound with total RNA[b]
1 light	1.3% ± 0.1%	0.5% ± 0.1%	1.3% ± 0.1%	2.0% ± 0.3%
1 dark	-[c]	-[c]	-[c]	-[c]
cisplatin	1.0% ± 0.1%	0.7% ± 0.1%	1.1% ± 0.1%	1.5% ± 0.2%

[a, b]The percentage of metal bound with genomic DNA or total RNA was calculated as follows:

$$\text{Percentage of metal bound with DNA (RNA)} = \frac{\text{Metal measured in DNA (RNA) sample (μmol)}}{\text{Metal in DNA sample + cell sample (μmol)}}$$

[c] Ruthenium level in DNA and RNA samples were under the detection limit (2ppb).

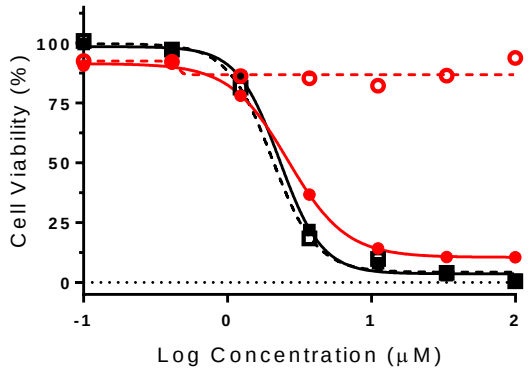

Figure S2.1 Cytotoxicity dose response of complex **1** (red lines) and cisplatin (black lines) in *E. coli* following photoirradiation (solid lines, filled circles) and dark condition (dashed lines, open circles).

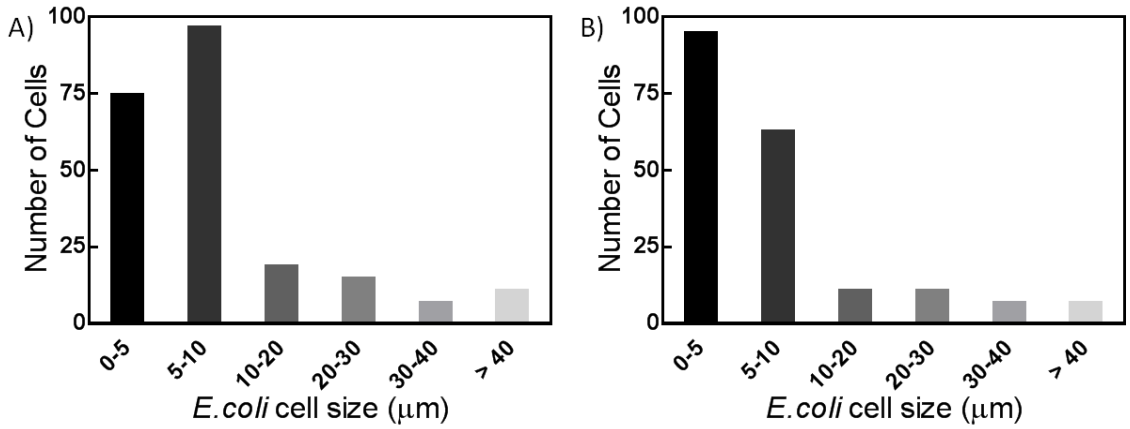

Figure S2.2 Size distribution histograms of *E. coli* filaments with treatment of A) rifampicin; and B) tetracycline. *E. coli* cells were treated with 3 μM of rifampicin and 48 μM of tetracycline (10x IC_{50}) for 6 hours.

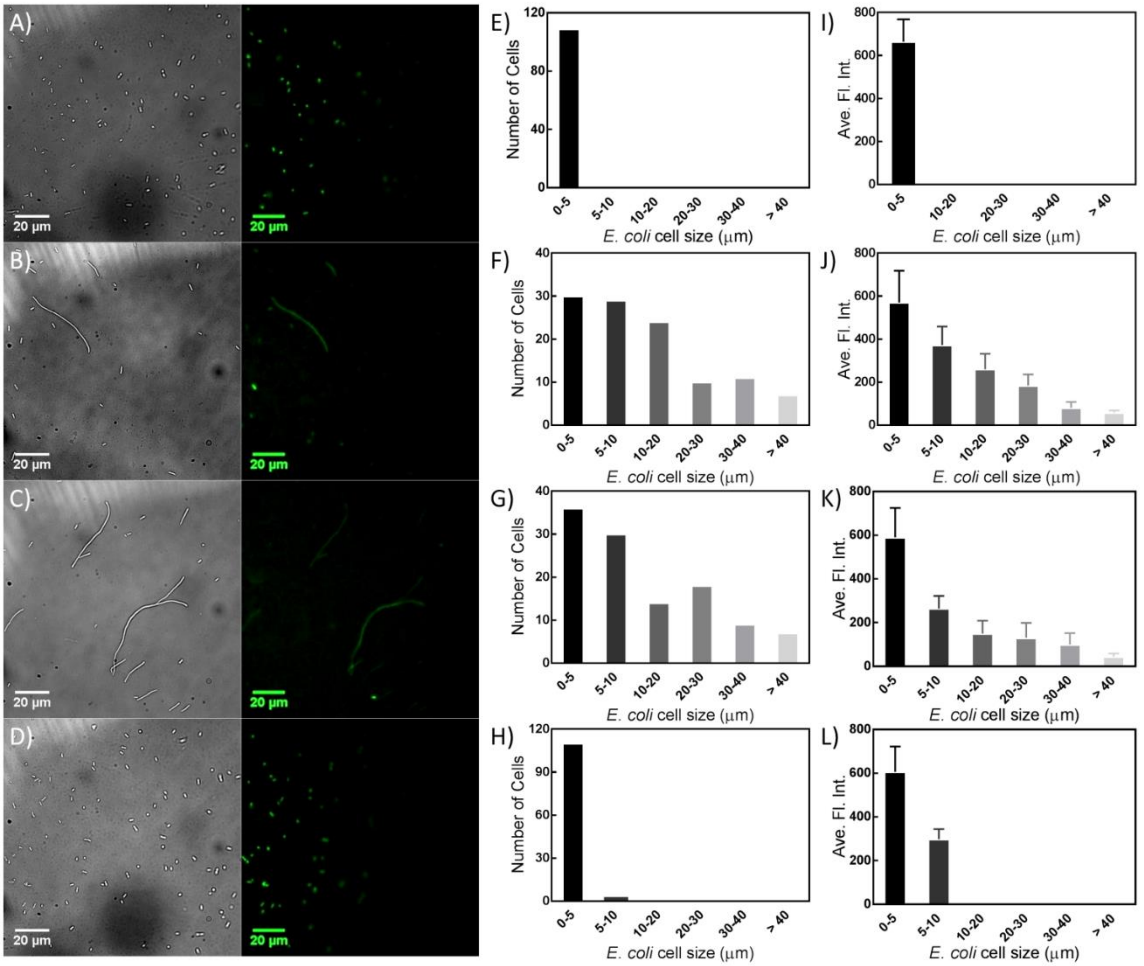

Figure S2.3 Complex **1** induces filamentous growth and decreased protein production in *E. coli*. A) - D) Bright field and fluorescent imaging of *E. coli* cells under different conditions; E) - H) Size distribution histograms of *E. coli* cells under different treatments; I)- L) Histograms of average fluorescence intensity (Ave. Fl. Int.) correlating to cell size with different treatments. Top through bottom panels: N. C. control, cisplatin, compound **1**with light, and compound 1 without light. Cells were treated with 40 μM each compound for 6 hours before imaging.

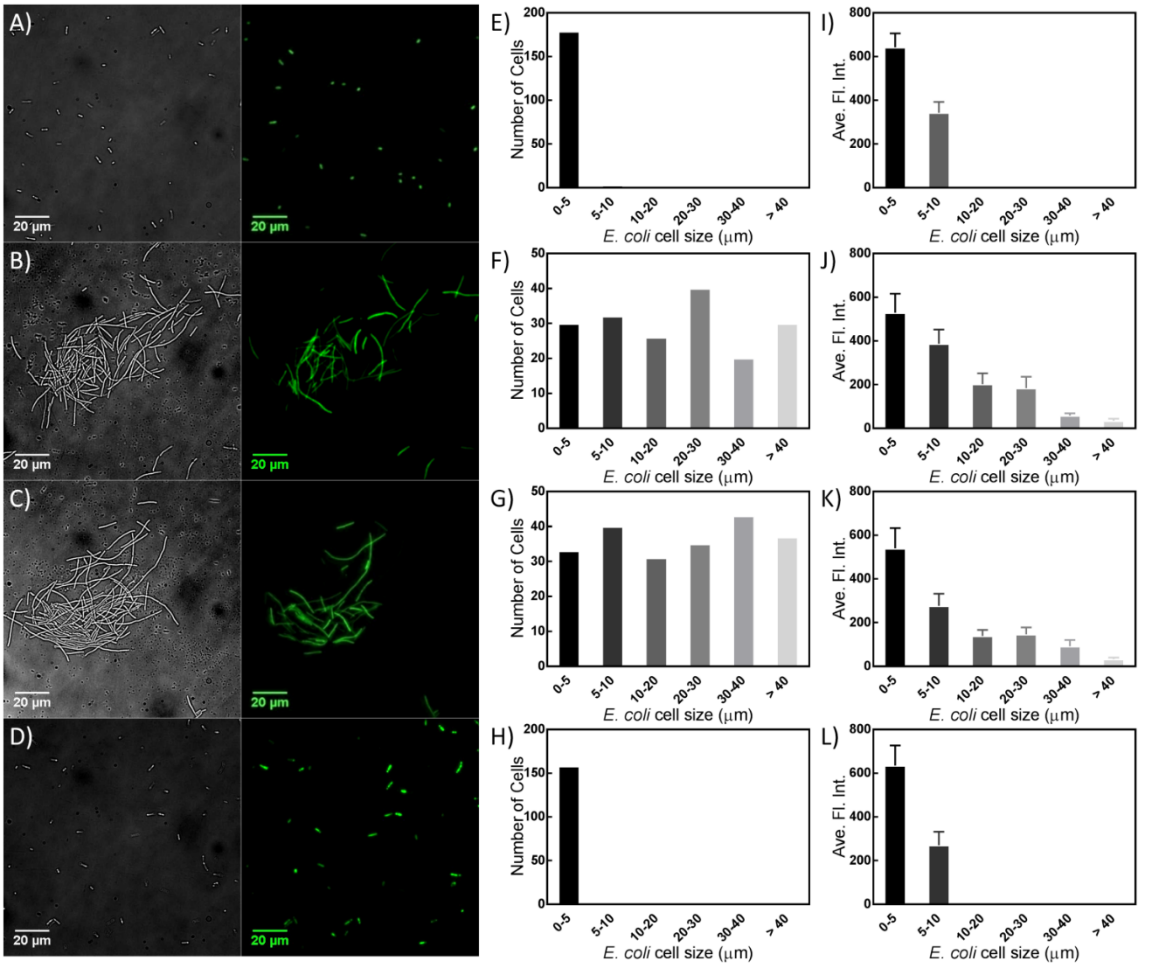

Figure S2.4 Complex **1** induces filamentous growth and decreased protein production in *E. coli*. A) - D) Bright field and fluorescent imaging of *E. coli* cells under different conditions; E) - H) Size distribution histograms of *E. coli* cells under different treatments; I)- L) Histograms of average fluorescence intensity (Ave. Fl. Int.) correlating to cell size with different treatments. Top through bottom panels: N. C. control, cisplatin, compound **1**with light, and compound **1**without light. Cells were treated with 40 μM each compound for 16 hours before imaging.

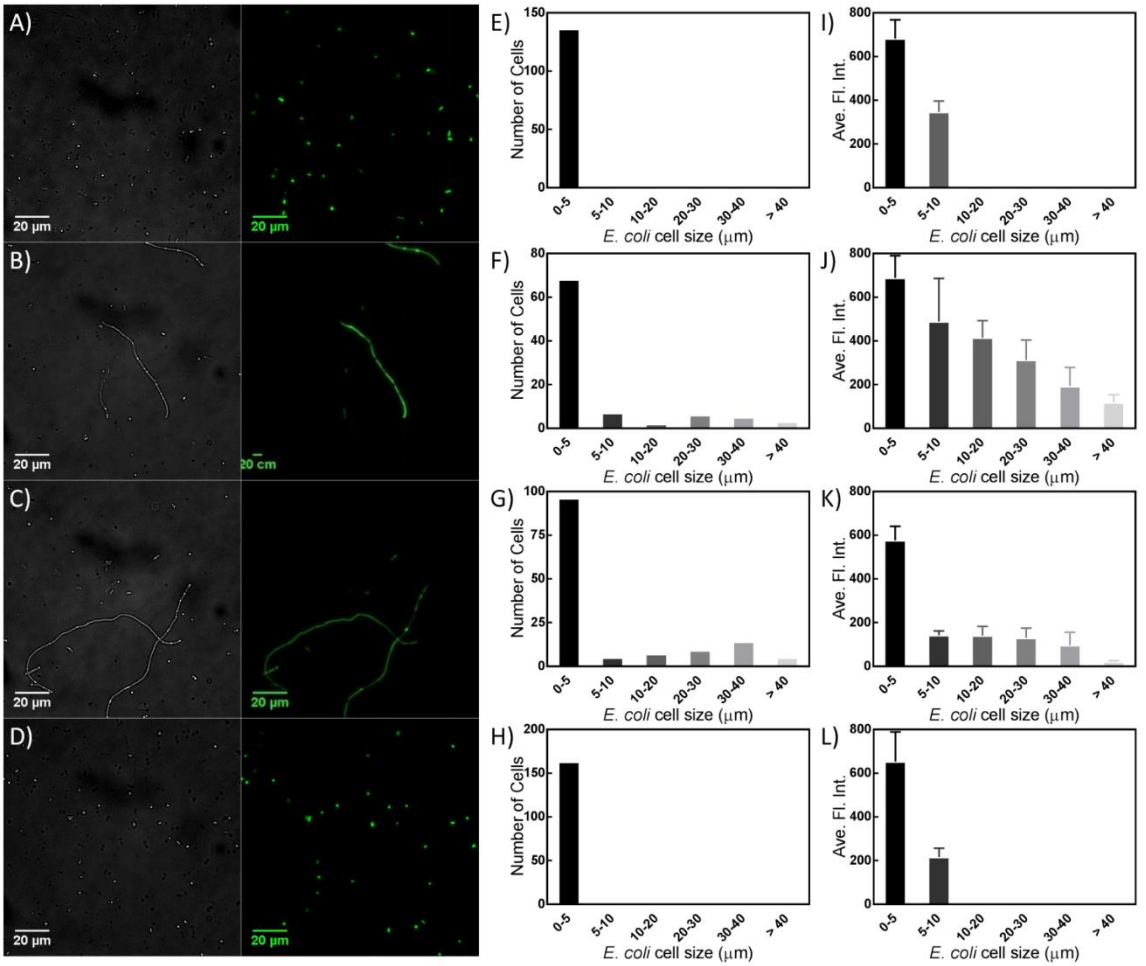

Figure S2.5 Complex **1** induces filamentous growth and decreased protein production in *E. coli*. A) - D) Bright field and fluorescent imaging of *E. coli* cells under different conditions; E) - H) Size distribution histograms of *E. coli* cells under different treatments; I)- L) Histograms of average fluorescence intensity (Ave. Fl. Int.) correlating to cell size with different treatments. Top through bottom panels: N. C. control, cisplatin, compound **1**with light, and compound **1**without light. Cells were treated with 100 μM each compound for 16 hours before imaging.

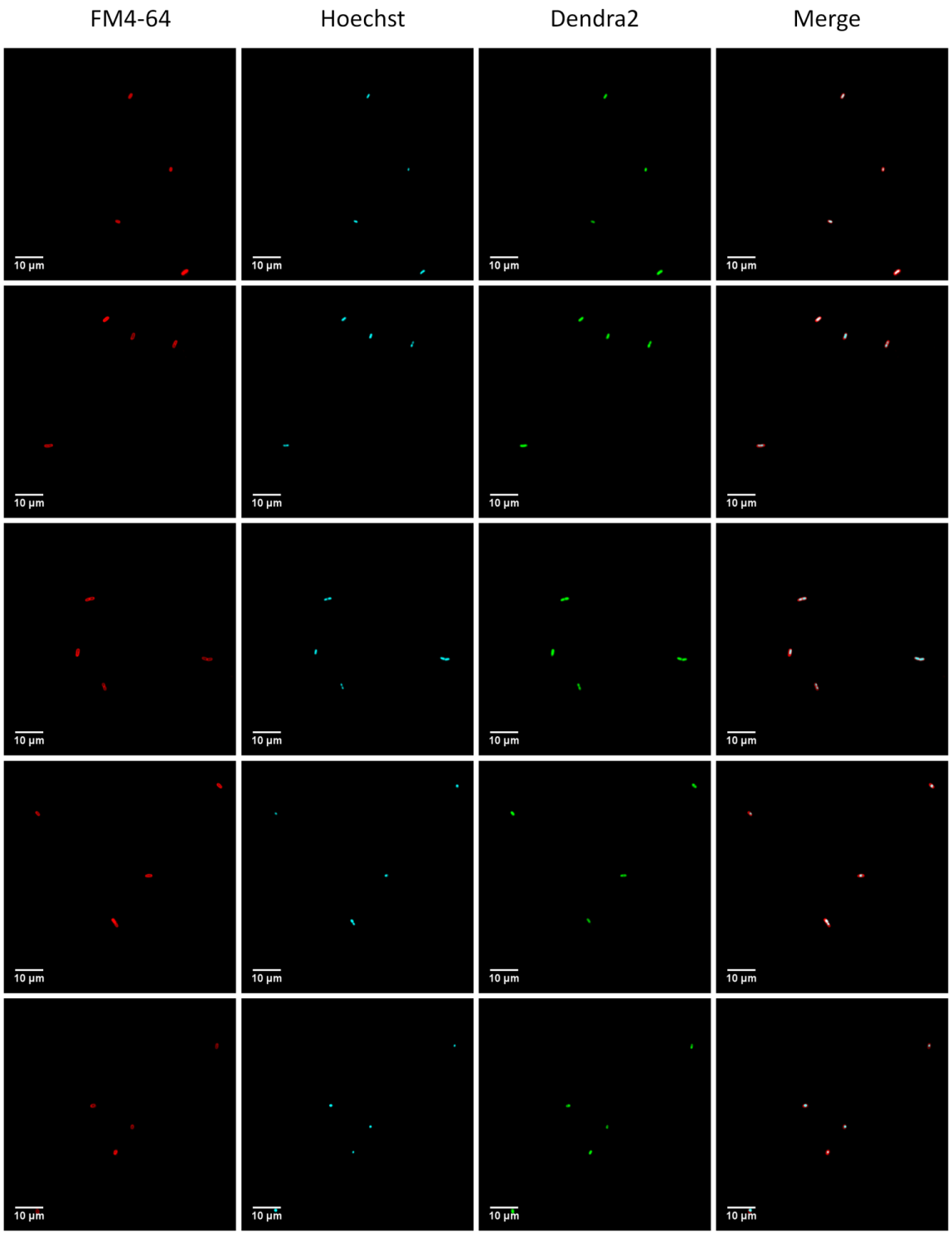

Figure S2.6 Supplemental fluorescent imaging of N. C. control. The merge is the combination of the Hoechst and FM4-64 membrane stain emission data.

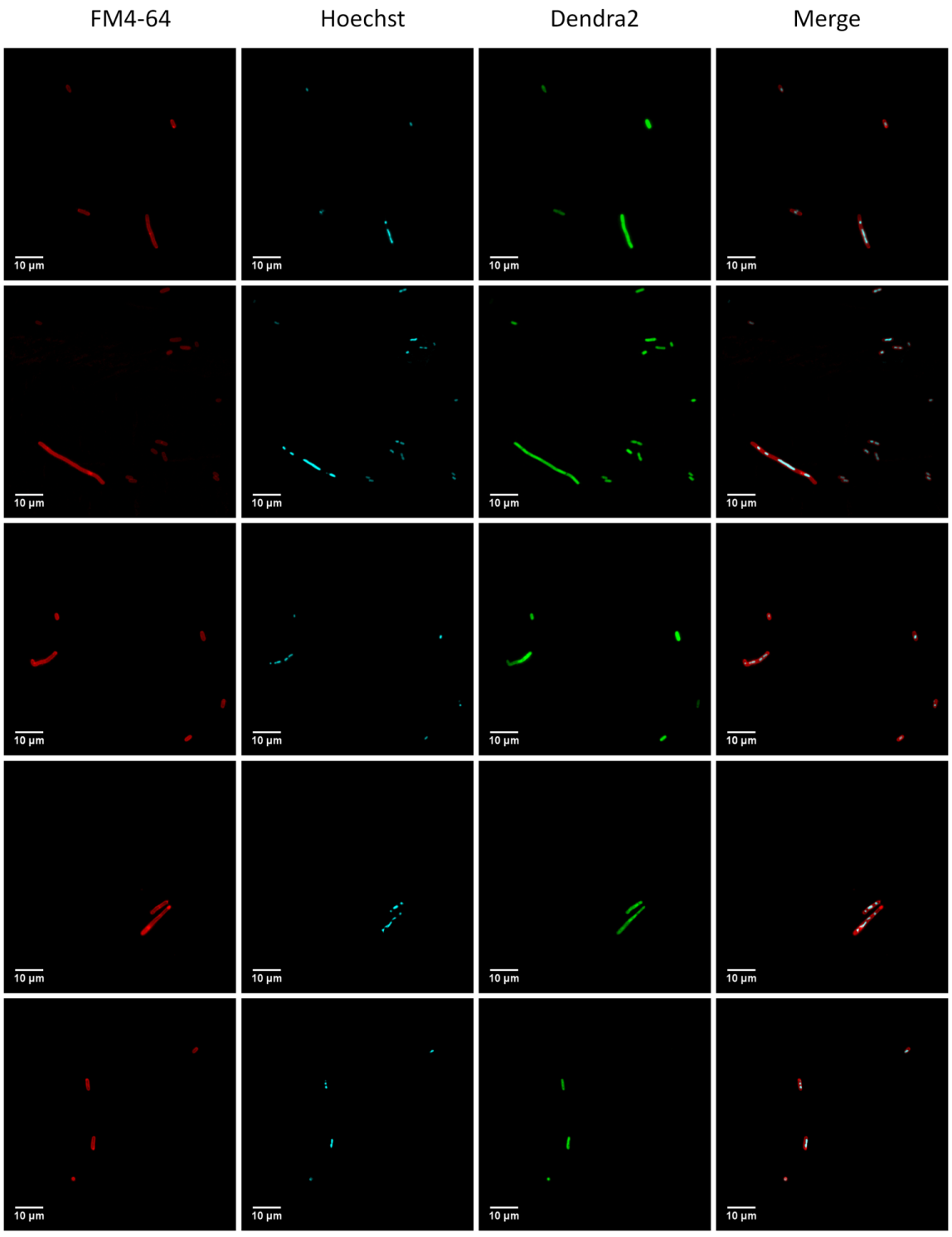

Figure S2.7 Supplemental fluorescent imaging of cisplatin. Cells were treated MIC for 6 hours before imaging. The merge is the combination of the Hoechst and FM4-64 membrane stain emission data.

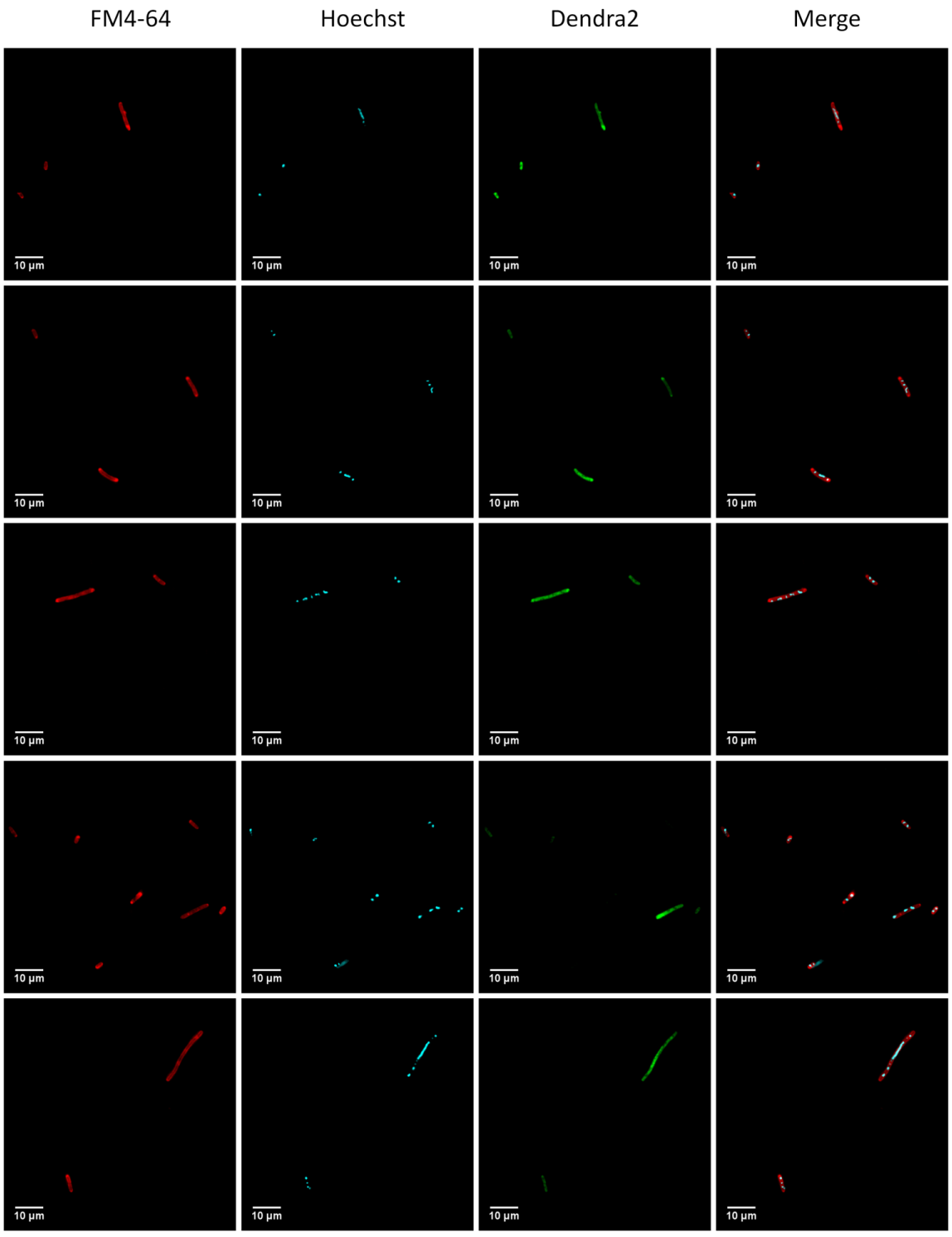

Figure S2.8 Supplemental fluorescent imaging of compound **1** with light. Cells were treated MIC for 6 hours before imaging. The merge is the combination of the Hoechst and FM4-64 membrane stain emission data.

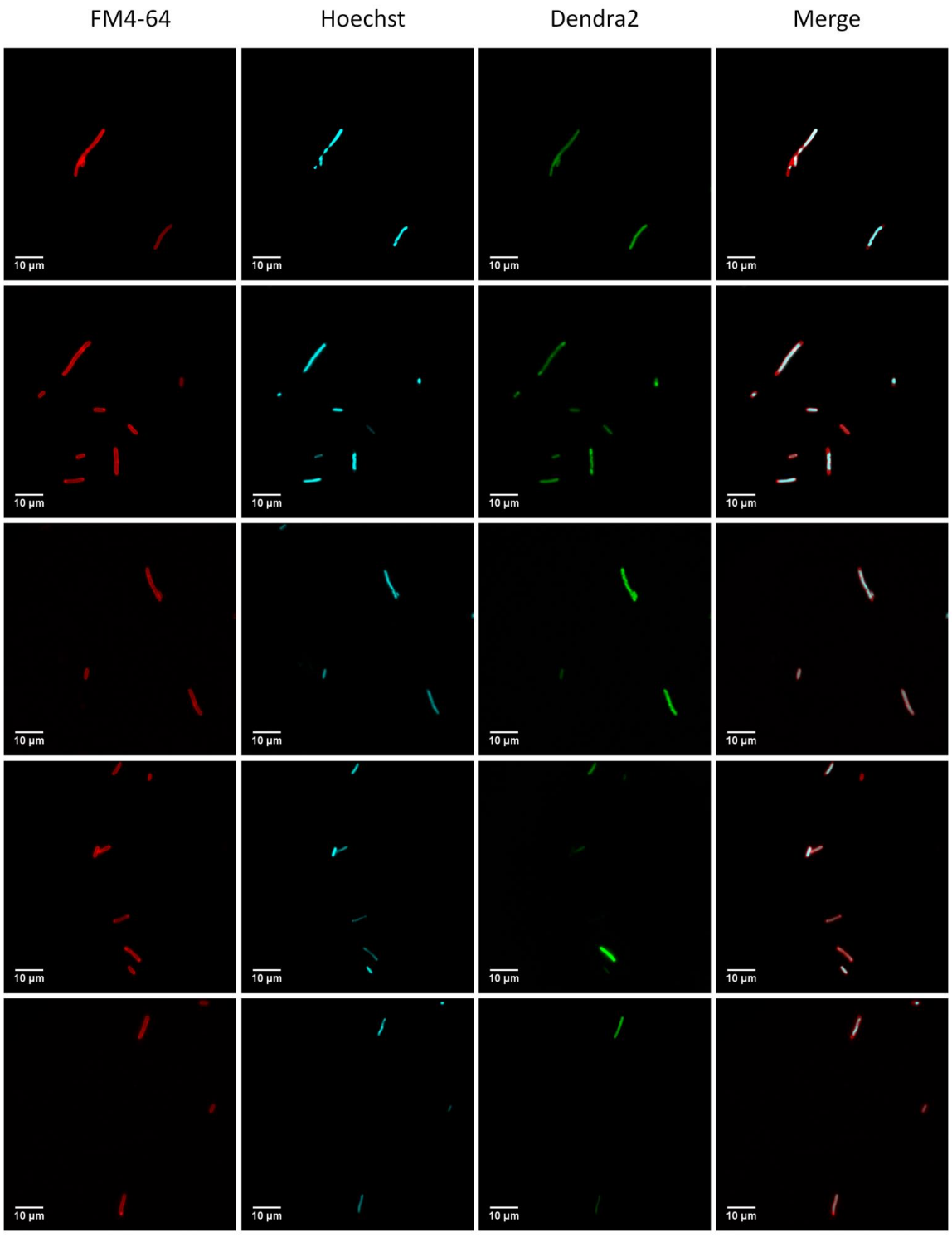

Figure S2.9 Supplemental fluorescent imaging of rifampicin. Cells were treated 10x MIC for 6 hours before imaging. The merge is the combination of the Hoechst and FM4-64 membrane stain emission data.

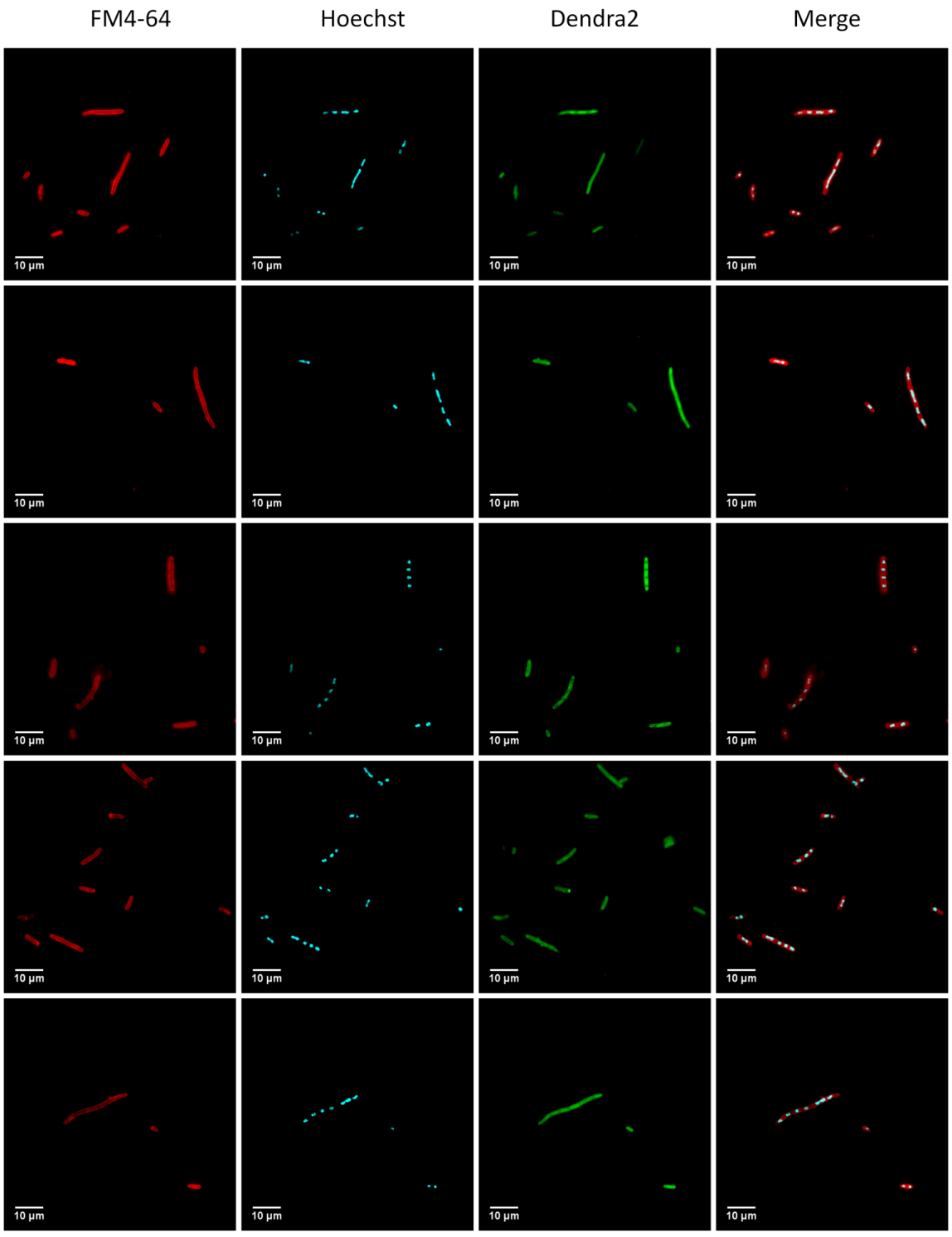

Figure S2.10 Supplemental fluorescent imaging of tetracycline. Cells were treated MIC for 6 hours before imaging. The merge is the combination of the Hoechst and FM4-64 membrane stain emission data.

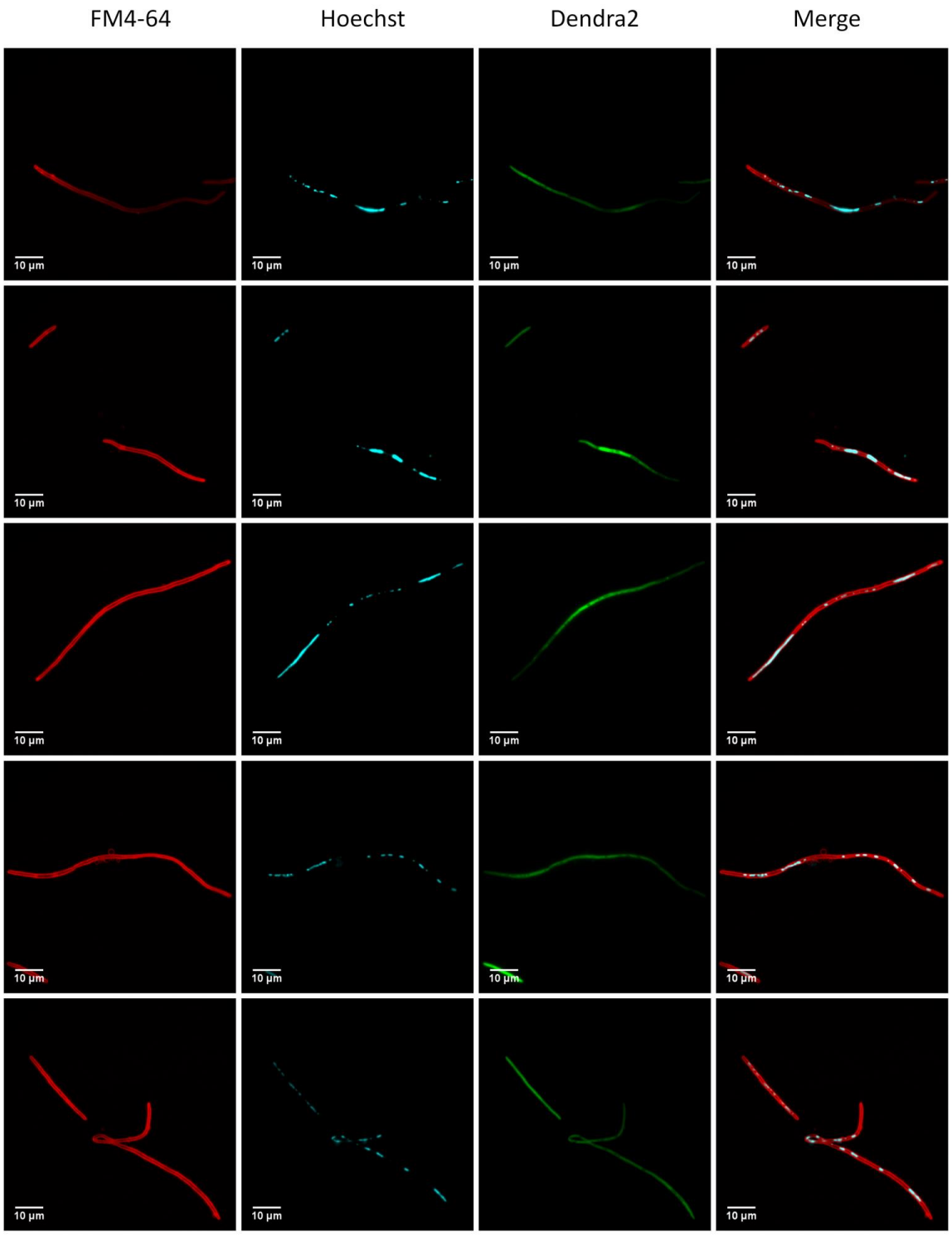

Figure S2.11 Supplemental fluorescent imaging of nalidixic acid. Cells were treated MIC for 6 hours before imaging. The merge is the combination of the Hoechst and FM4-64 membrane stain emission data.

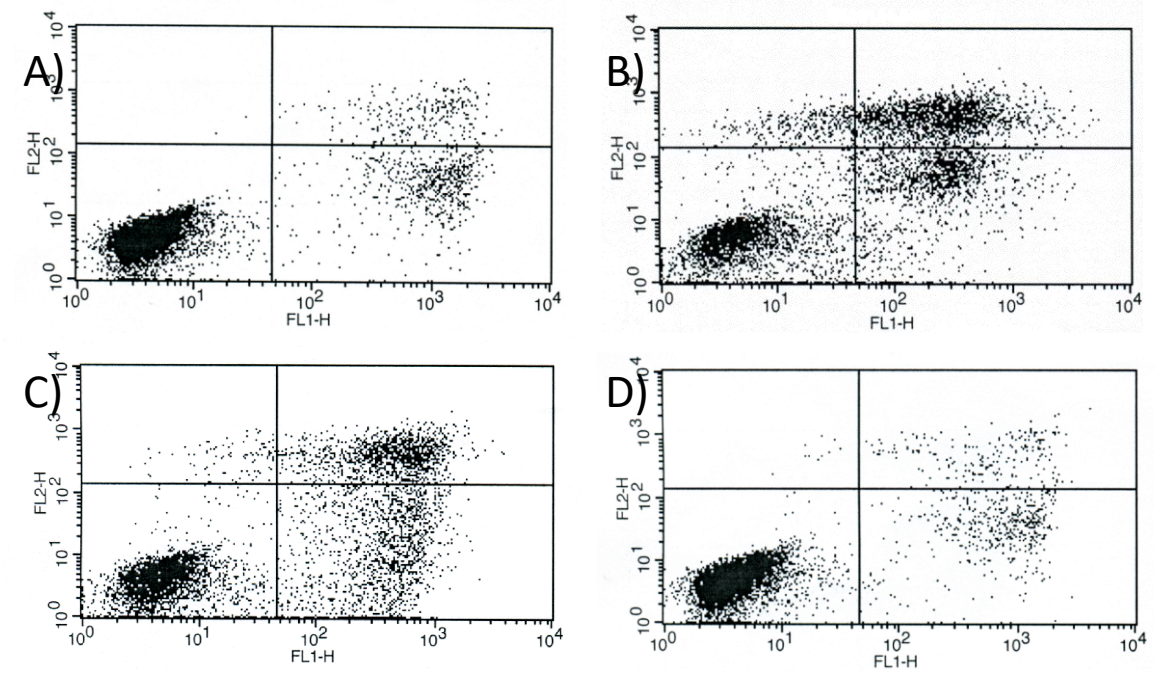

Figure S2.12 Flow cytometry analysis by FITC/Annexin-V and PI of apoptosis in HL60 cells. FITC-Annexin V (FL1-H) was used in combination with propidium iodide (FL2-H). A) N. C. control; B) cisplatin; C) compound **1** with light irradiation; D) compound **1** in dark. HL60 cells were treated with 20 μM compounds for 24 hours.

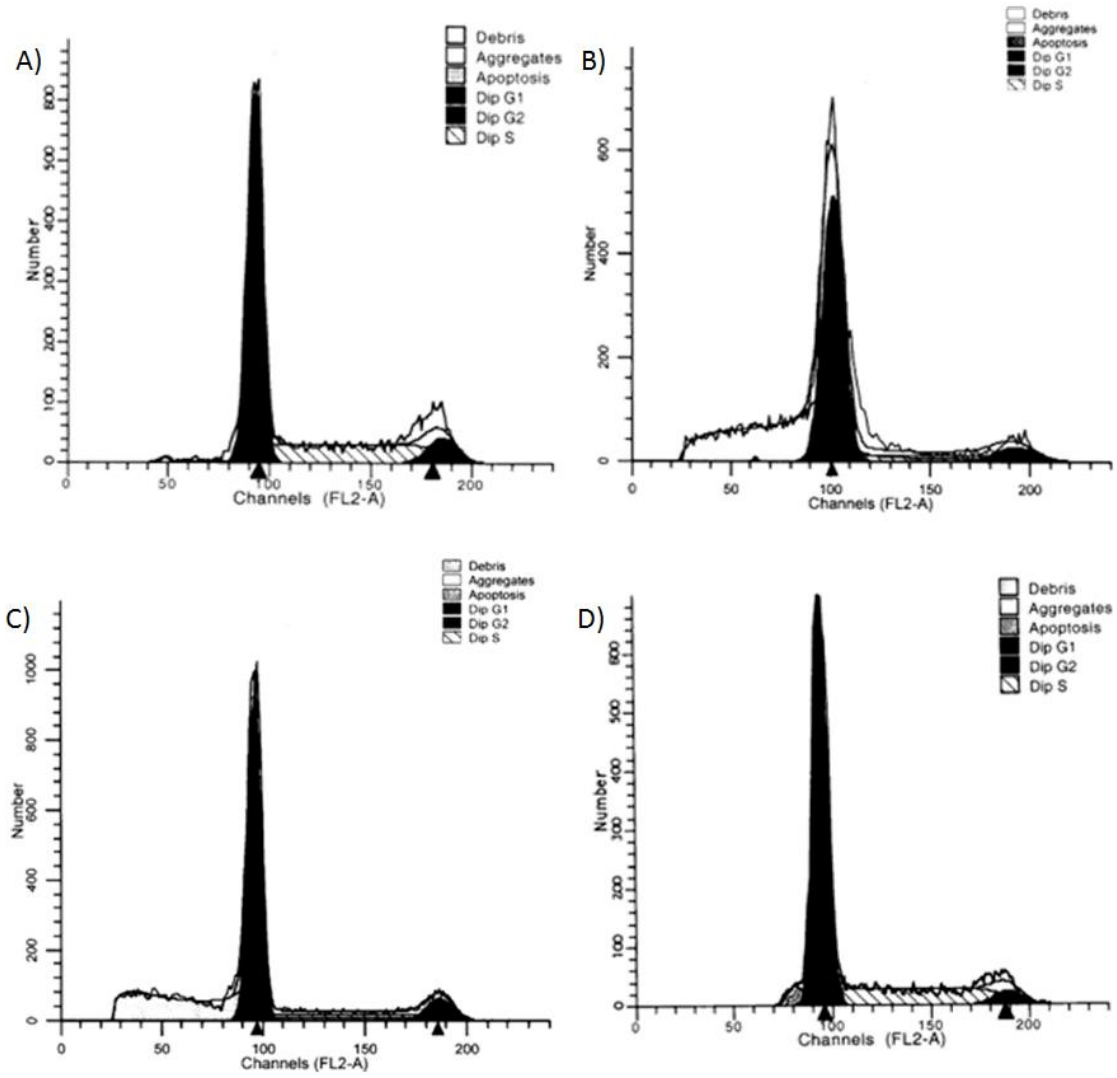

Figure S2.13 Flow cytometry analysis by propidium iodide of cell cycle arrest in HL60 cells. A) N. C. control; B) cisplatin; C) compound **1** with light irradiation; D) compound **1** in dark. HL60 cells were treated with compounds for 24 hours.

Calculation of the ratio of DNA and RNA nucleotides to metal based on data reported by DeRose *et al.*[188]:

The platinum content measured after 12 hours treatment of 100 μM cisplatin was used for this calculation.

Pt / DNA nt = 60.2×10^{-5}

DNA nt / Pt = $\frac{1}{60.2 \times 10^{-5}} = 1661{:}1$

Pt / RNA nt = 15.7×10^{-5}

RNA nt / Pt = $\frac{1}{15.7 \times 10^{-5}} = 6369{:}1$

Calculation of the ratio of DNA and RNA nucleotides to metal based on data reported from an IVTT assay[199] (at the IC_{50}):

DNA bp / Ru = 570:1

DNA nt / Ru = 1140:1

DNA bp / Pt = 300:1

DNA nt / Pt = 600:1

RNA nt / Ru = 610:1

RNA nt / Pt = 820:1

Calculation of the ratio of DNA and RNA nucleotides to metal at the IC_{50} to Dendra2 production inhibition based on data collected in AAS:

The DNA and RNA nt / mc ratio collected by AAS at 20μM is as follows:

DNA nt / Ru = 2000:1

DNA nt / Pt = 3000:1

RNA nt / Ru = 3800:1

RNA nt / Pt = 4700:1

Assuming the uptake is linearly proportional to the dosed concentration, the IC_{50} value to inhibit Dendra2 production in *E. coli* is 77 μM for compound **1** and 85 μM for cisplatin. Thus, a correction coefficient can be calculated to adjust the metal content to what would be obtained at the higher compound dose:

Compound **1**: $\frac{77}{20} = 3.8$

Cisplatin: $\frac{85}{20} = 4.3$

Then, at the IC_{50} to inhibit Dendra2 production, the theoretical metal to DNA or RNA nucleotides to metal ratio can be calculated as follows:

DNA nt / Ru $= \frac{2000}{3.8} = 520 : 1$

RNA nt / Ru $= \frac{3800}{3.8} = 1000 : 1$

DNA nt / Pt $= \frac{3000}{4.3} = 700 : 1$

RNA nt / Pt $= \frac{4700}{4.3} = 1090 : 1$

The average molecular weight values used in calculation for DNA base pairs and RNA nucleotides are 665 g/mol and 340 g/mol.

Appendix C. Supplemental tables and figures in chapter 4.

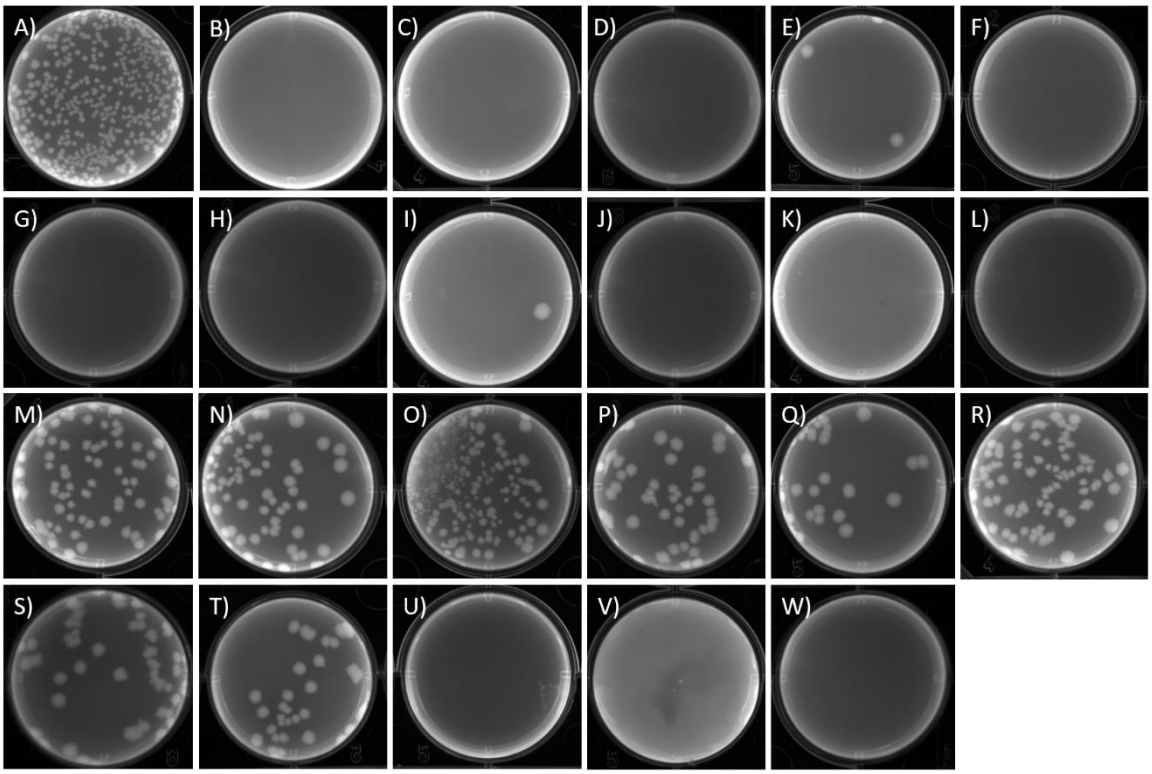

Figure S3.1 Colony formation after *E. coli* treated with A) untreated control, B) bleomycin, C) mitomycin C, D), ciprofloxacin, E) nalidixic acid, F) MMS, G) EMS, H) cisplatin, I) carboplatin, J) oxaliplatin, K) chlormethine, L) chlorambucil, M) BCEA, N) 4-NQO, O) puromycin, P) rifampicin, Q) rifaximin, R) tetracycline, S) chloramphenicol, T) kanamycin, U) doxorubicin, V) etoposide, W) mitoxantrone.

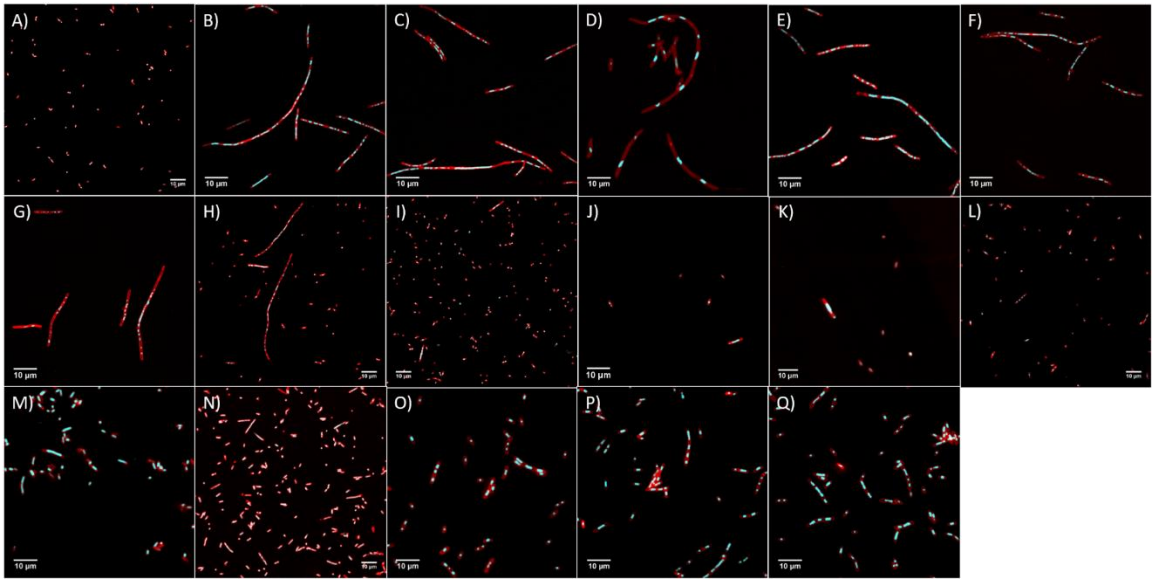

Figure S3.2 *E. coli* cells treated with A) untreated control, B) bleomycin, C) mitomycin C, D), ciprofloxacin, E) nalidixic acid, F) MMS, G) EMS, H) chlormethine, I) chlorambucil, J) BCEA, K) 4-NQO, L) puromycin, M) rifampicin, N) rifaximin, O) tetracycline, P) chloramphenicol, Q) kanamycin. All scale bars represent 10 µm.

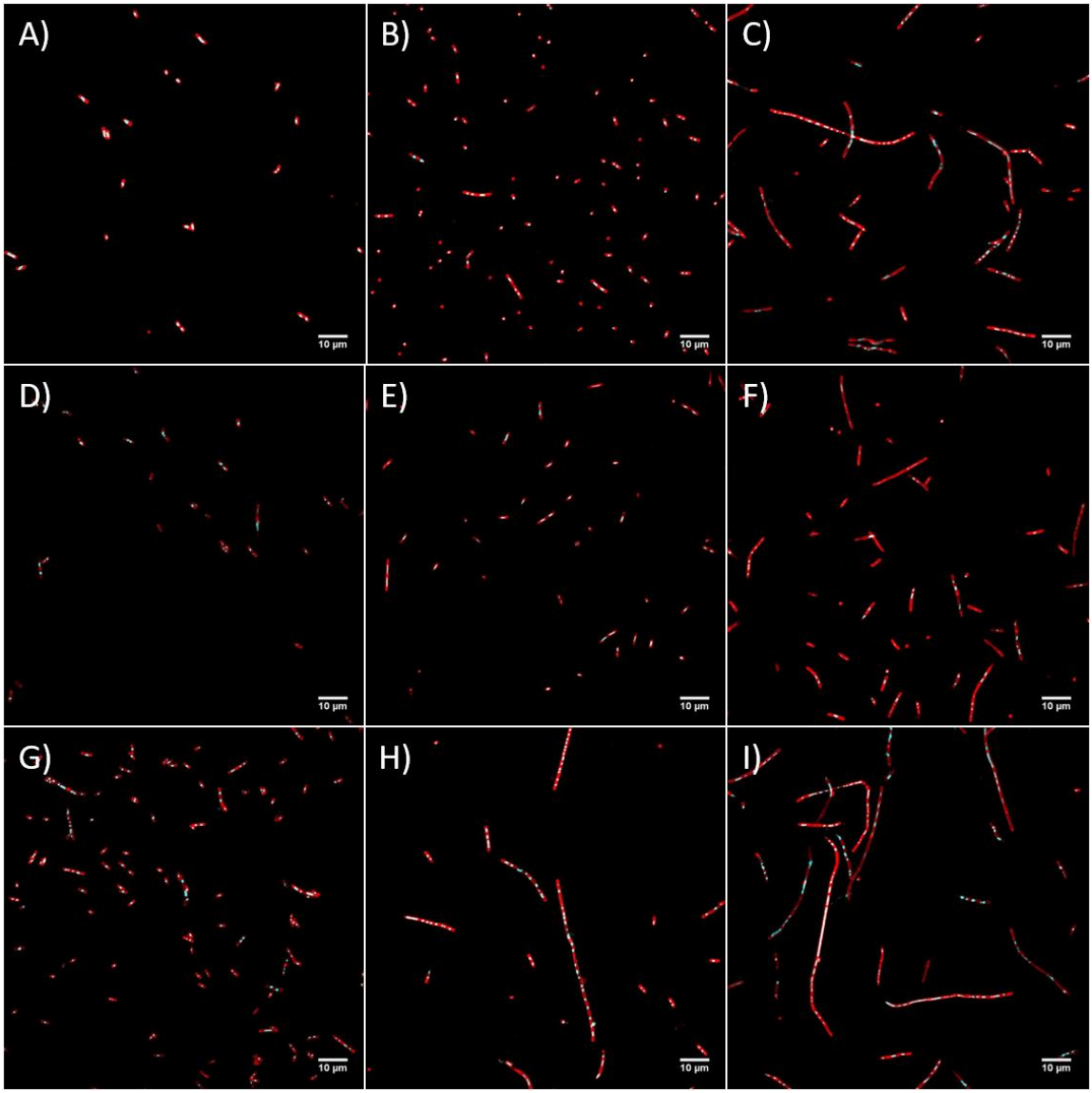

Figure S3.3 *E. coli* cells treated with carboplatin at A) 0.1 x MIC, B) 1 x MIC, and C) 5 x MIC; with cisplatin at D) 0.1 x MIC, E) 1 x MIC, and F) 5 x MIC; and with oxaliplatin at H) 0.1 x MIC, I) 1 x MIC, and J) 5 x MIC. All scale bars represent 10 µm.

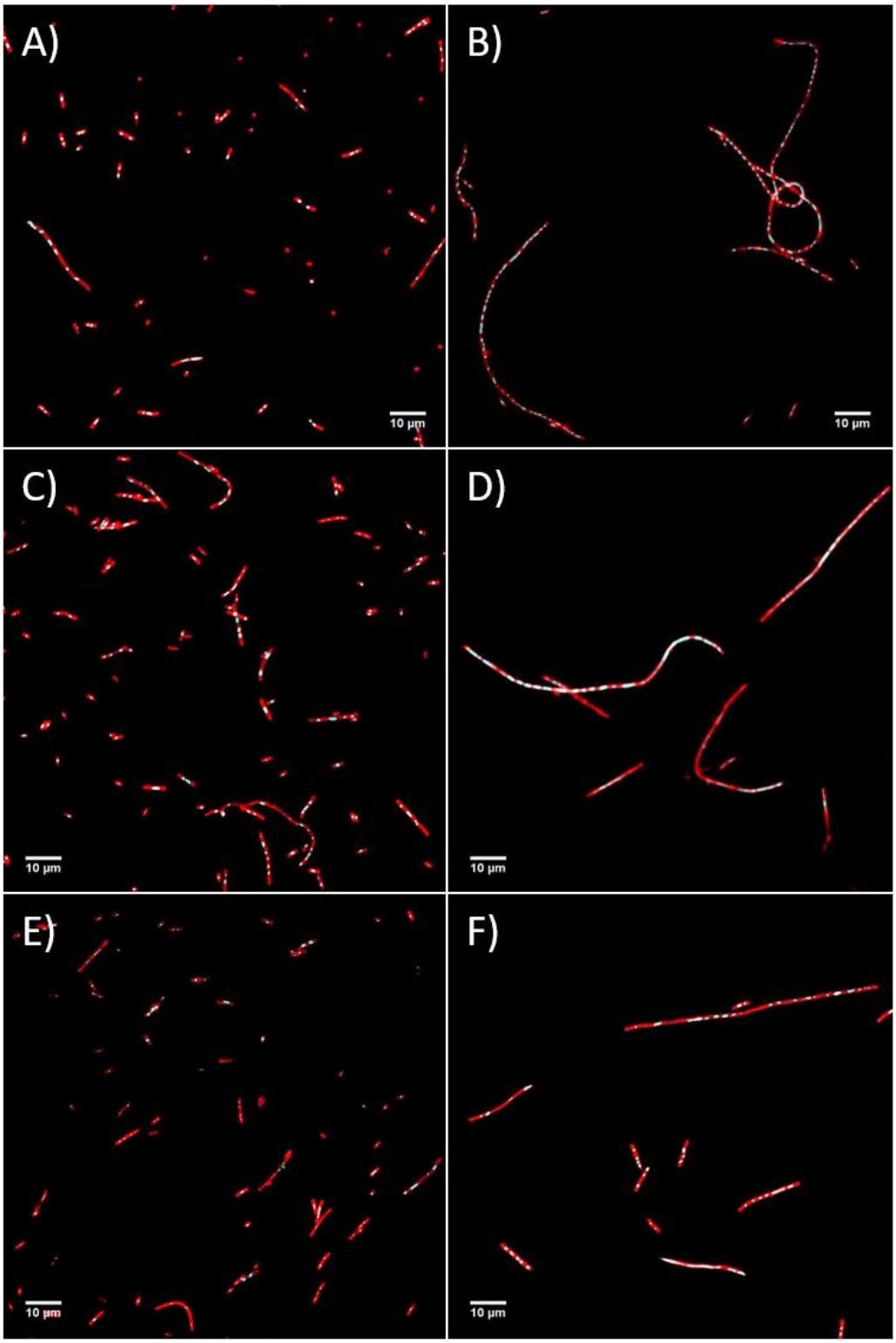

Figure S3.4 *E. coli* cells treated with etoposide at A) 0.1 x MIC, B) 1 x MIC; with doxorubicin at C) 0.1 x MIC, D) 1 x MIC; and with mitoxantrone at E) 0.1 x MIC, F) 1 x MIC. All scale bars represent 10 µm.

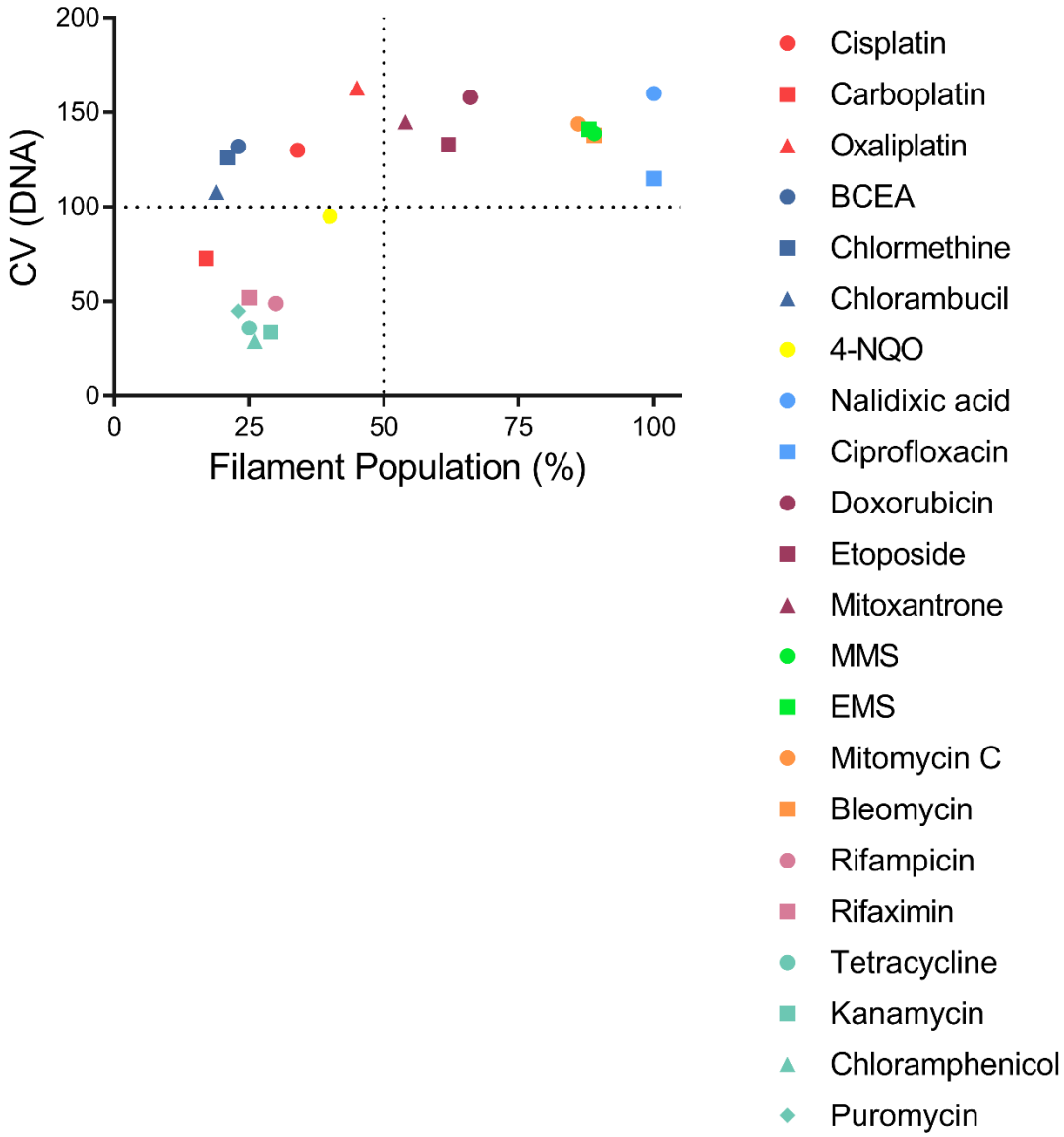

Figure S3.5 Distinguishing anticancer molecules with different mechanisms based on the phenotypic change observed in *E. coli*. Cells were treated with molecules at their MIC for 6 hours prior to imaging, translation inhibitors were dosed at 10 x MIC for phenotypic changes. Same phenotypic features as used for Figure 4.5 were analyzed with Prism 7.02.

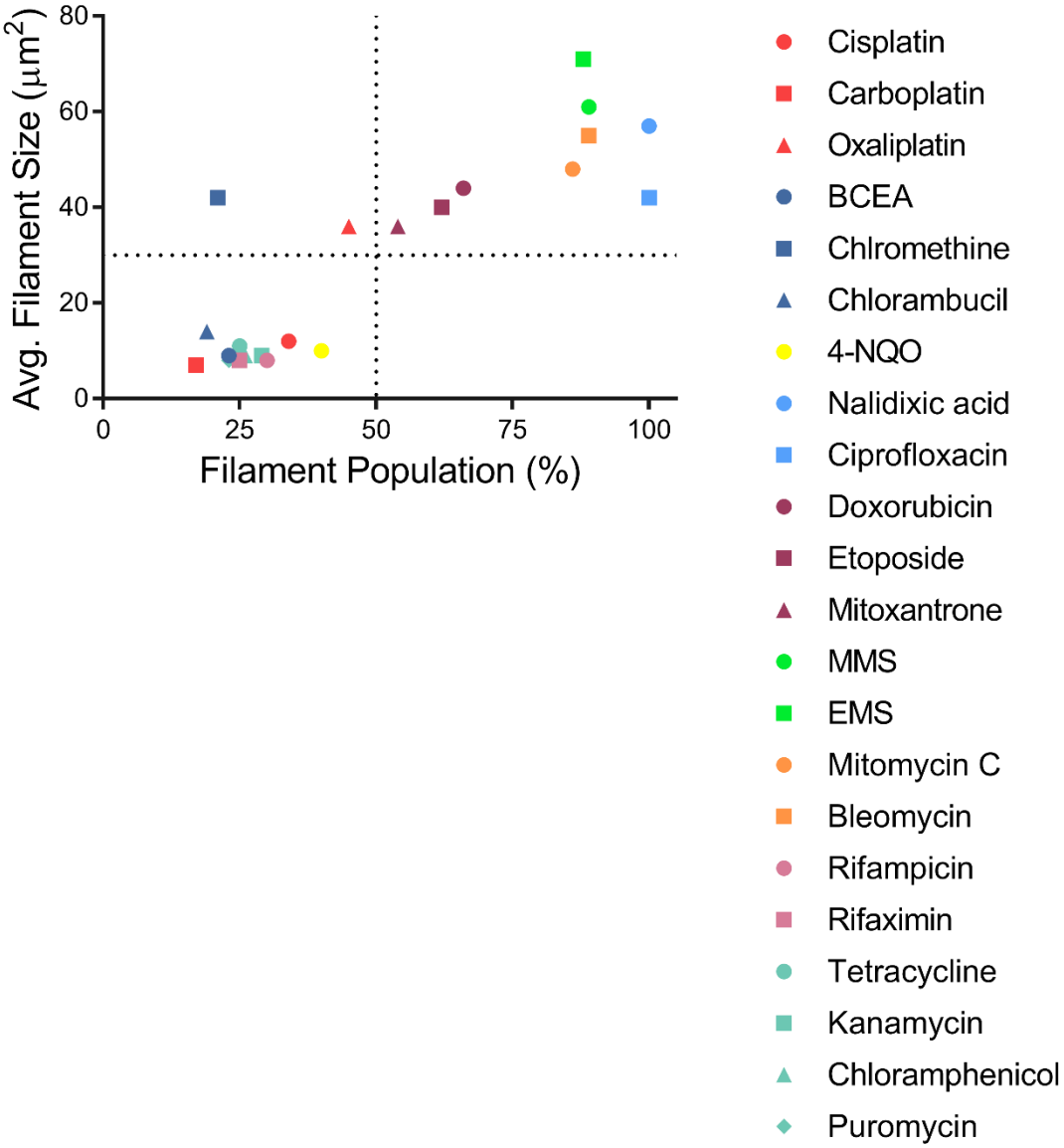

Figure S3.6 Distinguishing anticancer molecules with different mechanisms based on the phenotypic change observed in *E. coli*. Cells were treated with molecules at their MIC for 6 hours prior to imaging, translation inhibitors were dosed at 10 x MIC for phenotypic changes. Same phenotypic features as used for Figure 4.5 were analyzed with Prism 7.02.

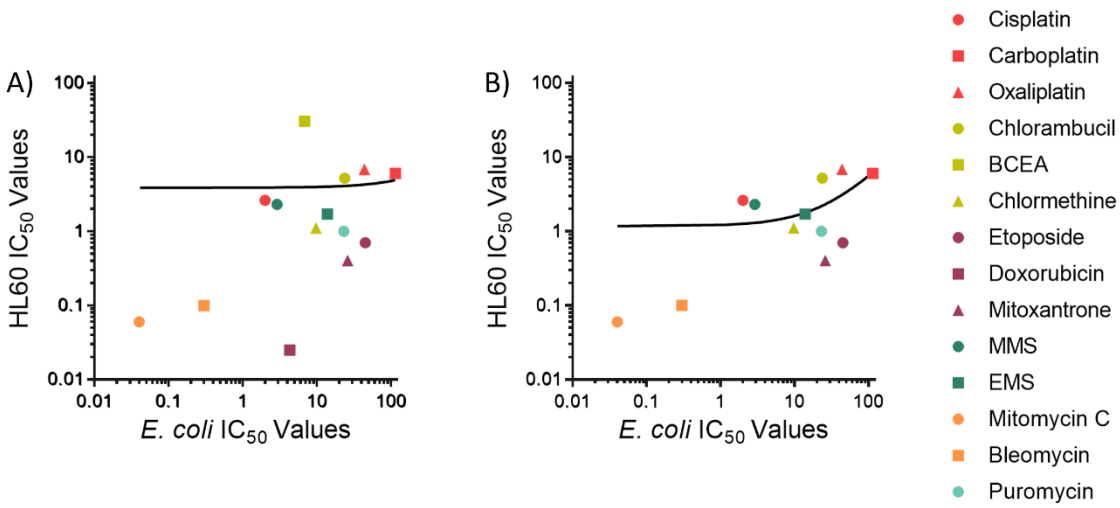

Figure S3.7 Correlation of cytotoxicity in cancer cells and *E. coli*. IC_{50} values in HL60 cells were determined 72 hours after treatement; IC_{50} values in *E. coli* cells were determined 16 hours after treatments. A) Linear regression fitness of all molecules. Liner regression, $y = 0.009x + 3.936$, $R^2 = 0.001$. B) Linear regress fitness of molecules but BCEA and Doxorubicin. Liner regression, $y = 0.045x + 1.191$, $R^2 = 0.368$. All data analysis was done with Prism 7.02.

Table S3.1 Comprehensive phenotypic profiling data obtained at MIC in *E. coli*.

Treatment	Mechanism of Action	DNA Damage	DNA Damage Repair	IC_{50} Growth Inhibition (μM)	IC_{50} Translation Inhibition (μM)
Cisplatin	DNA alkylating	Inter- and intra-strand crosslink at N7 of guanine	NER (nucleotide excision repair); MMR (mismatch repair)	2	85
Carboplatin	DNA alkylating			113.9	>300
Oxaliplatin	DNA alkylating	Inter- and intra-strand crosslink at N7 of purine		43.7	>300
BCEA	DNA alkylating	Inter- and intra-strand crosslink at N7 and N3 of purine	NER; DSBR (double strand break repair)	6.8	123
Chlormethine	DNA alkylating			9.7	52.6
Chlorambucil	DNA alkylating			23.7	231
4-NQO	DNA oxidizing damage	Oxidation at C8 of guanine (8-oxoG)	NER	12.8	> 300
Nalidixic acid	Bacterial DNA gyrase inhibitor	Double strand break	DSBR	1.2	4.3
Ciprofloxacin	Bacterial DNA gyrase inhibitor			1.5	5.5
Doxorubicin	Topoisomerase 2A inhibitor	DNA intercalation; double strand break	DSBR	4.3	9.7
Etoposide	Topoisomerase 2A inhibitor			44.9	174.5
Mitoxantrone	Topoisomerase 2A inhibitor			25.9	50.0
MMS	DNA alkylating	Mono adduct; double strand break	BER (base excision repair); DSBR	2.9	24.2
EMS	DNA alkylating			13.8	84.7
Mitomycin C	DNA alkylating	Double strand break	NER; DSBR	0.04	0.07
Bleomycin	ROS cleavage	Single and double strand break	DSBR	0.3	0.4
Rifampicin	Transcription inhibitor			0.3	2.8
Rifaximin	Transcription inhibitor			1.8	12.7

Table S3.1 Comprehensive phenotypic profiling data obtained at MIC in *E. coli*. (continued)

Treatment	MIC (μM)	IC_{50} Index	Filament Population (%)	Avg. Filament Size (μm^2)	Avg. DNA Pieces Per Cell	CV (DNA)	Colony Forming (%)
Cisplatin	4.4	43	34%	12 ± 6	5.1	130%	0%
Carboplatin	235.2	> 2.6	17%	7 ± 3	2.9	73%	0%
Oxaliplatin	93.3	> 6.7	45%	36 ± 31	5.9	163%	0%
BCEA	12.8	24	23%	9 ± 6	3.1	132%	65%
Chlormethine	19	5.2	21%	42 ± 30	5.3	126%	0%
Chlorambucil	63.5	9.7	19%	14 ± 10	4	108%	0%
4-NQO	32.1	> 23	40%	10 ± 7	3.9	95%	65%
Nalidixic acid	2.5	1.8	100%	57 ± 28	8.6	160%	0%
Ciprofloxacin	2.6	3.6	100%	42 ± 34	6.4	115%	0%
Doxorubicin	16.1	2.3	66%	44 ± 36	8.5	158%	0%
Etoposide	87.2	3.9	62%	40 ± 33	8.8	133%	0%
Mitoxantrone	62.4	1.9	54%	36 ± 24	7.5	145%	0%
MMS	10.8	8.3	89%	61 ± 55	8.2	139%	0%
EMS	25.7	6	88%	71 ± 34	7.5	141%	0%
Mitomycin C	0.09	1.8	86%	48 ± 35	9.2	144%	0%
Bleomycin	0.6	1.3	89%	55 ± 47	9.5	138%	0%
Rifampicin	0.6	9.3	30%	8 ± 3	1.2	49%	18%
Rifaximin	4.6	6.9	25%	8 ± 4	1.1	52%	17%

Table S3.2 Comprehensive phenotypic profiling data obtained at 10 x MIC in *E. coli.*

Treatment	Filament Population (%)	Avg. Filament Size (μm^2)	Avg. DNA Pieces Per Cell	CV (DNA)	Colony Forming (%)
Tetracycline	25%	11 ± 3	3.9	36%	36%
Kanamycin	29%	9 ± 5	3.5	34%	40%
Chloramphenicol	26%	9 ± 3	4.3	29%	40%
Puromycin	23%	8 ± 3	3.7	45%	47%

Table S3.3 Comprehensive phenotypic profiling data obtained at 0.1 x MIC in *E. coli.*

Treatment	Filament Population (%)	Avg. Filament Size (μm^2)	Avg. DNA Pieces Per Cell	CV (DNA)
Cisplatin	23%	9 ± 4	3.7	108%
Carboplatin	6%	7 ± 3	2.8	73%
Oxaliplatin	21%	13 ± 9	4.5	134%
Doxorubicin	38%	24 ± 18	5.1	122%
Etoposide	42%	22 ± 16	5	131%
Mitoxantrone	40%	28 ± 19	5.9	119%
EMS	44%	15 ± 6	3.7	96%

Appendix D. Supplemental tables and figures in chapter 5.

Note: Compound codes are chapter-specific. See Chapter 5 for HQ compound structures.

Table S4.1 Comprehensive phenotypic profiling data in *E. coli.*

Treatment	IC_{50} Growth Inhibition (μM)	IC_{50} Translation Inhibition (μM)	MIC (μM)	IC_{50} Index	Filament Population (%)	Avg. Filament Size (μm^2)	Avg. DNA Pieces Per Cell	CV (DNA)
HQ-2	3.9	20.5	8.5	3.6	39%	12 ± 5	41%	5.1
HQ-3	3.6	5.2	4.1	1.4	36%	9 ± 4	44%	3.3
HQ-4	27.5	5.5	41.9	0.2	30%	9 ± 5	59%	3.8
HQ-5	31.3	11.2	37.9	0.4	29%	8 ± 3	38%	3.2
HQ-6	26.2	2.9	32.7	0.1	18%	7 ± 3	41%	4.3
HQ-7	100.2	5.9	112.8	0.1	33%	10 ± 5	50%	3.8

Table S4.2 HQ-1 cytotoxicity and cellular metal uptake measured by ICP-OES in *E. coli*.

	IC50 (μM)	Cellular uptake[a]
HQ-1	1.3	50%

[a]Cellular uptake was calculated as metal content measured in cells divided by total metal content in both cell samples and cell culture media samples. Cellular uptake in *E. coli* cells were normalized to 10^9 cells. *E. coli* cells were treated with 2 μM of **HQ-1** for 2 hrs and 24 hrs. The metal levels in cells and media was measured by ICP-OES, and the number of metal atoms per cell was calculated using the cell number obtained using OD_{600} measurement. The metal levels were quantified by detection at three different wavelengths (n = 3).

Table S4.3 Pearson's correlation coefficients (PCC) of BODIPY conjugated HQ compounds with organelle markers.

	HQ-BODIPY			HQ-BODIPY-2			BODIPY		
CytERM-GFP	0.82	0.8	0.76	0.83	0.82	0.74	0.69	0.68	0.64
Mito-paGFP	0.33	0.31	0.3	0.49	0.34	0.27	0.55	0.41	0.34
GalT-GFP	0.45	0.4	0.3	0.47	0.45	0.25	0.46	0.43	0.33
Lys20-GFP	0.26	0.18	0.13	0.42	0.32	0.25	0.31	0.29	0.21
PNP-GFP	0.7	0.65	0.59	0.72	0.69	0.68	0.71	0.7	0.65
RPL10A-GFP	-0.04	-0.02	-0.02		N. D.[a]		0.03	0.029	0.02

[a]The colocalization of ribosome marker with **HQ-BODIPY-2** was not determined.

Table S4.4 Pearson's correlation coefficients (PCC) of PA-conjugated HQ compounds with organelle markers.

	HQ-PA			PA		
CytERM-GFP	0.79	0.72	0.64	0.13	0.11	0.08
Mito-paGFP	0.2	0.17	0.15	0.28	0.24	0.23
GalT-GFP	0.17	0.16	0.12	0.21	0.19	0.18
Lys20-GFP	0.18	0.16	0.1	0.25	0.19	0.18
PNP-GFP	0.13	0.09	0.05	0.15	0.11	0.07

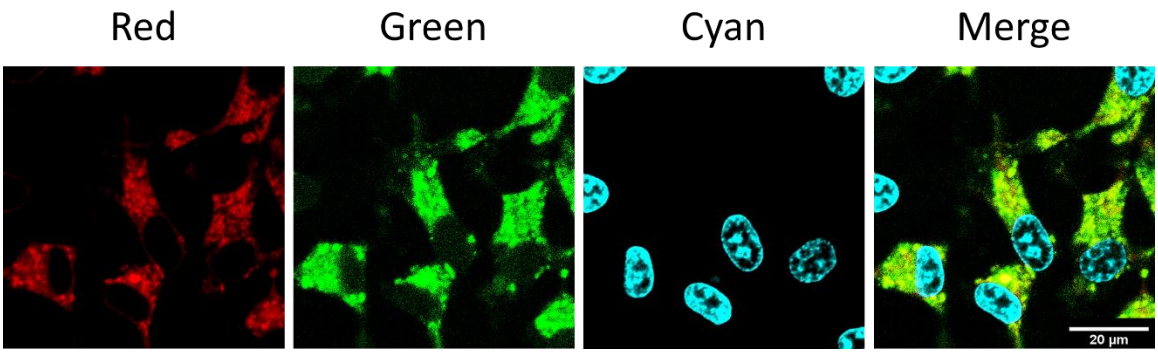

Figure S4.1 HQ compound shows partial colocalization with endoplasmic reticulum (ER). HEK cells stably expressing ER targeted transmembrane domain with GFP (CyTERM-GFP) were treated with 2 µM of **HQ-BODIPY-2** or free BODIPY for 6 hours prior to imaging, untreated cells were used as controls. Cells were incubated with Hoechst 33342 for 15 minutes before imaged with Nikon A1R confocal microscope. Red, BODIPY; Green, CytERM-GFP; Cyan, Hoechst 33342. All scale bars represent 20 µm.

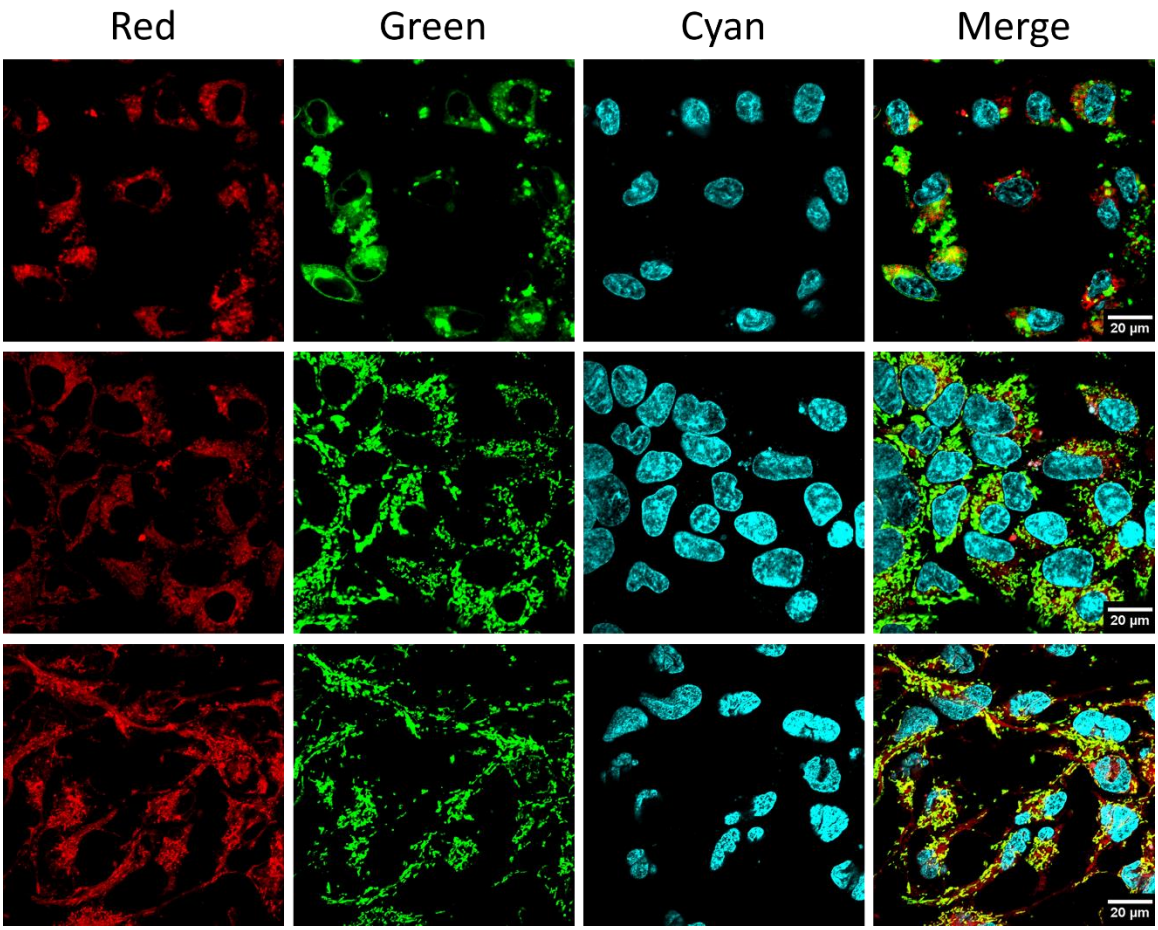

Figure S4.2 Cellular localization of HQ compound. HEK cells stably expressing human galactosyltransferase (GalT) with GFP (GalT-GFP, top), mitochondrial matrix-targeted photoactivable GFP (mito-PAGFP, middle), and human purine nucleoside phosphorylase with GFP (PNP-GFP, bottom) were treated with 2 µM of **HQ-BODIPY-2** or free BODIPY for 6 hours prior to imaging, untreated cells were used as controls. Cells were incubated with Hoechst 33342 for 15 minutes before imaged with Nikon A1R confocal microscope. Red, BODIPY; Green, GFP; Cyan, Hoechst 33342. All scale bars represent 20 µm.

References

1. Siegel, R. L.; Miller, K. D.; Jemal, A., Cancer Statistics, 2017. *CA: a cancer journal for clinicians* **2017,** *67* (1), 7-30.

2. McGuire, S., World Cancer Report 2014. Geneva, Switzerland: World Health Organization, International Agency for Research on Cancer, WHO Press, 2015. *Advances in nutrition (Bethesda, Md.)* **2016,** *7* (2), 418-9.

3. Urruticoechea, A.; Alemany, R.; Balart, J.; Villanueva, A.; Vinals, F.; Capella, G., Recent advances in cancer therapy: an overview. *Current pharmaceutical design* **2010,** *16* (1), 3-10.

4. Fujii, T.; Le Du, F.; Xiao, L.; Kogawa, T.; Barcenas, C. H.; Alvarez, R. H.; Valero, V.; Shen, Y.; Ueno, N. T., Effectiveness of an Adjuvant Chemotherapy Regimen for Early-Stage Breast Cancer: A Systematic Review and Network Meta-analysis. *JAMA oncology* **2015,** *1* (9), 1311-8.

5. Park, S. C.; Chun, H. J., Chemotherapy for Advanced Gastric Cancer: Review and Update of Current Practices. *Gut and Liver* **2013,** *7* (4), 385-393.

6. Rassnick, K. M.; Mauldin, G. E.; Al-Sarraf, R.; Mauldin, G. N.; Moore, A. S.; Mooney, S. C., MOPP chemotherapy for treatment of resistant lymphoma in dogs: a retrospective study of 117 cases (1989-2000). *Journal of veterinary internal medicine* **2002,** *16* (5), 576-80.

7. Chabner, B. A.; Longo, D. L., *Cancer Chemotherapy and Biotherapy: Principles and Practice*. Wolters Kluwer Health: 2011.

8. Wrigley, P. F. M., Cancer Chemotherapy Handbook. *Journal of the Royal Society of Medicine* **1980,** *73* (10), 758-758.

9. Kufe, D. W.; Holland, J. F.; Frei, E.; Society, A. C., *Cancer Medicine 6*. BC Decker: 2003.

10. Baudino, T. A., Targeted Cancer Therapy: The Next Generation of Cancer Treatment. *Current drug discovery technologies* **2015,** *12* (1), 3-20.

11. Huang, M.; Shen, A.; Ding, J.; Geng, M., Molecularly targeted cancer therapy: some lessons from the past decade. *Trends in Pharmacological Sciences 35* (1), 41-50.

12. Nagar, B.; Bornmann, W. G.; Pellicena, P.; Schindler, T.; Veach, D. R.; Miller, W. T.; Clarkson, B.; Kuriyan, J., Crystal structures of the kinase domain of c-Abl in complex with the small molecule inhibitors PD173955 and imatinib (STI-571). *Cancer research* **2002,** *62* (15), 4236-43.

13. Hantschel, O.; Rix, U.; Superti-Furga, G., Target spectrum of the BCR-ABL inhibitors imatinib, nilotinib and dasatinib. *Leukemia & lymphoma* **2008,** *49* (4), 615-9.

14. Shin, S. H.; Bode, A. M.; Dong, Z., Addressing the challenges of applying precision oncology. *npj Precision Oncology* **2017,** *1* (1), 28.

15. Lopez, J. S.; Banerji, U., Combine and conquer: challenges for targeted therapy combinations in early phase trials. *Nature Reviews Clinical Oncology* **2016,** *14*, 57.

16. Rosenberg, B.; Vancamp, L.; Krigas, T., Inhibition of cell division in Eschrichia coli by electrolysis products from a platinum electrode. *Nature* **1965,** *205*, 698-9.

17. Rosenberg, B.; Van Camp, L.; Grimley, E. B.; Thomson, A. J., The inhibition of growth or cell division in Escherichia coli by different ionic species of platinum(IV) complexes. *The Journal of biological chemistry* **1967,** *242* (6), 1347-52.

18. Rosenberg, B.; VanCamp, L.; Trosko, J. E.; Mansour, V. H., Platinum compounds: a new class of potent antitumour agents. *Nature* **1969,** *222* (5191), 385-6.

19. Basu, A.; Krishnamurthy, S., Cellular responses to Cisplatin-induced DNA damage. *Journal of nucleic acids* **2010,** *2010*.

20. Barabas, K.; Milner, R.; Lurie, D.; Adin, C., Cisplatin: a review of toxicities and therapeutic applications. *Veterinary and comparative oncology* **2008,** *6* (1), 1-18.

21. Johnstone, T. C.; Suntharalingam, K.; Lippard, S. J., The Next Generation of Platinum Drugs: Targeted Pt(II) Agents, Nanoparticle Delivery, and Pt(IV) Prodrugs. *Chemical reviews* **2016,** *116* (5), 3436-86.

22. Raymond, E.; Faivre, S.; Chaney, S.; Woynarowski, J.; Cvitkovic, E., Cellular and molecular pharmacology of oxaliplatin. *Molecular cancer therapeutics* **2002,** *1* (3), 227-35.

23. Sharp, S. Y.; Rogers, P. M.; Kelland, L. R., Transport of cisplatin and bis-acetato-ammine-dichlorocyclohexylamine Platinum(IV) (JM216) in human ovarian carcinoma cell lines: identification of a plasma membrane protein associated with cisplatin resistance. *Clinical cancer research : an official journal of the American Association for Cancer Research* **1995,** *1* (9), 981-9.

24. Cepeda, V.; Fuertes, M. A.; Castilla, J.; Alonso, C.; Quevedo, C.; Perez, J. M., Biochemical mechanisms of cisplatin cytotoxicity. *Anti-cancer agents in medicinal chemistry* **2007,** *7* (1), 3-18.

25. Boulikas, T.; Vougiouka, M., Cisplatin and platinum drugs at the molecular level. (Review). *Oncology reports* **2003,** *10* (6), 1663-82.

26. Ahmad, S., Platinum-DNA interactions and subsequent cellular processes controlling sensitivity to anticancer platinum complexes. *Chem Biodivers* **2010,** *7* (3), 543-66.

27. Galluzzi, L.; Senovilla, L.; Vitale, I.; Michels, J.; Martins, I.; Kepp, O.; Castedo, M.; Kroemer, G., Molecular mechanisms of cisplatin resistance. *Oncogene* **2012,** *31* (15), 1869-83.

28. Lin, X.; Okuda, T.; Holzer, A.; Howell, S. B., The copper transporter CTR1 regulates cisplatin uptake in Saccharomyces cerevisiae. *Molecular pharmacology* **2002,** *62* (5), 1154-9.

29. Masters, J. R.; Thomas, R.; Hall, A. G.; Hogarth, L.; Matheson, E. C.; Cattan, A. R.; Lohrer, H., Sensitivity of testis tumour cells to chemotherapeutic drugs: role of detoxifying pathways. *European journal of cancer (Oxford, England : 1990)* **1996,** *32A* (7), 1248-53.

30. Tang, C.; Yang, H.; Zhou, X., Advances of DNA damage repair and Cisplatin resistance mechanisms in lung cancer. *Zhongguo fei ai za zhi = Chinese journal of lung cancer* **2011,** *14* (12), 960-4.

31. Gillet, L. C.; Scharer, O. D., Molecular mechanisms of mammalian global genome nucleotide excision repair. *Chemical reviews* **2006,** *106* (2), 253-76.

32. Welsh, C.; Day, R.; McGurk, C.; Masters, J. R. W.; Wood, R. D.; Köberle, B., Reduced levels of XPA, ERCC1 and XPF DNA repair proteins in testis tumor cell lines. *International Journal of Cancer* **2004,** *110* (3), 352-361.

33. Köberle, B.; Masters, J. R. W.; Hartley, J. A.; Wood, R. D., Defective repair of cisplatin-induced DNA damage caused by reduced XPA protein in testicular germ cell tumours. *Current Biology* **1999,** *9* (5), 273-278.

34. Mansouri, A.; Ridgway, L. D.; Korapati, A. L.; Zhang, Q.; Tian, L.; Wang, Y.; Siddik, Z. H.; Mills, G. B.; Claret, F. X., Sustained activation of JNK/p38 MAPK pathways in response to cisplatin leads to Fas ligand induction and cell death in ovarian carcinoma cells. *The Journal of biological chemistry* **2003,** *278* (21), 19245-56.

35. Brozovic, A.; Fritz, G.; Christmann, M.; Zisowsky, J.; Jaehde, U.; Osmak, M.; Kaina, B., Long-term activation of SAPK/JNK, p38 kinase and fas-L expression by cisplatin is attenuated in human carcinoma cells that acquired drug resistance. *International journal of cancer. Journal international du cancer* **2004,** *112* (6), 974-85.

36. Kartalou, M.; Essigmann, J. M., Mechanisms of resistance to cisplatin. *Mutation research* **2001,** *478* (1-2), 23-43.

37. Fajac, A.; Da Silva, J.; Ahomadegbe, J. C.; Rateau, J. G.; Bernaudin, J. F.; Riou, G.; Benard, J., Cisplatin-induced apoptosis and p53 gene status in a cisplatin-resistant human ovarian carcinoma cell line. *International journal of cancer. Journal international du cancer* **1996,** *68* (1), 67-74.

38. Chresta, C. M.; Masters, J. R.; Hickman, J. A., Hypersensitivity of human testicular tumors to etoposide-induced apoptosis is associated with functional p53 and a high Bax:Bcl-2 ratio. *Cancer research* **1996,** *56* (8), 1834-41.

39. Kelland, L., The resurgence of platinum-based cancer chemotherapy. *Nat Rev Cancer* **2007,** *7* (8), 573-84.

40. Allardyce, C. S.; Dyson, P. J., Metal-based drugs that break the rules. *Dalton transactions (Cambridge, England : 2003)* **2016,** *45* (8), 3201-9.

41. Johnstone, T. C.; Suntharalingam, K.; Lippard, S. J., Third row transition metals for the treatment of cancer. *Philosophical transactions. Series A, Mathematical, physical, and engineering sciences* **2015,** *373* (2037).

42. Hesketh, P. J.; Kris, M. G.; Basch, E.; Bohlke, K.; Barbour, S. Y.; Clark-Snow, R. A.; Danso, M. A.; Dennis, K.; Dupuis, L. L.; Dusetzina, S. B.; Eng, C.; Feyer, P. C.; Jordan, K.; Noonan, K.; Sparacio, D.; Somerfield, M. R.; Lyman, G. H., Antiemetics: American Society of Clinical Oncology Clinical Practice Guideline Update. *Journal of clinical oncology : official journal of the American Society of Clinical Oncology* **2017,** *35* (28), 3240-3261.

43. Dilruba, S.; Kalayda, G. V., Platinum-based drugs: past, present and future. *Cancer Chemother Pharmacol* **2016,** *77* (6), 1103-24.

44. Bruno, P. M.; Liu, Y.; Park, G. Y.; Murai, J.; Koch, C. E.; Eisen, T. J.; Pritchard, J. R.; Pommier, Y.; Lippard, S. J.; Hemann, M. T., A subset of platinum-containing chemotherapeutic agents kills cells by inducing ribosome biogenesis stress. *Nature medicine* **2017,** *23* (4), 461-471.

45. Zdraveski, Z. Z.; Mello, J. A.; Farinelli, C. K.; Essigmann, J. M.; Marinus, M. G., MutS preferentially recognizes cisplatin- over oxaliplatin-modified DNA. *The Journal of biological chemistry* **2002,** *277* (2), 1255-60.

46. Ozdian, T.; Holub, D.; Maceckova, Z.; Varanasi, L.; Rylova, G.; Rehulka, J.; Vaclavkova, J.; Slavik, H.; Moudry, P.; Znojek, P.; Stankova, J.; de Sanctis, J. B.; Hajduch, M.; Dzubak, P., Proteomic profiling reveals DNA damage, nucleolar and ribosomal stress are the main responses to oxaliplatin treatment in cancer cells. *Journal of Proteomics* **2017,** *162*, 73-85.

47. Pasetto, L. M.; D'Andrea, M. R.; Rossi, E.; Monfardini, S., Oxaliplatin-related neurotoxicity: how and why? *Crit Rev Oncol Hematol* **2006,** *59* (2), 159-68.

48. Stojanovska, V.; McQuade, R.; Rybalka, E.; Nurgali, K., Neurotoxicity Associated with Platinum-Based Anti-Cancer Agents: What are the Implications of Copper Transporters? *Current medicinal chemistry* **2017,** *24* (15), 1520-1536.

49. Shimada, M.; Itamochi, H.; Kigawa, J., Nedaplatin: a cisplatin derivative in cancer chemotherapy. *Cancer Management and Research* **2013,** *5*, 67-76.

50. Wheate, N. J.; Walker, S.; Craig, G. E.; Oun, R., The status of platinum anticancer drugs in the clinic and in clinical trials. *Dalton transactions (Cambridge, England : 2003)* **2010,** *39* (35), 8113-27.

51. Choi, C.-H.; Cha, Y.-J.; An, C.-S.; Kim, K.-J.; Kim, K.-C.; Moon, S.-P.; Lee, Z. H.; Min, Y.-D., Molecular mechanisms of heptaplatin effective against cisplatin-resistant cancer cell lines: less involvement of metallothionein. *Cancer Cell International* **2004,** *4*, 6-6.

52. Lobaplatin. *Drugs in R & D* **2003,** *4* (6), 369-372.

53. McKeage, M. J., Lobaplatin: a new antitumour platinum drug. *Expert opinion on investigational drugs* **2001,** *10* (1), 119-28.

54. Harrap, K. R., Preclinical studies identifying carboplatin as a viable cisplatin alternative. *Cancer treatment reviews* **1985,** *12 Suppl A*, 21-33.

55. Knox, R. J.; Friedlos, F.; Lydall, D. A.; Roberts, J. J., Mechanism of cytotoxicity of anticancer platinum drugs: evidence that cis-diamminedichloroplatinum(II) and cis-diammine-(1,1-cyclobutanedicarboxylato)platinum(II) differ only in the kinetics of their interaction with DNA. *Cancer research* **1986,** *46* (4 Pt 2), 1972-9.

56. Kidani, Y.; Inagaki, K.; Iigo, M.; Hoshi, A.; Kuretani, K., Antitumor activity of 1,2-diaminocyclohexane--platinum complexes against sarcoma-180 ascites form. *Journal of medicinal chemistry* **1978,** *21* (12), 1315-8.

57. Machover, D.; Diaz-Rubio, E.; de Gramont, A.; Schilf, A.; Gastiaburu, J. J.; Brienza, S.; Itzhaki, M.; Metzger, G.; N'Daw, D.; Vignoud, J.; Abad, A.; Francois, E.; Gamelin, E.; Marty, M.; Sastre, J.; Seitz, J. F.; Ychou, M., Two consecutive phase II studies of oxaliplatin (L-OHP) for treatment of patients with advanced colorectal carcinoma who were resistant to previous treatment with fluoropyrimidines. *Annals of oncology : official journal of the European Society for Medical Oncology / ESMO* **1996,** *7* (1), 95-8.

58. Gibbons, G. R.; Wyrick, S.; Chaney, S. G., Rapid reduction of tetrachloro(D,L-trans)1,2-diaminocyclohexaneplatinum(IV) (tetraplatin) in RPMI 1640 tissue culture medium. *Cancer research* **1989,** *49* (6), 1402-7.

59. Rahman, A.; Roh, J. K.; Wolpert-DeFilippes, M. K.; Goldin, A.; Venditti, J. M.; Woolley, P. V., Therapeutic and pharmacological studies of tetrachloro(d,l-trans)1,2-diaminocyclohexane platinum (IV) (tetraplatin), a new platinum analogue. *Cancer research* **1988,** *48* (7), 1745-52.

60. Schilder, R. J.; LaCreta, F. P.; Perez, R. P.; Johnson, S. W.; Brennan, J. M.; Rogatko, A.; Nash, S.; McAleer, C.; Hamilton, T. C.; Roby, D.; et al., Phase I and pharmacokinetic study of ormaplatin (tetraplatin, NSC 363812) administered on a day 1 and day 8 schedule. *Cancer research* **1994,** *54* (3), 709-17.

61. Parker, R. J.; Vionnet, J. A.; Bostick-Bruton, F.; Reed, E., Ormaplatin sensitivity/resistance in human ovarian cancer cells made resistant to cisplatin. *Cancer research* **1993,** *53* (2), 242-7.

62. Anderson, H.; Wagstaff, J.; Crowther, D.; Swindell, R.; Lind, M. J.; McGregor, J.; Timms, M. S.; Brown, D.; Palmer, P., Comparative toxicity of cisplatin, carboplatin (CBDCA) and iproplatin (CHIP) in combination with cyclophosphamide in patients with advanced epithelial ovarian cancer. *European journal of cancer & clinical oncology* **1988,** *24* (9), 1471-9.

63. Bramwell, V. H.; Crowther, D.; O'Malley, S.; Swindell, R.; Johnson, R.; Cooper, E. H.; Thatcher, N.; Howell, A., Activity of JM9 in advanced ovarian cancer: a phase I-II trial. *Cancer treatment reports* **1985,** *69* (4), 409-16.

64. Johnstone, T. C.; Lippard, S. J., Improvements in the Synthesis and Understanding of the Iodo-bridged Intermediate en Route to the Pt(IV) Prodrug Satraplatin. *Inorganica Chim Acta* **2015,** *424*, 254-259.

65. Judson, I.; Cerny, T.; Epelbaum, R.; Dunlop, D.; Smyth, J.; Schaefer, B.; Roelvink, M.; Kaplan, S.; Hanauske, A., Phase II trial of the oral platinum complex JM216 in non-small-cell lung cancer: an EORTC early clinical studies group investigation. *Annals of oncology : official journal of the European Society for Medical Oncology* **1997,** *8* (6), 604-6.

66. Trudeau, M.; Stuart, G.; Hirte, H.; Drouin, P.; Plante, M.; Bessette, P.; Dulude, H.; Lebwohl, D.; Fisher, B.; Seymour, L., A phase II trial of JM-216 in cervical cancer: an NCIC CTG study. *Gynecologic oncology* **2002,** *84* (2), 327-31.

67. Bergamo, A.; Sava, G., Ruthenium complexes can target determinants of tumour malignancy. *Dalton transactions (Cambridge, England : 2003)* **2007,** (13), 1267-72.

68. Che, C. M.; Siu, F. M., Metal complexes in medicine with a focus on enzyme inhibition. *Current opinion in chemical biology* **2010,** *14* (2), 255-61.

69. Weidmann, A. G.; Komor, A. C.; Barton, J. K., Targeted Chemotherapy with Metal Complexes. *Comments on modern chemistry. Part A, Comments on inorganic chemistry : a journal of critical discussion of the current literature* **2014,** *34* (3-4), 114-123.

70. Deo, K. M.; Pages, B. J.; Ang, D. L.; Gordon, C. P.; Aldrich-Wright, J. R., Transition Metal Intercalators as Anticancer Agents—Recent Advances. *International Journal of Molecular Sciences* **2016,** *17* (11), 1818.

71. Ndagi, U.; Mhlongo, N.; Soliman, M. E., Metal complexes in cancer therapy – an update from drug design perspective. *Drug Design, Development and Therapy* **2017,** *11*, 599-616.

72. Ott, I.; Gust, R., Non platinum metal complexes as anti-cancer drugs. *Archiv der Pharmazie* **2007,** *340* (3), 117-26.

73. Jung, M.; Kerr, D. E.; Senter, P. D., Bioorganometallic Chemistry – Synthesis and Antitumor Activity of Cobalt Carbonyl Complexes. *Archiv der Pharmazie* **1997,** *330* (6), 173-176.

74. Ott, I.; Schmidt, K.; Kircher, B.; Schumacher, P.; Wiglenda, T.; Gust, R., Antitumor-Active Cobalt−Alkyne Complexes Derived from Acetylsalicylic Acid: Studies on the Mode of Drug Action. *Journal of medicinal chemistry* **2005,** *48* (2), 622-629.

75. Munteanu, C. R.; Suntharalingam, K., Advances in cobalt complexes as anticancer agents. *Dalton transactions (Cambridge, England : 2003)* **2015,** *44* (31), 13796-808.

76. Ott, I.; Abraham, A.; Schumacher, P.; Shorafa, H.; Gastl, G.; Gust, R.; Kircher, B., Synergistic and additive antiproliferative effects on human leukemia cell lines induced by combining acetylenehexacarbonyldicobalt complexes with the tyrosine kinase inhibitor imatinib. *J Inorg Biochem* **2006,** *100* (11), 1903-6.

77. Munteanu, C. R.; Suntharalingam, K., Advances in cobalt complexes as anticancer agents. *Dalton Transactions* **2015,** *44* (31), 13796-13808.

78. Chang, J. Y.; Lu, G. L.; Stevenson, R. J.; Brothers, P. J.; Clark, G. R.; Botting, K. J.; Ferry, D. M.; Tercel, M.; Wilson, W. R.; Denny, W. A.; Ware, D. C., Cross-bridged cyclen or cyclam Co(III) complexes containing cytotoxic ligands as hypoxia-activated prodrugs. *Inorganic chemistry* **2013,** *52* (13), 7688-98.

79. Lu, G. L.; Stevenson, R. J.; Chang, J. Y.; Brothers, P. J.; Ware, D. C.; Wilson, W. R.; Denny, W. A.; Tercel, M., N-alkylated cyclen cobalt(III) complexes of 1-(chloromethyl)-3-(5,6,7-trimethoxyindol-2-ylcarbonyl)-2,3-dihydro-1H-pyrrolo[3, 2-f]quinolin-5-ol DNA alkylating agent as hypoxia-activated prodrugs. *Bioorg Med Chem* **2011,** *19* (16), 4861-7.

80. Ng, C. H.; Kong, S. M.; Tiong, Y. L.; Maah, M. J.; Sukram, N.; Ahmad, M.; Khoo, A. S., Selective anticancer copper(II)-mixed ligand complexes: targeting of ROS and proteasomes. *Metallomics* **2014,** *6* (4), 892-906.

81. Santini, C.; Pellei, M.; Gandin, V.; Porchia, M.; Tisato, F.; Marzano, C., Advances in copper complexes as anticancer agents. *Chemical reviews* **2014,** *114* (1), 815-62.

82. Palermo, G.; Magistrato, A.; Riedel, T.; von Erlach, T.; Davey, C. A.; Dyson, P. J.; Rothlisberger, U., Fighting Cancer with Transition Metal Complexes: From Naked DNA to Protein and Chromatin Targeting Strategies. *ChemMedChem* **2016,** *11* (12), 1199-210.

83. Leon, I. E.; Cadavid-Vargas, J. F.; Di Virgilio, A. L.; Etcheverry, S. B., Vanadium, Ruthenium and Copper Compounds: A New Class of Nonplatinum Metallodrugs with Anticancer Activity. *Current medicinal chemistry* **2017,** *24* (2), 112-148.

84. Adhireksan, Z.; Davey, G. E.; Campomanes, P.; Groessl, M.; Clavel, C. M.; Yu, H.; Nazarov, A. A.; Yeo, C. H.; Ang, W. H.; Droge, P.; Rothlisberger, U.; Dyson, P. J.; Davey, C. A., Ligand substitutions between ruthenium-cymene compounds can control protein versus DNA targeting and anticancer activity. *Nature communications* **2014,** *5*, 3462.

85. Wu, B.; Davey, G. E.; Nazarov, A. A.; Dyson, P. J.; Davey, C. A., Specific DNA structural attributes modulate platinum anticancer drug site selection and cross-link generation. *Nucleic Acids Res* **2011,** *39* (18), 8200-12.

86. Shah, P. K.; Bhattacharjee, K.; Shukla, P. K., Mechanisms of reactions of Ru(iii)-based drug NAMI-A and its aquated products with DNA purine bases: a DFT study. *RSC Advances* **2016,** *6* (114), 113620-113629.

87. Stevens, S. K.; Strehle, A. P.; Miller, R. L.; Gammons, S. H.; Hoffman, K. J.; McCarty, J. T.; Miller, M. E.; Stultz, L. K.; Hanson, P. K., The anticancer ruthenium complex KP1019 induces DNA damage, leading to cell cycle delay and cell death in Saccharomyces cerevisiae. *Molecular pharmacology* **2013,** *83* (1), 225-34.

88. Irace, C.; Misso, G.; Capuozzo, A.; Piccolo, M.; Riccardi, C.; Luchini, A.; Caraglia, M.; Paduano, L.; Montesarchio, D.; Santamaria, R., Antiproliferative effects of ruthenium-based nucleolipidic nanoaggregates in human models of breast cancer in vitro: insights into their mode of action. *Scientific reports* **2017,** *7*, 45236.

89. Sava, G.; Zorzet, S.; Turrin, C.; Vita, F.; Soranzo, M.; Zabucchi, G.; Cocchietto, M.; Bergamo, A.; DiGiovine, S.; Pezzoni, G.; Sartor, L.; Garbisa, S., Dual Action of NAMI-A in inhibition of solid tumor metastasis: selective targeting of metastatic cells and binding to collagen. *Clinical cancer research : an official journal of the American Association for Cancer Research* **2003,** *9* (5), 1898-905.

90. Hartinger, C. G.; Jakupec, M. A.; Zorbas-Seifried, S.; Groessl, M.; Egger, A.; Berger, W.; Zorbas, H.; Dyson, P. J.; Keppler, B. K., KP1019, a new redox-active anticancer agent--preclinical development and results of a clinical phase I study in tumor patients. *Chemistry & biodiversity* **2008,** *5* (10), 2140-55.

91. Ang, W. H.; Casini, A.; Sava, G.; Dyson, P. J., Organometallic ruthenium-based antitumor compounds with novel modes of action. *Journal of Organometallic Chemistry* **2011,** *696* (5), 989-998.

92. Gill, M. R.; Thomas, J. A., Ruthenium(II) polypyridyl complexes and DNA--from structural probes to cellular imaging and therapeutics. *Chem Soc Rev* **2012,** *41* (8), 3179-92.

93. Wachter, E.; Heidary, D. K.; Howerton, B. S.; Parkin, S.; Glazer, E. C., Light-activated ruthenium complexes photobind DNA and are cytotoxic in the photodynamic therapy window. *Chemical communications (Cambridge, England)* **2012,** *48* (77), 9649-51.

94. Hidayatullah, A. N.; Wachter, E.; Heidary, D. K.; Parkin, S.; Glazer, E. C., Photoactive Ru(II) complexes with dioxinophenanthroline ligands are potent cytotoxic agents. *Inorganic chemistry* **2014,** *53* (19), 10030-2.

95. Wachter, E.; Howerton, B. S.; Hall, E. C.; Parkin, S.; Glazer, E. C., A new type of DNA "light-switch": a dual photochemical sensor and metalating agent for duplex and G-quadruplex DNA. *Chemical communications (Cambridge, England)* **2014,** *50* (3), 311-3.

96. Fong, J.; Kasimova, K.; Arenas, Y.; Kaspler, P.; Lazic, S.; Mandel, A.; Lilge, L., A novel class of ruthenium-based photosensitizers effectively kills in vitro cancer cells and in vivo tumors. *Photochemical & photobiological sciences : Official journal of the European Photochemistry Association and the European Society for Photobiology* **2015,** *14* (11), 2014-23.

97. Sainuddin, T.; Pinto, M.; Yin, H.; Hetu, M.; Colpitts, J.; McFarland, S. A., Strained ruthenium metal-organic dyads as photocisplatin agents with dual action. *J Inorg Biochem* **2016,** *158*, 45-54.

98. Imming, P.; Sinning, C.; Meyer, A., Drugs, their targets and the nature and number of drug targets. **2006,** *5*, 821.

99. Sonner, J. M.; Cantor, R. S., Molecular Mechanisms of Drug Action: An Emerging View. *Annual Review of Biophysics* **2013,** *42* (1), 143-167.

100. Mechanism matters. *Nature medicine* **2010,** *16* (4), 347-347.

101. Schenone, M.; Dancik, V.; Wagner, B. K.; Clemons, P. A., Target identification and mechanism of action in chemical biology and drug discovery. *Nature chemical biology* **2013,** *9* (4), 232-240.

102. (a) Kurita, K. L.; Linington, R. G., Connecting phenotype and chemotype: high-content discovery strategies for natural products research. *Journal of natural products* **2015,** *78* (3), 587-96; (b) Moffat, J. G.; Rudolph, J.; Bailey, D., Phenotypic screening in cancer drug discovery [mdash] past, present and future. *Nat Rev Drug Discov* **2014,** *13* (8), 588-602.

103. Kenneth, A. G.; Robbin, L. D.; Dunlay, R. T.; Albert, G.; Joanne, M. V.; Joseph, Z.; George, N. P.; Taylor, D. L., High-Content Screening: A New Approach to Easing Key Bottlenecks in the Drug Discovery Process. *Journal of Biomolecular Screening* **1997,** *2* (4), 249-259.

104. Eggert, U. S.; Mitchison, T. J., Small molecule screening by imaging. *Current Opinion in Chemical Biology* **2006,** *10* (3), 232-237.

105. Abraham, V. C.; Taylor, D. L.; Haskins, J. R., High content screening applied to large-scale cell biology. *Trends in Biotechnology* **2004,** *22* (1), 15-22.

106. Zock, J. M., Applications of High Content Screening in Life Science Research. *Combinatorial Chemistry & High Throughput Screening* **2009,** *12* (9), 870-876.

107. Garvey, C. M.; Spiller, E.; Lindsay, D.; Chiang, C.-T.; Choi, N. C.; Agus, D. B.; Mallick, P.; Foo, J.; Mumenthaler, S. M., A high-content image-based method for quantitatively studying context-dependent cell population dynamics. *Scientific reports* **2016,** *6*, 29752.

108. Ainscow, E., Statistical techniques for handling high content screening data. *European Pharmaceutical Review* **2007,** *12* (5), 30.

109. Xia, X.; Wong, S. T., Concise review: a high-content screening approach to stem cell research and drug discovery. *Stem cells (Dayton, Ohio)* **2012,** *30* (9), 1800-7.

110. High‐Content Screening for Drug Discovery and Target Validation. In *Wiley Handbook of Current and Emerging Drug Therapies*.

111. Buchser, W.; Collins, M.; Garyantes, T.; Guha, R.; Haney, S.; Lemmon, V.; Li, Z.; Trask, O. J., Assay development guidelines for image-based high content screening, high content analysis and high content imaging. **2014**.

112. Boutros, M.; Heigwer, F.; Laufer, C., Microscopy-Based High-Content Screening. *Cell 163* (6), 1314-1325.

113. HÃ1⁄4ser, J. Ã.; Mannhold, R.; Kubinyi, H.; Folkers, G., *High-Throughput Screening in Drug Discovery*. Wiley: 2006.

114. Flaumenhaft, R., 3.07 - Chemical Biology A2 - Taylor, John B. In *Comprehensive Medicinal Chemistry II*, Triggle, D. J., Ed. Elsevier: Oxford, 2007; pp 129-149.

115. Peach, K. C.; Bray, W. M.; Winslow, D.; Linington, P. F.; Linington, R. G., Mechanism of action-based classification of antibiotics using high-content bacterial image analysis. *Molecular bioSystems* **2013,** *9* (7), 1837-48.

116. Nonejuie, P.; Burkart, M.; Pogliano, K.; Pogliano, J., Bacterial cytological profiling rapidly identifies the cellular pathways targeted by antibacterial molecules. *Proceedings of the National Academy of Sciences of the United States of America* **2013,** *110* (40), 16169-74.

117. Montero Llopis, P.; Jackson, A. F.; Sliusarenko, O.; Surovtsev, I.; Heinritz, J.; Emonet, T.; Jacobs-Wagner, C., Spatial organization of the flow of genetic information in bacteria. *Nature* **2010,** *466* (7302), 77-81.

118. Yao, Z.; Kahne, D.; Kishony, R., Distinct single-cell morphological dynamics under beta-lactam antibiotics. *Molecular cell* **2012,** *48* (5), 705-712.

119. Nagaoka, K.; Matsumoto, M.; Oono, J.; Yokoi, K.; Ishizeki, S.; Nakashima, T., Azinomycins A and B, new antitumor antibiotics. I. Producing organism, fermentation, isolation, and characterization. *The Journal of antibiotics* **1986,** *39* (11), 1527-32.

120. Mirabelli, C. K.; Huang, C. H.; Fenwick, R. G.; Crooke, S. T., Quantitative measurement of single- and double-strand breakage of DNA in Escherichia coli by the antitumor antibiotics bleomycin and talisomycin. *Antimicrob Agents Chemother* **1985,** *27* (4), 460-7.

121. Umbreit, W. W., *Advances in Applied Microbiology*. Elsevier Science: 1961.

122. Moffat, J. G.; Rudolph, J.; Bailey, D., Phenotypic screening in cancer drug discovery - past, present and future. *Nat Rev Drug Discov* **2014,** *13* (8), 588-602.

123. Lee, J. A.; Uhlik, M. T.; Moxham, C. M.; Tomandl, D.; Sall, D. J., Modern phenotypic drug discovery is a viable, neoclassic pharma strategy. *Journal of medicinal chemistry* **2012,** *55* (10), 4527-38.

124. Hoelder, S.; Clarke, P. A.; Workman, P., Discovery of small molecule cancer drugs: successes, challenges and opportunities. *Molecular oncology* **2012,** *6* (2), 155-76.

125. Swinney, D. C.; Anthony, J., How were new medicines discovered? *Nature Reviews Drug Discovery* **2011,** *10*, 507.

126. Lippert, B., *Cisplatin: chemistry and biochemistry of a leading anticancer drug*. John Wiley & Sons: 1999.

127. Cohen, S. M.; Lippard, S. J., Cisplatin: from DNA damage to cancer chemotherapy. *Progress in nucleic acid research and molecular biology* **2001,** *67*, 93-130.

128. Hadjiliadis, N.; Sletten, E., *Metal complex-DNA interactions*. John Wiley & Sons: 2009.

129. Moucheron, C., From cisplatin to photoreactive Ru complexes: targeting DNA for biomedical applications. *New journal of chemistry* **2009,** *33* (2), 235-245.

130. Boerner, L. J.; Zaleski, J. M., Metal complex–DNA interactions: from transcription inhibition to photoactivated cleavage. *Current opinion in chemical biology* **2005,** *9* (2), 135-144.

131. Zeglis, B. M.; Pierre, V. C.; Barton, J. K., Metallo-intercalators and metallo-insertors. *Chemical Communications* **2007,** (44), 4565-4579.

132. Gill, M. R.; Derrat, H.; Smythe, C. G.; Battaglia, G.; Thomas, J. A., Ruthenium (II) Metallo-intercalators: DNA Imaging and Cytotoxicity. *ChemBioChem* **2011,** *12* (6), 877-880.

133. Gill, M. R.; Thomas, J. A., Ruthenium (II) polypyridyl complexes and DNA—from structural probes to cellular imaging and therapeutics. *Chemical Society Reviews* **2012,** *41* (8), 3179-3192.

134. Svensson, F. R.; Andersson, J.; Åmand, H. L.; Lincoln, P., Effects of chirality on the intracellular localization of binuclear ruthenium (II) polypyridyl complexes. *JBIC Journal of Biological Inorganic Chemistry* **2012,** *17* (4), 565-571.

135. Zava, O.; Zakeeruddin, S. M.; Danelon, C.; Vogel, H.; Gratzel, M.; Dyson, P. J., A Cytotoxic Ruthenium Tris(Bipyridyl) Complex that Accumulates at Plasma Membranes. *ChemBioChem* **2009,** *10*, 1796-1800.

136. (a) Puckett, C. A.; Barton, J. K., Methods to explore cellular uptake of ruthenium complexes. *Journal of the American Chemical Society* **2007,** *129* (1), 46-47; (b) Pucket, C. A.; Barton, J. K., Mechanism of Cellular Uptake of a Ruthenium Polypyridyl Complex. *Biochemistry*

2008, *47*, 11711-11716; (c) Pucket, C. A.; Barton, J. K., Fluorescein Redirects a Ruthenium-Octaarginine Conjugate to the Nucleus. *J Am Chem Soc* **2009,** *131*, 8738-8739; (d) Puckett, C. A.; Barton, J. K., Targeting a ruthenium complex to the nucleus with short peptides. *Bioorganic & medicinal chemistry* **2010,** *18* (10), 3564-3569; (e) Puckett, C. A.; Ernst, R. J.; Barton, J. K., Exploring the cellular accumulation of metal complexes. *Dalton Transactions* **2010,** *39* (5), 1159-1170.

137. Juris, A.; Balzani, V.; Barigelletti, F.; Campagna, S.; Belser, P. l.; Von Zelewsky, A., Ru (II) polypyridine complexes: photophysics, photochemistry, eletrochemistry, and chemiluminescence. *Coordination Chemistry Reviews* **1988,** *84*, 85-277.

138. Barton, J. K.; Basile, L. A.; Danishefsky, A.; Alexandrescu, A., Chiral probes for the handedness of DNA helices: enantiomers of tris (4, 7-diphenylphenanthroline) ruthenium (II). *Proceedings of the National Academy of Sciences* **1984,** *81* (7), 1961-1965.

139. Goldstein, B. M.; Barton, J. K.; Berman, H. M., Crystal and molecular structure of a chiral-specific DNA-binding agent: tris (4, 7-diphenyl-1, 10-phenanthroline) ruthenium (II). *Inorganic chemistry* **1986,** *25* (6), 842-847.

140. Rabilloud, T.; Strub, J. M.; Luche, S.; van Dorsselaer, A.; Lunardi, J., A comparison between Sypro Ruby and ruthenium II tris (bathophenanthroline disulfonate) as fluorescent stains for protein detection in gels. *Proteomics* **2001,** *1* (5), 699-704.

141. Castellano, F. N.; Lakowicz, J. R., A Water - Soluble Luminescence Oxygen Sensor. *Photochemistry and photobiology* **1998,** *67* (2), 179-183.

142. Lamanda, A.; Zahn, A.; Röder, D.; Langen, H., Improved ruthenium II tris (bathophenantroline disulfonate) staining and destaining protocol for a better signal - to - background ratio and improved baseline resolution. *Proteomics* **2004,** *4* (3), 599-608.

143. Garcìa - Fresnadillo, D.; Georgiadou, Y.; Orellana, G.; Braun, A. M.; Oliveros, E., Singlet - Oxygen (1Δg) Production by Ruthenium (II) complexes containing polyazaheterocyclic ligands in methanol and in water. *Helvetica chimica acta* **1996,** *79* (4), 1222-1238.

144. Alberts, B.; Johnson, A.; Lewis, J.; Walter, P.; Raff, M.; Roberts, K., Molecular Biology of the Cell 4th Edition: International Student Edition. Routledge: 2002.

145. Garcia-Fresnadillo, D.; Orellana, G., Interaction of Sulfonated ruthenium(II) Polypyridine Complexes with Surfactants Probed by Luminescence Spectroscopy. *Helv Chim Acta* **2001,** *84*, 2708-2730.

146. Friedman, A. E.; Kumar, C. V.; Turro, N. J.; Barton, J. K., Luminescence of ruthenium (II) polypyridyls: evidence for intercalative binding to Z-DNA. *Nucleic acids research* **1991,** *19* (10), 2595.

147. Zanarini, S.; Ciana, L. D.; Marcaccio, M.; Marzocchi, E.; Paolucci, F.; Prodi, L., Electrochemistry and electrochemiluminescence of [Ru (II)-tris (bathophenanthroline-disulfonate)] 4− in aprotic conditions and aqueous buffers. *The Journal of Physical Chemistry B* **2008,** *112* (33), 10188-10193.

148. Hergueta-Bravo, A.; Jiménez-Hernández, M. E.; Montero, F.; Oliveros, E.; Orellana, G., Singlet oxygen-mediated DNA photocleavage with Ru (II) polypyridyl complexes. *The Journal of Physical Chemistry B* **2002,** *106* (15), 4010-4017.

149. These data are consistent with earlier reports that the bathophenanthroline ligand increases the uptake of Ru(II) complexes; see ref 11a.

150. Gobeil, S.; Boucher, C.; Nadeau, D.; Poirier, G., Characterization of the necrotic cleavage of poly (ADP-ribose) polymerase (PARP-1): implication of lysosomal proteases. *Cell death and differentiation* **2001,** *8* (6), 588.

151. Leist, M.; Nicotera, P., The shape of cell death. *Biochemical and biophysical research communications* **1997,** *236* (1), 1-9.

152. Gill, M. R.; Garcia-Lara, J.; Foster, S. J.; Smythe, C.; Battaglia, G.; Thomas, J. A., A ruthenium (II) polypyridyl complex for direct imaging of DNA structure in living cells. *Nature chemistry* **2009,** *1* (8), 662-667.

153. Xu, W.; Zuo, J.; Wang, L.; Ji, L.; Chao, H., Dinuclear ruthenium (II) polypyridyl complexes as single and two-photon luminescence cellular imaging probes. *Chemical Communications* **2014,** *50* (17), 2123-2125.

154. Baggaley, E.; Gill, M. R.; Green, N. H.; Turton, D.; Sazanovich, I. V.; Botchway, S. W.; Smythe, C.; Haycock, J. W.; Weinstein, J. A.; Thomas, J. A., Dinuclear Ruthenium (II) Complexes as Two-Photon, Time-Resolved Emission Microscopy Probes for Cellular DNA. *Angewandte Chemie International Edition* **2014,** *53* (13), 3367-3371.

155. Pierroz, V.; Joshi, T.; Leonidova, A.; Mari, C.; Schur, J.; Ott, I.; Spiccia, L.; Ferrari, S.; Gasser, G., Molecular and cellular characterization of the biological effects of ruthenium (II) complexes incorporating 2-pyridyl-2-pyrimidine-4-carboxylic acid. *Journal of the American Chemical Society* **2012,** *134* (50), 20376-20387.

156. Wang, J.-Q.; Zhang, P.-Y.; Qian, C.; Hou, X.-J.; Ji, L.-N.; Chao, H., Mitochondria are the primary target in the induction of apoptosis by chiral ruthenium (II) polypyridyl complexes in cancer cells. *JBIC Journal of Biological Inorganic Chemistry* **2014,** *19* (3), 335-348.

157. Du, Y.; Fu, X.; Li, H.; Chen, B.; Guo, Y.; Su, G.; Zhang, H.; Ning, F.; Lin, Y.; Mei, W., Mitochondrial fragmentation is an important cellular event induced by ruthenium (II) polypyridyl complexes in osteosarcoma cells. *ChemMedChem* **2014,** *9* (4), 714-718.

158. Chen, T.; Mei, W.-J.; Wong, Y.-S.; Liu, J.; Liu, Y.; Xie, H.-S.; Zheng, W.-J., Chiral ruthenium polypyridyl complexes as mitochondria-targeted apoptosis inducers. *MedChemComm* **2010,** *1* (1), 73-75.

159. Chen, T.; Liu, Y.; Zheng, W.-J.; Liu, J.; Wong, Y.-S., Ruthenium polypyridyl complexes that induce mitochondria-mediated apoptosis in cancer cells. *Inorganic chemistry* **2010,** *49* (14), 6366-6368.

160. Joshi, T.; Pierroz, V.; Ferrari, S.; Gasser, G., Bis (dipyridophenazine)(2-(2′-pyridyl) pyrimidine-4-carboxylic acid) ruthenium (II) Hexafluorophosphate: A Lesson in Stubbornness. *ChemMedChem* **2014,** *9* (7), 1419-1427.

161. Blackmore, L.; Moriarty, R.; Dolan, C.; Adamson, K.; Forster, R. J.; Devocelle, M.; Keyes, T. E., Peptide directed transmembrane transport and nuclear localization of Ru (II) polypyridyl complexes in mammalian cells. *Chemical Communications* **2013,** *49* (26), 2658-2660.

162. Alvarez, M.; Villanueva, Á.; Acedo, P.; Cañete, M.; Stockert, J. C., Cell death causes relocalization of photosensitizing fluorescent probes. *Acta histochemica* **2011,** *113* (3), 363-368.

163. Snyder, J. W.; Lambert, J. D.; Ogilby, P. R., 5, 10, 15, 20-Tetrakis (N-Methyl-4-Pyridyl)-21 H, 23H-Porphine (TMPyP) as a Sensitizer for Singlet Oxygen Imaging in Cells: Characterizing the Irradiation-dependent Behavior of TMPyP in a Single Cell. *Photochemistry and photobiology* **2006,** *82* (1), 177-184.

164. Strauss, W. S.; Gschwend, M. H.; Sailer, R.; Schneckenburger, H.; Steiner, R.; Rück, A., Intracellular fluorescence behaviour of meso-tetra (4-sulphonatophenyl) porphyrin during photodynamic treatment at various growth phases of cultured cells. *Journal of Photochemistry and Photobiology B: Biology* **1995,** *28* (2), 155-161.

165. Howerton, B. S.; Heidary, D. K.; Glazer, E. C., Strained ruthenium complexes are potent light-activated anticancer agents. *J Am Chem Soc* **2012,** *134* (20), 8324-7.

166. Wang, D.; Lippard, S. J., Cellular processing of platinum anticancer drugs. *Nat Rev Drug Discov* **2005,** *4* (4), 307-320.

167. Ciarimboli, G., Membrane transporters as mediators of cisplatin side-effects. *Anticancer research* **2014,** *34* (1), 547-50.

168. Stewart, D. J., Mechanisms of resistance to cisplatin and carboplatin. *Critical Reviews in Oncology/Hematology* **2007,** *63* (1), 12-31.

169. Chen, D.; Milacic, V.; Frezza, M.; Dou, Q. P., Metal complexes, their cellular targets and potential for cancer therapy. *Current pharmaceutical design* **2009,** *15* (7), 777-91.

170. Frezza, M.; Hindo, S.; Chen, D.; Davenport, A.; Schmitt, S.; Tomco, D.; Dou, Q. P., Novel metals and metal complexes as platforms for cancer therapy. *Current pharmaceutical design* **2010,** *16* (16), 1813-25.

171. Romero-Canelon, I.; Sadler, P. J., Next-generation metal anticancer complexes: multitargeting via redox modulation. *Inorganic chemistry* **2013,** *52* (21), 12276-91.

172. Anighoro, A.; Bajorath, J.; Rastelli, G., Polypharmacology: challenges and opportunities in drug discovery. *Journal of medicinal chemistry* **2014,** *57* (19), 7874-87.

173. Schenone, M.; Dancik, V.; Wagner, B. K.; Clemons, P. A., Target identification and mechanism of action in chemical biology and drug discovery. *Nature chemical biology* **2013,** *9* (4), 232-40.

174. Baba, T.; Ara, T.; Hasegawa, M.; Takai, Y.; Okumura, Y.; Baba, M.; Datsenko, K. A.; Tomita, M.; Wanner, B. L.; Mori, H., Construction of Escherichia coli K-12 in-frame, single-gene knockout mutants: the Keio collection. *Molecular Systems Biology* **2006,** *2*, 2006.0008-2006.0008.

175. Blattner, F. R.; Plunkett, G., 3rd; Bloch, C. A.; Perna, N. T.; Burland, V.; Riley, M.; Collado-Vides, J.; Glasner, J. D.; Rode, C. K.; Mayhew, G. F.; Gregor, J.; Davis, N. W.; Kirkpatrick, H. A.; Goeden, M. A.; Rose, D. J.; Mau, B.; Shao, Y., The complete genome sequence of Escherichia coli K-12. *Science (New York, N.Y.)* **1997,** *277* (5331), 1453-62.

176. Frazer, K. A., Decoding the human genome. *Genome Research* **2012,** *22* (9), 1599-1601.

177. Neumann, B.; Walter, T.; Heriche, J. K.; Bulkescher, J.; Erfle, H.; Conrad, C.; Rogers, P.; Poser, I.; Held, M.; Liebel, U.; Cetin, C.; Sieckmann, F.; Pau, G.; Kabbe, R.; Wunsche, A.; Satagopam, V.; Schmitz, M. H.; Chapuis, C.; Gerlich, D. W.; Schneider, R.; Eils, R.; Huber, W.; Peters, J. M.; Hyman, A. A.; Durbin, R.; Pepperkok, R.; Ellenberg, J., Phenotypic profiling of the human genome by time-lapse microscopy reveals cell division genes. *Nature* **2010,** *464* (7289), 721-7.

178. Catrina, S. B.; Refai, E.; Andersson, M., The cytotoxic effects of the anti-bacterial peptides on leukocytes. *Journal of peptide science : an official publication of the European Peptide Society* **2009,** *15* (12), 842-8.

179. Vaucher, R. A.; Teixeira, M. L.; Brandelli, A., Investigation of the cytotoxicity of antimicrobial peptide P40 on eukaryotic cells. *Current microbiology* **2010,** *60* (1), 1-5.

180. Johnstone, T. C.; Alexander, S. M.; Lin, W.; Lippard, S. J., Effects of Monofunctional Platinum Agents on Bacterial Growth: A Retrospective Study. *Journal of the American Chemical Society* **2014,** *136* (1), 116-118.

181. Janovska, E.; Novakova, O.; Natile, G.; Brabec, V., Differential genotoxic effects of antitumor trans-[PtCl(2)(E-iminoether)(2)] and cisplatin in Escherichia coli. *J Inorg Biochem* **2002,** *90* (3-4), 155-8.

182. Brabec, V.; Pracharova, J.; Novakova, O.; Gibson, D.; Kasparkova, J., The induction of lysis in lysogenic strains of Escherichia coli by a new antitumor transplatin derivative and its DNA interactions. *Dalton transactions (Cambridge, England : 2003)* **2015,** *44* (8), 3573-82.

183. Carragher, N. O.; Brunton, V. G.; Frame, M. C., Combining imaging and pathway profiling: an alternative approach to cancer drug discovery. *Drug discovery today* **2012,** *17* (5-6), 203-14.

184. Peitz, I.; van Leeuwen, R., Single-cell bacteria growth monitoring by automated DEP-facilitated image analysis. *Lab on a Chip* **2010,** *10* (21), 2944-2951.

185. Lambert, R. J.; Pearson, J., Susceptibility testing: accurate and reproducible minimum inhibitory concentration (MIC) and non-inhibitory concentration (NIC) values. *Journal of applied microbiology* **2000,** *88* (5), 784-90.

186. Carson, C. F.; Hammer, K. A.; Riley, T. V., Broth micro-dilution method for determining the susceptibility of Escherichia coli and Staphylococcus aureus to the essential oil of Melaleuca alternifolia (tea tree oil). *Microbios* **1995,** *82* (332), 181-5.

187. Davison, H. C.; Low, J. C.; Woolhouse, M. E., What is antibiotic resistance and how can we measure it? *Trends in microbiology* **2000,** *8* (12), 554-9.

188. Hostetter, A. A.; Osborn, M. F.; DeRose, V. J., RNA-Pt adducts following cisplatin treatment of Saccharomyces cerevisiae. *ACS Chem Biol* **2012,** *7* (1), 218-25.

189. Calvori, C.; Frontali, L.; Leoni, L.; Tecce, G., Effect of rifamycin on protein synthesis. *Nature* **1965,** *207* (995), 417-8.

190. Wehrli, W., Rifampin: Mechanisms of Action and Resistance. *Reviews of Infectious Diseases* **1983,** *5*, S407-S411.

191. Campbell, E. A.; Korzheva, N.; Mustaev, A.; Murakami, K.; Nair, S.; Goldfarb, A.; Darst, S. A., Structural mechanism for rifampicin inhibition of bacterial rna polymerase. *Cell* **2001,** *104* (6), 901-12.

192. Speer, B. S.; Shoemaker, N. B.; Salyers, A. A., Bacterial resistance to tetracycline: mechanisms, transfer, and clinical significance. *Clinical microbiology reviews* **1992,** *5* (4), 387-99.

193. Salyers, A. A.; Speer, B. S.; Shoemaker, N. B., New perspectives in tetracycline resistance. *Molecular microbiology* **1990,** *4* (1), 151-6.

194. Nguyen, F.; Starosta, A. L.; Arenz, S.; Sohmen, D.; Donhofer, A.; Wilson, D. N., Tetracycline antibiotics and resistance mechanisms. *Biological chemistry* **2014,** *395* (5), 559-75.

195. Drlica, K.; Malik, M.; Kerns, R. J.; Zhao, X., Quinolone-mediated bacterial death. *Antimicrobial agents and chemotherapy* **2008,** *52* (2), 385-392.

196. Chai, Q.; Singh, B.; Peisker, K.; Metzendorf, N.; Ge, X.; Dasgupta, S.; Sanyal, S., Organization of Ribosomes and Nucleoids in Escherichia coli Cells during Growth and in Quiescence. *The Journal of biological chemistry* **2014,** *289* (16), 11342-11352.

197. Ang, W. H.; Brown, W. W.; Lippard, S. J., Preparation of Mammalian Expression Vectors Incorporating Site-Specifically Platinated-DNA Lesions. *Bioconjugate chemistry* **2009,** *20* (5), 1058-1063.

198. Ang, W. H.; Myint, M.; Lippard, S. J., Transcription Inhibition by Platinum DNA Cross-links in Live Mammalian Cells. *Journal of the American Chemical Society* **2010,** *132* (21), 7429-7435.

199. Heidary, D. K.; Glazer, E. C., A light-activated metal complex targets both DNA and RNA in a fluorescent in vitro transcription and translation assay. *Chembiochem* **2014,** *15* (4), 507-11.

200. Fron, E.; Van der Auweraer, M.; Moeyaert, B.; Michiels, J.; Mizuno, H.; Hofkens, J.; Adam, V., Revealing the excited-state dynamics of the fluorescent protein Dendra2. *The journal of physical chemistry. B* **2013,** *117* (8), 2300-13.

201. Adam, V.; Nienhaus, K.; Bourgeois, D.; Nienhaus, G. U., Structural basis of enhanced photoconversion yield in green fluorescent protein-like protein Dendra2. *Biochemistry* **2009,** *48* (22), 4905-15.

202. Woods, E.; Courtney, J.; Scholz, D.; Hall, W. W.; Gautier, V. W., Tracking protein dynamics with photoconvertible Dendra2 on spinning disk confocal systems. *Journal of microscopy* **2014,** *256* (3), 197-207.

203. Sandman, K. E.; Marla, S. S.; Zlokarnik, G.; Lippard, S. J., Rapid fluorescence-based reporter-gene assays to evaluate the cytotoxicity and antitumor drug potential of platinum complexes. *Chemistry & biology* **1999,** *6* (8), 541-551.

204. Domotor, O.; Hartinger, C. G.; Bytzek, A. K.; Kiss, T.; Keppler, B. K.; Enyedy, E. A., Characterization of the binding sites of the anticancer ruthenium(III) complexes KP1019 and KP1339 on human serum albumin via competition studies. *J Biol Inorg Chem* **2013,** *18* (1), 9-17.

205. Muller, P. A.; Vousden, K. H., Mutant p53 in cancer: new functions and therapeutic opportunities. *Cancer cell* **2014,** *25* (3), 304-17.

206. Marcel, V.; Catez, F.; Diaz, J. J., p53, a translational regulator: contribution to its tumour-suppressor activity. *Oncogene* **2015**.

207. Woods, D.; Turchi, J. J., Chemotherapy induced DNA damage response: convergence of drugs and pathways. *Cancer biology & therapy* **2013,** *14* (5), 379-89.

208. Elias, J.; Dimitrio, L.; Clairambault, J.; Natalini, R., The p53 protein and its molecular network: modelling a missing link between DNA damage and cell fate. *Biochimica et biophysica acta* **2014,** *1844* (1 Pt B), 232-47.

209. Brozovic, A.; Osmak, M., Activation of mitogen-activated protein kinases by cisplatin and their role in cisplatin-resistance. *Cancer letters* **2007,** *251* (1), 1-16.

210. Woessmann, W.; Chen, X.; Borkhardt, A., Ras-mediated activation of ERK by cisplatin induces cell death independently of p53 in osteosarcoma and neuroblastoma cell lines. *Cancer Chemother Pharmacol* **2002,** *50* (5), 397-404.

211. Peidis, P.; Papadakis, A. I.; Muaddi, H.; Richard, S.; Koromilas, A. E., Doxorubicin bypasses the cytoprotective effects of eIF2α phosphorylation and promotes PKR-mediated cell death. *Cell Death and Differentiation* **2011,** *18* (1), 145-154.

212. Persons, D. L.; Yazlovitskaya, E. M.; Cui, W.; Pelling, J. C., Cisplatin-induced Activation of Mitogen-activated Protein Kinases in Ovarian Carcinoma Cells: Inhibition of Extracellular Signal-regulated Kinase Activity Increases Sensitivity to Cisplatin. *Clinical Cancer Research* **1999,** *5* (5), 1007-1014.

213. Cuello-Garibo, J. A.; Meijer, M. S.; Bonnet, S., To cage or to be caged? The cytotoxic species in ruthenium-based photoactivated chemotherapy is not always the metal. *Chemical communications (Cambridge, England)* **2017,** *53* (50), 6768-6771.

214. Azar, D. F.; Audi, H.; Farhat, S.; El-Sibai, M.; Abi-Habib, R. J.; Khnayzer, R. S., Phototoxicity of strained Ru(ii) complexes: is it the metal complex or the dissociating ligand? *Dalton transactions (Cambridge, England : 2003)* **2017**.

215. Arnesano, F.; Banci, L.; Bertini, I.; Felli, I. C.; Losacco, M.; Natile, G., Probing the interaction of cisplatin with the human copper chaperone Atox1 by solution and in-cell NMR spectroscopy. *J Am Chem Soc* **2011,** *133* (45), 18361-9.

216. Luchinat, E.; Banci, L., A Unique Tool for Cellular Structural Biology: In-cell NMR. *The Journal of biological chemistry* **2016,** *291* (8), 3776-84.

217. Quach, D. T.; Sakoulas, G.; Nizet, V.; Pogliano, J.; Pogliano, K., Bacterial Cytological Profiling (BCP) as a Rapid and Accurate Antimicrobial Susceptibility Testing Method for Staphylococcus aureus. *EBioMedicine* **2016,** *4*, 95-103.

218. Wilson, M. Z.; Wang, R.; Gitai, Z.; Seyedsayamdost, M. R., Mode of action and resistance studies unveil new roles for tropodithietic acid as an anticancer agent and the gamma-glutamyl cycle as a proton sink. *Proceedings of the National Academy of Sciences of the United States of America* **2016,** *113* (6), 1630-5.

219. Cattley, R. C.; Radinsky, B. R., Cancer Therapeutics: Understanding the Mechanism of Action. *Toxicologic Pathology* **2004,** *32* (1_suppl), 116-121.

220. Joensuu, H., Escalating and de-escalating treatment in HER2-positive early breast cancer. *Cancer treatment reviews* **2017,** *52*, 1-11.

221. Bozic, I.; Reiter, J. G.; Allen, B.; Antal, T.; Chatterjee, K.; Shah, P.; Moon, Y. S.; Yaqubie, A.; Kelly, N.; Le, D. T.; Lipson, E. J.; Chapman, P. B.; Diaz, L. A., Jr.; Vogelstein, B.; Nowak, M. A., Evolutionary dynamics of cancer in response to targeted combination therapy. *Elife* **2013,** *2*, e00747.

222. Masui, K.; Gini, B.; Wykosky, J.; Zanca, C.; Mischel, P. S.; Furnari, F. B.; Cavenee, W. K., A tale of two approaches: complementary mechanisms of cytotoxic and targeted therapy resistance may inform next-generation cancer treatments. *Carcinogenesis* **2013,** *34* (4), 725-738.

223. Scott, D. E.; Bayly, A. R.; Abell, C.; Skidmore, J., Small molecules, big targets: drug discovery faces the protein–protein interaction challenge. **2016,** *15*, 533.

224. Lomenick, B.; Olsen, R. W.; Huang, J., Identification of Direct Protein Targets of Small Molecules. *ACS Chemical Biology* **2011,** *6* (1), 34-46.

225. Hopkins, A. L.; Groom, C. R., The druggable genome. *Nat Rev Drug Discov* **2002,** *1* (9), 727-30.

226. Cuatrecasas, P.; Wilchek, M.; Anfinsen, C. B., Selective enzyme purification by affinity chromatography. *Proceedings of the National Academy of Sciences of the United States of America* **1968,** *61* (2), 636-643.

227. Hirota, T.; Lee, J. W.; St John, P. C.; Sawa, M.; Iwaisako, K.; Noguchi, T.; Pongsawakul, P. Y.; Sonntag, T.; Welsh, D. K.; Brenner, D. A.; Doyle, F. J., 3rd; Schultz, P. G.; Kay, S. A., Identification of small molecule activators of cryptochrome. *Science (New York, N.Y.)* **2012,** *337* (6098), 1094-7.

228. Eggert, U. S., The why and how of phenotypic small-molecule screens. *Nature chemical biology* **2013,** *9* (4), 206-9.

229. Kang, J.; Hsu, C. H.; Wu, Q.; Liu, S.; Coster, A. D.; Posner, B. A.; Altschuler, S. J.; Wu, L. F., Improving drug discovery with high-content phenotypic screens by systematic selection of reporter cell lines. *Nature biotechnology* **2016,** *34* (1), 70-77.

230. Caie, P. D.; Walls, R. E.; Ingleston-Orme, A.; Daya, S.; Houslay, T.; Eagle, R.; Roberts, M. E.; Carragher, N. O., High-content phenotypic profiling of drug response signatures across distinct cancer cells. *Molecular cancer therapeutics* **2010,** *9* (6), 1913-26.

231. Fetz, V.; Prochnow, H.; Bronstrup, M.; Sasse, F., Target identification by image analysis. *Natural product reports* **2016,** *33* (5), 655-67.

232. Bray, M. A.; Singh, S.; Han, H.; Davis, C. T.; Borgeson, B.; Hartland, C.; Kost-Alimova, M.; Gustafsdottir, S. M.; Gibson, C. C.; Carpenter, A. E., Cell Painting, a high-content image-based assay for morphological profiling using multiplexed fluorescent dyes. *Nature protocols* **2016,** *11* (9), 1757-74.

233. Bougen-Zhukov, N.; Loh, S. Y.; Lee, H. K.; Loo, L. H., Large-scale image-based screening and profiling of cellular phenotypes. *Cytometry. Part A : the journal of the International Society for Analytical Cytology* **2017,** *91* (2), 115-125.

234. Kang, J.; Hsu, C. H.; Wu, Q.; Liu, S.; Coster, A. D.; Posner, B. A.; Altschuler, S. J.; Wu, L. F., Improving drug discovery with high-content phenotypic screens by systematic selection of reporter cell lines. *Nature biotechnology* **2016,** *34* (1), 70-7.

235. Klainer, A. S.; Perkins, R. L., Antibiotic-induced alterations in the surface morphology of bacterial cells: a scanning-beam electron miscroscopy study. *The Journal of infectious diseases* **1970,** *122* (4), 323-8.

236. Athamneh, A. I.; Alajlouni, R. A.; Wallace, R. S.; Seleem, M. N.; Senger, R. S., Phenotypic profiling of antibiotic response signatures in Escherichia coli using Raman spectroscopy. *Antimicrob Agents Chemother* **2014,** *58* (3), 1302-14.

237. Cushnie, T. P.; O'Driscoll, N. H.; Lamb, A. J., Morphological and ultrastructural changes in bacterial cells as an indicator of antibacterial mechanism of action. *Cellular and molecular life sciences : CMLS* **2016,** *73* (23), 4471-4492.

238. (a) Overbeck, T. L.; Knight, J. M.; Beck, D. J., A comparison of the genotoxic effects of carboplatin and cisplatin in Escherichia coli. *Mutation research* **1996,** *362* (3), 249-59; (b) Panda, P.; Taviti, A. C.; Satpati, S.; Kar, M. M.; Dixit, A.; Beuria, T. K., Doxorubicin inhibits E. coli division by interacting at a novel site in FtsZ. *The Biochemical journal* **2015,** *471* (3), 335-46; (c) Fram, R. J.; Sullivan, J.; Marinus, M. G., Mutagenesis and repair of DNA damage caused by nitrogen mustard, N,N'-bis(2-chloroethyl)-N-nitrosourea (BCNU), streptozotocin, and mitomycin C in E. coli. *Mutation research* **1986,** *166* (3), 299-42; (d) De Alencar, T. A.; Leitao, A. C.; Lage, C., Nitrogen mustard- and half-mustard-induced damage in Escherichia coli requires different DNA repair pathways. *Mutation research* **2005,** *582* (1-2), 105-15.

239. Johnstone, T. C.; Alexander, S. M.; Lin, W.; Lippard, S. J., Effects of Monofunctional Platinum Agents on Bacterial Growth – A Retrospective Study. *Journal of the American Chemical Society* **2014,** *136* (1), 116-118.

240. Azzam, M. E.; Algranati, I. D., Mechanism of Puromycin Action: Fate of Ribosomes after Release of Nascent Protein Chains from Polysomes. *Proceedings of the National Academy of Sciences* **1973,** *70* (12), 3866-3869.

241. Kim, S. Y.; Kim, S. J.; Kim, B. J.; Rah, S. Y.; Chung, S. M.; Im, M. J.; Kim, U. H., Doxorubicin-induced reactive oxygen species generation and intracellular Ca2+ increase are reciprocally modulated in rat cardiomyocytes. *Experimental & molecular medicine* **2006,** *38* (5), 535-45.

242. Wang, S.; Konorev, E. A.; Kotamraju, S.; Joseph, J.; Kalivendi, S.; Kalyanaraman, B., Doxorubicin Induces Apoptosis in Normal and Tumor Cells via Distinctly Different Mechanisms: INTERMEDIACY OF H2O2- AND p53-DEPENDENT PATHWAYS. *Journal of Biological Chemistry* **2004,** *279* (24), 25535-25543.

243. Vilenchik, M. M.; Knudson, A. G., Endogenous DNA double-strand breaks: production, fidelity of repair, and induction of cancer. *Proceedings of the National Academy of Sciences of the United States of America* **2003,** *100* (22), 12871-6.

244. Kang, Y. H.; Lee, K. A.; Kim, J. H.; Park, S. G.; Yoon, D. Y., Mitomycin C modulates DNA-double strand break repair genes in cervical carcinoma cells. *Amino acids* **2010,** *39* (5), 1291-8.

245. Roh, D. S.; Cook, A. L.; Rhee, S. S.; Joshi, A.; Kowalski, R.; Dhaliwal, D. K.; Funderburgh, J. L., DNA Cross-linking, Double-Strand Breaks, and Apoptosis in Corneal Endothelial Cells after a Single Exposure to Mitomycin C. *Investigative ophthalmology & visual science* **2008,** *49* (11), 4837-43.

246. Lundin, C.; North, M.; Erixon, K.; Walters, K.; Jenssen, D.; Goldman, A. S. H.; Helleday, T., Methyl methanesulfonate (MMS) produces heat-labile DNA damage but no detectable in vivo DNA double-strand breaks. *Nucleic Acids Res* **2005,** *33* (12), 3799-811.

247. Griffiths, A. J. F.; Depaula, A.; Young, P.; Miller, J. H.; Suzuki, D. T.; Lewontin, R. C.; Gelbart, W. M., *An Introduction to Genetic Analysis*. Macmillan Higher Education: 2003.

248. (a) Tounekti, O.; Kenani, A.; Foray, N.; Orlowski, S.; Mir, L. M., The ratio of single- to double-strand DNA breaks and their absolute values determine cell death pathway. *British Journal of Cancer* **2001,** *84* (9), 1272-1279; (b) Siddik, Z. H., Mechanisms of Action of Cancer Chemotherapeutic Agents: DNA-Interactive Alkylating Agents and Antitumour Platinum-Based Drugs. In *The Cancer Handbook*, John Wiley & Sons, Ltd: 2005; (c) Painter, R. B., Inhibition of DNA replicon initiation by 4-nitroquinoline 1-oxide, adriamycin, and ethyleneimine. *Cancer research* **1978,** *38* (12), 4445-9.

249. Chai, Q.; Singh, B.; Peisker, K.; Metzendorf, N.; Ge, X.; Dasgupta, S.; Sanyal, S., Organization of ribosomes and nucleoids in Escherichia coli cells during growth and in quiescence. *The Journal of biological chemistry* **2014,** *289* (16), 11342-52.

250. Morita, R.; Nakane, S.; Shimada, A.; Inoue, M.; Iino, H.; Wakamatsu, T.; Fukui, K.; Nakagawa, N.; Masui, R.; Kuramitsu, S., Molecular mechanisms of the whole DNA repair system: a comparison of bacterial and eukaryotic systems. *Journal of nucleic acids* **2010,** *2010*, 179594.

251. Inturi, S.; Tewari-Singh, N.; Agarwal, C.; White, C. W.; Agarwal, R., Activation of DNA damage repair pathways in response to nitrogen mustard-induced DNA damage and toxicity in skin keratinocytes. *Mutation research* **2014,** *0*, 53-63.

252. Ikenaga, M.; Takebe, H.; Ishii, Y., Excision repair of DNA base damage in human cells treated with the chemical carcinogen 4-nitroquinoline 1-oxide. *Mutation research* **1977,** *43* (3), 415-27.

253. Geronimo, I.; Denning, C. A.; Rogers, W. E.; Othman, T.; Huxford, T.; Heidary, D. K.; Glazer, E. C.; Payne, C. M., Effect of Mutation and Substrate Binding on the Stability of Cytochrome P450BM3 Variants. *Biochemistry* **2016,** *55* (25), 3594-606.

254. Kubanik, M.; Holtkamp, H.; Söhnel, T.; Jamieson, S. M. F.; Hartinger, C. G., Impact of the Halogen Substitution Pattern on the Biological Activity of Organoruthenium 8-Hydroxyquinoline Anticancer Agents. *Organometallics* **2015,** *34* (23), 5658-5668.

255. Prachayasittikul, V.; Prachayasittikul, S.; Ruchirawat, S.; Prachayasittikul, V., 8-Hydroxyquinolines: a review of their metal chelating properties and medicinal applications. *Drug Design, Development and Therapy* **2013,** *7*, 1157-1178.

256. Oliveri, V.; Vecchio, G., 8-Hydroxyquinolines in medicinal chemistry: A structural perspective. *Eur J Med Chem* **2016,** *120*, 252-74.

257. Yang, L.; Zhang, J.; Wang, C.; Qin, X.; Yu, Q.; Zhou, Y.; Liu, J., Interaction between 8-hydroxyquinoline ruthenium(II) complexes and basic fibroblast growth factors (bFGF): inhibiting angiogenesis and tumor growth through ERK and AKT signaling pathways. *Metallomics* **2014,** *6* (3), 518-31.

258. Liu, Y.-C.; Wei, J.-H.; Chen, Z.-F.; Liu, M.; Gu, Y.-Q.; Huang, K.-B.; Li, Z.-Q.; Liang, H., The antitumor activity of zinc(II) and copper(II) complexes with 5,7-dihalo-substituted-8-quinolinoline. *European Journal of Medicinal Chemistry* **2013,** *69*, 554-563.

259. Zou, B.-Q.; Qin, Q.-P.; Bai, Y.-X.; Cao, Q.-Q.; Zhang, Y.; Liu, Y.-C.; Chen, Z.-F.; Liang, H., Synthesis and antitumor mechanism of a new iron(iii) complex with 5,7-dichloro-2-methyl-8-quinolinol as ligands. *MedChemComm* **2017,** *8* (3), 633-639.

260. Qin, Q.-P.; Chen, Z.-F.; Qin, J.-L.; He, X.-J.; Li, Y.-L.; Liu, Y.-C.; Huang, K.-B.; Liang, H., Studies on antitumor mechanism of two planar platinum(II) complexes with 8-hydroxyquinoline: Synthesis, characterization, cytotoxicity, cell cycle and apoptosis. *European Journal of Medicinal Chemistry* **2015,** *92*, 302-313.

261. Kubista, B.; Schoefl, T.; Mayr, L.; van Schoonhoven, S.; Heffeter, P.; Windhager, R.; Keppler, B. K.; Berger, W., Distinct activity of the bone-targeted gallium compound KP46 against osteosarcoma cells - synergism with autophagy inhibition. *Journal of experimental & clinical cancer research : CR* **2017,** *36* (1), 52.

262. Zhang, H.-R.; Liu, Y.-C.; Meng, T.; Qin, Q.-P.; Tang, S.-F.; Chen, Z.-F.; Zou, B.-Q.; Liu, Y.-N.; Liang, H., Cytotoxicity, DNA binding and cell apoptosis induction of a zinc(ii) complex of HBrQ. *MedChemComm* **2015,** *6* (12), 2224-2231.

263. Martin-Santos, C.; Michelucci, E.; Marzo, T.; Messori, L.; Szumlas, P.; Bednarski, P. J.; Mas-Balleste, R.; Navarro-Ranninger, C.; Cabrera, S.; Aleman, J., Gold(III) complexes with hydroxyquinoline, aminoquinoline and quinoline ligands: Synthesis, cytotoxicity, DNA and protein binding studies. *J Inorg Biochem* **2015,** *153*, 339-45.

264. Heidary, D. K.; Howerton, B. S.; Glazer, E. C., Coordination of hydroxyquinolines to a ruthenium bis-dimethyl-phenanthroline scaffold radically improves potency for potential as antineoplastic agents. *Journal of medicinal chemistry* **2014,** *57* (21), 8936-46.

265. Kim, E. K.; Choi, E. J., Pathological roles of MAPK signaling pathways in human diseases. *Biochimica et biophysica acta* **2010,** *1802* (4), 396-405.

266. Cuadrado, A.; Nebreda, A. R., Mechanisms and functions of p38 MAPK signalling. *The Biochemical journal* **2010,** *429* (3), 403-17.

267. Wagner, E. F.; Nebreda, A. R., Signal integration by JNK and p38 MAPK pathways in cancer development. *Nat Rev Cancer* **2009,** *9* (8), 537-49.

268. Gdowski, A.; Panchoo, M.; Treuren, T. V.; Basu, A., Emerging therapeutics for targeting Akt in cancer. *Frontiers in bioscience (Landmark edition)* **2016,** *21*, 757-68.

269. Osaki, M.; Oshimura, M.; Ito, H., PI3K-Akt pathway: its functions and alterations in human cancer. *Apoptosis : an international journal on programmed cell death* **2004,** *9* (6), 667-76.

270. Manning, B. D.; Cantley, L. C., AKT/PKB signaling: navigating downstream. *Cell* **2007,** *129* (7), 1261-74.

271. Chen, Z.-F.; Gu, Y.-Q.; Song, X.-Y.; Liu, Y.-C.; Peng, Y.; Liang, H., Synthesis, crystal structure, cytotoxicity and DNA interaction of 5,7-dichloro-8-quinolinolato-lanthanides. *European Journal of Medicinal Chemistry* **2013,** *59*, 194-202.

272. Chen, Z.-F.; Wei, J.-H.; Liu, Y.-C.; Liu, M.; Gu, Y.-Q.; Huang, K.-B.; Wang, M.; Liang, H., High antitumor activity of 5,7-dihalo-8-quinolinolato cerium complexes. *European Journal of Medicinal Chemistry* **2013,** *68*, 454-462.

273. Martin Santos, C.; Cabrera, S.; Rios-Luci, C.; Padron, J. M.; Lopez Solera, I.; Quiroga, A. G.; Medrano, M. A.; Navarro-Ranninger, C.; Aleman, J., Novel clioquinol and its analogous

platinum complexes: importance, role of the halogen substitution and the hydroxyl group of the ligand. *Dalton transactions (Cambridge, England : 2003)* **2013,** *42* (37), 13343-8.

274. Bochkov, Y. A.; Palmenberg, A. C., Translational efficiency of EMCV IRES in bicistronic vectors is dependent upon IRES sequence and gene location. *BioTechniques* **2006,** *41* (3), 283-4, 286, 288 passim.

275. Telpalo-Carpio, S. A.; Diaz-Mitoma, F.; Moreno-Cuevas, J. E.; Aguilar-Yanez, J. M., Internal ribosome entry site (IRES) from Encephalomyocarditis virus (EMCV) as a tool for shuttle expression plasmids. *Biochemical and biophysical research communications* **2015,** *468* (4), 548-53.

276. Kyrpides, N. C.; Woese, C. R., Universally conserved translation initiation factors. *Proceedings of the National Academy of Sciences* **1998,** *95* (1), 224-228.

277. Gonzalez-Almela, E.; Williams, H.; Sanz, M. A.; Carrasco, L., The Initiation Factors eIF2, eIF2A, eIF2D, eIF4A, and eIF4G Are Not Involved in Translation Driven by Hepatitis C Virus IRES in Human Cells. *Frontiers in microbiology* **2018,** *9*, 207.

278. Chamond, N.; Deforges, J.; Ulryck, N.; Sargueil, B., 40S recruitment in the absence of eIF4G/4A by EMCV IRES refines the model for translation initiation on the archetype of Type II IRESs. *Nucleic Acids Res* **2014,** *42* (16), 10373-84.

279. Lopez-Lastra, M.; Rivas, A.; Barria, M. I., Protein synthesis in eukaryotes: the growing biological relevance of cap-independent translation initiation. *Biological research* **2005,** *38* (2-3), 121-46.

280. Costantini, L. M.; Fossati, M.; Francolini, M.; Snapp, E. L., Assessing the tendency of fluorescent proteins to oligomerize under physiologic conditions. *Traffic (Copenhagen, Denmark)* **2012,** *13* (5), 643-9.

281. Costantini, L. M.; Fossati, M.; Francolini, M.; Snapp, E. L., Assessing the Tendency of Fluorescent Proteins to Oligomerize under Physiologic Conditions. *Traffic (Copenhagen, Denmark)* **2012,** *13* (5), 643-649.

282. Dougherty, J. D., The Expanding Toolkit of Translating Ribosome Affinity Purification. *The Journal of Neuroscience* **2017,** *37* (50), 12079-12087.

283. Garrett, R. A., *The Ribosome: Structure, Function, Antibiotics, and Cellular Interactions*. ASM Press: 2000.

284. Schaub, B. E.; Berger, B.; Berger, E. G.; Rohrer, J., Transition of Galactosyltransferase 1 from Trans-Golgi Cisterna to the Trans-Golgi Network Is Signal Mediated. *Molecular Biology of the Cell* **2006,** *17* (12), 5153-5162.

285. Chen, T.; Liu, Y.; Z, W.-J.; Liu, J.; Wong, Y.-S., Ruthenium Polypyridyl Complexes That Induce Mitochondria-Mediated Apoptosis in Cancer Cells. *Inorganic chemistry* **2010,** *49*, 6366-6368.

286. Qian, C.; Wang, J.-Q.; Song, C.-L.; Wang, L.-L.; Ji, L.-N.; Chao, H., The induction of mitochondria-mediated apoptosis in cancer cells by ruthenium(II) asymmetric complexes. *Metallomics* **2013,** *5*, 844-854.

287. Karbowski, M.; Arnoult, D.; Chen, H.; Chan, D. C.; Smith, C. L.; Youle, R. J., Quantitation of mitochondrial dynamics by photolabeling of individual organelles shows that mitochondrial fusion is blocked during the Bax activation phase of apoptosis. *The Journal of Cell Biology* **2004,** *164* (4), 493-499.

288. Lo, K. K.-W.; Tsang, K. H.-K.; Sze, K.-S.; Chung, C.-K.; Lee, T. K.-M.; Zhang, K. Y.; Hui, W.-K.; Li, C.-K.; Lau, J. S.-Y.; Ng, D. C.-M.; Zhu, N., Non-covalent binding of luminescent transition metal polypyridine complexes to avidin, indole-binding proteins and estrogen receptors. *Coordination Chemistry Reviews* **2007,** *251* (17), 2292-2310.

289. Campagna, S.; Puntoriero, F.; Nastasi, F.; Bergamini, G.; Balzani, V., Photochemistry and Photophysics of Coordination Compounds: Ruthenium. In *Photochemistry and Photophysics of Coordination Compounds I*, Balzani, V.; Campagna, S., Eds. Springer Berlin Heidelberg: Berlin, Heidelberg, 2007; pp 117-214.

290. Kowada, T.; Maeda, H.; Kikuchi, K., BODIPY-based probes for the fluorescence imaging of biomolecules in living cells. *Chemical Society Reviews* **2015,** *44* (14), 4953-4972.

291. Pakhomov, A. A.; Deyev, I. E.; Ratnikova, N. M.; Chumakov, S. P.; Mironiuk, V. B.; Kononevich, Y. N.; Muzafarov, A. M.; Martynov, V. I., BODIPY-based dye for no-wash live-cell staining and imaging. *BioTechniques* **2017,** *63* (2), 77-80.

292. Sugawara, T.; Hirasawa, A.; Hashimoto, K.; Tsujimoto, G., Differences in the subcellular localization of α1-adrenoceptor subtypes can affect the subtype selectivity of drugs in a study with the fluorescent ligand BODIPY FL-prazosin. *Life Sciences* **2002,** *70* (18), 2113-2124.

293. Cummins, T. D.; Higdon, A. N.; Kramer, P. A.; Chacko, B. K.; Riggs, D. W.; Salabei, J. K.; Dell'Italia, L. J.; Zhang, J.; Darley-Usmar, V. M.; Hill, B. G., Utilization of fluorescent probes for the quantification and identification of subcellular proteomes and biological processes regulated by lipid peroxidation products. *Free radical biology & medicine* **2013,** *59*, 56-68.

294. Maekawa, M.; Fairn, G. D., Molecular probes to visualize the location, organization and dynamics of lipids. *Journal of Cell Science* **2014,** *127* (22), 4801.

295. Zhang, H.; Chen, X.; Lan, J.; Liu, Y.; Zhou, F.; Wu, D.; You, J., Silver-mediated direct C-H amination of BODIPYs for screening endoplasmic reticulum-targeting reagents. *Chemical communications (Cambridge, England)* **2018,** *54* (26), 3219-3222.

296. Thongboonkerd, V., *Proteomics of Human Body Fluids: Principles, Methods, and Applications*. Humana Press: 2008.

297. Zhang, R.; Ye, Z.; Yin, Y.; Wang, G.; Jin, D.; Yuan, J.; Piper, J. A., Developing Red-Emissive Ruthenium(II) Complex-Based Luminescent Probes for Cellular Imaging. *Bioconjugate Chemistry* **2012,** *23* (4), 725-733.

298. Byrne, A.; Burke, C. S.; Keyes, T. E., Precision targeted ruthenium(ii) luminophores; highly effective probes for cell imaging by stimulated emission depletion (STED) microscopy. *Chemical Science* **2016,** *7* (10), 6551-6562.

299. Liu, Z.; Gao, K.; Wang, B.; Yan, H.; Xing, P.; Zhong, C.; Xu, Y.; Li, H.; Chen, J.; Wang, W.; Sun, S., A dinuclear ruthenium(II) complex as turn-on luminescent probe for hypochlorous acid and its application for in vivo imaging. *Scientific reports* **2016,** *6*, 29065.

300. Boynton, A. N.; Marcelis, L.; McConnell, A. J.; Barton, J. K., A Ruthenium(II) Complex as a Luminescent Probe for DNA Mismatches and Abasic Sites. *Inorganic chemistry* **2017,** *56* (14), 8381-8389.

301. Dunn, K. W.; Kamocka, M. M.; McDonald, J. H., A practical guide to evaluating colocalization in biological microscopy. *American Journal of Physiology - Cell Physiology* **2011,** *300* (4), C723-C742.

302. Adler, J.; Parmryd, I., Quantifying colocalization by correlation: The Pearson correlation coefficient is superior to the Mander's overlap coefficient. *Cytometry Part A* **2010,** *77A* (8), 733-742.

VITA

Yang Sun

Personal Information

Place of Birth: Hengshui, Hebei P. R. China

Education

Beijing Normal University

Beijing P. R. China

Bachelors of Science in Biotechnology (2008)

University of Kentucky

Lexington, KY U. S. A.

Doctor of Philosophy (2018)

Awards and Scholarships

Research Challenge Trust Fund Fellowship – 2016 – 2017 academic year

Kentucky Opportunity Fellowship – 2012 – 2013 academic year

Kentucky Excellence Fellowship – 2010 – 2011 academic year

Honorable Mention of 39th Annual Naff Symposium Poster Session – Spring 2013

Publications

Submitted or in preparation

Sun, Y.; Dickerson, M.; Howerton, B.; Glazer, E. C., Modifying charge and hydrophilicity of simple Ru(II) polypyridyl complexes radically alters biological activities: old complexes, surprising new tricks. *Inorganic Chemistry*, **2014**, *53* (19), 10370-7.

Sun, Y.; Heidary, D. K.; Zhang, Z.; Richards, C. I.; Glazer, E. C.; *E. coli* as a Model System for Rapid Investigations of the Mechanism of Actions of Cytotoxic Metal Complexes. *Manuscript in preparation*